MATERIAL CHARACTERIZATION AND DESIGN RECOMMENDATIONS FOR MECHANICALLY STABILIZED EARTH RETAINING WALLS

A Dissertation

by

VISHAL SAMBAIAH DANTAL

Submitted to the Office of Graduate and Professional Studies of
Texas A&M University
in partial fulfillment of the requirements for the degree of

DOCTOR OF PHILOSOPHY

Chair of Committee,	Charles P. Aubeny
Co-Chair of Committee,	Giovanna Biscontin
Committee Members,	Robert L. Lytton
	Christopher C. Mathewson
Head of Department,	Robin Autenrieth

December 2013

Major Subject: Civil Engineering

ABSTRACT

Since its appearance in 1970s, mechanically stabilized earth (MSE) walls have become a majority among all types of retaining walls due to their economics and satisfactory performance. The Texas Department of Transportation has primarily adopted the Federal Highway Administration and American Association of State Highway and Transportation Officials (AASHTO) guidelines for design of MSE walls.

The research addresses three main issues expressed by TxDOT in their design and material selection process. The literature review in this research addresses the current practice and guidelines adopted by TxDOT as well as other Department of Transportations.

The first part of this dissertation explains the laboratory test performed on backfill materials used in Texas. The material classification was carried out according to TxDOT specifications and the laboratory test consist of performing state-of-the-art large scale triaxial test on large particles to evaluate engineering properties of backfill materials and a consolidated undrained test on a backfill material with higher amount fine particles present in that soil.

The second part of this addresses the issues on global stability and failure modes associated with it. A Fast Lagrangian Analysis of Continua (FLAC) program was used to asseses possible failure modes for MSE walls with different geometries and soil parameters for retained and foundation soils.

Finally, a parametric study was performed for sliding analysis using AASTHO recommended design parameters and comparing them with modified design parameters calculated from FLAC simulations for different geometries and soil parameters. Similarly, a parametric study was performed to address bearing capacity issues for MSE walls and justification of AASHTO recommendation with German code (EBGEO) for MSE walls.

The outcome this research shows that, the friction angle (ϕ) for the backfill materials used in Texas is higher than AASHTO recommended values for large particles size type backfills. From FLAC simulations it shows that the global failure mechanism for MSE walls is dependent on type of soil properties used as retained and foundation soils. The parametric study shows that a modified parameters can be used for sliding analysis and for bearing capacity analysis a combination of Vesic's and German code can be used.

DEDICATION

To my parents, sister and maternal grandmother for helping me and supporting me throughout my life.

ACKNOWLEDGEMENTS

I would like to thank my committee co-chair, Dr. Charles P. Aubeny and Dr. Giovanna Biscontin for their immense guidance and encouragement for doing this research, and my committee members, Dr. Lytton and Dr. Mathewson for being part of my research committee and support.

I would like to express sincere thanks to Texas Department of Transportation for funding this project. I would also like to extend my thanks to Project Director at TxDOT Mr. Sean Yoon and Dr. Dov Leshchinsky for their technical advises.

I would like to thank a graduate student, Mackenzie Garton for helping in laboratory testing and being a part of this research, and thanks also goes to Adam White and Marcus Rasulo for their help in different laboratory work for this research. I would like to sincerely thank business coordinator at Texas A&M Transportation Institute, Ms. Maria Medrano for helping out on purchasing equipment and managing business side of this research. Thanks also goes to my friends (Michelle Bernhardt, Ryan Beemer, Ahran Song, Deeyvid Saez and Mackenzie Garton), colleagues, department faculty and staff for making my time at Texas A&M University a great experience.

Finally, thanks to my mother, father and sister for their encouragement and patience.

TABLE OF CONTENTS

Page

LIST OF FIGURES

Page

LIST OF TABLES

Page

1. INTRODUCTION

The Mechanically Stabilized Earth (MSE) retaining walls have been used for many different purposes such as supporting bridges, residential/commercial buildings, sound walls, roadways, and railroads. Invented by the French architect and engineer, Henri Vidal in 1960s, MSE walls have gradually become a widely accepted retaining wall type. The MSE wall was introduced to the US in 1970s and the first MSE wall was built in the state of California in 1972. So far, over 60,000 MSE walls higher than 35 ft are in service at the US highway system (Alzamora and Barrows 2007). Approximately 9,000,000 ft^2 (850,000 m^2) were added into the US transportation system annually, which accounted for more than half of all types of retaining wall usage (Berg et al. 2009). Texas Department of Transportation (TxDOT) is one of the leading transportation organizations in the application of MSE walls in US. MSE walls accounted for more than 80 percent of TxDOT retaining walls according to statistical data collected between August 1, 2006 and June 20, 2007 (Galvan 2007). The MSE walls constructed by TxDOT comprised more than 20 percent of the MSE walls constructed annually in the US transportation system.

The MSE walls have become the preferred retaining wall type because they are less expensive, easier to construct, more tolerable to differential settlement, and perform better under seismic loading compared with other types of retaining walls (Christopher et al. 2005). Besides routinely retaining soil/rock mass, MSE walls have been built to support various heavily loaded superstructures, such as bridges and towers (Adams et al. 2011).

This research encompasses different aspects of MSE wall components required in selection of materials and assumption of design parameters. In the following section-2, it includes a literature review on materials used by TxDOT and other transportation governing agencies, followed by an overview on current design assumptions and procedures for MSE walls adopted by TxDOT. Section-3 explains the tests performed on backfill materials provided by TxDOT. This section starts with a material procurement from borrow pits and processing these materials according to TxDOT specifications before testing them. A testing procedure for large scale triaxial test is also explained in this section.

Section-4 focuses on a numerical simulations performed using Fast Lagrangian Analysis of Continua (FLAC) for global stability of MSE walls with different geometries and different material properties for retaining soils. A parametric study is performed in this research to better understand the effect of different geometries, different material properties for retaining and foundation soils on sliding analysis and bearing capacity analysis of MSE walls. This parametric study is documented in Section-5 for sliding and bearing capacity analysis using AASHTO, 2002 guidelines for forces acting on the wall and as well as forces calculated from FLAC simulations.

Finally, section-5 concludes findings from all the above chapters on MSE walls for testing backfill materials, performing numerical simulations and conducting statistical analysis on backfill materials. This chapter also provides recommendations for design assumptions in terms of material properties and on design methodology to be used for MSE wall.

1.1 Background

The main purpose of retaining walls is to provide a support to other structures and contain an earth forces from the vertical cut-out of slope. Typically MSE walls are used for supporting bridges, retaining walls for commercial/residential buildings, supporting cut-out slope and other roadway structures. The MSE walls are constructed using select backfill with certain specifications, reinforcements and wall face units (concrete).

1.1.1 Typical MSE Wall Geometries

The typical height of MSE walls ranges from 6 ft to 20 ft depending upon the project requirements. The current recommendation for the width of the wall is 8ft or 0.7H whichever is higher, where H is the height of the wall. Three different type of wall configurations are widely used by department of transportation are as shown in Figure 1-Figure 3 below.

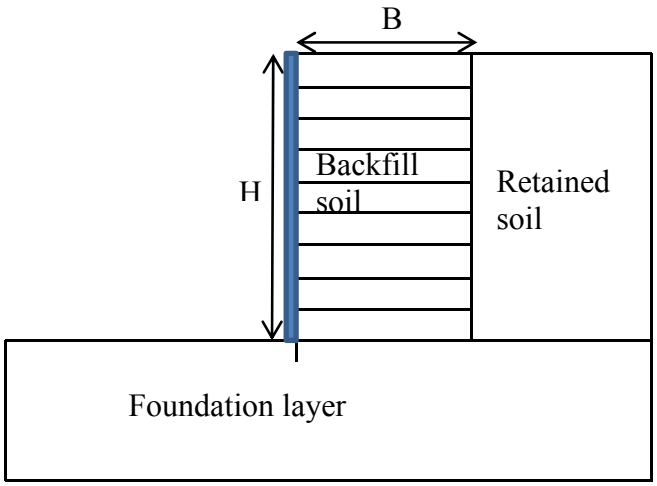

Figure 1. Typical MSE Wall Configuration with No Backslope.

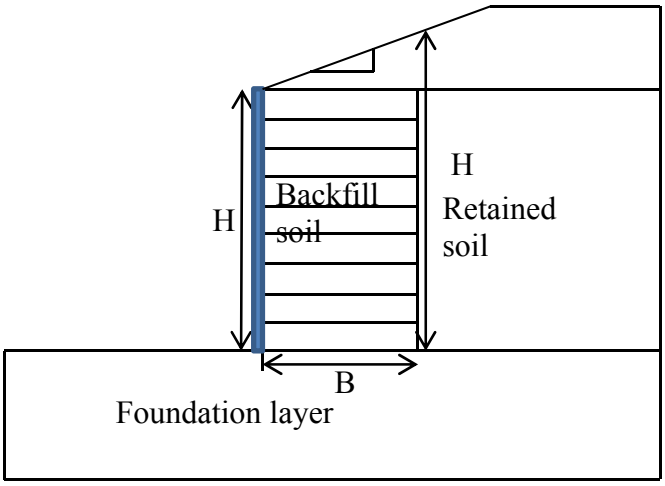

Figure 2. MSE Wall Configuration with Backslope.

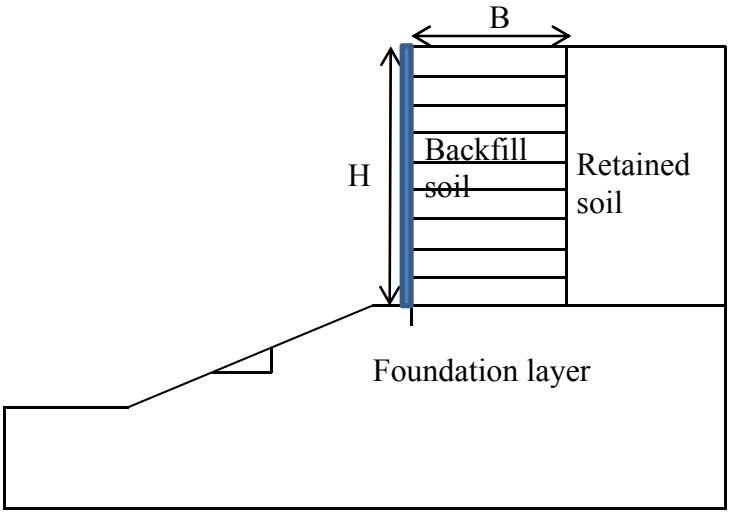

Figure 3. MSE Wall Configuration with Fore-slope.

1.1.2 Reinforcement Materials Used

Different department of transportation specifies different type of reinforcements for MSE walls. There two different type of reinforcements in terms of materials i.e geosynthetic and metal reinforcement. TxDOT specifies steel reinforcements in form of

strips. The metal strips used for reinforcement can be plain in surface or ribbed. The ribbed one gives additional surface area for resistance against horizontal pullout force and increases a friction factor for design calculations (AASHTO 2002). The geosynthetic type of reinforcement can come different forms, most widely used type is in form of plastic sheets or in form of hexagonal grid pattern. The wall face units comes in different size and shapes depends on the manufacturers. Generally these wall units are made of concrete and if a geosynthetics are used as reinforcements then a place-in concreting can be done.

1.1.3 Current Design Procedures and Failure Modes

Most department of transportation's adopts a design procedures from American Association of State Highway and Transportation Officials (AASHTO) design guidelines or Federal Highway Administration (FHWA) design guidelines for MSE walls with few state specific recommendations. TxDOT adopts AASHTO design guidelines for metal strips as reinforcement. According to TxDOT the internal stability design is conducted by the vendor of wall face units and of reinforcement supplier. The external stability analysis is checked for following potential external failure modes shown in Figure 4 and the factor of safety against these failure mode are presented in Table 1.

Table 1. Factor of Safety against External Failure Modes (AASHTO 2002)

Failure Mode	Factor of Safety
Bearing	1.5
Overturning	2.0
Bearing capacity	2.5

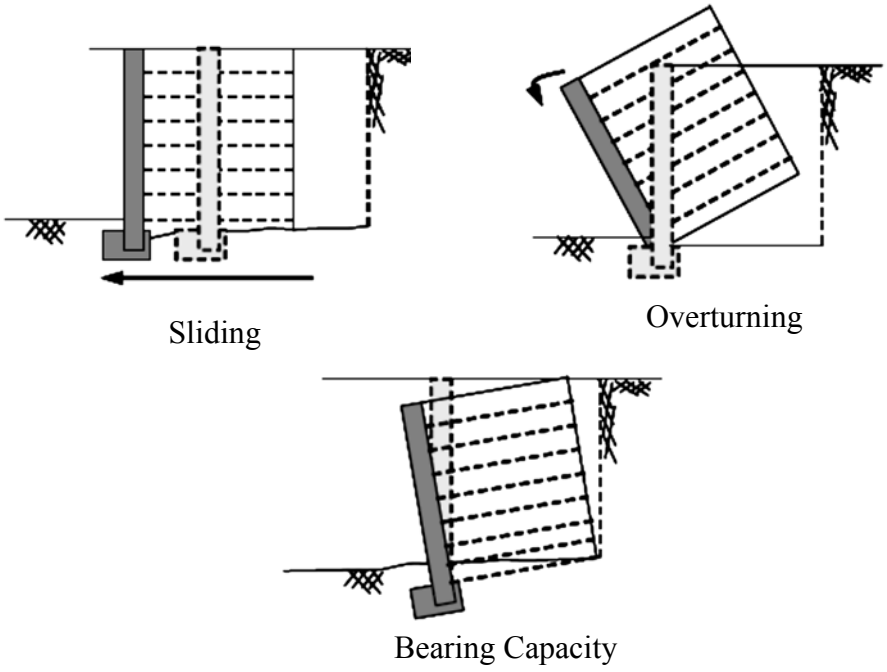

Figure 4. Potential External Failure Modes for MSE Walls (after (FHWA 2009)).

2. LITERATURE REVIEW

Since the initial appearance of MSE walls in 70's, these type of walls have been widely used and integrated in lot of highway projects. This section focuses on the following aspects of the MSE wall design:

- Materials: backfill material types, material properties, and related standard specifications.
- Design: required minimum factors of safety, bearing capacity check, minimum reinforced length, and global stability.

2.1 Overview of Backfill Material Used in MSE Walls

2.1.1 Type A, B, and D

Various types of backfill materials have been used in MSE wall construction. Existing AASHTO specifications for construction of MSE walls call for the use of high quality of free-draining granular material (AASHTO 2002). TxDOT allows four types of backfill materials in MSE walls as listed in Table 2 (TxDOT 2004). According to Item 423 of TxDOT material specifications, the allowable amount of material passing a #200 sieve for backfill types A, B and D ranges from 0 to 15 percent, and there is no plasticity index (PI) requirement listed. These specifications are slightly different from FHWA requirements for fine contents (<15 percent) and PI value (<6). The gradation of each type of backfills deviates from FHWA specifications are shown in Figure 5. However, the friction angle is directly adopted from FHWA guidelines without any modifications. FHWA does not specify the unit weight of backfill materials to be used, but TxDOT

uses two sets of aggregate unit weight values for select backfill in current practice as presented in Table 3.

Table 2. Material Parameters Used by TxDOT (Yoon 2011).

Type of Fill	Material	Short-term		Long-term		Unit weight (lb/ft^3)
		c (psf)	ϕ (deg)	c (psf)	ϕ (deg)	
Reinforced fill	Types A, B, and D	0	34	0	34	125
	Type C	0	30	0	30	125
Retained fill	Controlled fill, PI<30	750	0	0	30 or PI correlation	125
Foundation soil (fill)	Controlled fill, PI<30	750	0	0	30 or PI correlation	125

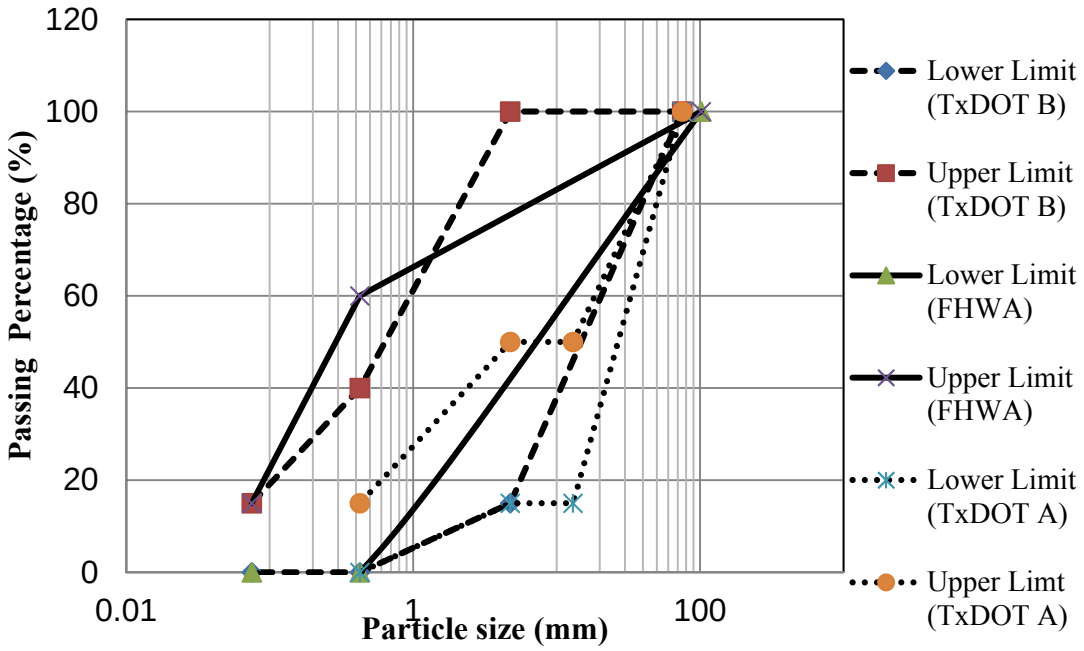

Figure 5. TxDOT MSE Wall Backfill Material Gradation (Developed from TxDOT Standard Specification 2004 and (FHWA 2009)).

Table 3. Unit Weights for Select Backfill (TxDOT 2012).

	Unit Weight	Internal Stability	External Stability
Type A, B, and D	105 pcf	Pullout	Sliding, Overturning, Eccentricity
	125 pcf	Rupture	Bearing

Both the friction angle and the unit weight of backfill materials have significant influence on the calculated factor of safety (FOS). Duncan (2000) completed a study on the variation of parameters for the calculation of FOS, which indicated that a variation of friction angle between 34° and 28° could influence the calculated FOS against sliding by up to 25 percent, and the variation of unit weight between 127 lb/ft^3 and 113 lb/ft^3 could influence the calculated FOS by approximately 10 percent. Harr (1984) and Kulhawy (1992) indicate that the variation of the friction angle of the foundation soil can lead 13 percent variation of the calculated FOS. The material properties are influenced by the material type as well as the construction quality. Mooney et al. (2008) indicated that the inadequate compaction often occurred at the zones within 3–4 ft of the wall facing.

2.1.2 Type C

TxDOT Type C material specifications permit a fines content of more than 15 percent, which is an unsuitable backfill material according to FHWA specifications (Berg et al. 2009). Note that TxDOT allows use of Type C only for temporary walls. It is also usually considered a marginal fill in practice. There is an argument that the FHWA specification is too conservative in its limitation on the fines content, since the National Concrete Masonry Association (NCMA) adopted a 35 percent fines content criterion

(NCMA 2002) for marginal fills. It was claimed that the marginal backfill material, if appropriately used, could lead to a well-performing MSE wall with 20–30 percent cost saving compared with the MSE walls using AASHO/FHWA specified backfill material (Christopher et al. 2005). FHWA (2001) presented cases of MSE walls and reinforced slopes design and construction, including several case histories on utilizing various backfill materials such as glacial till, decomposed granite, and sandy clay soils with geo-reinforcement. Overall, the performance of structures has been satisfactory with no major problems observed.

However, studies (Dodson 2010) also showed that inappropriate usage of the marginal fill can cause excessive lateral deformation of walls, vertical settlement of reinforced fill, movement, and cracking of the facing. Once the above-mentioned problems occurred, the repair/remedy cost would make the total cost much high than the construction cost of the MSE walls using AASHTO/FHWA specified backfill materials (Dodson 2010). The usage of marginal backfill material has been debated for long time. NCHRP has sponsored a seven-year project (Project 24-22) entitled "Selecting Backfill Materials for Mechanically Stabilized Earth (MSE) Retaining Walls."(Allen 2013) The project was extended for another year and thus the final report is not publically available. A common concern of using marginal fill in MSE walls is that the marginal backfill cannot effectively dissipate excessive water pressure. As a result, it increases the lateral force on MSE walls and softens the backfill material. With regard to this issue, Bobet (2002) conducted extensive laboratory pullout tests along with numerical analyses to determine the relation between drained and undrained pullout capacities for different soil

types, overburden pressures as well as scale and permeability effects in the dissipation of excess pore pressures. It was observed that (1) drained and undrained pullout capacities varied depending on the amount of silt. The pullout capacity decreased from clean sand to 5percent silt in sand, and increased when amount of silt was between 5 to 10 percent, and then decreased when there was 10 to 15 and 35percent silt in sand; (2) pullout capacity increased with larger overburden pressure; (3) the undrained pullout capacity was always smaller than the drained one except for clean sand, for which it was identical; (4) the dissipation of pore pressure was very rapid for hydraulic conductivity larger than 10^{-2} cm/sec and very slow with hydraulic conductivity smaller than 10^{-3} cm/sec; and (5) for hydraulic conductivity smaller than 10^{-3} cm/sec, consolidation time increased along with the larger reinforcement length, based on numerical analyses. The deficiency of marginal backfill materials has been reflected in many failure cases (Reddy et al. 2003). Keller (1995) documented case histories with poorly- and well-performing MSE walls typically constructed with native soil backfill on low and moderate standard rural roads as presented in Table 4.

Table 4. Local Marginal Materials Used in Forest Service Structures (after (Keller 1995)).

Site	Wall Type	USC Unified Soil Classification	% Minus 200 Sieve	PI	ϕ (deg)	C (kPa)	Comments
Goat Hill Plumas NF (National Forest)	Welded wire (4.6 m)	SM SC SM	21 20 23	5 8 4	34 31 27	9.6 14.4 16.7	4% settlement on face
Mosquito R. Tahoe NF	Welded wire (8.2 m)	SM ML	22 50	NP 6	- -	- -	Minor settlement, vegetated
L.North Fork Plumas NF	Reinforced fill (1:1, 15.2 m)	SM ML	38 55	2 3	34 33	4.8 7.2	Minor slumping, well vegetated
Gallatin Lassen NF	HSE-concrete face with wire (3.8 m)	GW	1+	NP	30+	-	Minor face panel separation
B.Longville Plumas NF	Welded wire (5.5 m)	CL SM	50+	-	26	9.6	Poor foundation, 3% settlement
Grave Plumas NF	Geotextile (2.7 m)	SM	26	NP	35	40.7	Irregular face, no fill loss
Butt Valley Plumas NF	Tire-Faced (3.1 m)	SC	38	8	26	19.2	10% face settlement
Thomjac Klamath NF	Timber-Faced (4.6 m)	SM	27	NP	30+	0	Minimal settlement
Stump Spring Sierra NF	Welded Wire (6.8 m)	SM SC	- 42	- 15	- -	- -	Performing well, Min. Settlement
Pulga Plumas NF	Welded Wire (5.9 m)	SM GM	- 44	- 4	- 29	- 9.6	Mod. Settlement, poor compaction
Agness Siskiyou NF	Chainlink Fencing (to 6.7 m)	GM SM	- 15	- NP	- -	- -	Min. settlement, Min. corrosion, face vegetated
Camp 5 Hill Willamette NF	Wood Chips+ Geotextile (8.5 m)	GP	0	NP	34	0	5% Settlement, Continuing chips decomposition

Currently, TxDOT recommends use of cement-stabilized Type C backfill when required or as approved along with special drainage provisions for temporary MSE walls. Stabilizing Type C backfill with 5 percent hydraulic cement by dry weight of the backfill material should be followed by compaction of the backfill within 2 hours of mixing. In addition, properties to indicate the potential aggressiveness of the backfill material metal reinforcement needs to be measured as follows. (TxDOT 2004)

- pH between 5.5 and 10.0 as determined by Tex-128-E (TxDOT 1999a).
- Electrical resistivity more than 3000 ohm-cm as determined by Tex-129-E (TxDOT 1999b). Material resistivity between 1500 and 3000 ohm-cm may be used if the chloride content and sulfate content are less than 100 ppm and 200 ppm, respectively, as determined from Tex-620-J (TxDOT 2005).

TxDOT project 0-4177 (Rathje et al. 2006) conducted a study on using crushed concrete and recycled asphalt pavement (RAP) as backfill to ensure long-term integrity of MSE walls. With respect to durability, expansion of compacted crushed concrete was monitored over a period of 70 to 100 days under various detrimental conditions. The expansion of most samples was negligible except for the samples that had suffered Alkali-Silica Reaction (ASR) or sulfate attack. However, there is a concern about drainage property of crushed concrete. The hydraulic conductivity of crushed concrete (CC) ranged from 10^{-4} to 10^{-5} cm/s over confining pressures of 5 to 50 psi while the typical crushed limestone backfill material exhibits 10^{-3} cm/s hydraulic conductivity. The lower hydraulic conductivity for crushed concrete may be due to the re-cementation of CC particles with pore water and reducing the pore size. For the RAP samples, creep

testing was conducted to evaluate durability of the material. The results indicated that the creep potential in RAP is significant, similar to that of clays under undrained conditions. Drainage testing of RAP showed hydraulic conductivities ranging from 0.5×10^{-3} to 4×10^{-3} cm/s over confining pressures of 5 to 50 psi using a triaxial apparatus, exhibiting higher drainage compared to crushed concrete. The study recommended use of crushed concrete as backfill unless the material was crushed from concrete structures that have suffered sulfate attack, along with adequate drains and high permittivity filter fabrics. The California Department of Transportation (CalTrans 2004) specifies the following criteria for MSE walls with extensible soil reinforcement (geosynthetics) as shown in Table 5.

Table 5. Property Requirements for MSE Walls with Extensible Soil Reinforcement (Caltrans 2004).

Test	Requirement	California Test
Sand Equivalent	30 min.	217
Plasticity Index	10 max.	204
Durability Index	35 min.	229
pH	4.5 to 9.0	643

The durability test is conducted to provide a measure of the relative resistance of an aggregate to producing clay sized fines when subjected to prescribed methods of interparticle abrasion in the presence of water in accordance with California Test 229 (CalTrans 2004). As per AASHTO (2002) backfill material should be free of shale or other soft, poor durability particles. Magnesium sulfate soundness should be less than 30 percent after four cycles in accordance with AASHTO T 104 (AASHTO 2007). The

organic content in soil should be less than 1 percent measured as per AASHTO T 267 (AASHTO 2008). It is necessary to use clean gravel with minimum fines and to use wet sieve analysis to avoid misrepresentation of clay clumps as a large size particle. The aggressiveness of backfill material should be identified in terms of electrochemical properties, pH, resistivity, and salt contents. For different types of soils, their aggressive soil environments are shown in Table 6 below.

Table 6. Aggressive Soil Environments (Elias et al. 2009).

Environment	Prevalence	Characteristics
Acid-Sulfate soils	Appalachian Regions	Pyritic,pH<4.5,SO_4 (1000–9000 ppm), Cl^- (200–600 ppm)
Sodic Soils	Western States	pH>9, high in salts including SO_4 and Cl^-
Calcareous Soils	FL, TX, NM, and Western states	High in carbonates, alkaline but pH<8.5, mildly corrosive
Organic Soils	FL(Everglades), GA, NC, MI, WI, MN	Contain organic material in excess of 1% facilitating microbial induced corrosion
Coastal Environments	Eastern, Southern and Western Seaboard States and Utah	Atmospheric salts and salts laden soils in marine environments
Road Deicing Salts	Northern States	Deicing liquid contain salts that can infiltrate into soils
Industrial Fills	Slag, cinders, fly-ash, mine tailings	Either acidic or alkaline and may have high sulfate and chloride content

2.2 Internal Stability Design

The report prepared by WSDOT (Allen et al. 2001) establishes guidelines for a simplified method of analysis for internal stability of MSE walls and a comparison with methods such as the coherent gravity method and FHWA structure stiffness method. The difference in these methods is how the vertical soil stress is calculated. The coherent gravity method assumes that internally the wall acts as a rigid body and an overturning moment is transmitted through the reinforced soil mass. This report uses case histories of instrumented MSE walls from 1972 to 1991 to compare the prediction accuracy of the simplified method to that of the other methods in design codes. The simplified method is based on the determination of coefficient of earth pressure within reinforced soil (K_r) using K_r/K_a vs. depth diagram where K_a is coefficient of active earth pressure and FHWA structure stiffness method equation to evaluate horizontal loads in the reinforcement. The FHWA structure stiffness method and the simplified method do not consider an overturning moment in internal vertical stress computations but do consider it for external bearing stress computation (Allen et al. 2001).

Currently, the simplified method is adopted in AASHTO design specifications for internal stability design. As per AASHTO design specifications, the internal stability of MSE walls is evaluated using a simplified coherent gravity approach. The vertical stress is the result of gravity forces from soil self-weight within and immediately above the reinforced wall backfill and any surcharge loads present. Equations used to calculate vertical stress are stated below. The lateral earth pressure coefficient Kr is determined by

applying a multiplier to the active earth pressure coefficient. The active earth pressure is calculated using the Coulomb method assuming no wall friction.

$$K_a = tan^2\left(45 - \frac{\phi'}{2}\right) \quad \text{(Eq. 1)}$$

$$K_a = \frac{sin^2(\theta + \phi')}{sin^3\theta\left(1 + \frac{sin\phi'}{sin\theta}\right)} \quad \text{(Eq. 2)}$$

$$\sigma_h = \sigma_v K_r + \Delta\sigma_h \quad \text{(Eq. 3)}$$

$$T_{max} = \sigma_h S_v \quad \text{(Eq. 4)}$$

Where

K_a = Coefficient of active earth pressure

ϕ = Angle of internal friction of retaining soil.

θ = Inclination angle of face of wall with vertical.

σ_v = Vertical stress.

σ_h = Horizontal stress.

T_{max} = Maximum horizontal force.

S_v = vertical spacing between reinforcement strips

Eq. 2 can be used only when the wall face is battered. In Eq. 3, $\Delta\sigma_h$ is the horizontal stress at the reinforcement location resulting from a concentrated horizontal load. As per a report prepared by Liang (2004), the locus of maximum tensile forces in the reinforcement defines the critical limiting failure surface, which is affected by both reinforcement spacing and length. Based upon this approach a new method of analyzing

internal stability is developed in this report. The method called Virtual Soil Wedge Analysis has been developed to estimate a reinforcement spacing and length. In this method, required parameters are angle of internal friction of back fill material, unit weight of backfill, vertical reinforcement spacing, and coverage ratio. The horizontal earth pressure distribution along the vertical axis is related to the unit weight of the soil, overburden height and a factor that corresponds to the effect of the lateral confinement, and embracement that restrains or prevents the lateral soil movements at the point of consideration. The lateral earth pressure is expressed as:

$$\sigma_h = \gamma h I_c \qquad \text{(Eq. 5)}$$

Where I_c is the embracement factor, which is different from the lateral earth pressure coefficients, h is the height of the wall and γ is the unit weight of soil. In this Eq.5 the embracement factor is related to the slope of the virtual soil wedge and reinforcement layout. This report concludes that the required length of reinforcement is controlled by the internal stability requirements rather than the external stability. This results in significant savings in materials and construction of reinforced earth walls.

As per TxDOT geotechnical manual (TxDOT 2012), the internal stability design is performed by MSE wall suppliers. Reinforcement loads calculated for internal stability design are dependent on the extensibility and material type of reinforcement. The vertical stress for internal stability analysis are calculated as shown in Figure 6 for live load and dead loads. Modes for internal stability failures includes, soil reinforcement rupture, soil reinforcement pullout, internal sliding, failure at face connection, and bulging of face connections (Holtz and Lee 2002). The load in the

reinforcement is determined at two critical locations, i.e., at the zone of maximum stress and at the connection with the wall face, to assess the internal stability of the wall system. It is important for the engineer in charge to evaluate calculations provided by wall supplier as they can be useful for calculating external stability of the system.

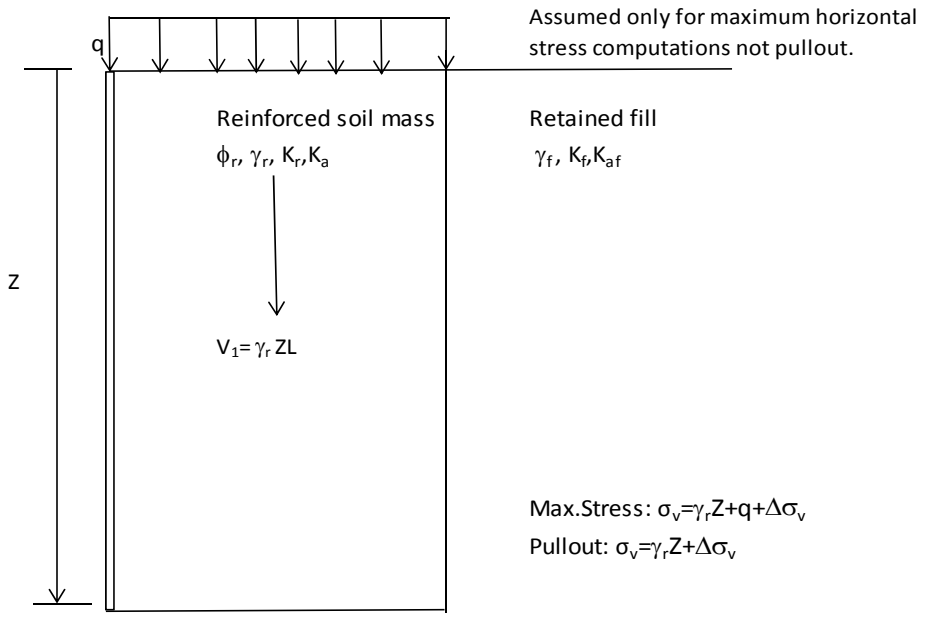

Figure 6. Calculation of Vertical Stress for Horizontal Back Slope Condition, including Live Load and Dead Load Surcharges for Internal Stability Design (AASHTO 2002).

2.3 Minimum Reinforcement Length

FHWA and AASHTO require minimum length of 0.7H or 8 ft in the public transportation sectors. The NCMA design manual (NCMA 2002) specifies a minimum length of 0.6H, which has been widely used in the private sectors. Nowadays, the 0.7H or 8 ft criterion has been used worldwide based on investigation of simple wall

geometries and external stability analyses. However, the 0.7H or 8 ft criterion needs further rational analysis or statistical data.

From this perspective, the opinion from a recognized world expert in MSE walls, Dr. Dov Leshchinsky, on the 0.7H or 8 ft criterion is reported below (personal communication with Dr.Leshchinsky, 2011)

> *The original FHWA specification on the 0.7H rule was a simple adoption of what has been used by Victor Elias, a pioneer of MSE walls in the US and one of the authors of a few FHWA publications on MSE walls. In the '70s–'80s, the MSE wall designs were implemented in a trial-and-error approach by hand. Considering a backfill of friction angle of 30°, in most instances a metallic strip length of 0.7H would satisfy the stability. Victor Elias personally specified 0.7H for two purposes: 1) it is a good starting point for trial-and-error analysis; and 2) it is a check to warn him a possible error if the length is significantly longer or shorter than 0.7H.*

Even though the adoption of 0.7H initially seemed unreasonable, a number of studies have shown that the minimum reinforcement length criterion is sometimes conservative and it is effective to ensure the serviceability of constructed MSE walls. Ling and Leshchinsky (2003) and Ling et al. (2005) showed that the deformations increase when reinforcement length decreases. Apart from that, Ling and Leshchinsky (2003) also stated that the spacing of reinforcement affects the distribution of maximum reinforcement force along the wall height. Chew et al. (1991) reported that decreasing reinforcement length from 0.7H to 0.5H resulted in an approximate 50 percent increase

in MSE wall deformations. Therefore, the minimum length, though lacking of solid basis, has been kept in the FHWA guidelines. Admittedly, a minimum reinforcement length to ensure serviceability is influenced by a number of factors such as the quality of backfill, compaction, wall facing unit, and reinforcement. A minimum length of 0.3H and 0.45H has been successfully used in Japan by considering the backfill quality and construction procedure that had a shoring wall in front of the structure to remove any external horizontal loads applying to the reinforced section (Morrison et al. 2006).

The specification of a minimum length of 8 ft for reinforcement is based largely on considerations for constructability rather than stability. Within a 3 ft zone near the back of the MSE wall facing, light weight compaction equipment is used to avoid exerting excessive pressure on the facing. The width of a typical roller is about 5 ft. To prevent a roller stepping within 3 ft of the facing, 8 ft is about the minimum acceptable length of the reinforced zone.

The TxDOT geotechnical manual sets minimum earth reinforcement to 8 ft or 0.7H as to ensure proper performance of the wall in place. Furthermore, a reinforcement length should be evaluated for project-specific requirements based on wall backfill type, wall embedment, wall drainage, and any conflicts within the reinforced zone of the wall. Special consideration should be given to walls that are subject to inundation. Type B backfill is the default backfill for permanent walls, but Type D backfill must be specified for walls that are subject to inundation. Walls to be placed in front of bridge abutments should have a 1.5 ft minimum and 3 ft desirable clearance from the back of the wall panels to the face of the abutment cap to facilitate wall construction. Standard

specification Item 423 governs the design and construction of this wall type (TxDOT 2004).

2.4 External Stability

The FHWA guidelines for external stability analysis are adopted from guidelines for rigid retaining walls such as gravity walls and cantilever walls. The adopted external stability analysis was from the FHWA research project titled "Mechanically Stabilized Earth Walls and Reinforced Soil Slopes Design and Construction Guidelines" (FHWA 2001). Overall, sliding and overturning have demonstrated consistency between design and performance. However, disagreement exists on the method used for the bearing capacity analysis. Apart from this, design of MSE wall for external stability should ensure that there will be adequate FOS as specified in standards. A proper understanding of the system of forces and the distribution of vertical stress within the reinforced soil mass is important for evaluation of external stability (Liang 2004). External stability design for MSE walls should include analyses for base sliding failure between wall and foundation soil, bearing capacity failure and for overall slope stability (Holtz and Lee 2002).

2.5 Bearing Capacity

Bearing capacity theory was derived by (Terzaghi 1943) based on Prandtl's theory (1920) for plastic failure of metal under rigid punches. For a rigid footing, punching failure occurs when there is compression of the soil under the footing,

accompanied by shear in the vertical direction at the edge of the footing as shown in Figure 7. There is no heave at the edge of the footing, but heave may occur at a certain distance from the edge of the footing. Relatively large settlement is a characteristic of the ultimate bearing capacity failure. Terzaghi proposed the equation below to calculate the ultimate bearing capacity:

$$q_u = cN_c + \gamma D_f N_q + \frac{1}{2}\gamma BN\gamma \qquad \text{(Eq. 6)}$$

However, the usage of the Terzaghi's bearing capacity equation for MSE wall has been in dispute. As described above, the classic Terzaghi's equation was derived based on punching rigid metal, but the MSE wall backfill mass, though reinforced, is still relatively flexible. Using Eq. 6 to calculate bearing capacity yields a conservative result. Another argument against the application of the equation for bearing capacity is that the bearing capacity failure mode is not realistic at all, especially when there is a slope adjacent to the toe of the MSE wall (Leshchinsky 2006).

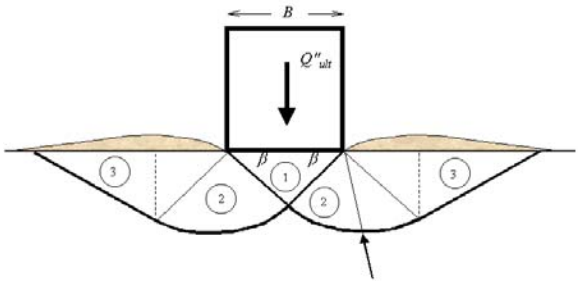

Figure 7. Ultimate Bearing Capacity of Rigid Footing.

At the elevation of leveling pads, only one side is surcharged by backfill materials, thus the surcharge term on the bearing capacity equation is completely ignored in current practice as shown in Figure 8(a). To increase the bearing capacity, the reinforcement length has to increase to give a larger term of ½γBNγ. The increase of the reinforcement length becomes crucial, even when the foundation soil is cohesionless. There is a motivation for at least partially considering the surcharge provided by the backfill materials as shown by Figure 8(b). It has been argued that a bearing capacity failure may lead to rotation about the toe of the MSE wall and separation between reinforced zone and retained zone. However, the MSE wall backfills are loose materials and a distinct separation is unlikely to occur. In recent years, there has been a tendency to unify bearing capacity analysis and global stability analysis. An insufficient bearing capacity for MSE wall will not simply induce punching failure, since there is always lateral force. As a result, the MSE wall movement will dominantly be rotation.

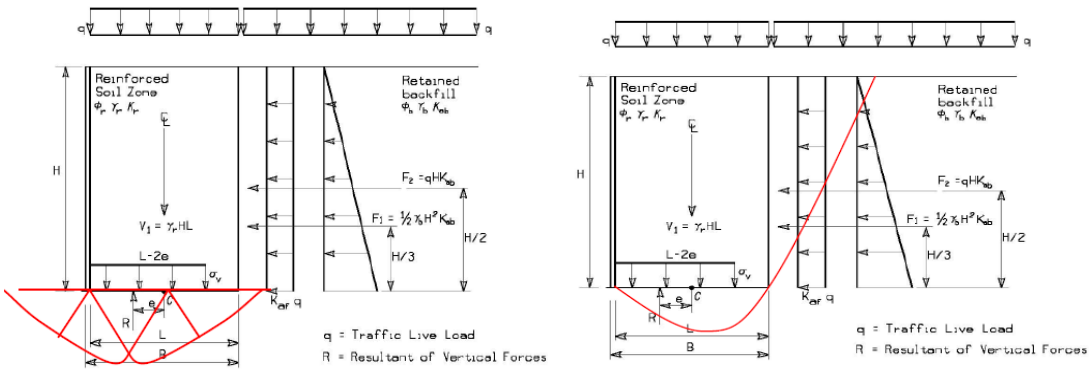

Figure 8. Bearing Capacity of Retaining Walls: (a) Assumed Bearing Failure Zone of Current Practice and (b) Possible Failure Zone.

2.6 Sliding and Overturning

Analysis for the potential for sliding and overturning of rigid wall has been well calibrated by practice. Strictly speaking, sliding analysis based on limit equilibrium is the only analysis that completely satisfies equilibrium (Leshchinsky and Han 2004). Thus, there is almost no dispute on the methods used for checking sliding and overturning. However, researchers and practitioners are concerned about the reliability of calculated FOS for MSE wall against sliding and overturning. A study completed by Chalermyanont and Benson (2005) indicated that the spatial variability of the backfill properties could influence the calculated FOS significantly. For instance, if the target FOS against sliding and overturning are 1.2 and 1.1, respectively, the material spatial variation along the wall may lead to about 2 percent and 0.4 percent probability of failure (i.e., FOS <1) even without considering uncertainties in FOS calculations. The spatial variation of the properties of backfill materials can influence the results for different reasons, such as non-uniform compaction, construction sequence, and reinforcement. The spatial variation is almost inevitable even when a strict QA/QC procedure is adopted. However, this variability is not considered when calculating the FOS for a rigid retaining wall. Duncan (2000) recommended using reliability analysis as a complement to FOS analysis, but it is often deemed too complicated to be practical. TxDOT has adopted the FOSs listed in Table 7, which are also specified by AASHTO (2002) and NCMA. In the table, the FOSs recommended by other agencies were listed for comparison. No consideration of the spatial variation has been included, which

results in higher probability of failure than for rigid retaining wall designed with the same FOS.

Table 7. Summary of Factor of Safety Used in MSE Design Check.

Failure Mode	TxDOT	WisDOT (WisDOT 2006)	Caltrans (CalTrans 2004)
Sliding	FOS ≥ 1.5	1.5 for spread footings on soil or rock and 1.0 for pile footings	1.5
Overturning	FOS ≥ 2.0	1.5 for footings on piles or rock 2.0 for footings on soil	1.5
Bearing capacity	1.3 (Global)	1.3 (Global)	3.0
Eccentricity, e	e < L/6 (middle third)	n/a	e < L/6 for wall footing on soil e < L/4 for wall footing on rock
Pullout	FOS ≥ 1.5	1.5	1.5

3. LABORATORY TEST ON BACKFILL MATERIALS

The laboratory test performed on backfill materials were on the request of TxDOT to quantify the engineering properties of locally available backfill materials. The main purpose of this laboratory testing was to compare the final results in terms of angle of internal friction with AASHTO, 2002 recommended values for backfill materials. The AASHTO, 2002 design guidelines suggests to use 34^0 as an angle of internal friction for backfill materials and currently TxDOT has adopted same recommendations. This section explains the steps followed to test the backfill material from procuring from borrow pit to large scale triaxial testing. The materials tested in this research were provided by TxDOT from their approved borrow pits within Texas. The material obtained was processed and classified according to TxDOT specifications (TxDOT 2004) the first subsection explains the material classification process and then sample preparation and followed by testing procedure for large scale triaxial test. The following few parts of this section are also a part of a Master's thesis on Large Scale Triaxial testing of MSE backfill materials by Mackenzie Garton (Garton 2013). The details test results and data interpretation from test results are presented in that Master's Thesis. The consolidated undrained testing part in this section was performed by an author of this research.

3.1 Material Classification

As per TxDOT specifications, there are four different types of backfill material namely, Type A, Type B, Type C, and Type D. The specification for these types of backfill is given below in Table 8. The backfill materials were obtained from TxDOT specified borrow sites. The Type A and D backfills were obtained in Waco, Texas, Type B was obtained in Bryan, Texas, and Type C was obtained in Beaumont, Texas. A total of 72 6in diameter consolidated drained triaxial compression tests were conducted according to ASTM D7181 (ASTM 2011a) on Types A, B, and D MSE wall backfill materials. A total of 24 2in consolidated undrained tests were performed according to ASTM D4767 (ASTM 2011b) on Type C backfill material.

Table 8. Select Backfill Gradation Limits (TxDOT 2004).

Type	Sieve Size	Percent Retained
A	3 in.	0
	1/2 in.	50-100
	No. 4	See Note
	No. 40	85-100
B	3 in.	0
	No. 4	See Note
	No. 40	40-100
	No. 200	85-100
C	3 in.	0
	No. 4	See Note
	No. 200	85-100
D	3 in.	0
	3/8 in.	85-100

Note: Backfill is considered rock backfill only if 85% or more material is retained on the No. 4 sieve

As the specifications allow a range of gradations for each type of material, it was necessary to test over that range to determine the boundary limits of the behavior associated with each type of material. Four different gradations were tested for each type of material as listed in Table 9. Additionally, three different confining stresses were used as confining stress increases with depth in MSE walls. These confining stresses were found by assuming a backfill unit weight of 125 pcf and assuming a coefficient of lateral earth pressure at rest of 0.5. Wall heights of 10, 15, and 20 ft resulted in confining stresses of 4.3, 6.5, and 8.7 psi, respectively.

Table 9. Tested Backfill Gradations.

Type	Particle Size -mm (Sieve Size)	% Passing			
		A1	**A2**	**A3**	**A4**
A	75 (3")	100	100	100	100
	12.5 (1/2")	0	16.67	33.33	45.00
	4.75 (#4)	0	10.00	20.00	30.00
	0.425 (#40)	0	5.00	10.00	15.00
	0.075 (#200)	0	3.33	6.67	10.00
B		**B1**	**B2**	**B3**	**B4**
	75 (3")	100	100	100	100
	12.5 (1/2")	35	45	60	75
	4.75 (#4)	15	25	45	60
	0.425 (#40)	0	6	10	30
	0.075 (#200)	0	4	6	15
C		**C1**	**C2**	**C3**	**C4**
	4.75 (#4)	100	100	100	100
	2 (#10)	50	60	70	80
	0.85 (#20)	35	45	55	65
	0.425 (#40)	25	35	45	55
	0.075 (#200)	0	10	20	30
D		**D1**	**D2**	**D3**	**D4**
	75 (3")	100	100	100	100
	12.5 (1/2")	0	5.00	10.00	15.00
	4.75 (#4)	0	3.33	6.67	10.00
	0.425 (#40)	0	3.33	6.67	10.00
	0.075 (#200)	0	3.33	6.67	10.00

Sieve analysis was performed according to ASTM D422 (ASTM 2007) on backfill material to classify the received backfill material in its field conditions, as well as to anticipate the need for additional material. The borrow gradation curve in comparison to the TxDOT specification limits is shown for Type A material in Figure 9, Type B in Figure 10, Type C in Figure 11 and Type D in Figure 12. For Types B and D, actual gradations were outside of the TxDOT specifications; however as each material was sieved into separate particles size ranges and remixed at desired percentages this meant additional material was required to have adequate quantities of each particle size for testing. Type C gradation limits were estimated due to the ambiguity in the backfill specifications of having a minimum of 85 percent retained on the No. 4 sieve, while 70 percent can be retained on the No. 200 sieve.

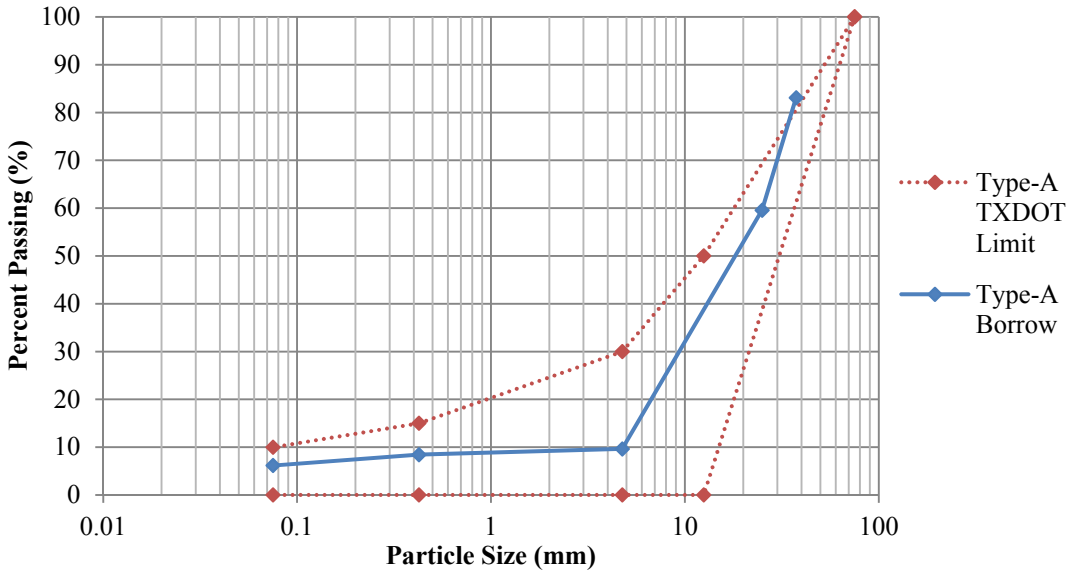

Figure 9. Type A Borrow Gradation.

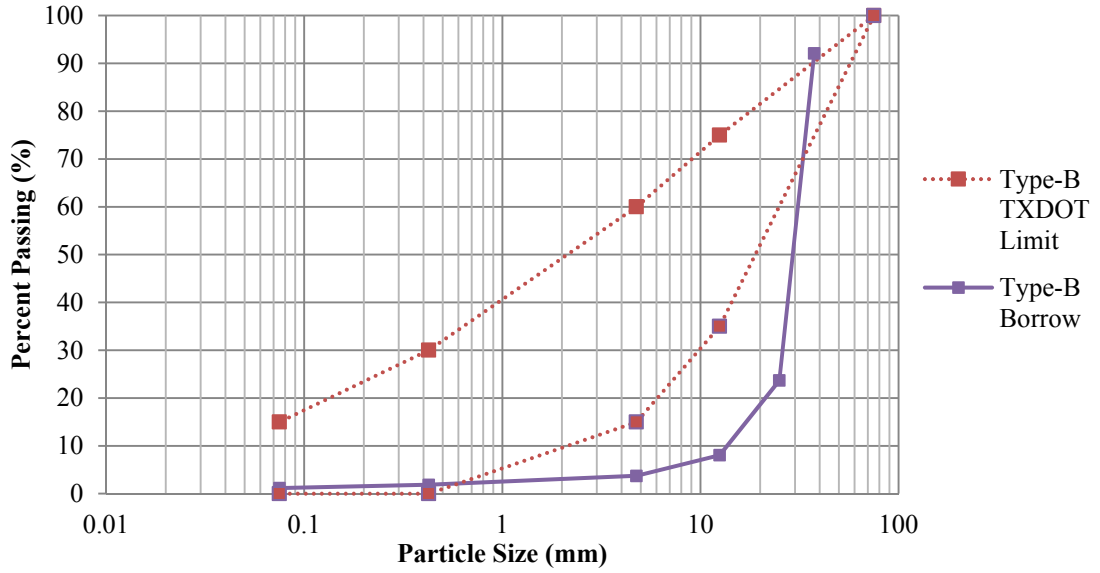

Figure 10. Type B Borrow Gradation.

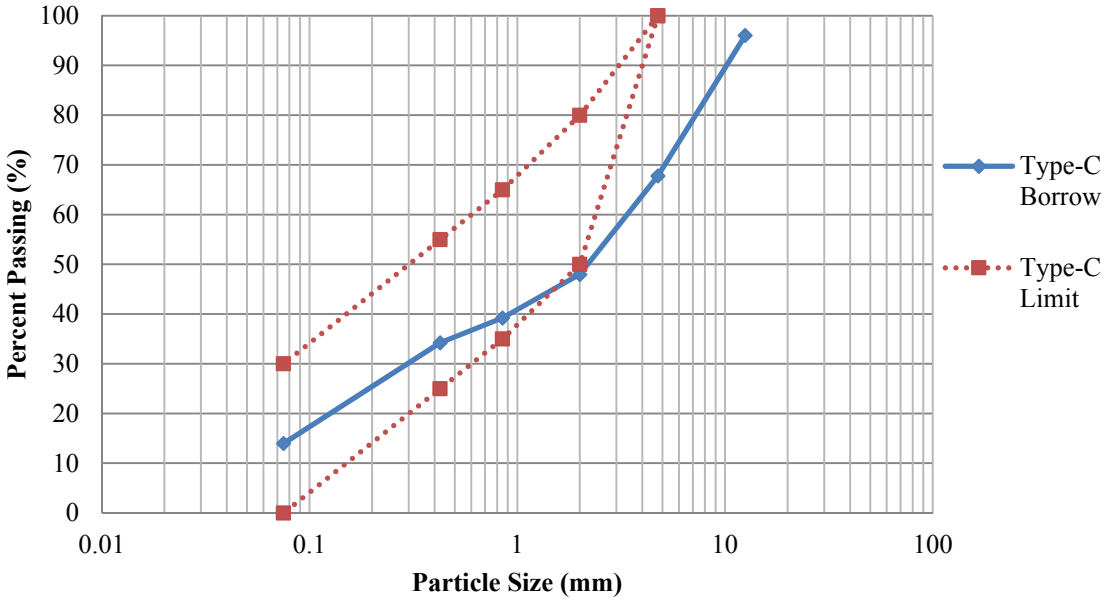

Figure 11. Type C Borrow Gradation.

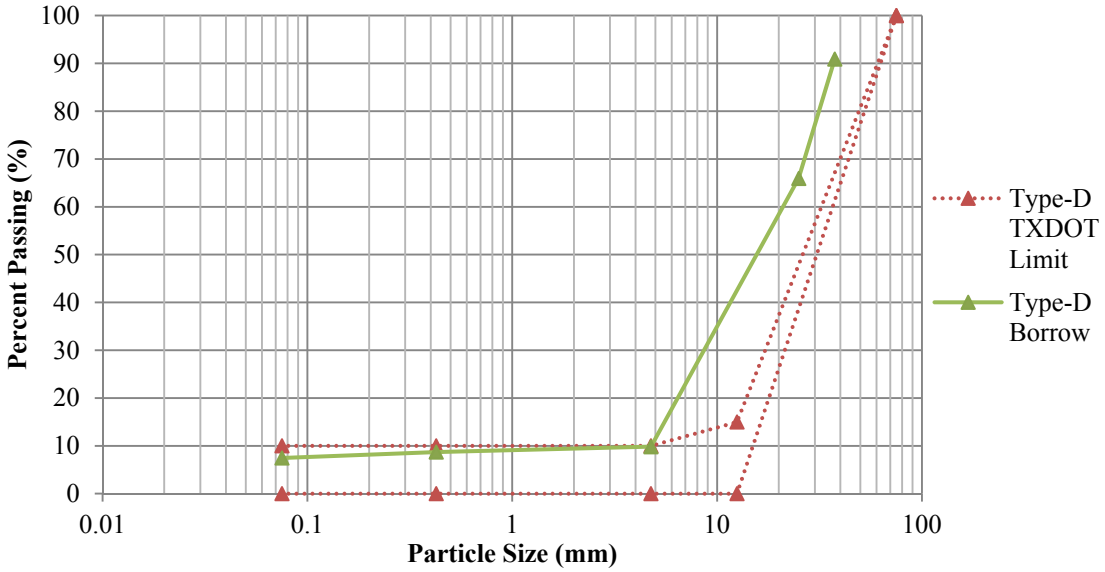

Figure 12. Type D Borrow Gradation.

Due to differences in the parent rock of the borrow material, bulk specific gravity testing was performed according to ASTM C29 (ASTM 2009) on the 1in particles of each material. Table 10 summarizes the results of this testing. All three backfill materials are limestone, however, Type B limestone seemed to be a more dense material than Types A and D. The specific gravity test for Type C was performed according to ASTM D854 (ASTM 2010) on each particle size used in Type C and then weight average for different gradation used. The results for Type C are presented in Table 11.

Table 10. Specific Gravity Test Results.

Type	Bulk Specific Gravity	Bulk Saturated Surface Dry Specific Gravity	Apparent Specific Gravity
A	2.20	2.35	2.60
B	2.52	2.56	2.64
D	2.31	2.46	2.71

Table 11. Specific Gravity Test Results for Type C.

Gradation	Specific Gravity
C1	2.647
C2	2.654
C3	2.661
C4	2.669

Fines were classified using the Atterberg Limits tests to determine plasticity. Test results in Table 12 show that all of the fines used were relatively low plasticity.

Table 12. Atterberg Limits of Passing the #200 Sieve

Type	LL	PL	PI	Fines Classification
A	18	13.4	4.6	CL-ML
B	-	Non-Plastic	-	ML
C	24.6	14.1	10.5	CL
D	20.2	11.5	8.7	CL

Maximum density testing was performed on large particulate backfill (Types A, B, and D) by compacting a sample with blows from a modified proctor hammer in a 1/3 cubic foot unit weight mold. The unit weight bucket had a diameter of 8in and a height of 11.5in, which allowed more particle organization, while simulating the test specimen compacted inside the split mold. Initial tests were performed to determine the optimum number of layers and blows per layers, which were 5 layers at 50 blows per layer. Results of maximum density testing are shown below in Table 13. Standard Proctor compaction was performed on Type C materials at different gradation to find optimum moisture content and maximum dry density, test data are shown below in Table 13.

Table 13. Maximum Density Test Results.

Gradation	Dry Unit Weight (pcf)	Gradation	Dry Unit Weight (pcf)	Gradation	Dry Unit Weight (pcf)	Gradation	Optimum MC (%)	Maximum Dry Unit Weight (pcf)
A1	94.65	B1	98	D1	93.45	C1	7.2	120.6
A2	99.7	B2	113.4	D2	98	C2	8.9	129.4
A3	99.1	B3	122.7	D3	98.1	C3	9.7	128.4
A4	109.8	B4	137.9	D4	98.3	C4	9.5	126.3

3.2 Sample Preparation

Samples were prepared for testing in three major steps: mixing, compacting, and mounting. The first step was to mix the proper gradation of soil according to specifications listed above in Table 8. Prior to testing, particles had been wet sieved into

five particle size ranges as shown in Figure 13. All particles except those passing the #200 sieve were oven dried in order to control the moisture content of the sample.

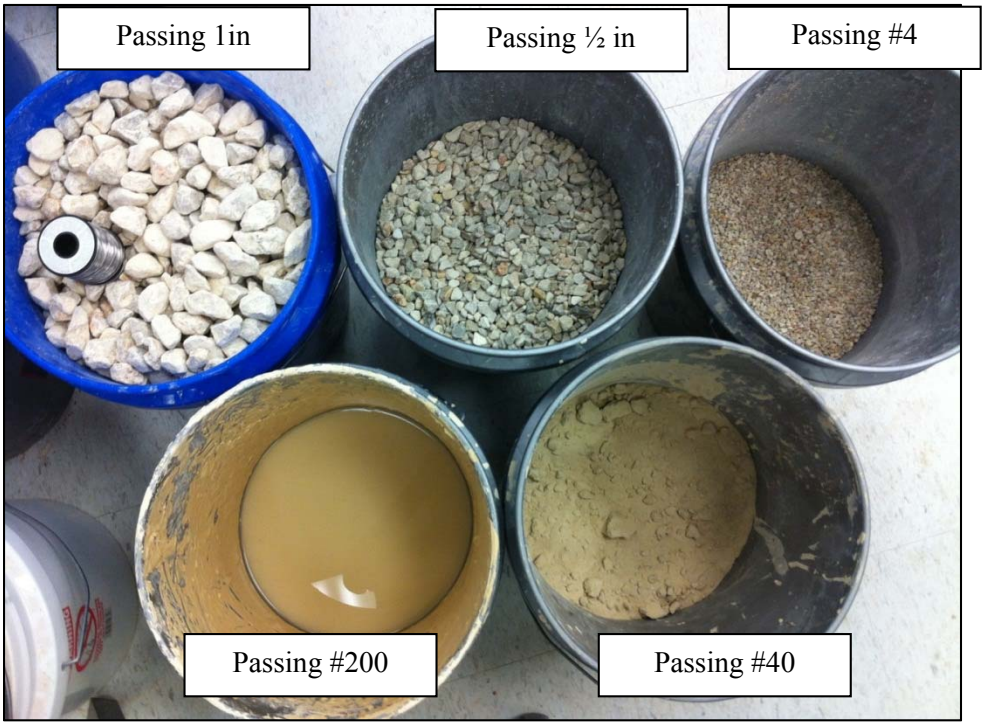

Figure 13. Sorted Particle Sizes of Type B Material.

Samples weights were estimated using values slightly above maximum dry unit weights and assuming a sample height of 12in with diameter of 6in. Individual particle sizes were weighed and added to the mix. The moisture content was taken on the passing #200 material, thus allowing for the correct amount of solids to be added and the moisture content of the total sample to be calculated. To avoid particle segregation as much as possible, judgment was used in determining total sample moisture contents and water was added if deemed necessary, in order for particles to clump together. Typically,

more well-graded samples required more water. Samples were then thoroughly mixed for even distribution of particles as shown in Figure 14.

Figure 14. Sample Mixing of Passing #200 for Type D Material.

The next step was to compact the specimen inside a 6in diameter split mold on the base of the triaxial chamber to avoid difficult maneuvers required to mount the 20 plus pound specimen. A 0.025in latex membrane was attached to the bottom cap using a rubber O-ring and stretched over the top of the split mold. Vacuum was applied to the exterior of the split mold to pull the membrane tight to avoid pinching. A porous stone and filter paper were then placed at the bottom of the mold. Wet paper towel was placed

around the O-ring of the chamber base to prevent granular material from falling into the seal.

Material was poured in one 400 mL scoop per layer. Each layer was then heavily tamped using a rubber mallet. Six 4.45-lb lab weights were then placed on top of the material and 50 blows of the rubber mallet were evenly distributed around the outside of the split mold as shown in Figure 15. This was repeated for a total of about 8 layers, until the level of backfill reached approximately 12in in height.

Figure 15. Compaction of Specimen.

Particles at the top of the cylinder were then arranged to provide as level of a surface as possible. Filter paper, a porous stone, and top cap were then placed on top of

the specimen and the latex membrane was fastened to the top cap using a rubber O-ring. A regulated partial vacuum of 1.5 psi was then applied through a drain line at the bottom of the sample to help confine the sample. The split mold was released, and the initial sample height was recorded.

Due to the high occurrence of membrane rupture during compaction, an additional 0.025in membrane was checked for leaks and then placed around the sample. The interior was lubricated with petroleum jelly and the ends were fastened with O-rings to provide a water tight seal. The sample was then leveled to provide complete axial loading from the piston as shown in Figure 16. Drain lines were then connected to the top of the sample and vacuum was moved from the bottom to the top of the sample.

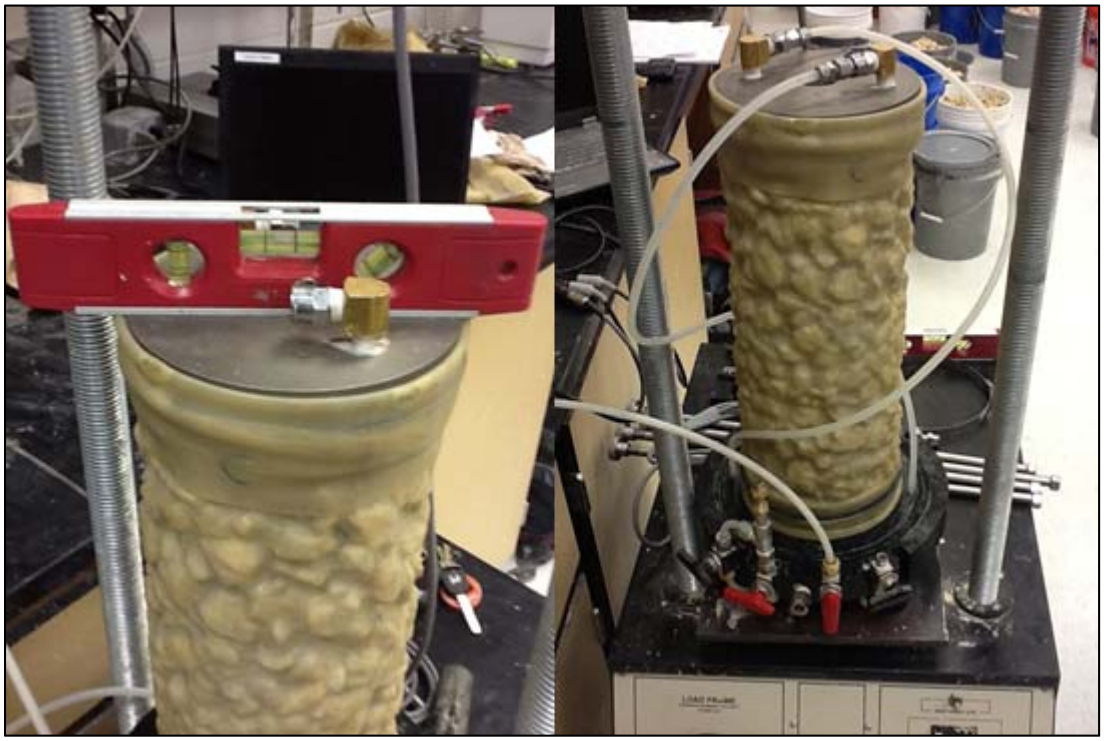

Figure 16. Leveling Top Cap of Specimen and Final Prepared Specimen.

The acrylic chamber and piston were then placed on top of the base and fastened with threaded metal bars to seal the chamber. The piston was set and locked in its designated indention on the top cap of the specimen.

The chamber was then filled from the bottom with water and vented at the top to avoid excess pressure build up and to expel air out of the top of the chamber. Once air bubbles were removed, a pressure transducer was placed in the top port and the bottom port was connected to the pressure panel, where an initial confining stress of 0.5 psi was placed on the sample to confine the sample during saturation. Between the confining stress and the vacuum, the sample received a net confinement of 2.0 psi prior to consolidation and shearing.

3.3 Large Scale Triaxial Testing Apparatus

A large scale triaxial testing system was developed in April 2012 to conduct consolidated drained triaxial compression testing on MSE wall backfill material. The system, shown in Figure 17, consisted of a triaxial chamber manufactured to our specifications by Trautwein Soil Testing Equipment.

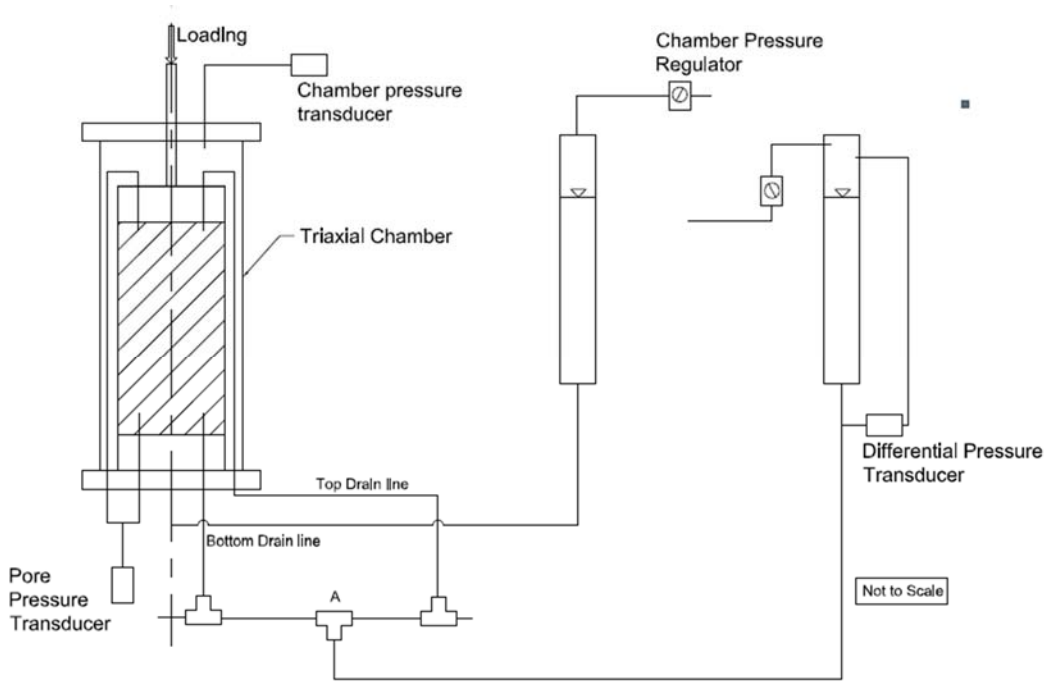

Figure 17. Large Diameter Triaxial Schematic.

Following ASTM D7181 Standard Test Method for Consolidated Drained Triaxial Compression Test for Soils (ASTM 2011a), which states the diameter of sample must be at least 6 times larger than the maximum particle size; a maximum of 1in particle was tested in the device. A height to diameter ratio of 2 was used to minimize the effect of end friction, resulting in samples approximately 12 in tall. Samples were tested at full saturation and water was used as the confining medium.

The chamber was fitted with a 1in linear ball bearing piston at the top for applying axial loading. While the chamber cap contains a port for measuring applied confining pressures, the chamber base is fitted with a port for applying confining pressures and four 1/4in drain lines, which connect to the exterior of the chamber with

one way exterior ball valves, in order to provide adequate drainage to the top and bottom of the sample. Pore pressure measurements are taken by a pressure transducer located between the top and bottom drain line ports on one side of the sample. Attached to the remaining drain line ports is a series of two-way valves connecting the sample to the back pressure system, which allows air to be flushed from the system during initial sample saturation. Figure 18 shows a picture of the actual test chamber. In the interior of the chamber, 6in diameter top and bottom caps connect the drain lines to the sample. The caps contain a small groove to allow even distribution of flow between sides of the sample. Thick sintered brass porous stones, 1/8in in size, were placed on the top and bottom of the sample along with filter paper to allow for adequate drainage while attempting to slow down the migration of soil particles into the drainage lines.

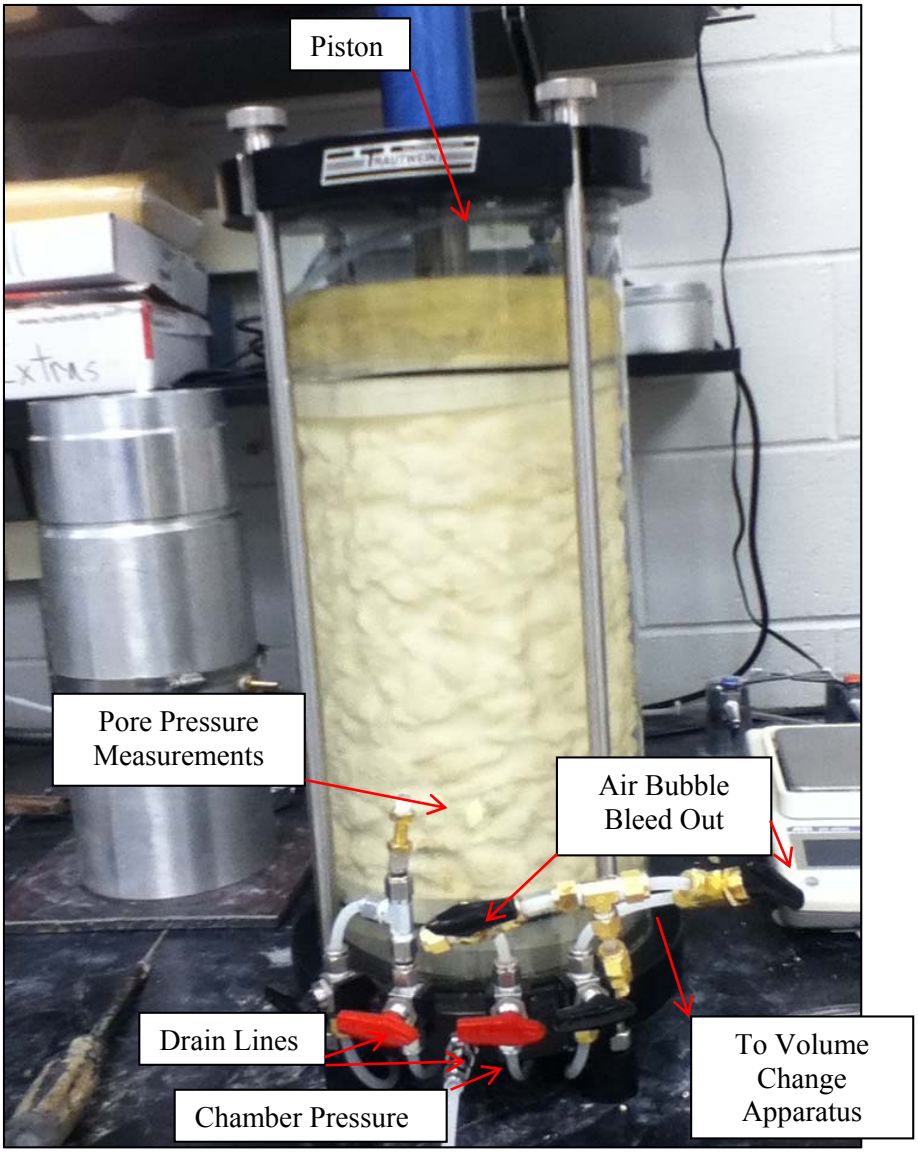

Figure 18. Large Scale Triaxial Chamber.

A Trautwein pressure panel, shown in Figure 19 with an accuracy of 0.1 psi was used to regulate back pressure and confining pressure. While the panel connected directly into the chamber to provide confining pressures, it did not have enough capacity to measure continuous volume change. Due to time constraints, early tests were

performed taking manual volume change measurements until a volume change apparatus was developed using a ¾ in transparent PVC pipe with back pressure applied to the top of the water column. The device was connected at the bottom by a tube to the sample drain lines, as seen in Figure 19. A differential pressure transducer was plumbed in between the top and the bottom of the clear PVC pipe, which recorded the change in differential pressure due to the height of the water column and could thus be calibrated to produce volume change within the known diameter pipe

Figure 19. Trautwein Pressure Panel (Left) and Volume Change Device (Right) Used in Testing.

An Omega LC101-3k load cell, PX602-100 pressure transducers, and PX409-2.5 differential pressure transducer were used to record force, pressure, and volume change characteristics. The displacement rate was set on the load frame to be 1.5 mm/min or a strain rate of 0.005/min. Data were acquired using a National Instruments (NI) Hi-Speed USB Carrier data acquisition box (NI USB 9162) with 24-bit full bridge analog input and an additional with 10 volt external power supply. Data were processed using NI's LabVIEW program to record time and millivolt readings of the sensors. Figure 20 shows a screenshot of the basic program.

Figure 20. Data Acquisition Program.

3.4 Testing Procedure

The sample must be saturated in order to measure volumetric changes in the sample during shearing. Deaired water was introduced into the bottom of the specimen from a pressurized water tank and pulled upward with the help of the vacuum at the top until water began to run into the vacuum line. At this point, the vacuum was removed and the sample drain lines were connected to the volume change apparatus, which was filled to the top with water. Even with the filter paper as a barrier against fines migration, some fines still escaped the sample. Water was allowed to run through the sample and drain lines, in order to drive air bubbles out of the specimen. At this time, the second pressure transducer was connected between the drain lines on the left side of the chamber. Once satisfactory air bubble removal had occurred, the chamber pressure and back pressure inside the sample were slowly raised above atmospheric pressure to allow for the dissolution of any air left in the sample. This process known as back pressure saturation was allowed to occur for a minimum of 30 minutes, before a B-value check was performed to verify saturation. During the B-value check, drain lines to the sample were closed and initial confining and pore pressure readings were taken. The confining pressure was increased by 0.5 psi, and the pore pressure response was record. The B-value is equal to the change in pore pressure over the change in confining pressure and theoretically should equal 1 at 100 percent saturation. As reaching this goal could take multiple days, it was decided that a B-value of at least 0.9 was reasonable to continue testing due to the scale of the test and the stiffness of the specimen.

Once the desired saturation was reached, the sample was isotropically consolidated at the desired confining pressure of the test. Volume change of the specimen was recorded to find the initial volume of the specimen for volumetric strain calculations and to monitor the end of consolidation. Typically, this happened within minutes due to the high porosity and stiffness of the sample. This also served as a good indicator of membrane leakage if volume change did not stabilize.

Following consolidation, the piston was unlocked and the sample was sheared at a constant strain rate of 0.5 percent/min. Ideally, samples were sheared to 15 percent strain, however in Type B materials the radial deformation of the sample exceeded the interior chamber diameter prior to 15 percent strain.

3.5 Consolidated Undrained Triaxial Testing

Type C material obtained from Beaumont, Texas, was classified as gravely- sand and as per TxDOT specification this material can be used as backfill for temporary MSE walls. It is important to know an undrained strength and effective friction angle of these materials and to assess the effect of pore pressure on the strength of material. Therefore a consolidated undrained (CU) triaxial test was performed as per ASTM 4767 to obtain these parameters.

3.5.1 Sample Preparation

The material obtained for Type C was sieved and separated in required particle size and then mixed to appropriate proportions to meet the tested backfill gradation criteria. For each gradation a standard proctor compaction test ASTM 698 (ASTM 2012)

was performed to find the optimum moisture content and max dry density. Using this optimum water content a sample is prepared in a 2in split mold by taking required weight of sample to compact as much as can in a 14.9 in^3 volume of sample as shown in Figure 21. The relative compaction for samples was greater than 95 percent. The sample is then placed on a bottom cap of triaxial chamber and then a latex membrane is placed around the sample as shown in Figure 22.

Figure 21. Sample Placed on the Bottom Cap of Triaxial Chamber.

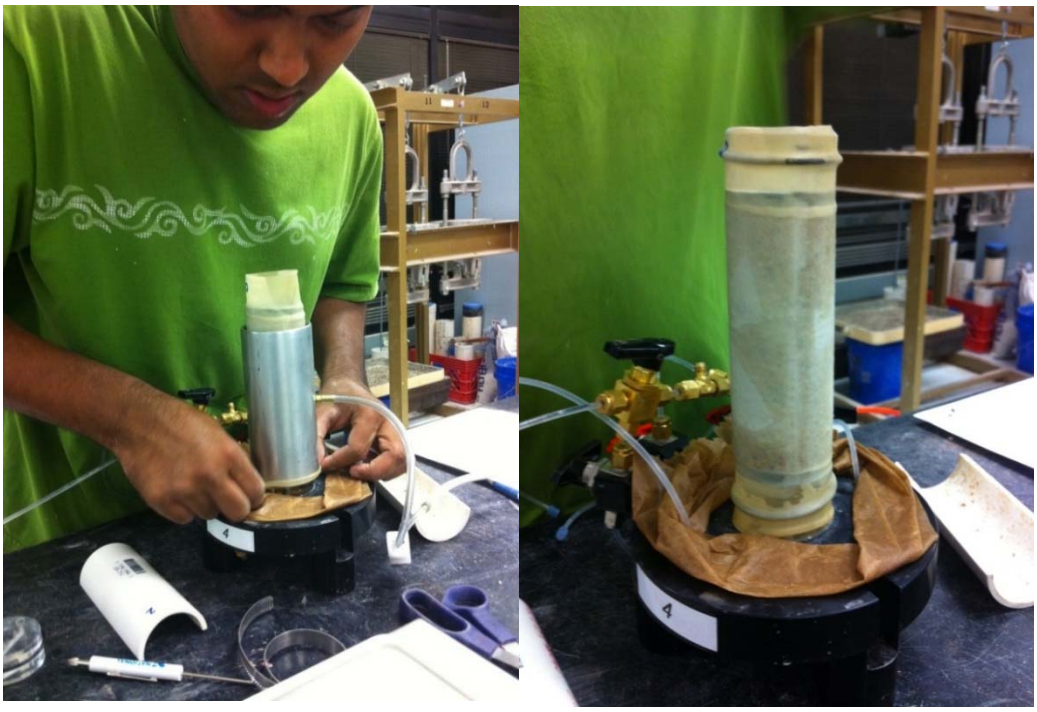

Figure 22. Stretching Membrane on Spreader and Placing Membrane on Sample.

3.5.2 Testing Procedure

The testing procedure for CU test is followed as per ASTM-4767. The procedure is similar to the one explained for CD test, except during the shearing phase drain lines are closed so that the pore pressure will develop during the test. The correction applied during calculations is different than one applied for large scale CD test. The corrections were used from ASTM-4767. The consolidated undrained test has three important steps to follow: (1) saturation, (2) consolidation, and (3) undrained shearing.

During saturation stage, the sample is connected to a panel to allow water to pass through, the chamber pressure port is connected to a panel, and a small pressure differential is applied between confining pressure and back pressure. The pore pressure

line from the top cap is opened to atmosphere so the air bubbles can escape out easily. After all the bubbles from system are removed, the cell pressure and back pressure is increased slowly to 16.00 psi and 15.50 psi, respectively; this way the effective confining pressure to the sample is 0.50 psi. The sample is left 6–8 hours for saturation and then a B-value check is performed. Once the B-value is reached to a desired value, sample is then consolidated to required effective confining pressure.

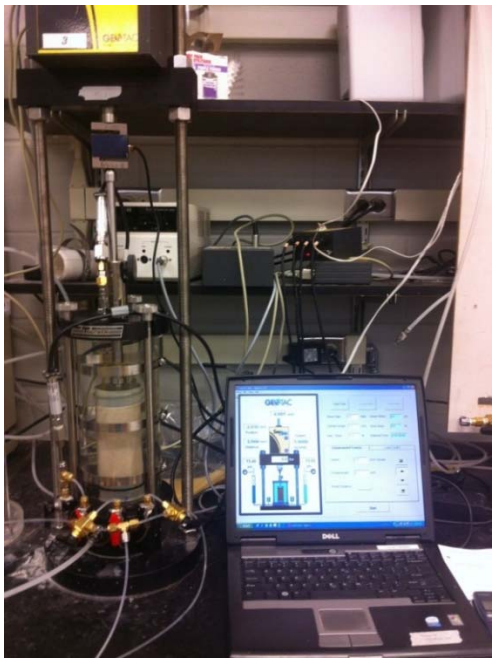

Figure 23. Geotac Loading Frame and Geotac Sigma-CU Program Used to Perform Triaxial CU Test.

The consolidation stage is lasts for 4–5 hours to confirm that the sample is gone through a primary consolidation phase. During this stage, a volume of water leaving the sample is recorded using differential transducer. The load frame used for this test is servo controlled and maintains a constant load on the sample to compensate the piston

uplift due to a confining pressure. The Geotec load frame shown in Figure 23 also allows us to record the displacement of piston while maintaining the constant load. These measurements are essential in calculating consolidated area of sample. All the calculations are performed per ASTM-4767 for the CU test (ASTM 2011b). The shearing stage is performed after the consolidation stage. The rate of shearing used for these tests was 5 percent axial stain per hour and sample was sheared to 20 percent axial strain. The sample usually failed at 4–6 percent axial strain. During shearing, the pore pressure ports connecting to panel were closed to ensure there was no drainage. Figure 24 shows the CU-program used to record parameters during the test, i.e., axial load, axial displacement, pore pressure, and cell pressure.

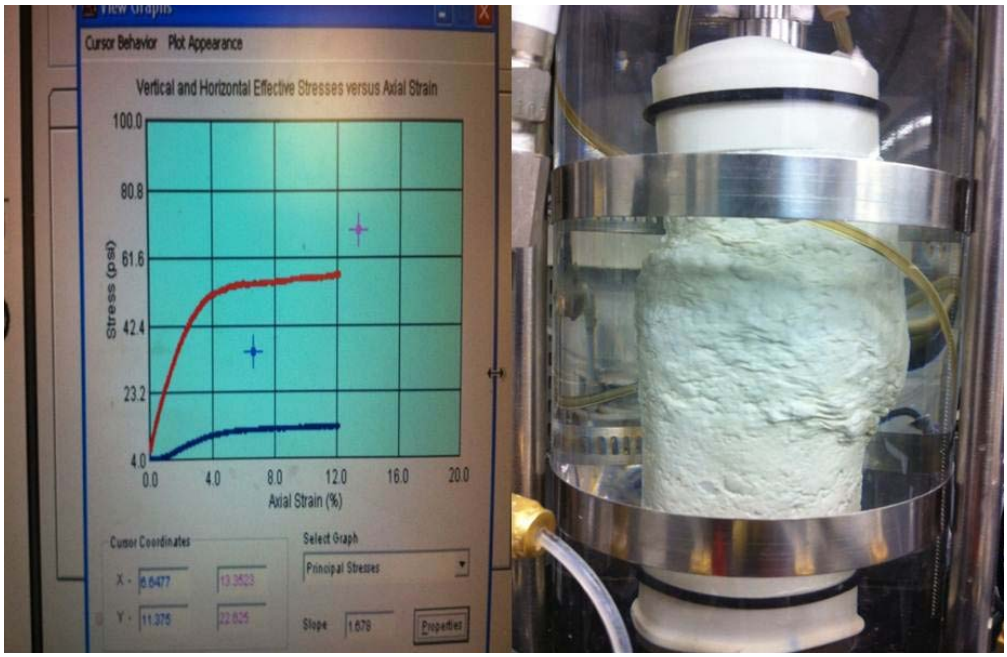

Figure 24. Stress-Strain Curve on Sigma-CU Program and Deformed Sample at 20 percent Axial Strain.

3.6 Calculations and Corrections

The calculations and data reduction are done per ASTM 4767. Initially the height of sample and wet density of sample are measured. During consolidation phase the volume of water leaving the sample is measured as well as change in height of sample was measured. These two measured values are used to calculate consolidated area of sample before shearing.

$$H_c = H_o - \Delta H_o \quad \text{(Eq. 7)}$$

H_o = initial height of sample.

ΔH_o = change in height of sample at end of consolidation.

$$A_c = (V_o - \Delta V_c)/H_c \quad \text{(Eq. 8)}$$

A_c = consolidated area of sample.

V_o = initial volume of sample.

ΔV_c = change in volume of sample during consolidation.

These values are used to calculate stresses and strains during shearing phase. During the shearing phase additional data were measured such as axial load, cell pressure, pore pressure, and displacement by measuring the position of servo motor. During undrained shearing, the current area of the specimen must be updated as follows:

$$A = A_c/(1 - \varepsilon_1) \quad \text{(Eq. 9)}$$

A = current area during shearing.

ε_1 = axial strain in decimal format.

The deviator stress is then:

$$\sigma_1 - \sigma_3 = \mathrm{P/A} \qquad \text{(Eq. 10)}$$

A membrane correction is applied to the above deviator stress:

$$\Delta(\sigma_1 - \sigma_3) = \frac{(4\mathrm{E_m t_m \varepsilon})}{\mathrm{D_c}} \qquad \text{(Eq. 11)}$$

The data obtained from these calculations are plotted in three types of graph, i.e., stress-axial strain curve, pore pressure-axial strain, and p-q curve for effective and total stresses. Note p= (σ_1+ σ_3)/2 and q = (σ_1− σ_3)/2.

3.6.1 Corrections

Test data were corrected for piston friction, piston uplift, membrane effects, and changing cross-sectional area. The piston friction was calculated using the procedure outlined by (Germaine and Ladd 1988) where the pressure inside the empty chamber is increased until the piston lifts up and then decreased until the piston drops. The average of these pressures times the cross sectional area of the piston was used to correct the load for a piston friction of 6.5 lb. The piston uplift was compensated by zeroing the load when contact was made with the sample during loading. Axial and radial effects of the membrane were corrected using the following equations from (Kuerbis and Vaid 1990):

$$\sigma_{am} = \sigma_a - \frac{4E_M t_0 \left(2 + \varepsilon_v + \varepsilon_{Ma}\right)\left(\varepsilon_v + 3\varepsilon_{Ma}\right)}{3D_0 \left(2 - \varepsilon_v + \varepsilon_{Ma}\right)} \qquad \text{(Eq. 12)}$$

$$\sigma_{rm} = \sigma_r - \frac{4E_M t_0 \left(2 + \varepsilon_v + \varepsilon_{Ma}\right)\varepsilon_v}{3D_0 \left(2 - \varepsilon_v + \varepsilon_{Ma}\right)} \qquad \text{(Eq. 13)}$$

where σ_{am} and σ_{rm} = the corrected axial and radial stresses.

σ_a and σ_r = the applied axial and radial stress.

E_M = the elastic modulus of the membrane.

t_0 = the unstretched membrane thickness.

D_0 = the unstretched membrane diameter.

ε_{Ma} and ε_V = the axial strain and the volumetric strain.

This equation assumes a thin hollow cylindrical shell and is only applicable if no visible membrane buckling occurs.

Finally, the cross-sectional area was corrected according to (Germaine and Ladd 1988) where the sample experiences an idealized parabolic or barreling deformation as shown in Figure 25. The equation for this area correction is:

$$A_c = A_0 \left[-\frac{1}{4} + \frac{\sqrt{25 - 20\varepsilon_a - 5\varepsilon_a^2}}{4\left(1 - \varepsilon_a\right)} \right]^2 \qquad \text{(Eq. 14)}$$

where A_c = the corrected area.

A_0 = the initial cross sectional area of the specimen.

ε_a = the axial strain in the specimen.

Figure 25. Parabolic Deformation of Test Specimen.

3.6.2 Test Results

The Figure 26 below shows the test results for Type-A1 at different confining pressure with zero amount of fines in the specimen. The stress-strain curve for Type-A1 presented in Figure 26a shows that at lower confining pressure there is no peak in stress-curve and with increasing confining pressure there is an increase in deviator stress at same strain value. This is typical trend for granular soils at drained condition (Holtz and

Kovacs 2011). Similarly, the plots of volumetric strain to axial strain for Type-A1 are shown in Figure 26b for different confining pressure. The volumetric strain was calculated by measuring the change in volume of sample by measuring the amount of pore water entering or exiting from sample. These volumetric strain plots shows that the sample behave dilative at lower confining pressure and contractive at higher confining pressure which is typical for drained triaxial testing of granular soils (Holtz and Kovacs 2011).

The results for consolidated undrained tests performed on Type-C1 are presented in Figure 27 below. The stress strain curve for this type shows that there is a peak in deviator stress at failure for high confining pressure and there is a positive change in pore pressure at same strain. The change in pore pressure was recorded during the shearing phase using differential pressure transducer.

The detailed plots and test result for these laboratory tests on Type A, B, C & D are presented in Appendix A.

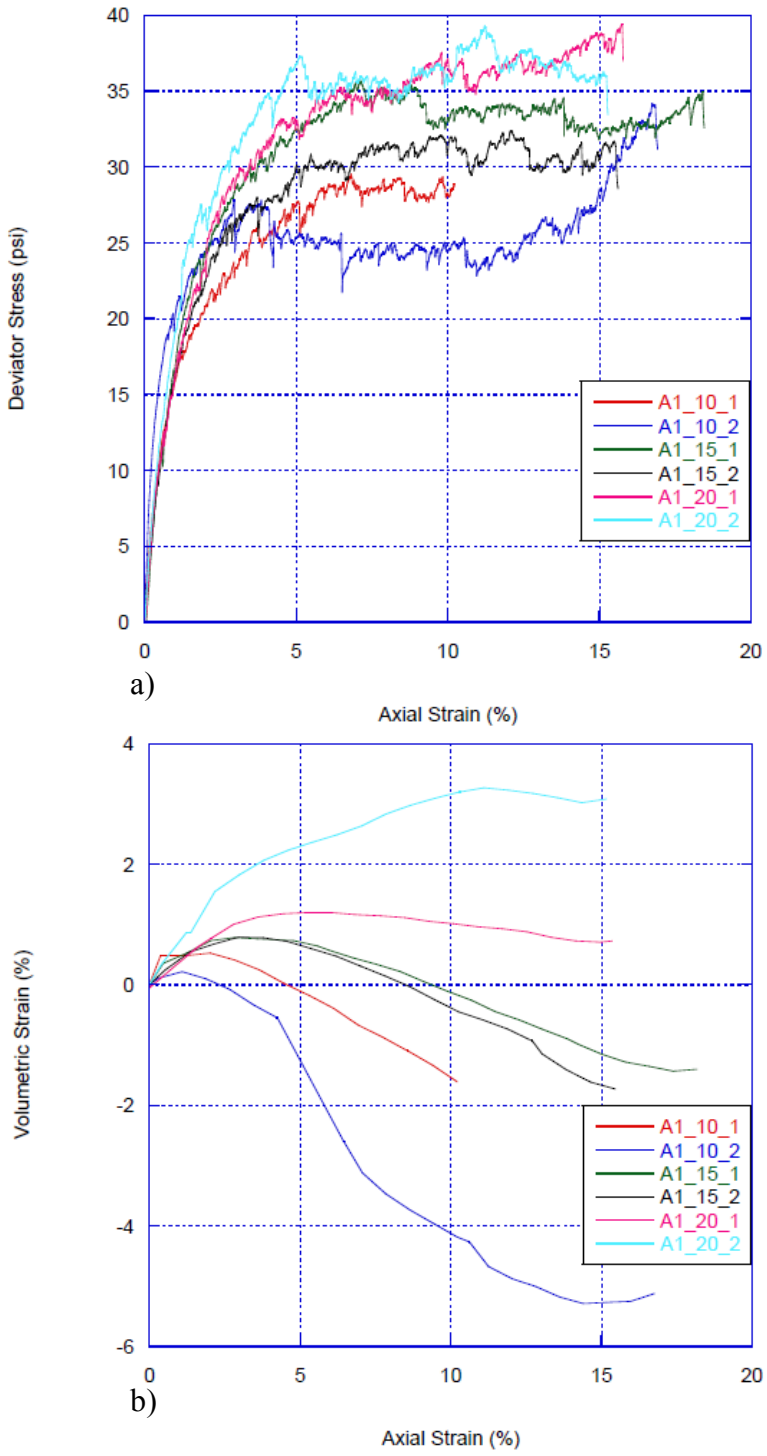

Figure 26. Test results for a Gradation Type A1; a) Stress-Strain Curves; b) Volumetric Strain Curves.

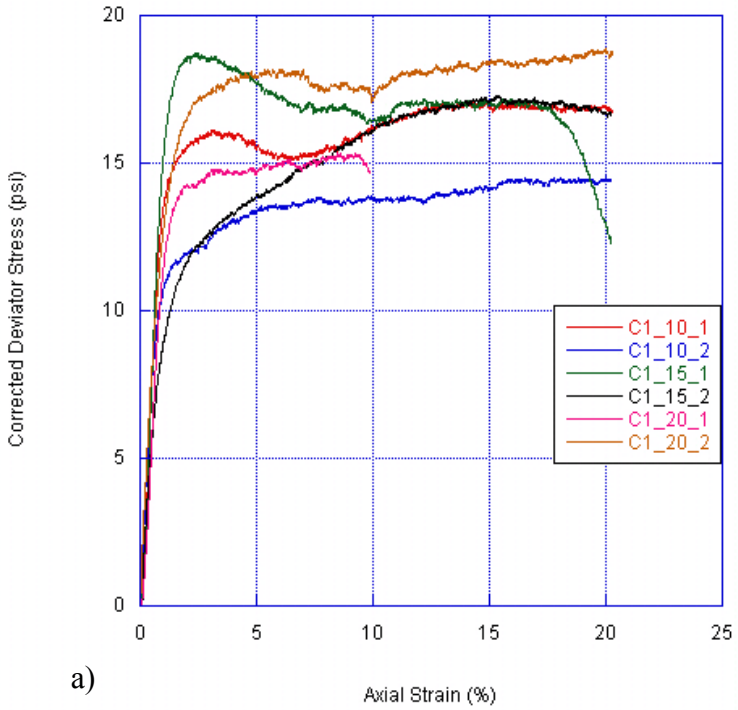

a)

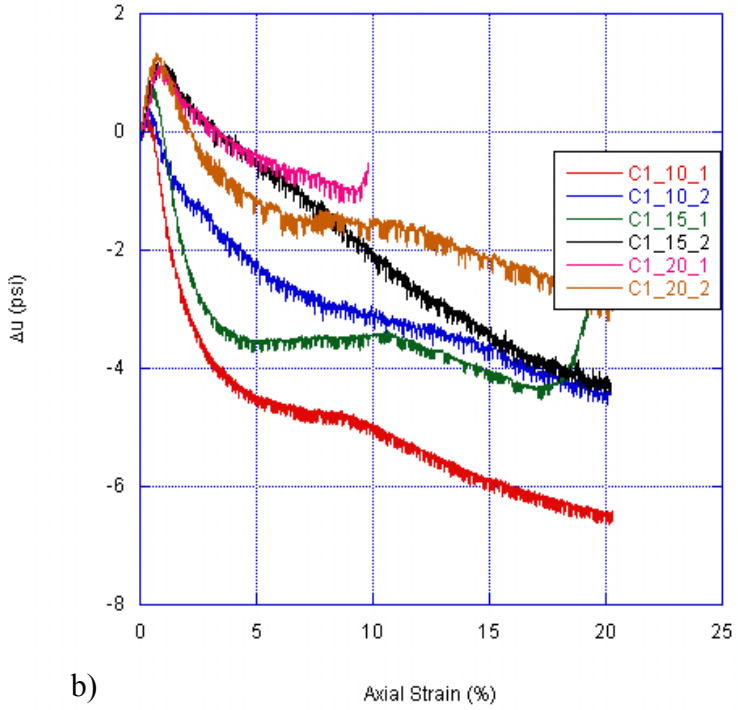

b)

Figure 27 Test results for a Gradation Type C1; a) Stress-Strain Curves; b) Change in Pore Pressure Curves.

3.6.3 Calculations of Friction Angles

Friction angles for each test were calculated using the differential stress at 10 percent strain and assuming cohesion of the material was zero. Data for each gradation were plotted in p-q space as shown in Figure 28, where p is equal to the average of the major and minor principal stress and q is equal to half of the differential stress. A friction angle was determined using a liner regression of the data to find the slope of the line (K_f), while again forcing the intercept to be zero. The sine of the friction angle is equal to the slope of the line in p-q space.

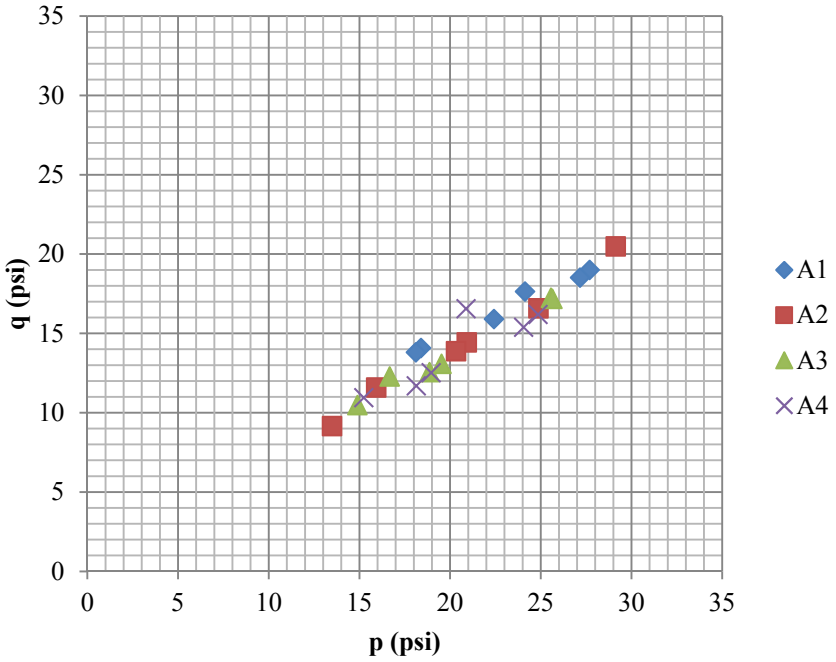

Figure 28. Type A Material p-q Diagram.

3.7 Conclusions

The relevant data include the minimum and maximum internal friction angles unit weights for backfill Types A, B, C, and D. The unit weight of materials was calculated as per ASTM C29 for Types A, B, and D and for Type C it was calculated by performing standard compaction test. Table 14–Table 15 show data for above mentioned materials. Table 14 shows drained and undrained strength parameters for Type C materials. For the confining pressures tested the Type C soils exhibited dilative behavior; therefore, the drained strength is actually less than the undrained strength, since negative pore pressures develop under such conditions.

Table 14. Laboratory Test Results for Type C Material.

Gradation	Maximum Undrained Friction Angles (°)	Minimum Undrained Friction Angles (°)	Maximum Drained Friction Angles (°)	Minimum Drained Friction Angles (°)	Dry Unit Weight (pcf)
C1	29.4	26.2	40.3	27.8	120.6
C2	28.3	26.2	47.4	30.1	129.4
C3	32.0	22.6	50.9	33.7	128.4
C4	32.3	23.6	26.4	23.0	126.3

Table 15. Laboratory Results for Types A, B, and D.

Gradation	Friction Angles (°)				Dry Unit Weight (pcf)	Dry Unit Weight (pcf)	
	Max.	Min.	Mean	Standard Deviation		Mean	Standard Deviation
A1	49.9	43.0	44.3	3.3	94.65	100.81	6.40
A2	46.8	41.8			99.7		
A3	47.5	41.8			99.1		
A4	45.9	39.8			109.8		
B1	53.4	48.5	47.4	5.8	98	118.00	16.73
B2	53.2	48.3			113.4		
B3	48.4	43.5			122.7		
B4	41.7	31.8			137.9		
D1	47.2	41.6	44.2	4.7	93.45	96.96	2.34
D2	47.0	36.5			98		
D3	51.6	38.4			98.1		
D4	41.7	35.8			98.3		

4. NUMERICAL SIMULATIONS

The main objective of numerical simulations was to identify the failure surfaces and safety factors for different retaining geometries supported by MSE walls. The FLAC program was used to perform the analyses. A parametric study was performed to investigate the effects of the following variables on MSE wall stability: a non-horizontal fore-slope, a non-horizontal back slope, foundation soil strength, backfill soil strength, and backfill soil density. The scope of the parametric study is illustrated in Figure 29-Figure 30.

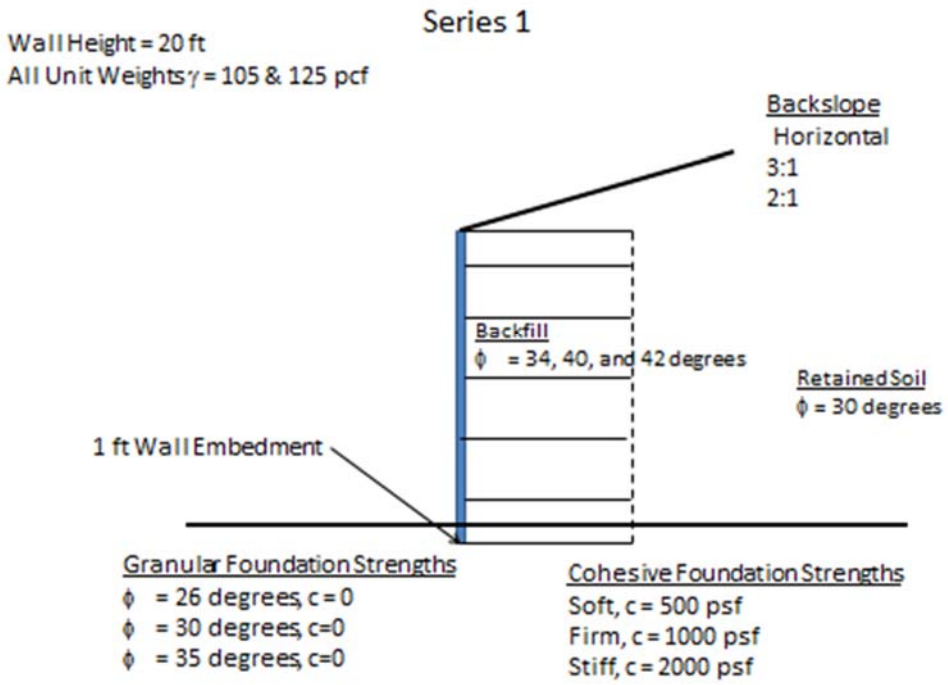

Figure 29. Effect of Non-Horizontal Back Slope.

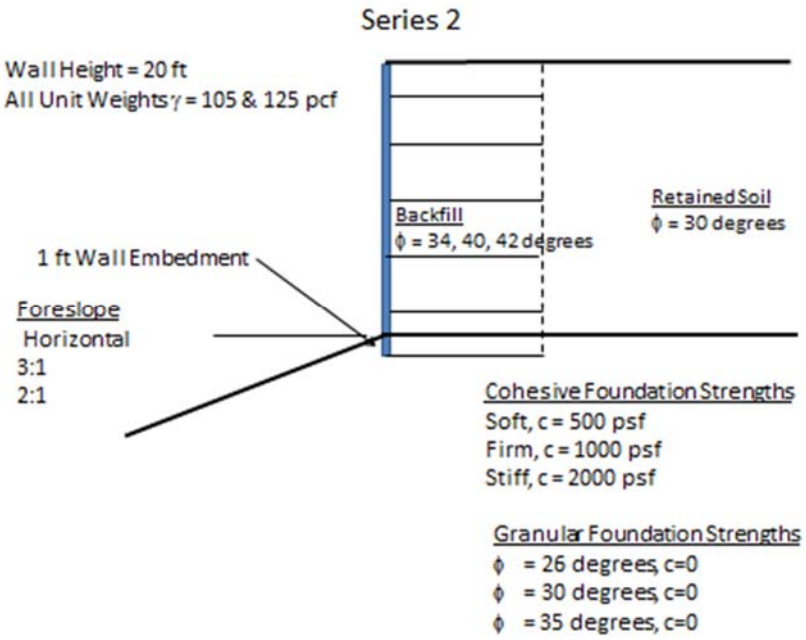

Figure 30. Effect of Non-Horizontal Fore-Slope.

4.1 Global Stability

Critics of the use of a bearing capacity analysis to evaluate MSE wall stability maintain that the actual failure mechanism for MSE walls is a global stability failure that is not well represented by a bearing capacity failure mechanism (Leshchinsky 2012). This section assesses whether a classical bearing capacity can provide meaningful inputs for MSE wall design.

4.1.1 Material Properties Used for Numerical Simulation

To compute FOS for each case mentioned above by using FLAC program, certain material properties are used. For frictional backfill and foundation materials values presented in Table 16 are used. For cohesive foundation materials values are

tabulated in, Table 17 and properties for backfill material are same as for both foundation materials.

Table 16. Material Properties for Frictional Backfill and Frictional Foundation Material.

Type	Elastic modulus* (psf)	Bulk modulus (psf)	Shear modulus (psf)	ν (Poisson's ratio)	ϕ
Foundation	2.116 E6	3.643 E6	0.364 E6	0.4516	26
	2.116 E6	3.643 E6	0.364 E6	0.4516	30
	4.232 E6	7.287 E6	0.728 E6	0.4516	35
Backfill	4.232 E6	7.287 E6	0.728 E6	0.4516	34
					40
					42

* Elastic modulus for sand is taken as $1000*P_{atm}$ where P_{atm}=2116.216 psf (Kulhawy and Mayne 1990)

Table 17. Material Properties for Cohesive Foundation Material.

Type	Elastic modulus* (psf)	Bulk modulus (psf)	Shear modulus (psf)	ν (Poisson's ratio)	C_u (psf)
Soft	$40*P_{atm}$=84.648 E3	141.081 E3	30.231 E3	0.4	500
Firm	$80*P_{atm}$	282.162 E3	60.463 E3		1000
Stiff	$200*P_{atm}$	705.405 E3	151.158 E3		2000

* Where P_{atm} =2116.216 psf (Kulhawy and Mayne 1990)

The dimension for a wall panel is used per TxDOT guidelines and 0.7H for the length of strips. The dimensions used for MSE walls with horizontal back slope is shown in Figure 31. The 20-ft high MSE wall is built in stages according to individual panel height. The panel height used is 5 ft and total wall height is 20 ft, therefore the MSE wall is built in four stages as shown in Figure 32. After each stage of the wall, the equilibrium forces were solved for a self-weight condition. The wall panel was modeled as an elastic member with an elastic modulus of a concrete. Whereas strips were modeled as a metal strips with vertical spacing of 1.5 ft and horizontal spacing of 3 ft. The material property for strips was used such as f* of 2.05 thickness of strip as 0.12in and width as 4in, according to a report by Rathje et al. (2006). The elastic modulus for concrete used in this analysis was 4.4957×10^{8} (psf).

4.1.2 Horizontal Back Slope

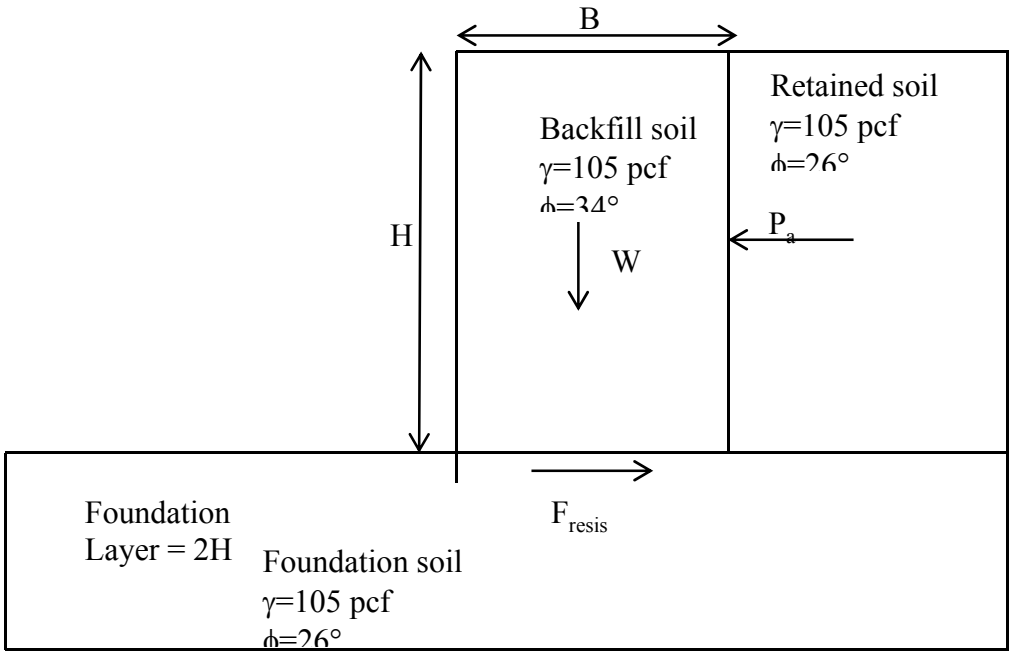

Figure 31. Dimensions and Properties Used for Series 1 Case 1.

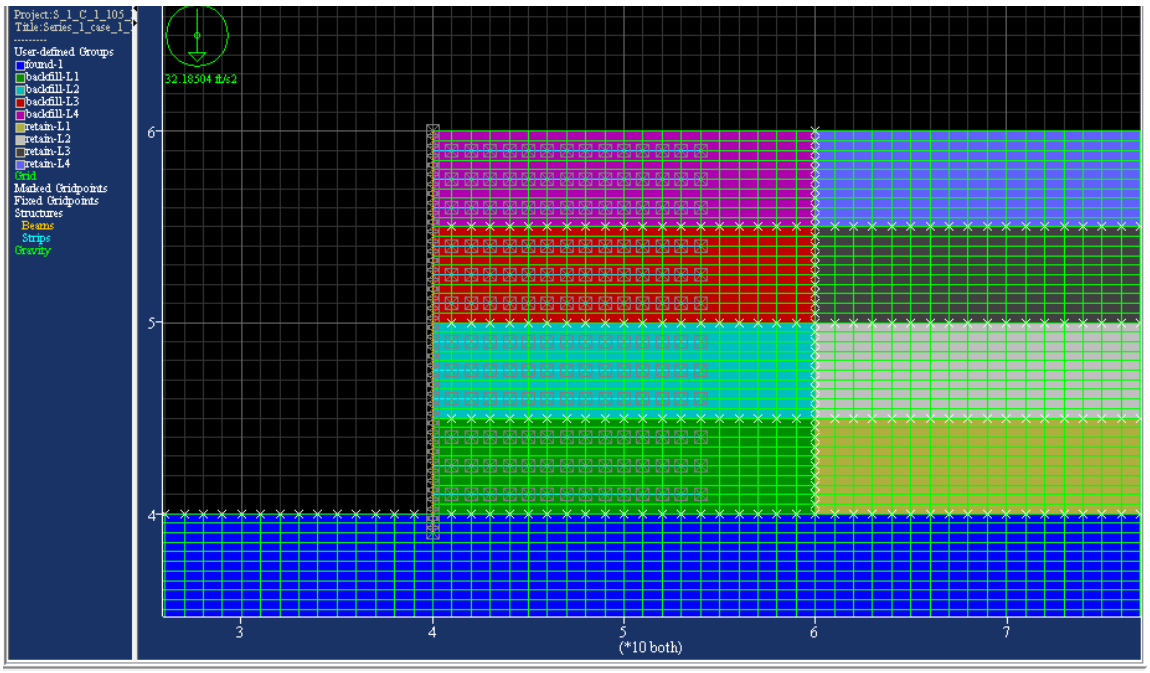

Figure 32. Concrete Panels and Strips Length Used for Series 1 Case 1.

The specific equations used in the bearing capacity analysis were as follows:

$$Q = B'\left[cN_c i_c + B'\gamma N_\gamma i_\gamma g_\gamma / 2\right] \qquad \text{(Eq. 15)}$$

where c = cohesion

$N_c = (N_q - 1) \cot \phi$

$N\gamma = (N_q - 1) \tan (1.4 \phi)$

$N_q = \exp (\pi \tan \phi) \tan^2 (\pi/4 + \phi/2)$

$i_c = (1 - 2 \alpha / \pi)^2$

$i_\gamma = (1 - \alpha / \phi)^2$

$g_\gamma = (1-\tan\delta)^2$.

ϕ = friction angle.

B’ = B – 2e.

B = base width of MSE wall.

e = eccentricity of load on foundation.

δ = ground inclination on toe-side of wall.

α = angle of foundation load from vertical.

The eccentricity e and angle of foundation load α are determined by resolving earth pressure, soil self-weight, and surcharge loads acting on the foundation. Apart from bearing capacity analysis and FOS for bearing capacity, sliding block failure, and FOS for it is also calculated using following equations:

$$P_a = 0.5 K_a \gamma_{ret} H_a^2 \qquad \text{(Eq. 16)}$$

where K_a= coefficient of active earth pressure.

γ_{ret}= unit weight for retained soil.

H_a = Equivalent Height of retained soil exerting active pressure on the wall.

$$F_{resist} = N \tan \phi_{found} \qquad \text{(Eq. 17)}$$

where N= total normal acting on the base of wall due to self-weight.

ϕ_{found} = friction angle for foundation soil.

$$FOS_{bearing} = \frac{Q}{N} \qquad \text{(Eq. 18)}$$

$$FOS_{sliding} = \frac{F_{resist}}{P_a} \quad \text{(Eq. 19)}$$

Table 18 shows the FOSs computed by FLAC for the case of a 20-ft high MSE wall with reinforcement length of 14 ft and a horizontal back slope. The corresponding plots of maximum shear strain rate for these cases are shown in Figure 33-Figure 34. The foundation soil used in these cases is purely frictional material with no cohesion. The bottom row of Table 18 presents the factors of safety from a classical bearing capacity analysis for the following cases presented. The backfill friction angle has no influence on the outcome of the classical bearing analysis. The detailed figures for each case for this series is shown in Appendix B. In this appendix figures for all series for sands and clays are presented. Figure 34 represents a typical failure mechanism for sands used for foundation layer and for retaining layers.

Table 18. Series 1 Case 1: Horizontal Back Slope with Frictional Foundation Soil.

Backfill Friction Angle (degrees)	**Factor of Safety**					
	ϕ_{found}= 26°		**ϕ_{found}= 30°**		**ϕ_{found}= 35°**	
	γ - backfill (pcf)		**γ - backfill (pcf)**		**γ - backfill (pcf)**	
	105	125	105	125	105	125
ϕ = 34	1.01	1.02	1.18	1.19	1.42	1.36
ϕ = 40	1.01	1.02	1.18	1.19	1.42	1.36
ϕ = 42	1.01	1.02	1.18	1.19	1.42	1.36
Bearing Capacity Analysis*	0.27	0.27	1.11	1.11	4.49	4.49
Sliding Stablity*	1.81	1.81	2.55	2.55	3.90	3.90

* The factor of safety for these conditions was calculated according to AASHTO (2002).

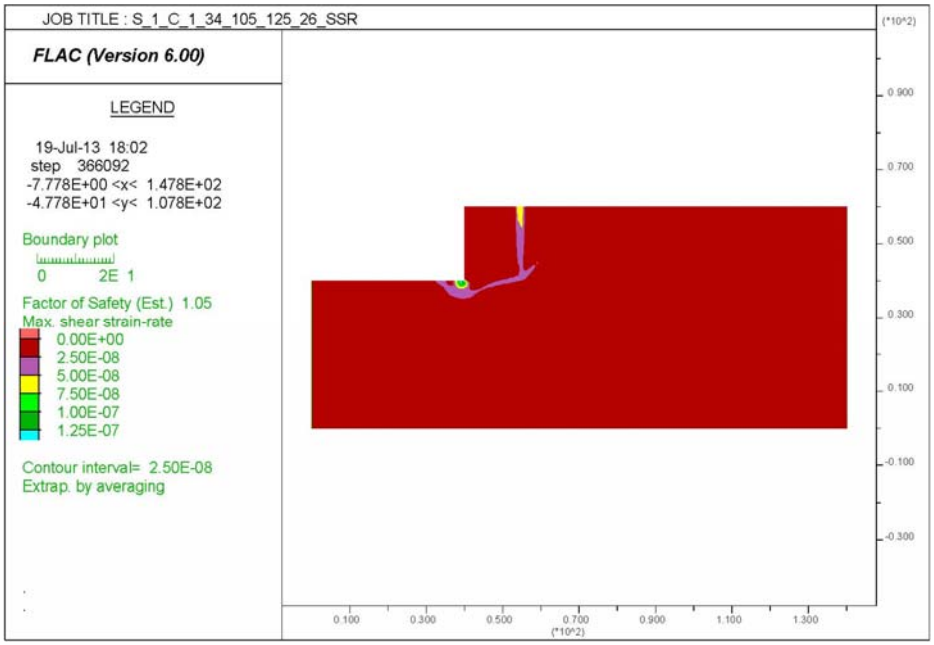

Figure 33. Series 1 Case 1 Foundation Angle ϕ=26°, Backfill Angle ϕ=34°, and γ_{back}=105 pcf γ_{retain}=125 pcf Maximum Shear Strain Rate.

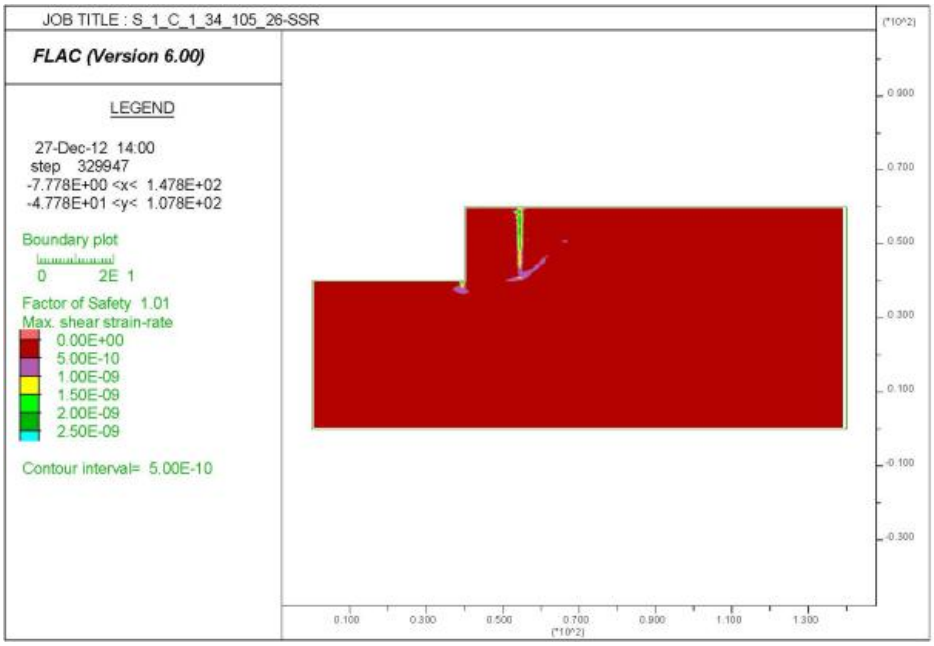

Figure 34. Series 1 Case 1 Foundation Angle ϕ=26°, Backfill Angle ϕ=34°, and γ=105 pcf Maximum Shear Strain Rate.

The analyses indicate the following:

- The dominant failure mechanism involves a wedge behind the reinforced portion of the wall, with a relatively shallow combined bearing-sliding failure at the base of the wall.
- The active wedge behind the wall is trying to move downward under the influence of gravity and the wall is pushed horizontally away from active wedge. Therefore its shows a vertical shear strain line behind the wall, which proves the failure mechanism. There was no interface material used in the simulation between wall and retaining soil.
- The backfill friction angle has negligible influence on global stability.
- Increasing or decreasing the unit weight of the backfill in conjunction with the retained soil has no influence on the safety factor. A denser retained soil will increase the active thrust; however, a denser backfill will increase the shearing resistance in similar proportion. The worst case scenario, a retained soil unit weight γ = 125 pcf in conjunction with a backfill unit weight γ = 105 pcf was considered and the results from FLAC simulation for this case were slightly different as the results for a unit weight of γ = 125 pcf for both soils. Figure 33 shows the result for this case. The failure mechanism is slightly different in terms of sliding mechanism without an active wedge at the back due to lower unit weight of backfill, which resulted in less force required to slide.
- For weak foundations (ϕ_{found}= 26° and 30°) the bearing capacity analysis significantly underestimates the actual factor of safety. This is a likely

consequence of the conservative assumption that the full overburden stress due to the backfill acts on the foundation. In actuality, the shearing resistance in the backfill and retained soil will likely reduce the pressure acting on the foundation.

- For strong foundations (ϕ_{found}= 35°) the FOS against bearing failure is well above the FOS against a wall failure. This is likely to the fact that when the foundation is sufficiently strong, the failure mechanism switches to a different mode.
- The FOS against sliding consistently overestimates the FOS against failure. This is a likely consequence of the assumption inherent in a sliding analysis that there is no interaction between bearing resistance and sliding resistance at the base of the backfill. Assuming no interaction between sliding and bearing resistance is generally unconservative, especially when dealing with weak foundations.
- The active wedge behind the reinforced zone tends to move downward under the influence of gravity as the wall is moves horizontally away from active wedge. Since the backfill is stiffer than the retained soil, significant strain occurs across the retained-backfill boundary. No interface material used in the simulation between wall and retaining soil. The figures show strain rate contours at the failure state, not the working stress state. Accordingly, the strain rate contours do not represent what would be seen in the field where stresses and strains are well below the failure level.

Given the conservatism of bearing capacity analyses for MSE walls on relatively weak foundations, the following alternatives may be considered:

1. Use the bearing capacity as a screening tool for determining whether a more sophisticated global stability analysis is needed.
2. Apply a semi-empirical correction to the bearing capacity analysis to match FLAC calculations.
3. Discontinue the use of the bearing capacity analysis and only perform the global stability analysis.

In the opinion of a researcher, the third alternative is too extreme. Although the existing bearing capacity is conservative, it is simple to perform and, in the least, it can be used as a screening tool for determining if more sophisticated analysis is warranted. In cases of high FOSs, it can avoid more costly analyses.

The FOS values from FLAC analysis using cohesive soil properties for Series 1 Case 1 are presented in Table 19. C_u=500 psf is considered as soft clays, Cu=1000 psf as firm clays, and C_u=2000 psf as stiff clays.

Table 19. Series 1 Case 1: Cohesive Foundation Soils.

Backfill Friction Angle (degrees)	Factor of Safety					
	C_u=500 psf		C_u=1000 psf		C_u=2000 psf	
	γ - backfill (pcf)		γ - backfill (pcf)		γ - backfill (pcf)	
	105	125	105	125	105	125
ϕ = 34	1.03	0.85	1.62	1.44	2.22	2.09
ϕ = 40	1.03	0.85	1.62	1.44	2.22	2.09
ϕ = 42	1.03	0.85	1.62	1.44	2.22	2.09

Figure 35–Figure 36 shows the results for this case. For soft clays the failure is more representative of bearing capacity type failure. The firm and stiff clays show a sliding type failure with stresses more concentrated behind the wall.

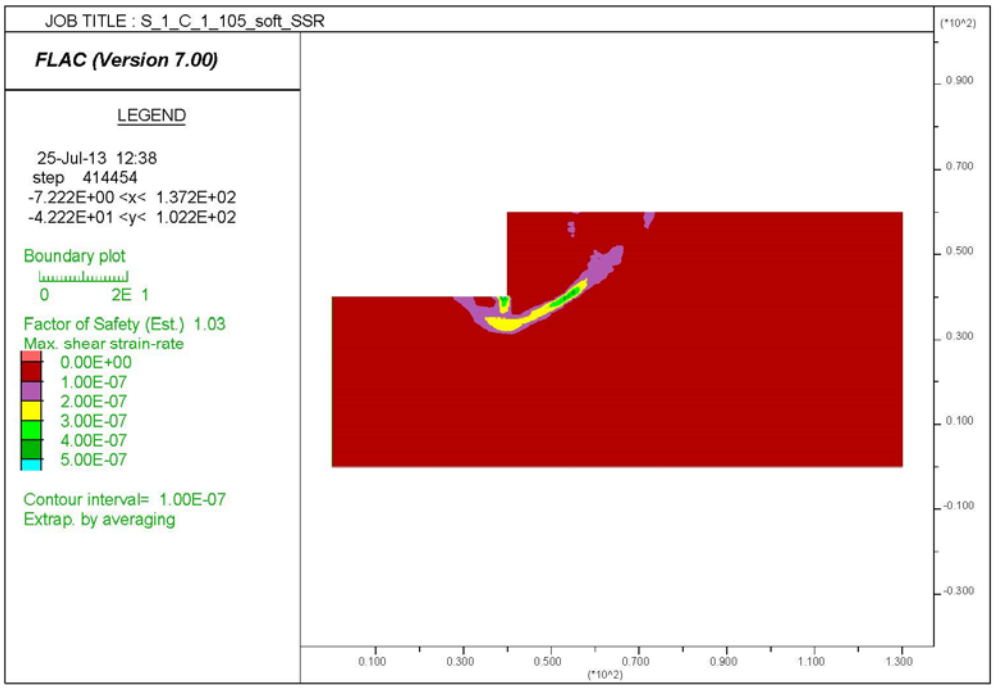

Figure 35. Series 1 Case 1 Foundation C_u=500 psf, Backfill Angle ϕ=34°, and γ=105 pcf Maximum Shear Strain Rate.

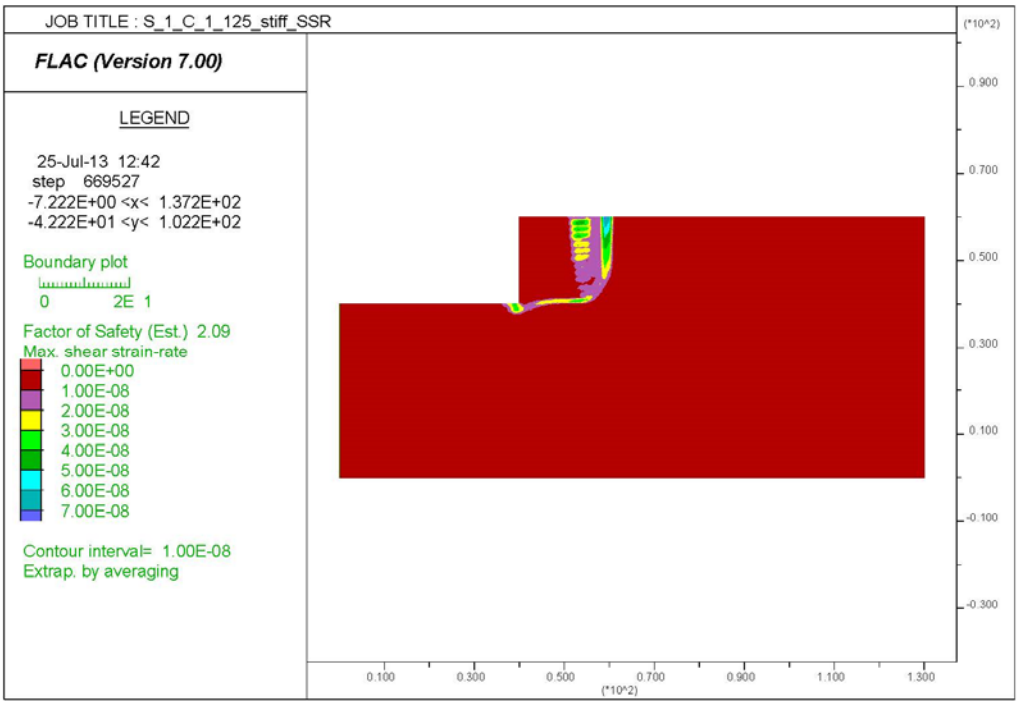

Figure 36. Series 1 Case 1 Foundation C_u=2000 psf, Backfill Angle ϕ=34°, and γ=125 pcf Maximum Shear Strain Rate.

Additionally, few more simulations were carried out to see the effect of thickness of foundation layer for cohesive soils especially for stiff clays. Table 20 shows the different factor of safety for different foundation layer thickness. A foundation layer of 2 times the wall height shows higher factor of safety than the foundation layer equal to the height of wall. The Figure 37 shows the shear strain rate contours for foundation layer equal to the height of wall.

Table 20. Factor of Safety Comparison for Series 1 Case 1 with Different Depth.

Backfill Friction Angle (degrees)	Factor of Safety					
	C_u=2000 psf (2H)		C_u=2000 psf (H)		Percent Different from 2H to H Foundation Depth (%)	
	γ - backfill (pcf)		γ - backfill (pcf)			
	105	125	105	125	105	125
ϕ = 34	2.22	2.09	1.48	1.37	6.22%	6.22%
ϕ = 40	2.22	2.09	1.48	1.37	6.22%	6.22%
ϕ = 42	2.22	2.09	1.48	1.37	6.22%	6.22%

* it is the difference in FOS when foundation depth is 2 times the wall height to 1 time the wall height.

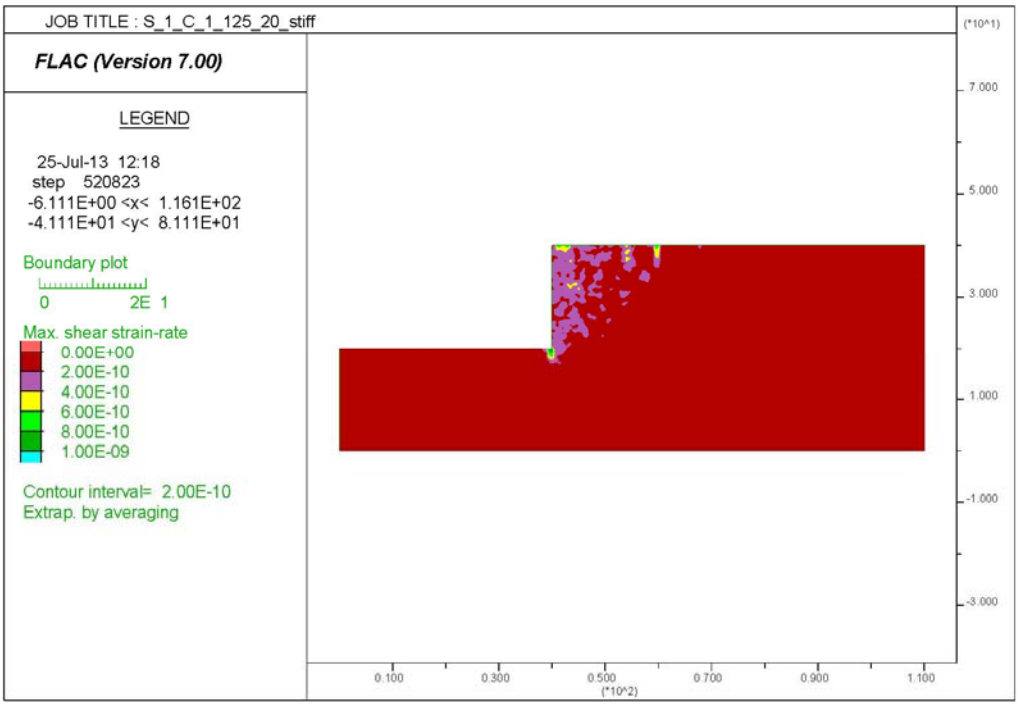

Figure 37. Series 1 Case 1 Foundation C_u=2000 psf, Backfill Angle ϕ=34°, and γ=105 pcf Maximum Shear Strain Rate. Foundation Depth Equals to Wall Height.

4.1.3 3H:1V Back Slope

Table 21 shows the FOSs computed by FLAC for the case of a 20-ft high MSE wall with reinforcement length of 14 ft and a 3H:1V back slope as shown in Figure 38. The corresponding plots of maximum shear strain rate for these cases are shown in Appendix B. The figures shown below from Figure 39–Figure 42 are with prominent failure surface. The bottom row of Table 21 presents the FOSs from a classical bearing capacity analysis for the cases presented in this section. The backfill friction angle has no influence on the outcome of the classical bearing analysis.

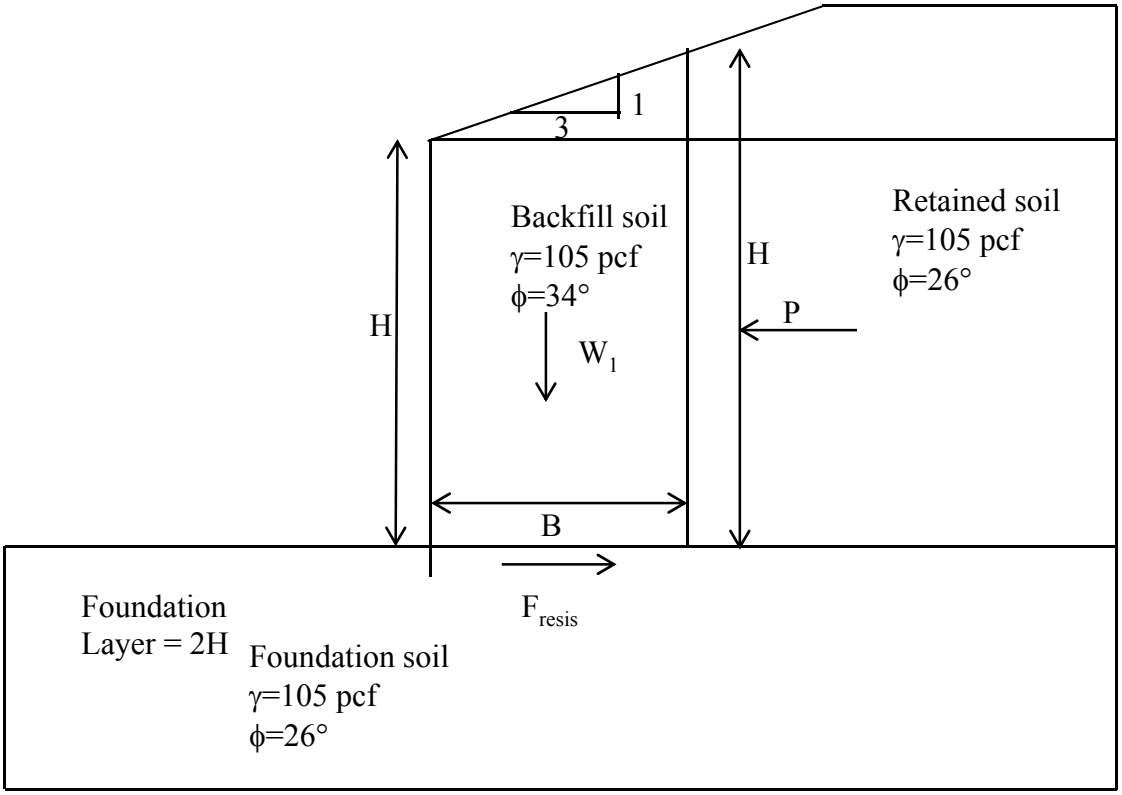

Figure 38. Dimensions and Properties Used for Series 1 Case 2.

Table 21. Series 1 Case 2: Back Slope 3:1 with Frictional Foundation Soil.

Backfill Friction Angle (degrees)	Factor of Safety					
	ϕ_{found}= 26°		ϕ_{found}= 30°		ϕ_{found}= 35°	
	γ - backfill (pcf)		γ - backfill (pcf)		γ - backfill (pcf)	
	105	125	105	125	105	125
ϕ = 34	0.78	0.78	0.90	0.90	1.17	1.17
ϕ = 40	0.78	0.78	0.90	0.90	1.17	1.17
ϕ = 42	0.78	0.78	0.90	0.90	1.17	1.17
Bearing Capacity Analysis	0.0002	0.0002	0.69	0.69	3.37	3.37
Sliding Analysis	0.97	0.97	2.16	2.16	3.41	3.41

Table 22. Series 1 Case 2: Cohesive Foundation Soils.

Backfill Friction Angle (degrees)	Factor of Safety					
	C_u=500 psf		C_u=1000 psf		C_u=2000 psf	
	γ - backfill (pcf)		γ - backfill (pcf)		γ - backfill (pcf)	
	105	125	105	125	105	125
ϕ = 34	0.64	0.54	1.28	1.08	1.98	1.84
ϕ = 40	0.64	0.54	1.28	1.08	1.98	1.84
ϕ = 42	0.64	0.54	1.28	1.08	1.98	1.84

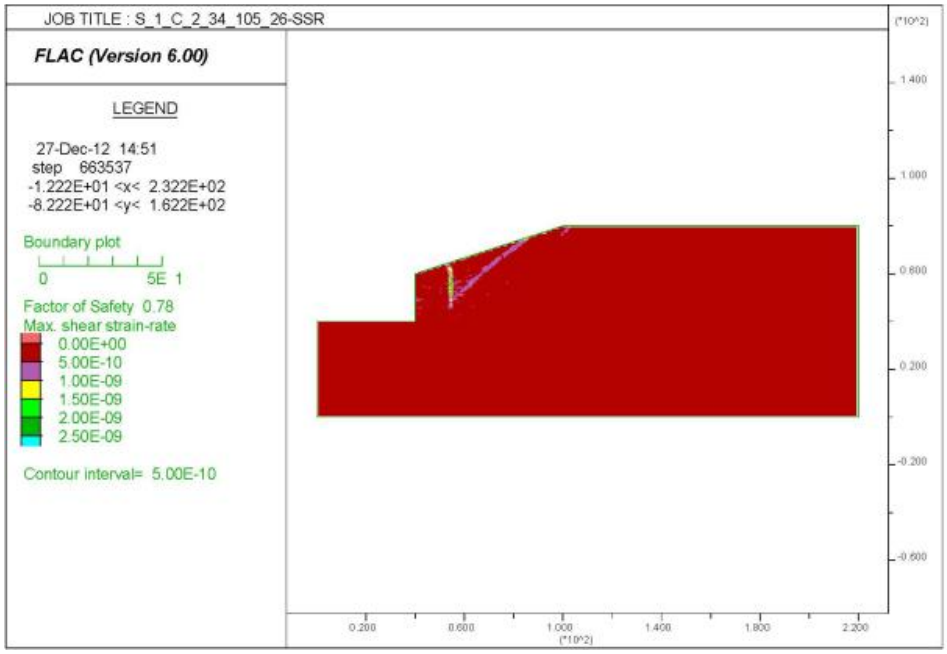

Figure 39. Series 1 Case 2 Foundation Angle ϕ=26°, Backfill Angle ϕ=34°, and γ=105 pcf Maximum Shear Strain Rate.

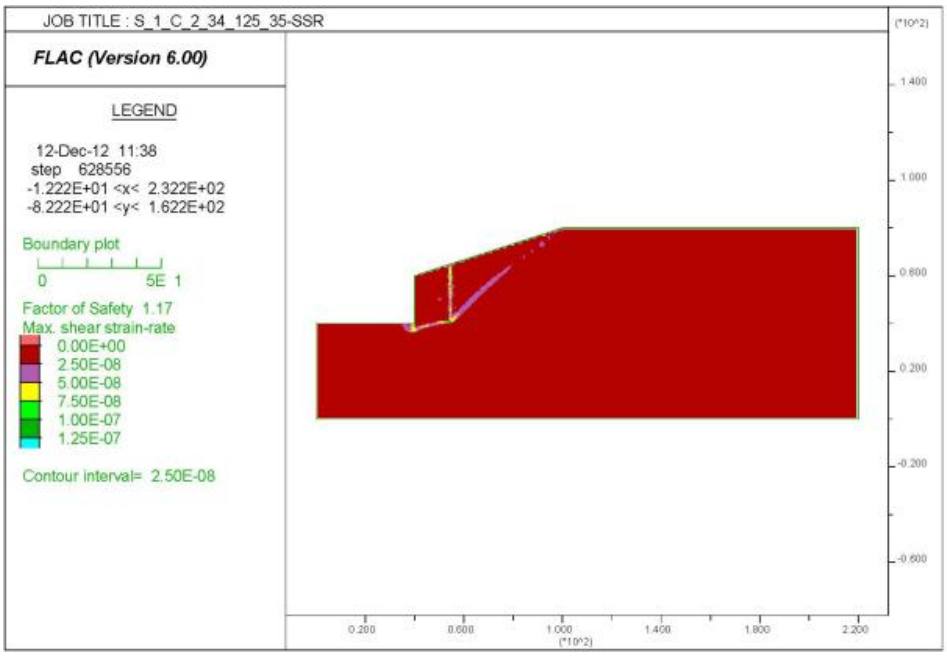

Figure 40. Series 1 Case 2 Foundation Angle ϕ=35°, Backfill Angle ϕ=34°, and γ=125 pcf Maximum Shear Strain Rate.

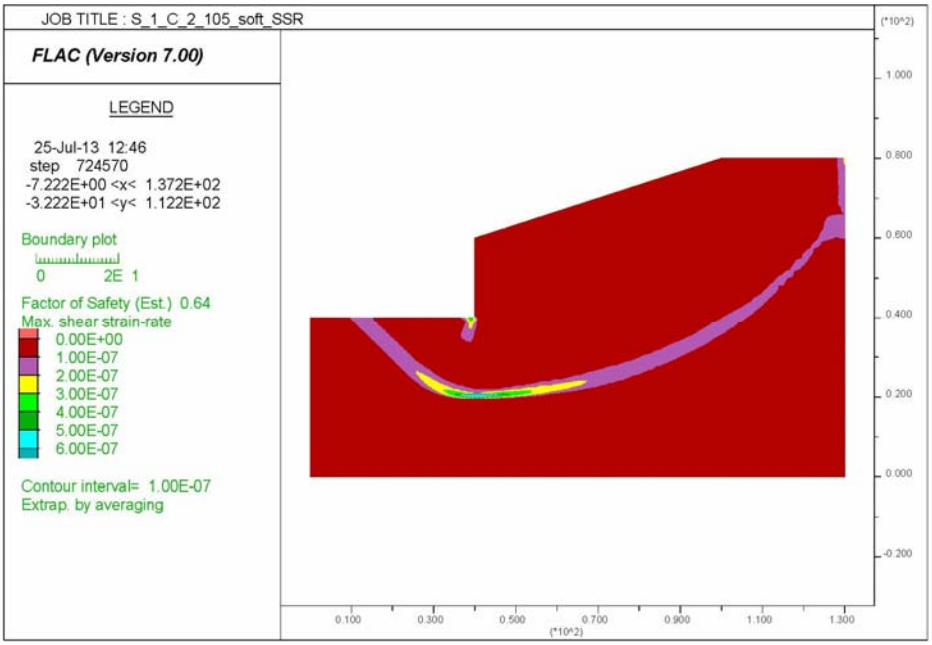

Figure 41. Series 1 Case 2 Foundation C_u=500 psf, Backfill Angle ϕ=34°, and γ=105 pcf Maximum Shear Strain Rate.

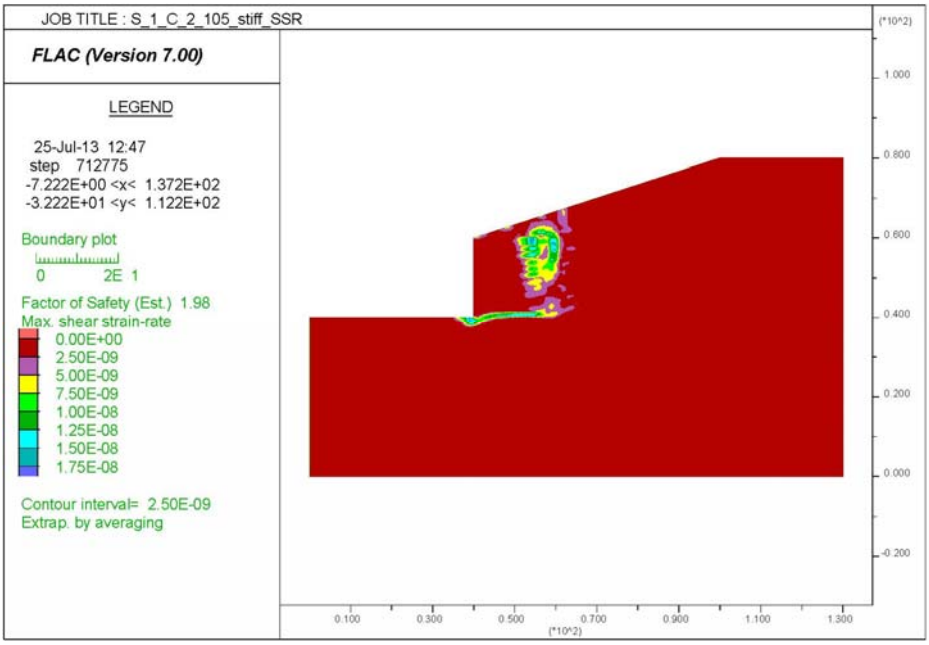

Figure 42. Series 1 Case 2 Foundation C_u=2000 psf, Backfill Angle ϕ=34°, and γ=105 pcf Maximum Shear Strain Rate.

For low foundation strengths (ϕ_{found}= 26° and ϕ_{found}= 30°) the classical bearing capacity differs from the finite difference solution significantly. This may be because bearing capacity equation does not consider the side friction between wall and retained soil. In the case of ϕ_{found}= 26°, the classical bearing capacity analysis is highly conservative, while it is slightly unconservative in the case of ϕ_{found}= 30°. For the stronger foundation (ϕ_{found}= 35°) the safety factor against bearing failure exceeds the more accurate finite difference solution by almost 2 times. As indicated previously, this may be because failure will tend to occur outside the foundation when the foundation strength is sufficiently high; i.e., a distinctly different failure mechanism governs. The failure surface for each case differs slightly for each of the cases considered. For low unit weight and low foundation friction angles, failure mechanism is mainly a sliding type with a small wedge behind the wall. By contrast, for higher unit weight and higher friction angle for retained soil the wedge behind the wall becomes wider with an angle of 41° with horizontal. The angle for wedge of retained soil varies from 40°–41°. The sliding analysis consistently gives a higher safety factor than either the bearing capacity analysis or the finite difference analysis.

These findings again support the notion that, while the bearing capacity analysis is not as reliable as a method that can analyze a global slope/wall failure, it can provide an indicator as to when failure through the foundation can be a problem. Accordingly, in the least it can be used as a preliminary analysis tool for determining when more sophisticated analyses should be used.

Similarly, a FLAC simulations were carried out to the see the effect of thickness of foundation layer on the FOS and the results are tabulated in Table 23 and a shear strain rate plot for foundation layer equal to height of the wall is shown in Figure 43.

Table 23. Factor of Safety Comparison for Series 1 Case 2 with Different Depth.

Backfill Friction Angle (degrees)	Factor of Safety					
	C_u=2000 psf (2H)		C_u=2000 psf (H)		Percent different from 2H to H foundation depth* (%)	
	γ - backfill (pcf)		γ - backfill (pcf)			
	105	125	105	125	105	125
ϕ = 34	1.98	1.84	1.37	1.44	44.5 %	27.7%
ϕ = 40	1.98	1.84	1.37	1.44	44.5%	27.7%
ϕ = 42	1.98	1.84	1.37	1.44	44.5%	27.7%

* it is the difference in FOS when foundation depth is 2 times the wall height to 1 time the wall height.

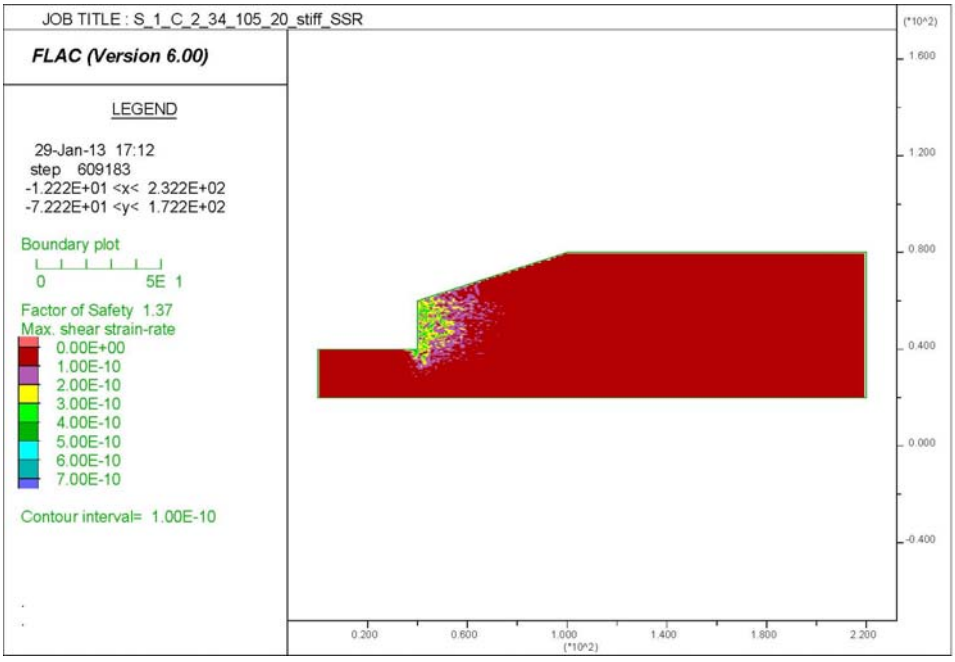

Figure 43. Series 1 Case 2 Foundation C_u=2000 psf, Backfill Angle ϕ=34°, and γ=105 pcf Maximum Shear Strain Rate. Foundation Depth Equals to Wall Height.

4.1.4 2H:1V Back Slope

In this case the back slope angle for taken as 2H: 1V, which is steeper than previous case as shown in Figure 44. Results from FLAC analysis are presented below in Table 24 and Table 25. In this table FOS safety for bearing capacity and for sliding is also presented. Figures associated with this case are presented in Appendix B. Figure 45–Figure 48 present a few representative results with visible failure surfaces.

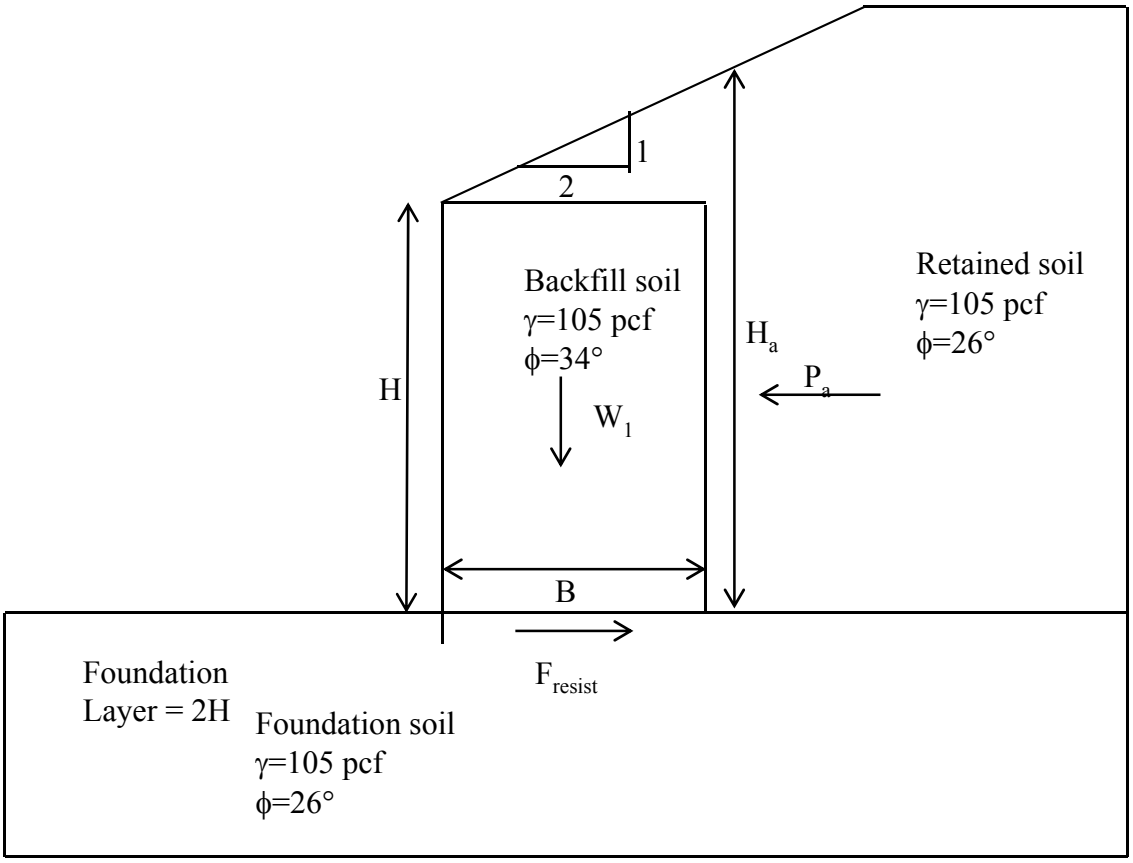

Figure 44. Dimensions and Properties Used for Series 1 Case 3.

Table 24. Series 1 Case 3: Back Slope 2:1 with Frictional Foundation Soil.

Backfill Friction Angle (degrees)	Factor of Safety					
	ϕ_{found}= 26°		ϕ_{found}= 30°		ϕ_{found}= 35°	
	γ - backfill (pcf)		γ - backfill (pcf)		γ - backfill (pcf)	
	105	125	105	125	105	125
ϕ = 34	0.61	0.62	0.72	0.66	0.91	0.92
ϕ = 40	0.61	0.62	0.72	0.66	0.91	0.92
ϕ = 42	0.61	0.62	0.72	0.66	0.91	0.92
Bearing Capacity Analysis	0.000	0.000	0.0001	0.0001	0.26	0.26
Sliding Analysis	0.65	0.65	0.98	0.98	1.58	1.58

Table 25. Series 1 Case 3: Cohesive Foundation Soils.

Backfill Friction Angle (degrees)	Factor of Safety					
	C_u=500 psf		C_u=1000 psf		C_u=2000 psf	
	γ - backfill (pcf)		γ - backfill (pcf)		γ - backfill (pcf)	
	105	125	105	125	105	125
ϕ = 34	0.55	0.49	1.16	0.98	2.41	No Convergence
ϕ = 40	0.55	0.49	1.16	0.98	2.41	
ϕ = 42	0.55	0.49	1.16	0.98	2.41	

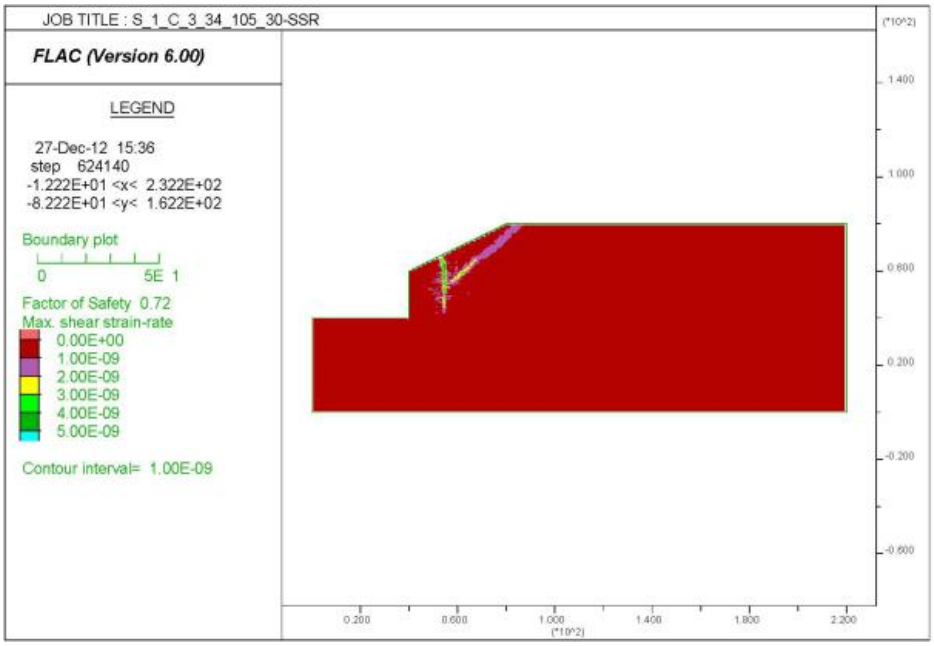

Figure 45. Series 1 Case 3 Foundation Angle ϕ=30°, Backfill Angle ϕ=34°, and γ=105 pcf Maximum Shear Strain Rate.

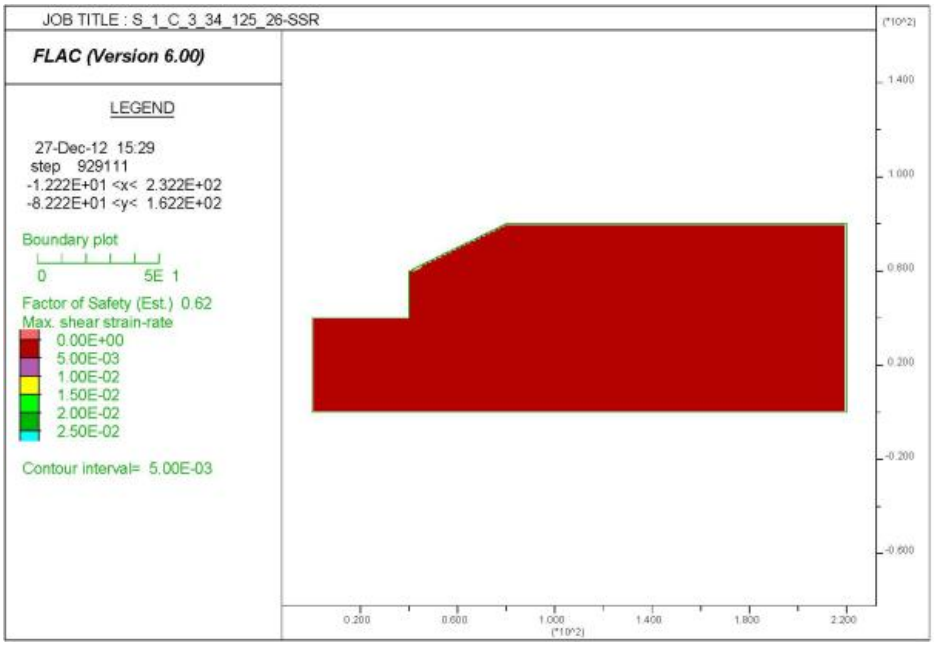

Figure 46. Series 1 Case 3 Foundation Angle ϕ=26°, Backfill Angle ϕ=34°, and γ=125 pcf Maximum Shear Strain Rate.

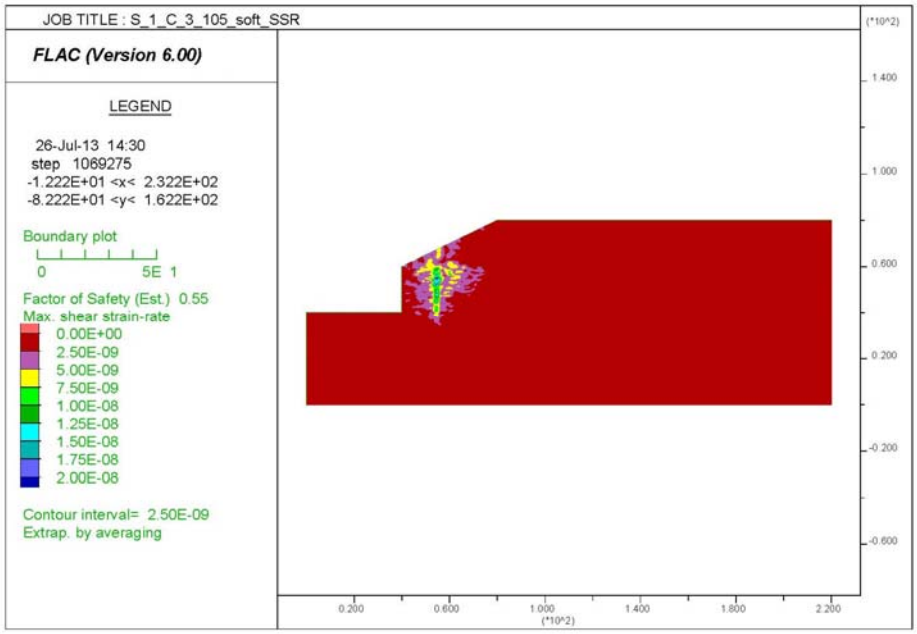

Figure 47. Series 1 Case 3 Foundation C_u=500 psf, Backfill Angle ϕ=34°, and γ=105 pcf Maximum Shear Strain Rate.

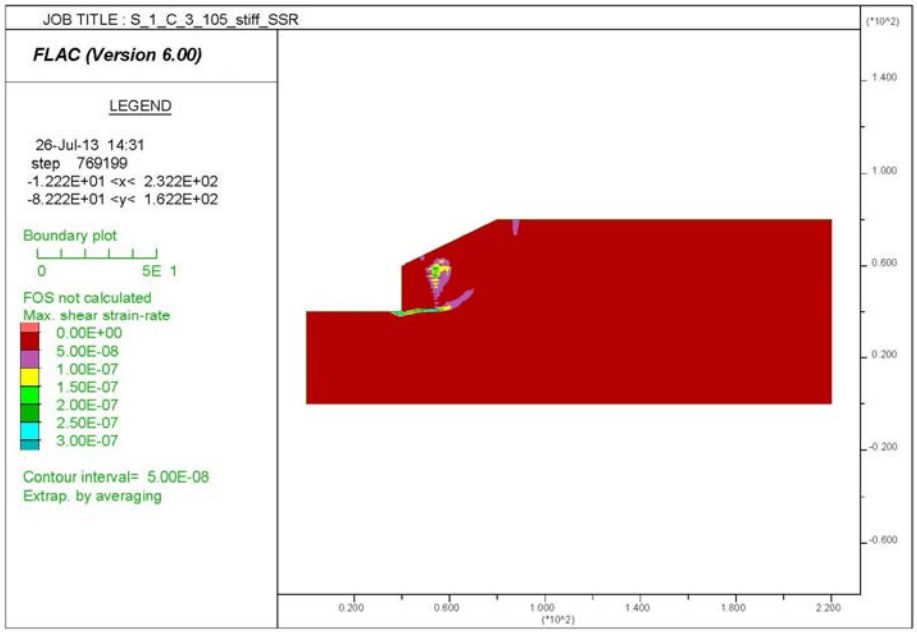

Figure 48. Series 1 Case 3 Foundation C_u=2000 psf, Backfill Angle ϕ=34°, and γ=105 pcf Maximum Shear Strain Rate.

The results from FLAC analysis show low values for ϕ_{found}= 26°, which is due to the fact that failure occurred on a back slope surface instead a wedge failure influencing the wall.

- The failure surface for ϕ_{found}= 30° had a wedge behind the wall with an angle of 32° with horizontal.
- The factor of safety from FLAC simulation for this case compared to 3H:1V back slope are reduced by 20–26 percent.
- The results for this case are different and should be verified with type of failure surface before considering it.
- The FOSs for bearing capacity are highly conservative and for sliding the values are higher than FLAC simulation data.

4.1.5 3H:1V Fore-Slope

In this series 3H:1V fore-slope is considered with depth equals to 1H wall height and the depth of foundation as 2H wall height below the fore-slope shown in Figure 49. Complete results for this case are presented in Appendix B. Figure 50–Figure 54 present a few representative plots from entire analysis for this case.

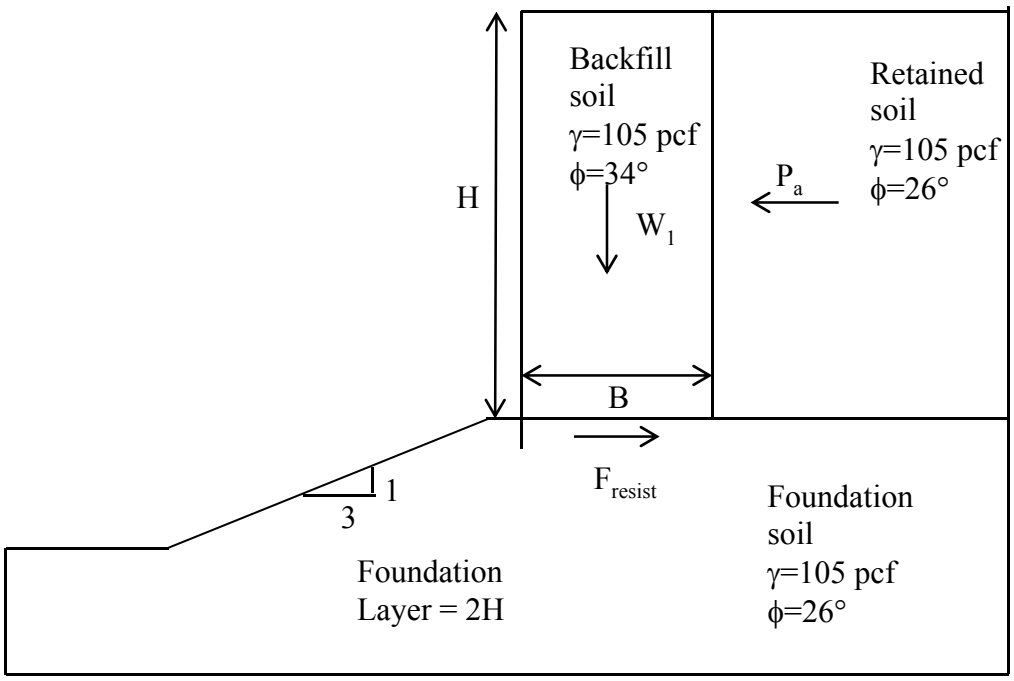

Figure 49. Dimensions and Properties Used for Series 2 Case 2.

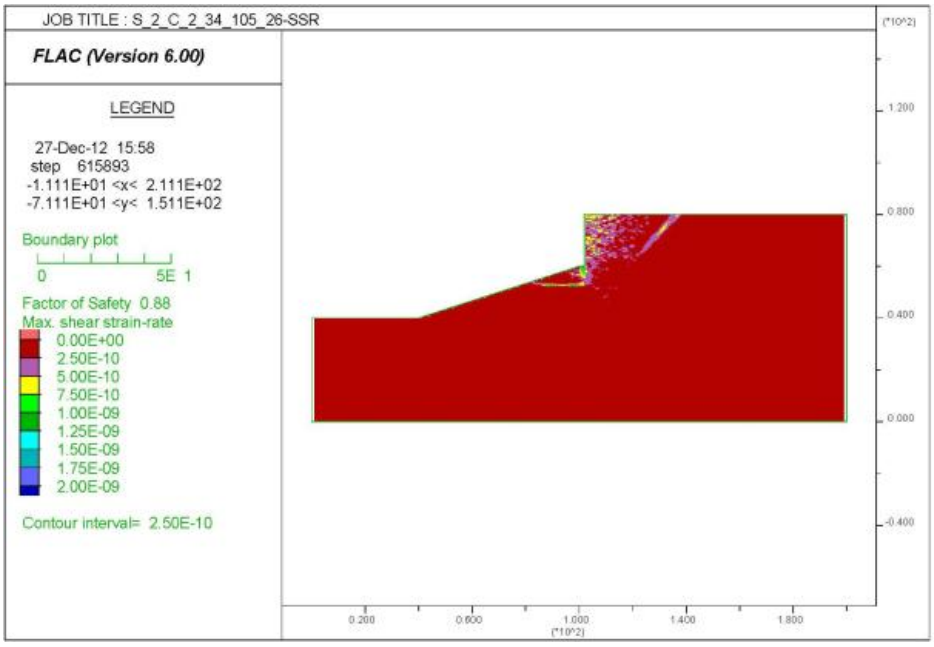

Figure 50. Series 2 Case 2 Foundation Angle ϕ=26°, Backfill Angle ϕ=34°, and γ=105 pcf Maximum Shear Strain Rate.

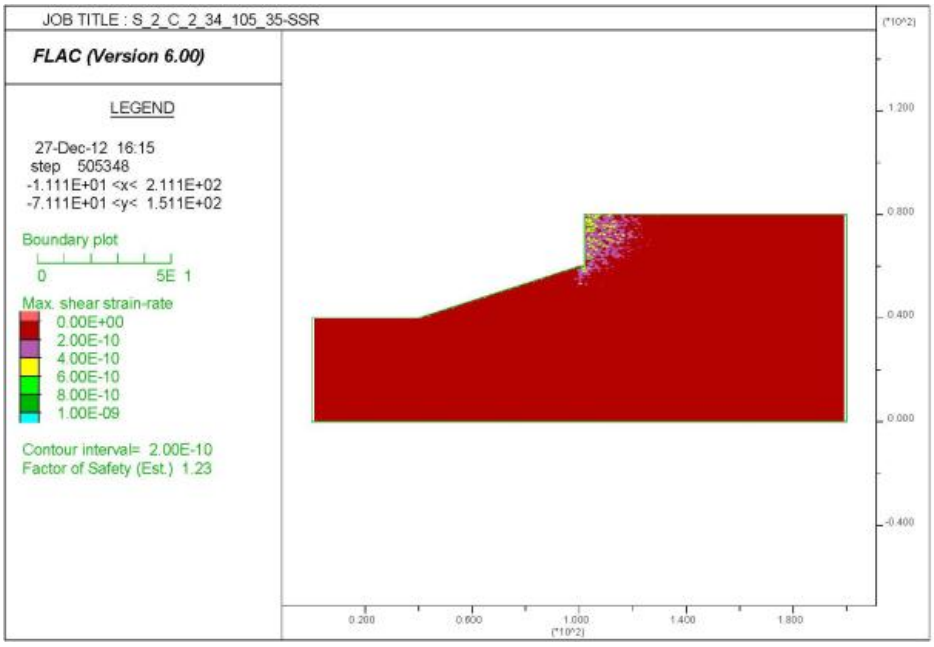

Figure 51. Series 2 Case 2 Foundation Angle ϕ=35°, Backfill Angle ϕ=34°, and γ=105 pcf Maximum Shear Strain Rate.

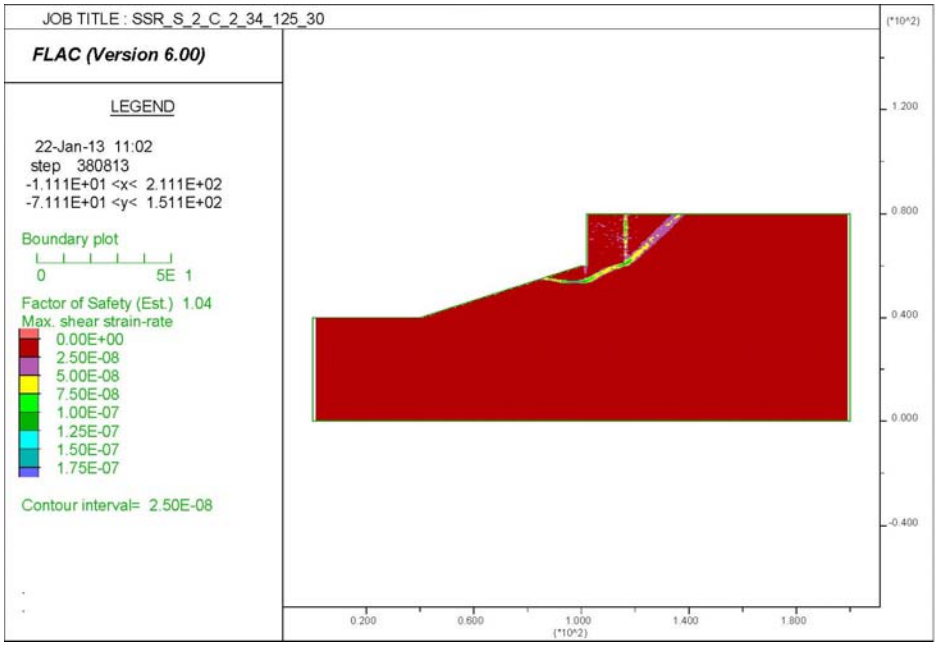

Figure 52. Series 2 Case 2 Foundation Angle ϕ=30°, Backfill Angle ϕ=34°, and γ=125 pcf Maximum Shear Strain Rate.

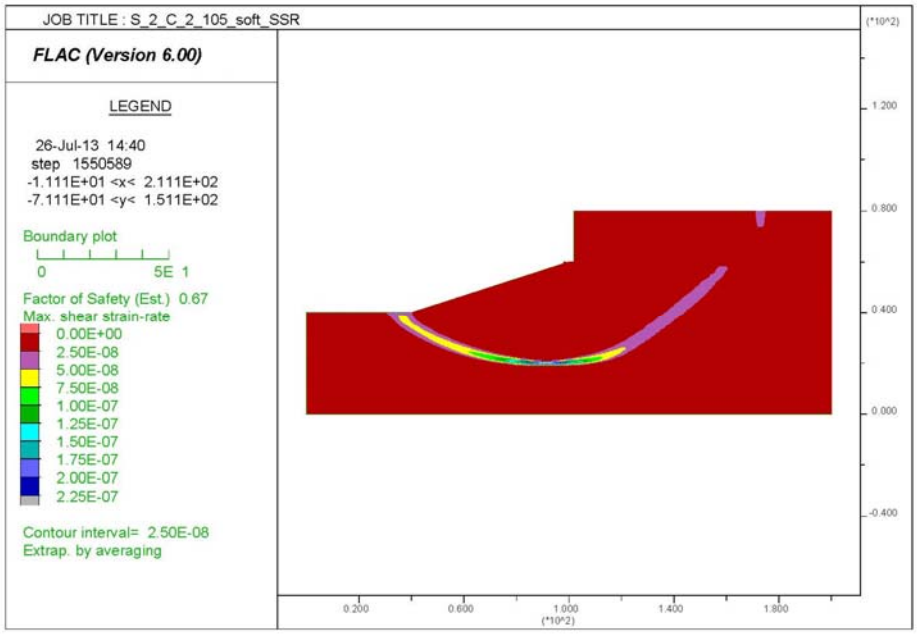

Figure 53. Series 2 Case 2 Foundation C_u=500 psf, Backfill Angle ϕ=34°, and γ=105 pcf Maximum Shear Strain Rate.

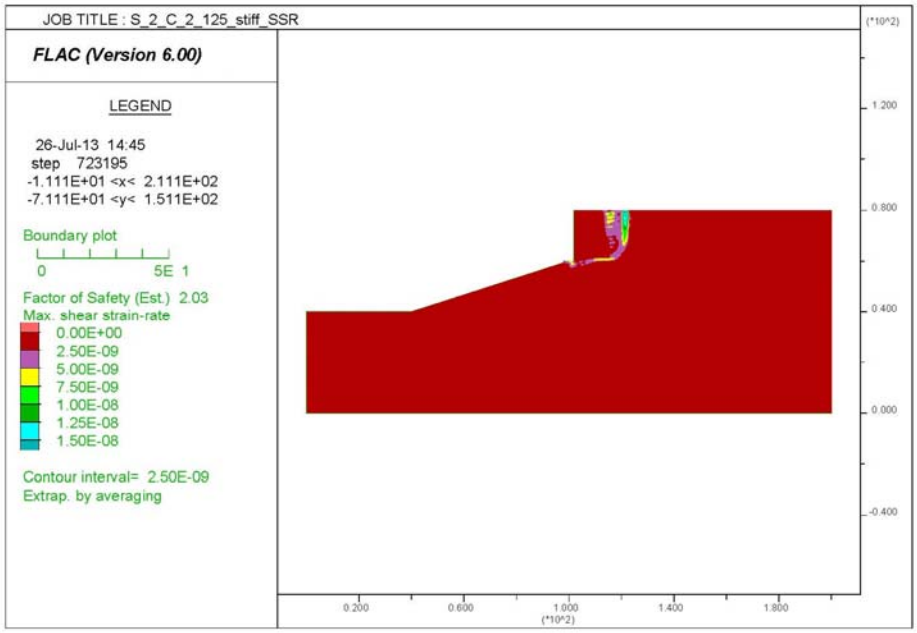

Figure 54. Series 2 Case 2 Foundation C_u=2000 psf, Backfill Angle ϕ=34°, and γ=105 pcf Maximum Shear Strain Rate.

Table 26-Table 27 below shows results from FLAC simulation as well as for bearing capacity analysis. The results for (ϕ_{found}= 26° and ϕ_{found}= 30°) foundations soils have different values for different unit weights. The lower unit weight foundation soils shows sliding failure, whereas, the failure surface for stronger foundation soils goes through fore-slope showing a general failure surface. The wedge type failure surface formed behind the wall has an angle of 42° with horizontal. The FOS from bearing capacity analysis shows values toward the conservative side while FOSs from sliding analysis show slightly unconservative values.

Table 26. Series 2 Case 2: Fore-Slope 3:1 with Frictional Foundation Soil.

Backfill Friction Angle (degrees)	Factor of Safety					
	ϕ_{found}= 26°		ϕ_{found}= 30°		ϕ_{found}= 35°	
	γ - backfill (pcf)		γ - backfill (pcf)		γ - backfill (pcf)	
	105	125	105	125	105	125
ϕ = 34	0.88	0.83	1.03	1.04	1.24	1.24
ϕ = 40	0.88	0.83	1.03	1.04	1.24	1.24
ϕ = 42	0.88	0.83	1.03	1.04	1.24	1.24
Bearing Capacity Analysis	0.12	0.12	0.49	0.49	2.00	2.00
Sliding Analysis	1.81	1.81	2.55	2.55	3.76	3.76

Table 27. Series 2 Case 2: Cohesive Foundation Soils.

Backfill Friction Angle (degrees)	Factor of Safety					
	C_u=500 psf		C_u=1000 psf		C_u=2000 psf	
	γ - backfill (pcf)		γ - backfill (pcf)		γ - backfill (pcf)	
	105	125	105	125	105	125
ϕ = 34	No Convergence	No Convergence	1.23	No Convergence	2.63	2.21
ϕ = 40			1.23		2.63	2.21
ϕ = 42			1.23		2.63	2.21

4.1.6 2H:1V Fore-Slope

The case discussed in this section has a higher fore-slope angle to see its effects on FLAC simulations. The complete results for this case are presented in Appendix B. Figure 55–Figure 60 present representative plots for this case, which are used here to explain the results for this case.

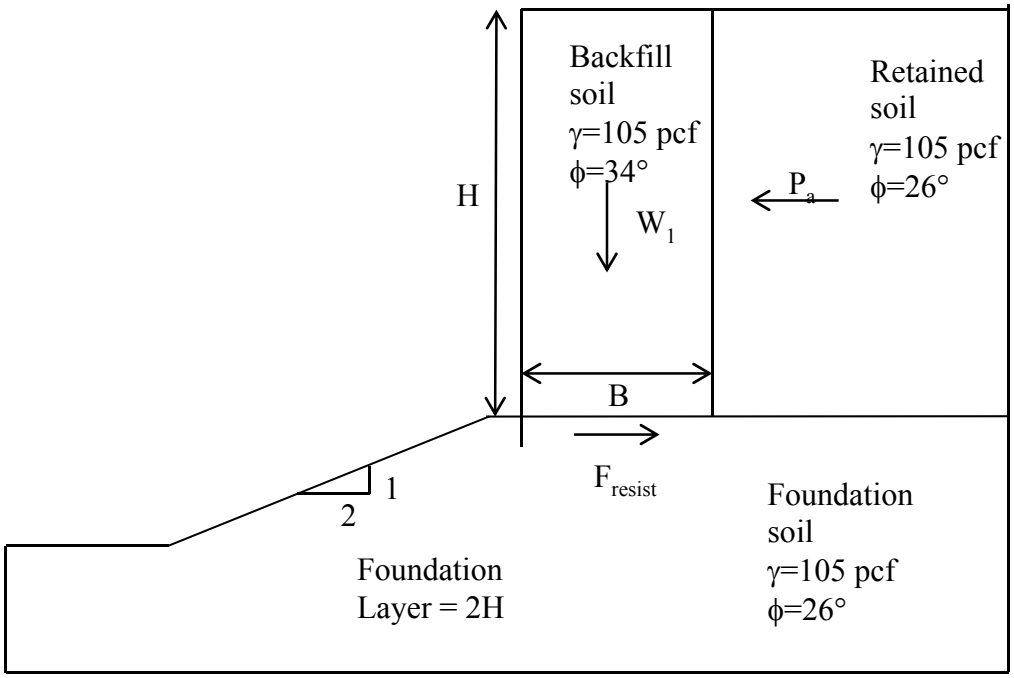

Figure 55. Dimensions and Properties Used for Series 2 Case 3.

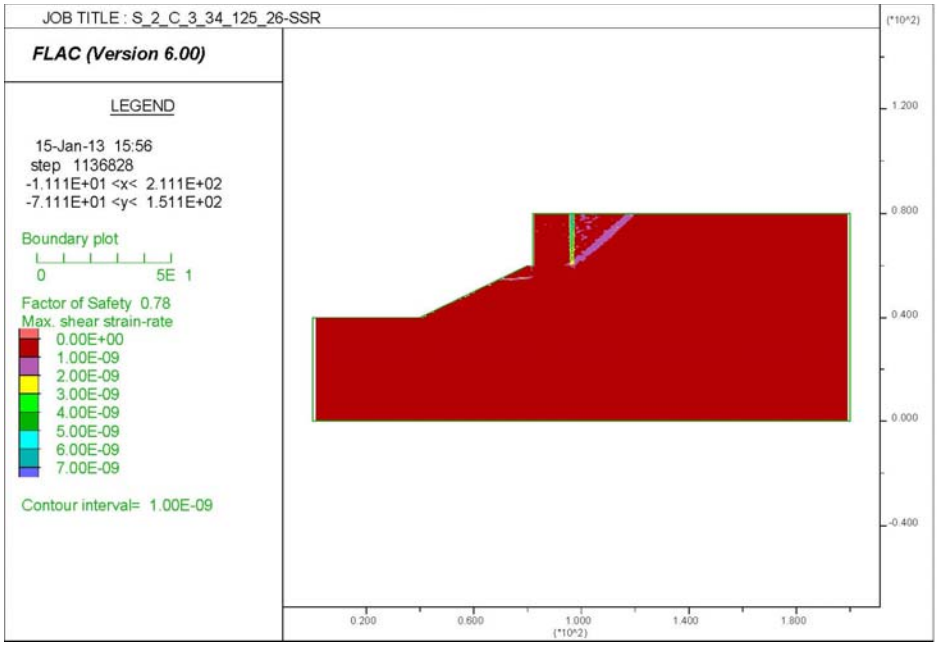

Figure 56. Series 2 Case 3 Foundation Angle ϕ=26°, Backfill Angle ϕ=34°, and γ=125 pcf Maximum Shear Strain Rate.

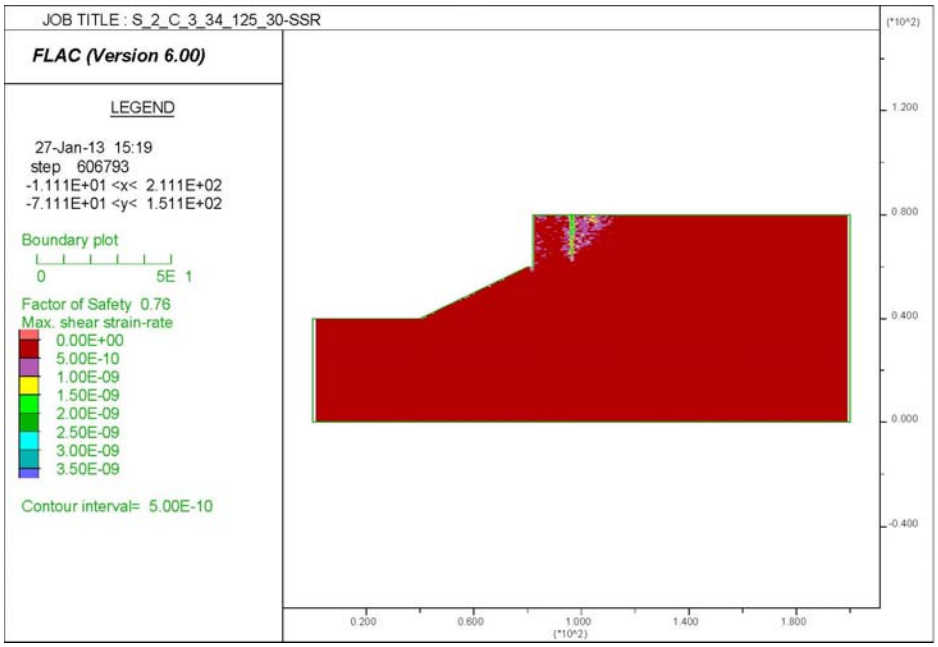

Figure 57. Series 2 Case 3 Foundation Angle ϕ=30°, Backfill Angle ϕ=34°, and γ=125 pcf Maximum Shear Strain Rate.

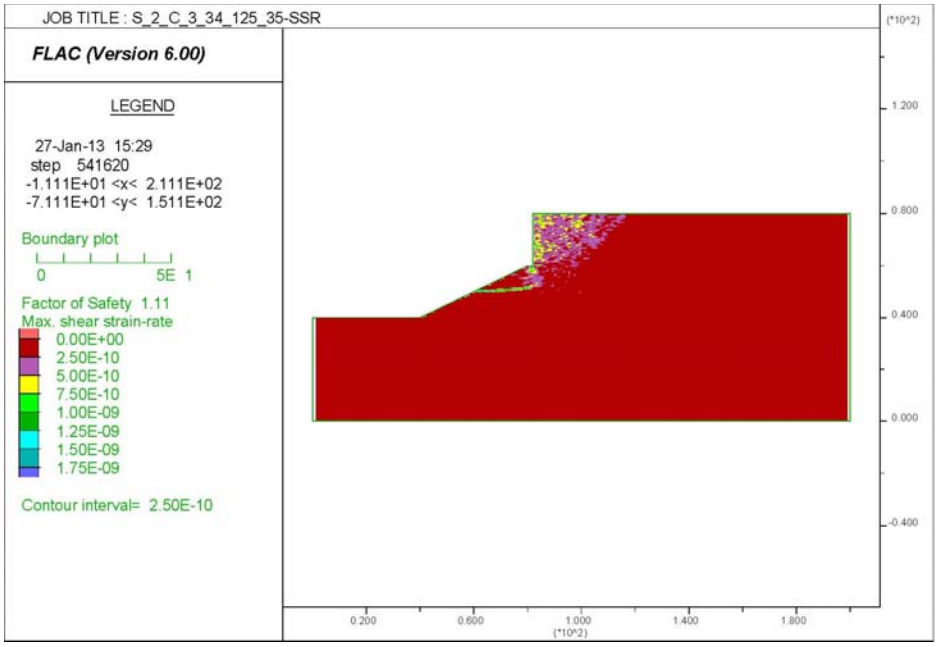

Figure 58. Series 2 Case 3 Foundation Angle ϕ=35°, Backfill Angle ϕ=34°, and γ=125 pcf Maximum Shear Strain Rate.

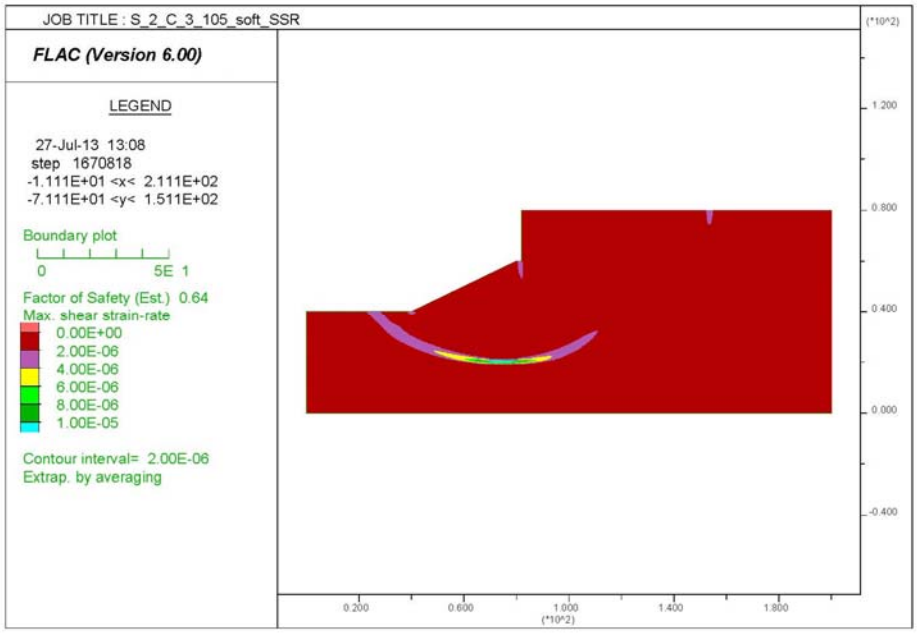

Figure 59. Series 2 Case 3 Foundation C_u=500 psf, Backfill Angle ϕ=34°, and γ=105 pcf Maximum Shear Strain Rate.

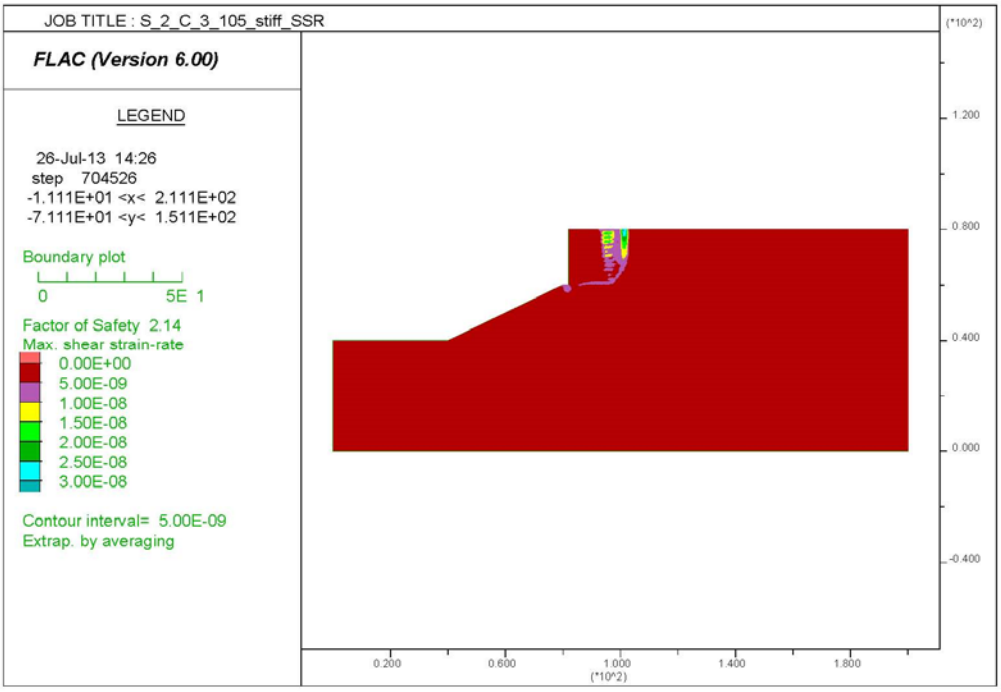

Figure 60. Series 2 Case 3 Foundation C_u=2000 psf, Backfill Angle ϕ=34°, and γ=105 pcf Maximum Shear Strain Rate.

Table 28-Table 29 shows FOS values from a FLAC simulation as well as from a bearing capacity and sliding analysis. The results from the bearing capacity analysis are highly conservative for low foundation strengths but for high foundation strengths it is close to FLAC analysis, which suggests that failure would be a bearing capacity failure. Values from the sliding analysis lean toward being unconservative. With increase in fore-slope angle the FOS values decrease from its previous case by 11–26 percent. The angle of failure wedge behind the wall is 42.3° with horizontal.

Table 28. Series 2 Case 3: Fore-Slope 2:1 with Frictional Foundation Soil.

Backfill Friction Angle (degrees)	Factor of Safety					
	ϕ_{found}= 26°		ϕ_{found}= 30°		ϕ_{found}= 35°	
	γ - backfill (pcf)		γ - backfill (pcf)		γ - backfill (pcf)	
	105	125	105	125	105	125
ϕ = 34	0.78	0.78	0.88	0.76	1.11	1.11
ϕ = 40	0.78	0.78	0.88	0.76	1.11	1.11
ϕ = 42	0.78	0.78	0.88	0.76	1.11	1.11
Bearing Capacity Analysis	0.068	0.068	0.278	0.278	1.12	1.12
Sliding Analysis	1.81	1.81	2.55	2.55	3.76	3.76

Table 29. Series 2 Case 3: Fore-Slope 2:1 with Cohesive Foundation Soils.

Backfill Friction Angle (degrees)	Factor of Safety					
	C_u=500 psf		C_u=1000 psf		C_u=2000 psf	
	γ - backfill (pcf)		γ - backfill (pcf)		γ - backfill (pcf)	
	105	125	105	125	105	125
ϕ = 34	0.64	0.52	1.25	1.05	2.14	2.12
ϕ = 40	0.64	0.52	1.25	1.05	2.14	2.12
ϕ = 42	0.64	0.52	1.25	1.05	2.14	2.12

5. PARAMETRIC STUDY

5.1 Parametric Study for Sliding and Overturning Analysis

This section assesses the effect of unit weight and strength of the backfill and retaining soils on sliding and overturning factors of safety. Two different types of wall geometry with cohesionless soil were performed. First, a wall with geometry of 20 ft height and no back slope was considered, and then a wall of 20 ft height with 3H:1V back slope was considered.

5.1.1 Horizontal Back Slope

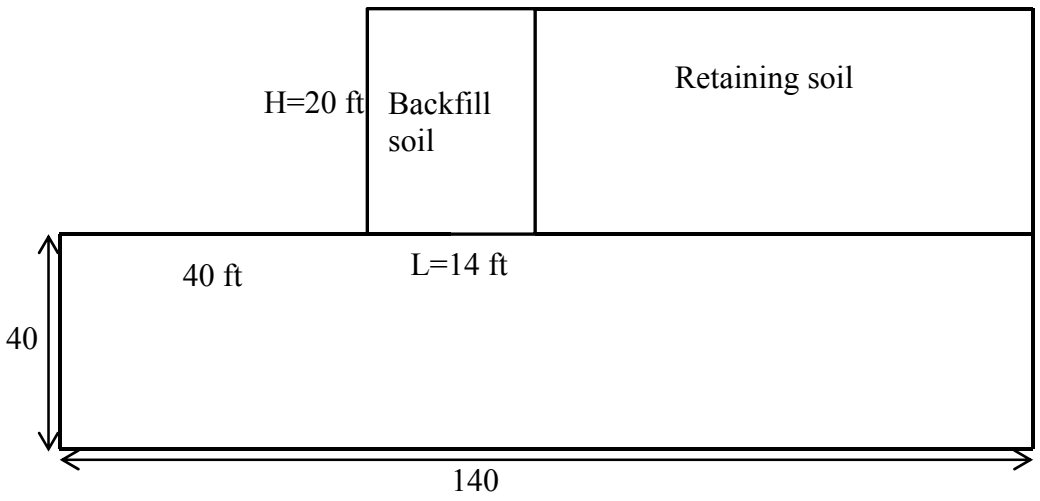

Figure 61. MSE Wall with 20 ft Wall Height and No Back Slope.

For the MSE wall with a geometry shown above Figure 61, initially a unit weight of 105 pcf was assigned to the backfill and retaining soils and then it was increased to 125 pcf for backfill soil with 105 pcf for retaining soil and vice versa to see the effect on FOS against sliding. The results for this parametric study are presented below. The

equations used to calculate FOS for sliding and FOS for overturning are shown. These equations are as per AASHTO 2002 manual for MSE retaining walls (AASHTO 2002):

$$F_{driving} = \frac{1}{2} K_a \times \gamma_{ret} \times H^2 \quad \text{(Eq. 20)}$$

$$F_{resisting} = W \times tan\delta_b \quad \text{(Eq. 21)}$$

$$W = \gamma_{back} \times L \times H \quad \text{(Eq. 22)}$$

$$FOS_{Sliding} = \frac{F_{resisting}}{F_{driving}} \quad \text{(Eq. 23)}$$

$$M_{driving} = \frac{1}{2} K_a \times \gamma_{ret} \times H^2 \times \frac{H}{3} \quad \text{(Eq. 24)}$$

$$M_{resisting} = W \times \frac{L}{2} \quad \text{(Eq. 25)}$$

$$FOS_{overturning} = \frac{M_{resisting}}{M_{driving}} \quad \text{(Eq. 26)}$$

To have a better understanding of an effect of unit weight of backfill and retaining soils on FOS for sliding and overturning, it is necessary to plot different FOS values for different $\phi_{retaining}$ and $\phi_{foundation}$ with respect to ratio of unit weights. For an above given geometry, FOS values with respect to ratio of unit weights are plotted for three different $\phi_{retaining}$ in an one plot by fixing $\phi_{foundation}$ and repeating the same procedure for different $\phi_{foundation}$. Noting that retained soil and backfill unit weights can plausibly vary from 105–125 pcf, the density ratio $\gamma_{back}/\gamma_{retain}$ in Figure 62–Figure 65 can realistically be considered to vary from 0.84–1.19. Thus, an adverse distribution of unit weights say γ_{back} = 105 pcf and γ_{retain} = 125 pcf-can lead to safety factors on the order of 20 percent lower than would occur for the case of a homogeneous ($\gamma_{back}/\gamma_{retain}$ =1) unit weight distribution. The overall implications of this issue are significant but not

necessarily very serious. For example, for the case of a relatively low strength foundation, ϕ_{found} = 26°, the FOS for the uniform unit weight case is about 2.1. For a fairly severe adverse case $\gamma_{back}/\gamma_{retain}$ =0.84, the FOS reduces to about 1.5, which is still acceptable. Nevertheless, the potential for a reduced safety factor due to an adverse distribution of unit weights should be kept in mind, particularly for situations of low FOS walls.

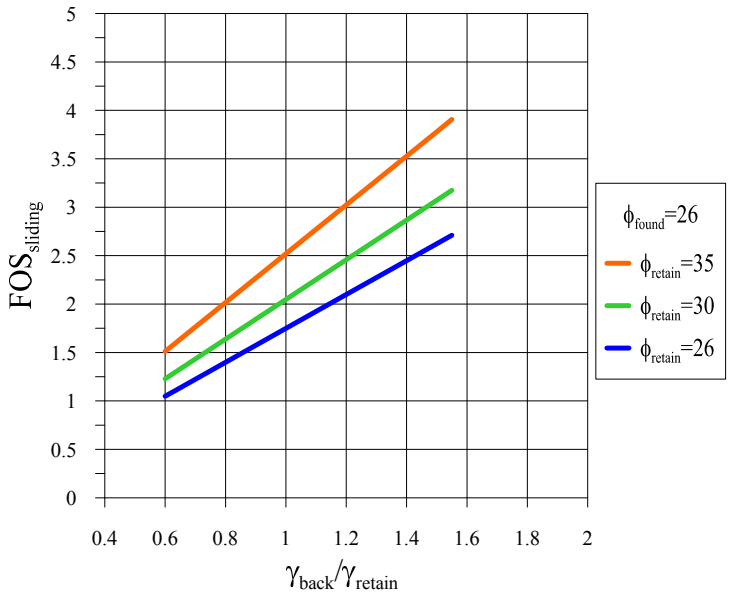

Figure 62. Factor of Safety against Sliding for 20 ft Wall Height with No Back Slope for Different $\phi_{retaining}$ at a Constant ϕ_{found}=26°.

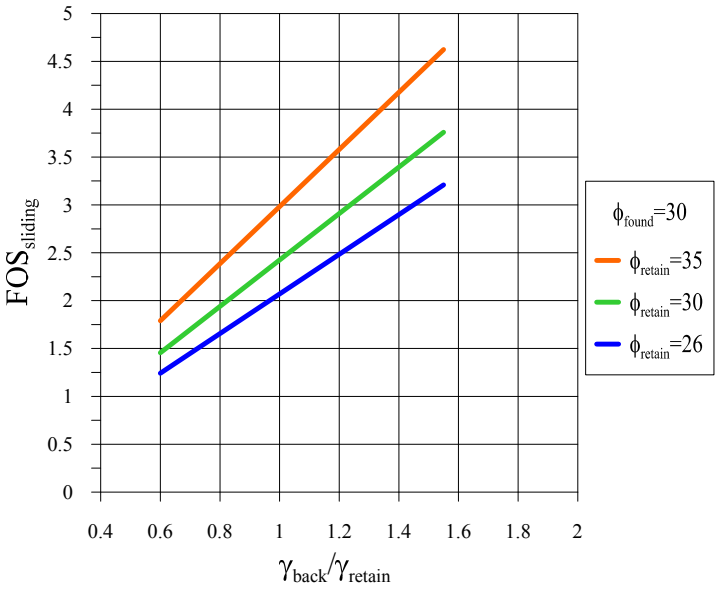

Figure 63. Factor of Safety against Sliding for 20 ft Wall Height with No Back Slope for Different $\phi_{retaining}$ at a Constant ϕ_{found}=30°.

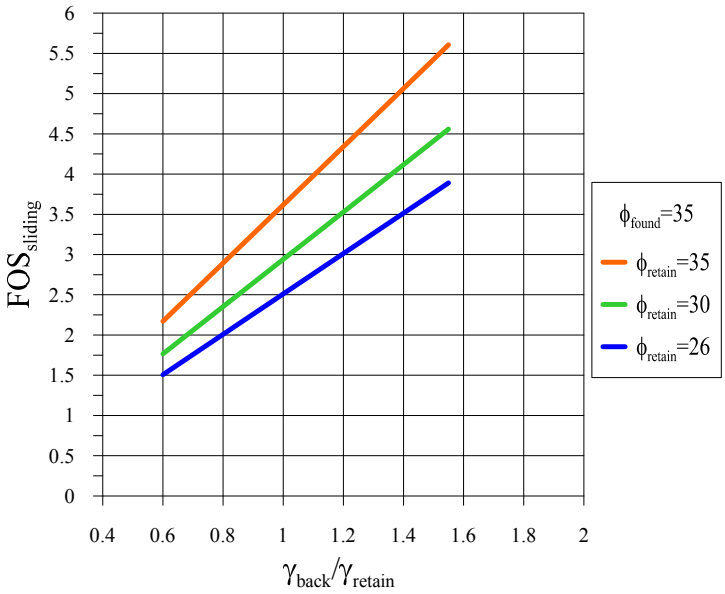

Figure 64. Factor of Safety against Sliding for 20 ft Wall Height with No Back Slope for Different $\phi_{retaining}$ at a Constant ϕ_{found}=35°.

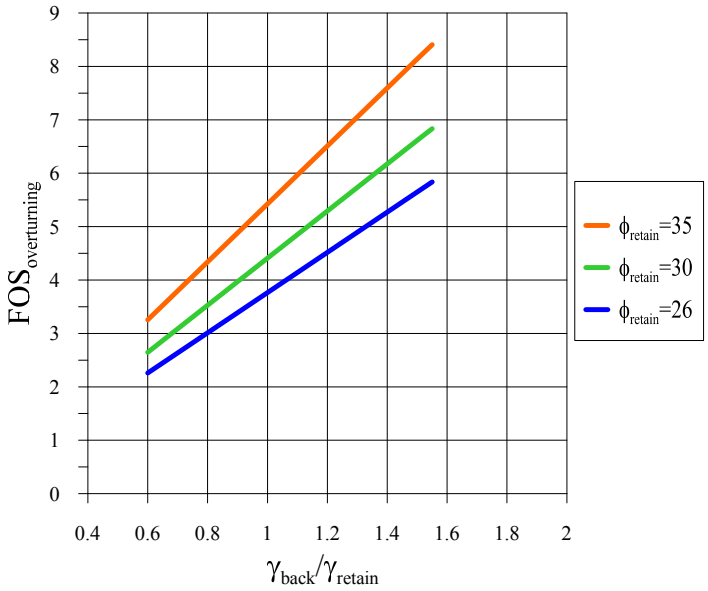

Figure 65. Factor of Safety against Overturning for 20 ft Wall Height with No Back Slope for Different $\phi_{retaining}$.

A detailed analysis of the influence of ϕ (retaining) and ϕ (foundation) on FOS for two different weights for retaining and backfill soils is plotted below. These plots shown in Figure 66-Figure 71 clearly demonstrates the effect of ϕ (foundation) on FOS.

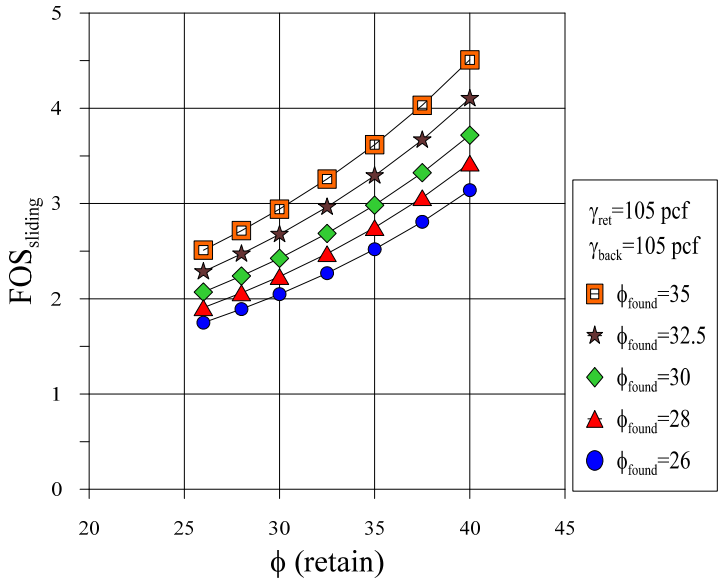

Figure 66. Factor of Safety against Sliding for 20 ft Wall Height with No Back Slope with γ_{ret}=105 pcf and γ_{back}=105 pcf for Different Friction Angles.

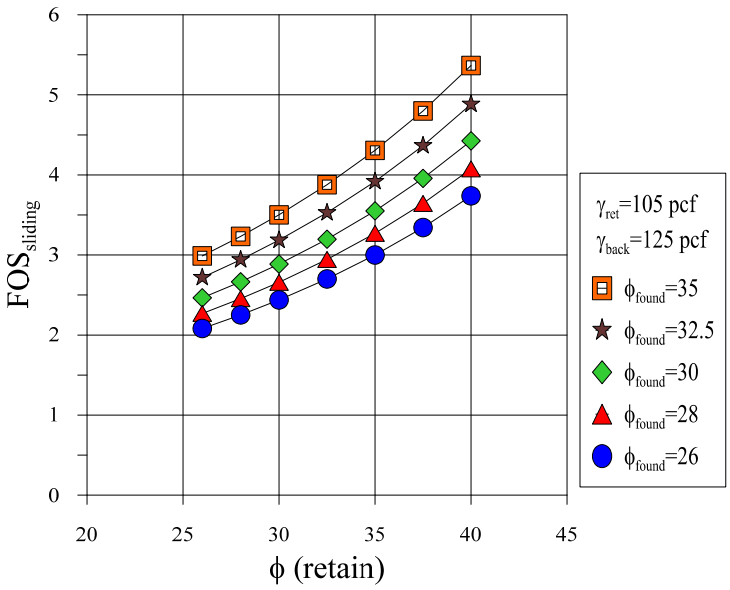

Figure 67. Factor of Safety against Sliding for 20 ft Wall Height with No Back Slope with γ_{ret}=105 pcf and γ_{back}=125 pcf for Different Friction Angles.

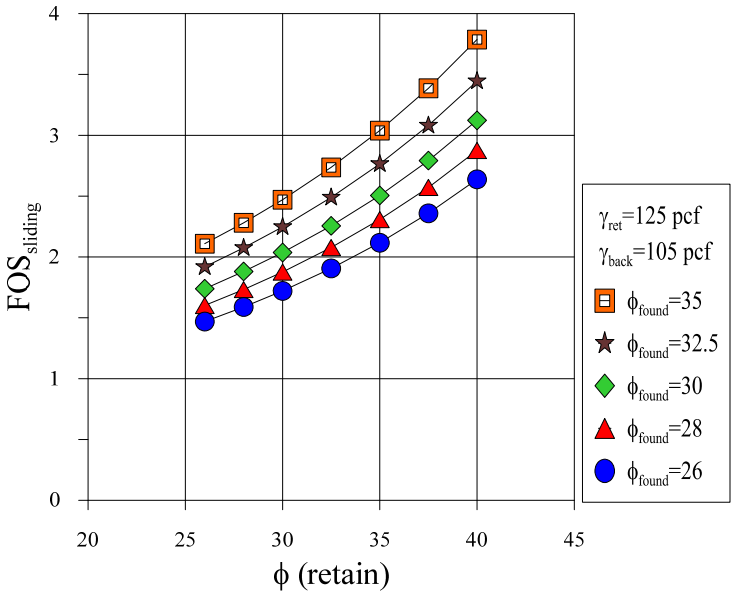

Figure 68. Factor of Safety against Sliding for 20 ft Wall Height with No Back Slope with γ_{ret}=125 pcf and γ_{back}=105 pcf for Different Friction Angles.

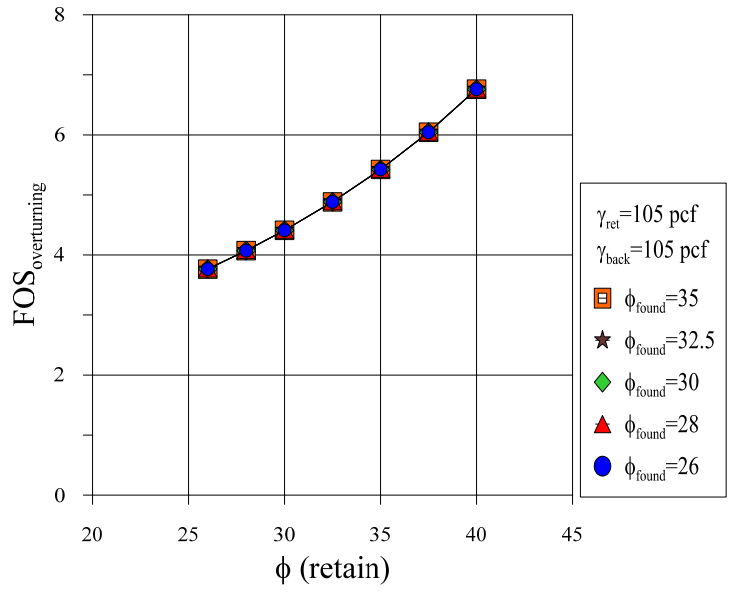

Figure 69. Factor of Safety against Overturning for 20 ft Wall Height with No Back Slope with γ_{ret}=105 pcf and γ_{back}=105 pcf for Different Friction Angles.

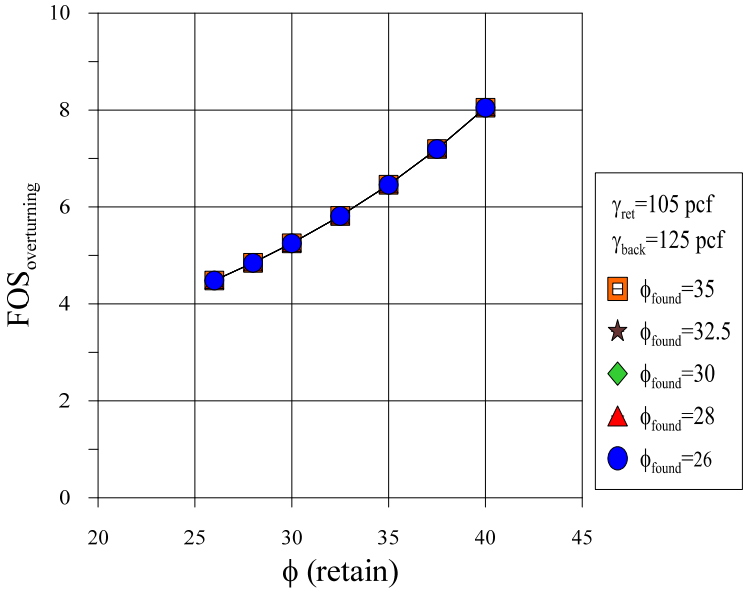

Figure 70. Factor of Safety against Overturning for 20 ft Wall Height with No Back Slope with γ_{ret}=105 pcf and γ_{back}=125 pcf for Different Friction Angles.

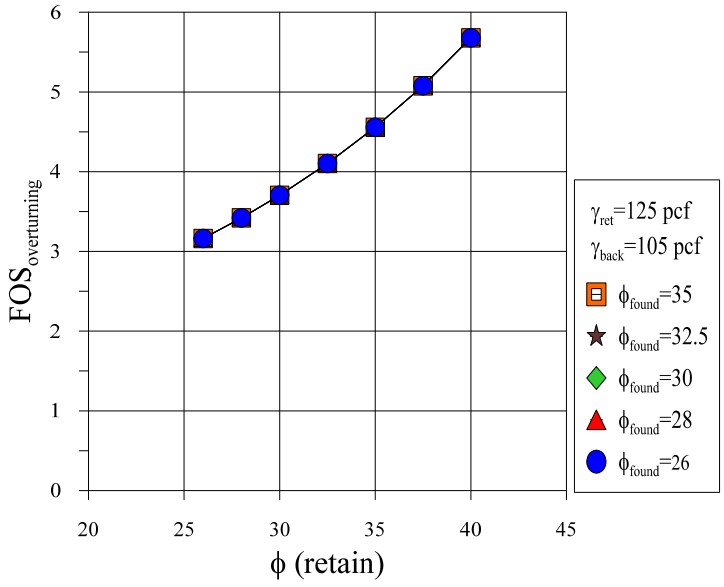

Figure 71. Factor of Safety against Overturning for 20 ft Wall Height with No Back Slope with γ_{ret}=125 pcf and γ_{back}=105 pcf for Different Friction Angles.

5.1.2 3H:1V Back Slope

Similarly, a parametric study was conducted on a MSE wall with 3H:1V back slope for a 20 ft wall height as shown in Figure 72. The results are presented below in Figure 73-Figure 76 for sliding analysis and overturning analysis with the same criterion used for no back slope case.

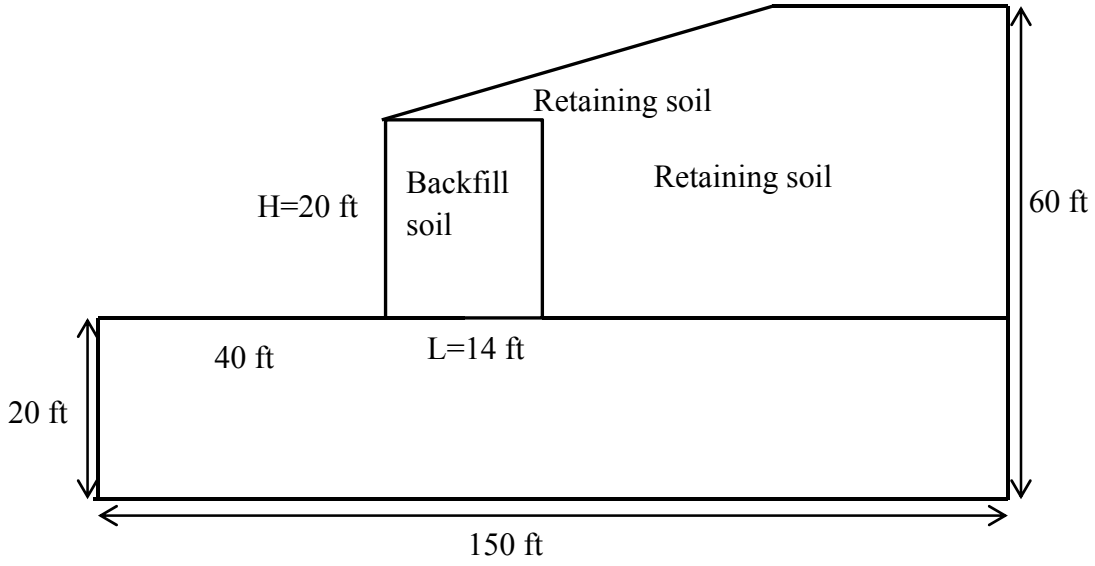

Figure 72. MSE Wall with 20 ft Wall and 3H:1V Back Slope.

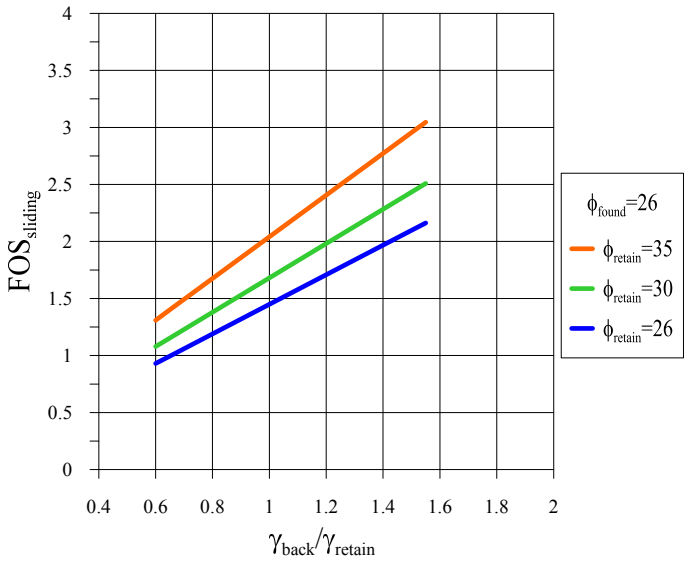

Figure 73. Factor of Safety against Sliding for 20 ft Wall Height with 3H:1V Back Slope for Different $\phi_{retaining}$ at a Constant ϕ_{found}=26°.

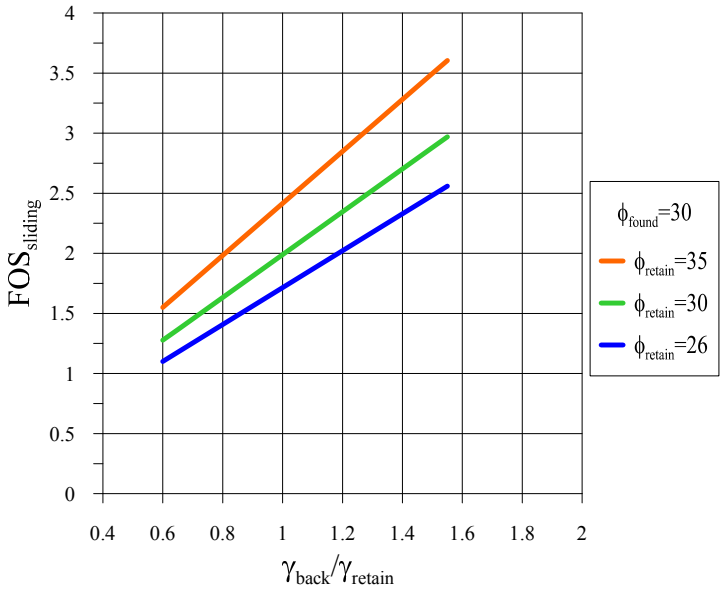

Figure 74. Factor of Safety against Sliding for 20 ft Wall Height with 3H:1V Back Slope for Different $\phi_{retaining}$ at a Constant ϕ_{found}=30°.

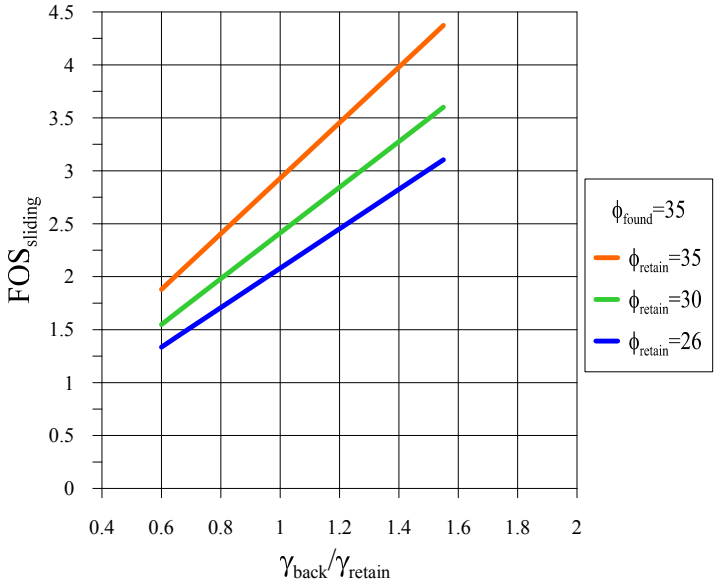

Figure 75. Factor of Safety against Sliding for 20 ft Wall Height with 3H:1V Back Slope for Different $\phi_{retaining}$ at a Constant ϕ_{found}=35°.

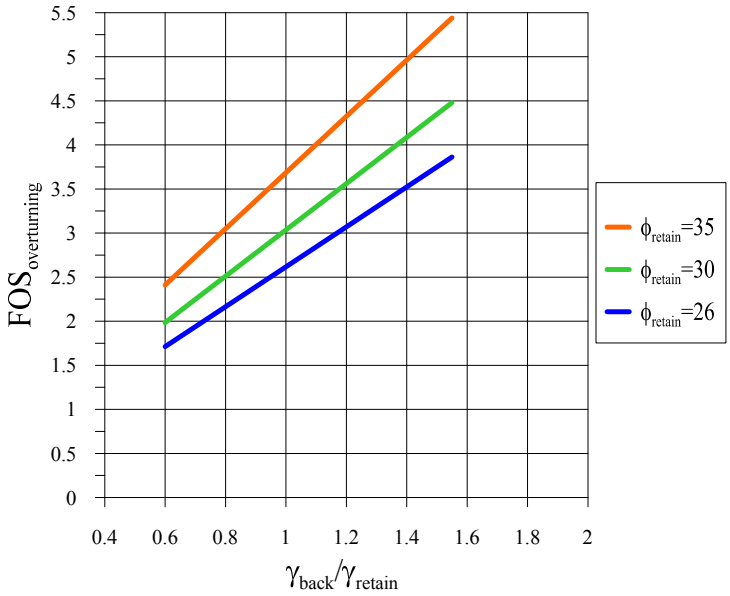

Figure 76. Factor of Safety against Overturning for 20 ft Wall Height with 3H:1V Back Slope for Different $\phi_{retaining}$.

Similarly, a detailed analysis is carried out as it was done for horizontal back slope case to the see the effect of ϕ foundation and ϕ retained on FOS sliding and overturning. The results from this detailed analysis is shown in Figure 77-Figure 82

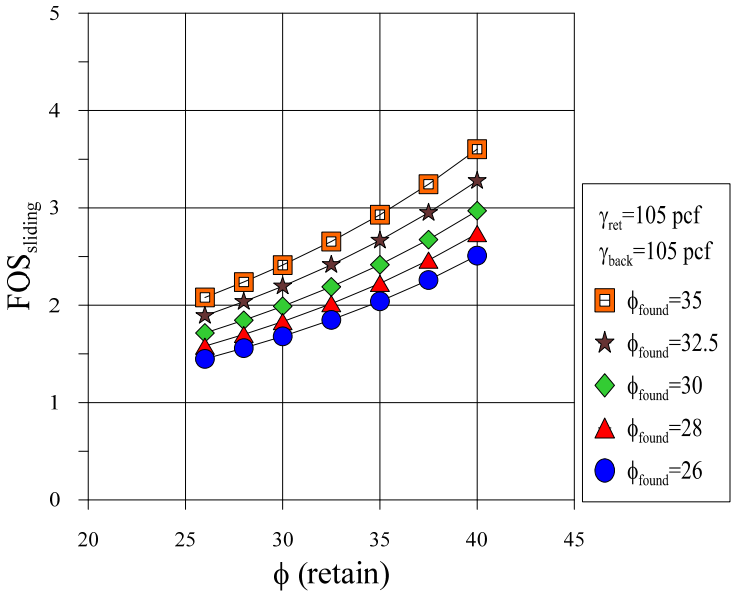

Figure 77. Factor of Safety against Sliding for 20 ft Wall Height with 3H:1V Back Slope with γ_{ret}=105 pcf and γ_{back}=105 pcf for Different Friction Angles.

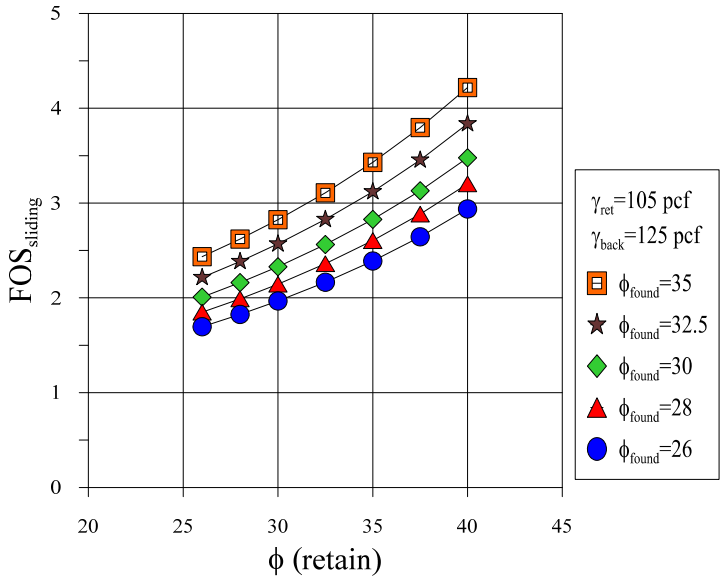

Figure 78. Factor of Safety against Sliding for 20 ft Wall Height with 3H:1V Back Slope with γ_{ret}=105 pcf and γ_{back}=125 pcf for Different Friction Angles.

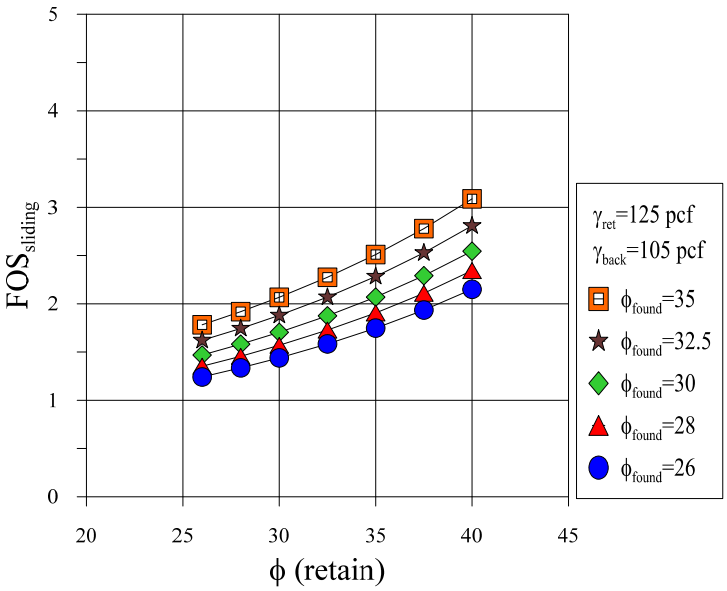

Figure 79. Factor of Safety against Sliding for 20 ft Wall Height with 3H:1V Back Slope with γ_{ret}=125 pcf and γ_{back}=105 pcf for Different Friction Angles.

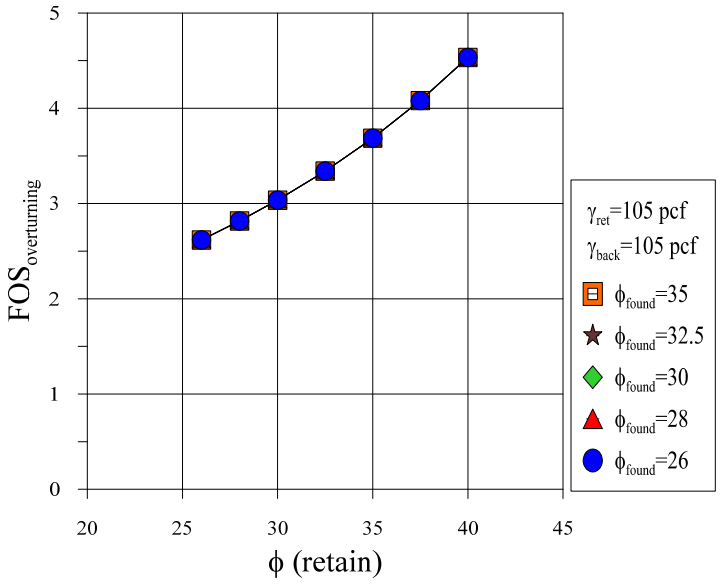

Figure 80. Factor of Safety against Overturning for 20 ft Wall Height with 3H:1V Back Slope with γ_{ret}=105 pcf and γ_{back}=105 pcf for Different Friction Angles.

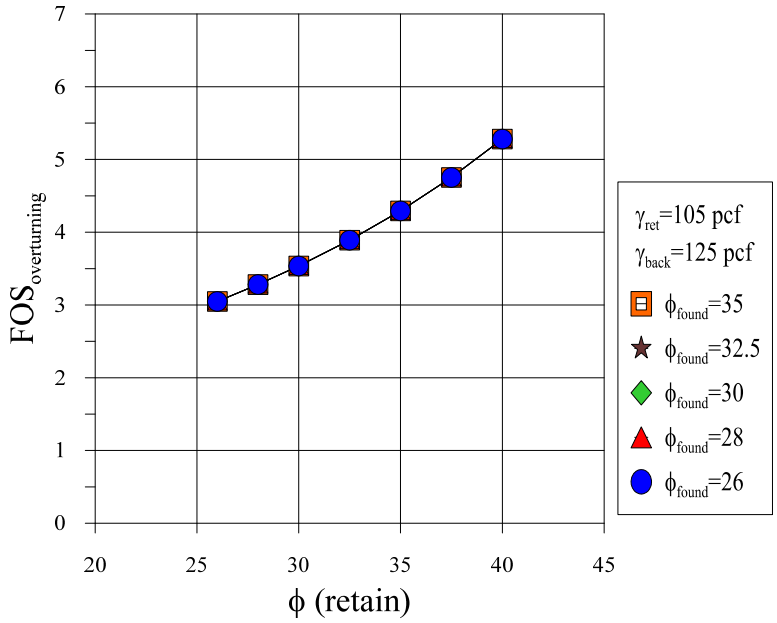

Figure 81. Factor of Safety against Overturning for 20 ft Wall Height with 3H:1V Back Slope with γ_{ret}=105 pcf and γ_{back}=125 pcf for Different Friction Angles.

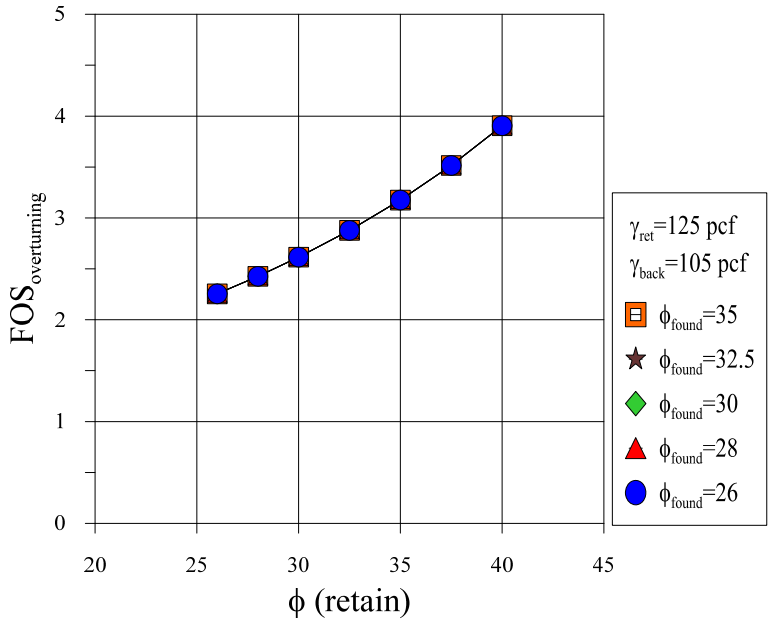

Figure 82. Factor of Safety against Overturning for 20 ft Wall Height with 3H:1V Back Slope with γ_{ret}=125 pcf and γ_{back}=105 pcf for Different Friction Angles.

5.1.3 Conclusion

The results from the above cases shows that it is important to consider the effect of unit weight of backfill and retaining soils on FOS calculations.

- Increasing γ_{back} from 105 pcf to 125 pcf with γ_{ret} maintained at a constant value of 105 pcf increases the FOS against sliding by 19 percent and FOS against overturning by 19 percent for the case of a wall height of 20 ft with no back slope.
- Increasing γ_{ret} from 105 pcf to 125 pcf with γ_{back} maintained at a constant value of 105 pcf decreases the FOS against sliding and FOS against sliding by 16 percent for the case of a wall height of 20ft with no back slope.

- For a wall height of 20 ft and 3H:1V back slope, increasing the unit weight of backfill from 105 pcf to 125 pcf increases the FOS against sliding by 17 percent and the FOS against overturning by 16.5 percent as compared to assigning same unit weights for both types of soils.
- For a wall height of 20 ft and 3H:1V back slope, the FOS against sliding decreases by 14.3 percent and the FOS against overturning decreases by 13.9 percent when the unit weight of the retained soil is increased from 105 pcf to 125 pcf with a constant backfill unit weight of 105 pcf.

  In general, the ratio $\gamma_{back}/\gamma_{retain}$ has a significant influence on FOS for sliding as well as overturning.

5.2 Parametric Study Using FLAC Simulations

5.2.1 Analysis for Pure Frictional Soils

The FLAC simulations are performed for two different geometries and for two different soil types via sands and clays. This section describes the model parameters used two different wall types and the effect of variation of material parameters.

5.2.1.1 Model Geometry

A total of three wall geometries are considered for this parametric study as shown in Figure 83-Figure 85. First, two 20-ft walls are considered, one with no back slope and the other with 3H:1V back slope. In addition, a 10-ft wall with no back slope is analyzed. The figures below show the three walls analyzed. All walls are use 5-ft panel heights. For the 20 ft wall the length of reinforcement is 14 ft (0.7H), and for 10 ft

wall an 8 ft reinforcement length is used (AASHTO). The embedment depth was taken as zero for this study, recognizing that the results will be slightly conservative.

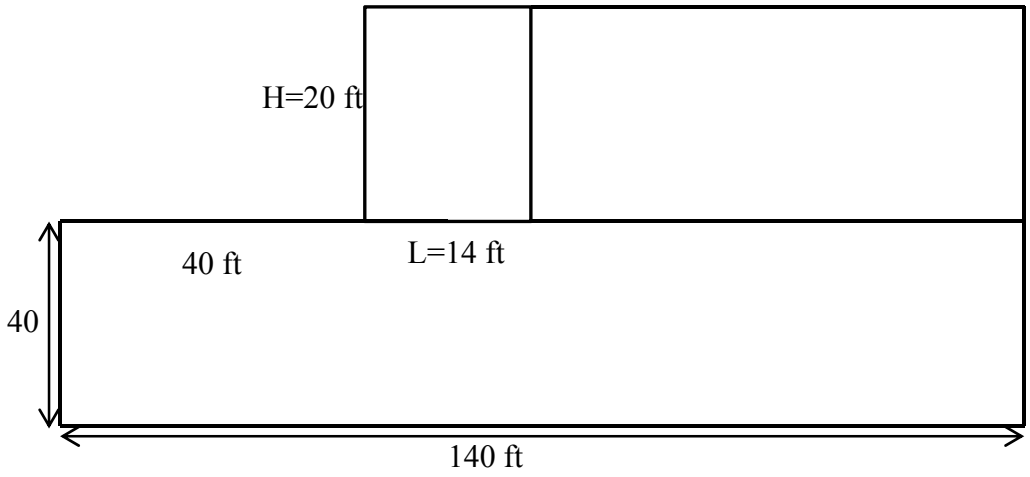

Figure 83. MSE Wall with 20 ft Wall Height and No Back Slope Model Geometry for FLAC.

The dimensions shown above in Figure 83 are used for FLAC simulation for 20 ft wall height. The 90-ft width of model was judged to be sufficiently large to minimize boundary effects. The depth of foundation was taken as twice the wall height, again, to minimize boundary effects. The selected grid size was 0.5 ft in y-direction and 1 ft in x-direction. The grid density was judged fine enough for this MSE wall model.

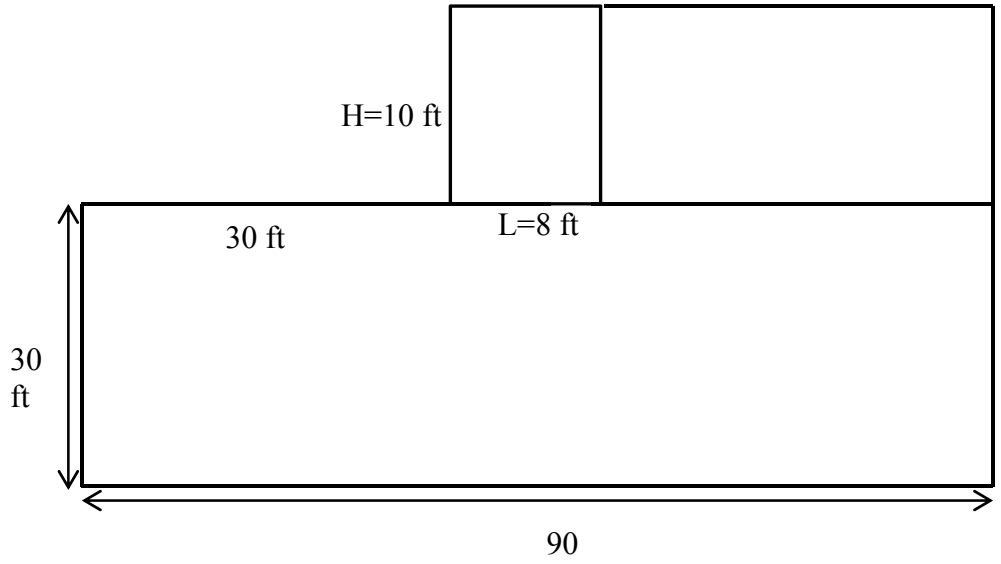

Figure 84. MSE Wall with 10 ft Wall Height and No Back Slope.

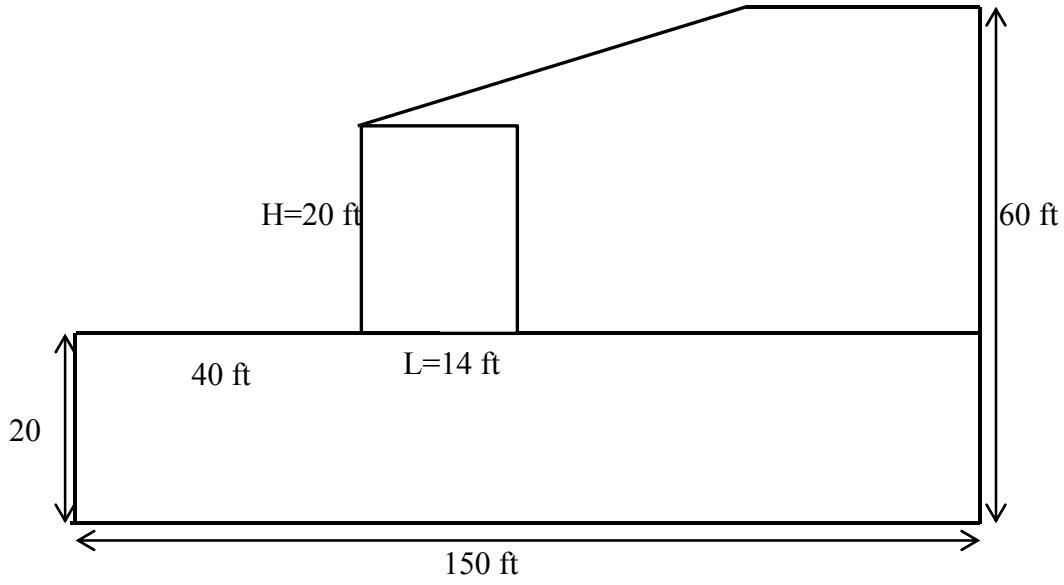

Figure 85. MSE Wall with 20 ft Wall and 3H:1V Back Slope.

These figures show dimensions used for the wall geometries used in the FLAC simulations to calculate stresses at the back boundary of the backfill and at the base of

MSE wall. Stresses calculated from FLAC are used to compute design parameters that are used to calculate FOS for sliding and comparing these parameters with AASHTO design AASHTO (2002).

5.2.1.2 Material Parameters

The soil model used in this study is Mohr-Coulomb model for backfill, retaining wall, and for foundation soils. Table 30 lists the properties for these soils. The model was run with a dilation angle and without a dilation angle to see the effect on stresses and on FOS. The dilation angle values used in this parametric study was 10°. Friction properties for retaining soils and foundation soils are modified as shown in Table 31 for each case to see the effect of foundation soil on sliding friction as well as an effect of retaining soils on base friction.

Table 30. Material Properties for Frictional Backfill, Retaining Materials and Frictional Foundation Material.

Type	Elastic modulus* (psf)	Bulk modulus (psf)	Shear modulus (psf)	ν (Poisson's ratio)	ϕ
Foundation	2.116 E6	3.643 E6	0.364 E6	0.4516	26
					28
					30
					32.5
	4.232 E6	7.287 E6	0.728 E6	0.4516	35
Retaining	2.116 E6	3.643 E6	0.364 E6	0.4516	26
					28
					30
					32.5
	4.232 E6	7.287 E6	0.728 E6	0.4516	35
					37.5
					40
Backfill	4.232 E6	7.287 E6	0.728 E6	0.4516	34

* Elastic modulus for sand is taken as $1000*P_{atm}$ where P_{atm}=2116.216 psf (Kulhawy and Mayne 1990)

Table 31. Matrix of Properties Changed in FLAC Simulation for Three Different Wall Types.

		MSE wall with backfill ϕ=34°, γ=105 pcf						
		ϕ(retain)						
		26	28	30	32.5	35	37.5	40
ϕ (found)	26	x	x	x	x	x	x	x
	28	x	x	x	x	x	x	x
	30	x	x	x	x	x	x	x
	32.5	x	x	x	x	x	x	x
	35	x	x	x	x	x	x	x

5.2.1.3 Boundary Conditions

The boundary conditions for all three wall geometries are as follows. Zero displacement is imposed in the x and y directions at the base of model, and in the x direction on both sides of the model. MSE wall panels used in this model are 5 ft high, and zero relative displacement is imposed at the junctions between the panels. Each panel has three strips in the vertical direction (i.e., y direction) and two strips in the horizontal direction (i.e., z direction) for a total of six strips per panel. The spacing for these strips is shown in Figure 86. The wall is constructed without embedment to simplify the stress calculations. The length for strips used in this model is 14 ft (i.e., 0.7H) for 20 ft wall and 8 ft for 10 ft wall height.

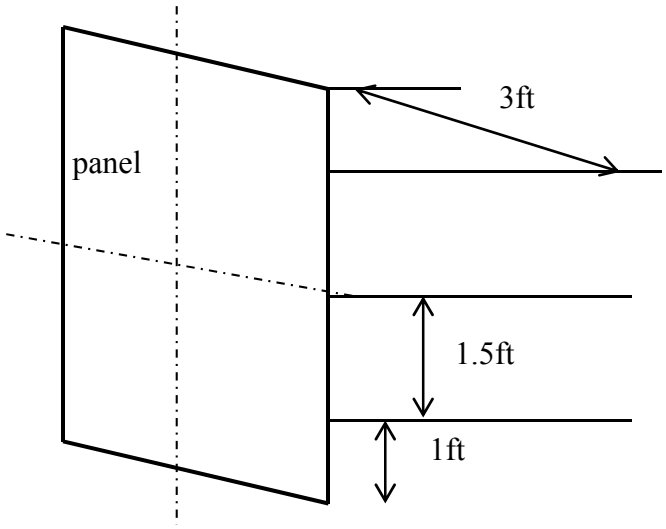

Figure 86. Strips Spacing for Each Panel of MSE Wall.

5.2.1.4 FLAC Calculation Process

Each analysis is solved in stages to simulate the construction sequence for an actual MSE wall. First a foundation layer is solved for equilibrium conditions under gravity loads and then the first MSE wall layer is added and solved for same loads for equilibrium condition. This sequence is continued to build 20 ft wall in 4 layers and 10 ft wall in 2 layers. Once the wall is solved for equilibrium conditions, the model was solved for failure condition by reducing the strength of material. In this case, strength was reduced by reducing a friction value from the assigned value to a minimum friction value to have a failure displacement.

$$FOS\ flac\ = \frac{\tan(\phi)eq}{\tan(\phi)f} \qquad \text{(Eq. 27)}$$

Figure 87–Figure 92 show FOSs calculated from FLAC for three types of walls with and without dilation angle. After solving for the equilibrium and failure states, the

stresses generated in x and y direction are recorded for entire model. Stresses at the base of wall and between retain and backfill were used to find the total forces acting on the wall as well as to calculate design parameters. A total of 210 cases were solved for both equilibrium and failure conditions.

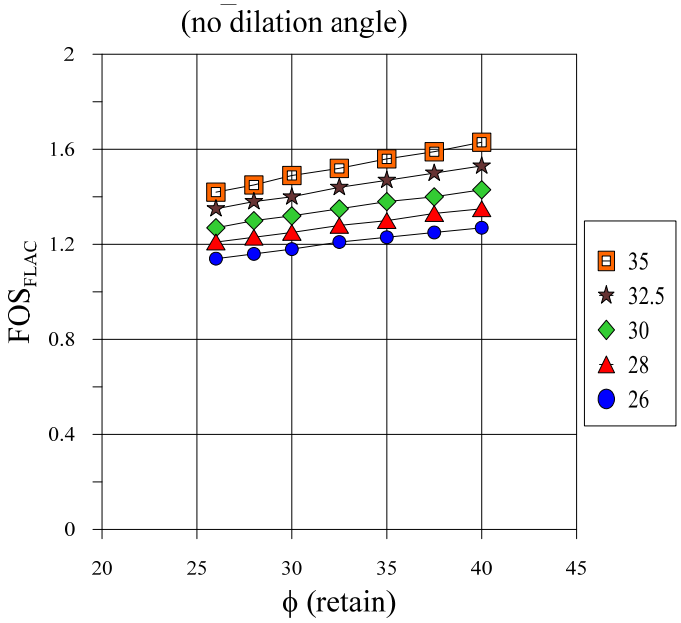

Figure 87. FLAC FOS with Respect to ϕ (Retain) for 10 ft Wall Height with No Dilation Angle.

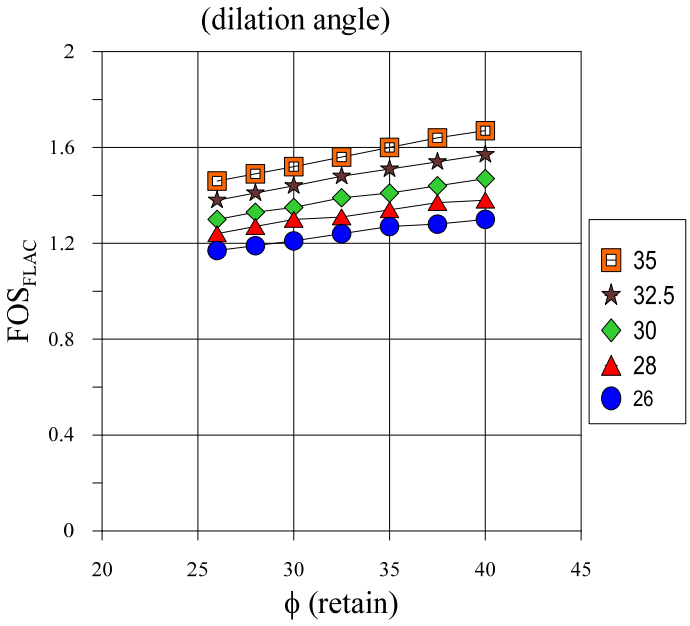

Figure 88. FLAC FOS with Respect to ϕ (Retain) for 10 ft Wall Height with Dilation Angle.

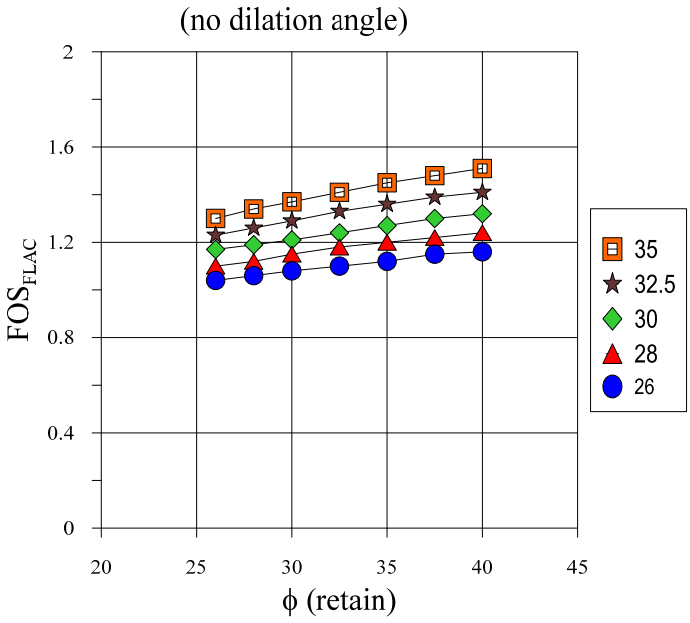

Figure 89. FLAC FOS with Respect to ϕ (Retain) for 20 ft Wall Height with No Dilation Angle.

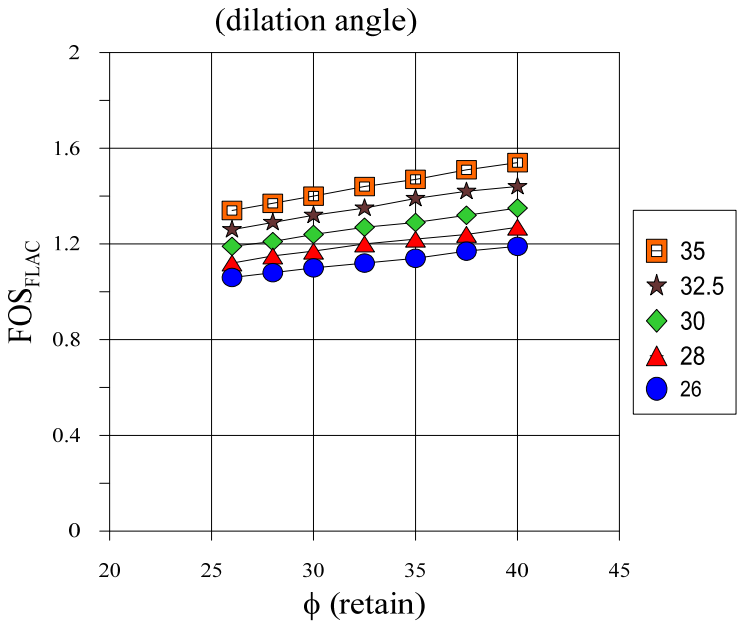

Figure 90. FLAC FOS with Respect to ϕ (Retain) for 20 ft Wall Height with Dilation Angle.

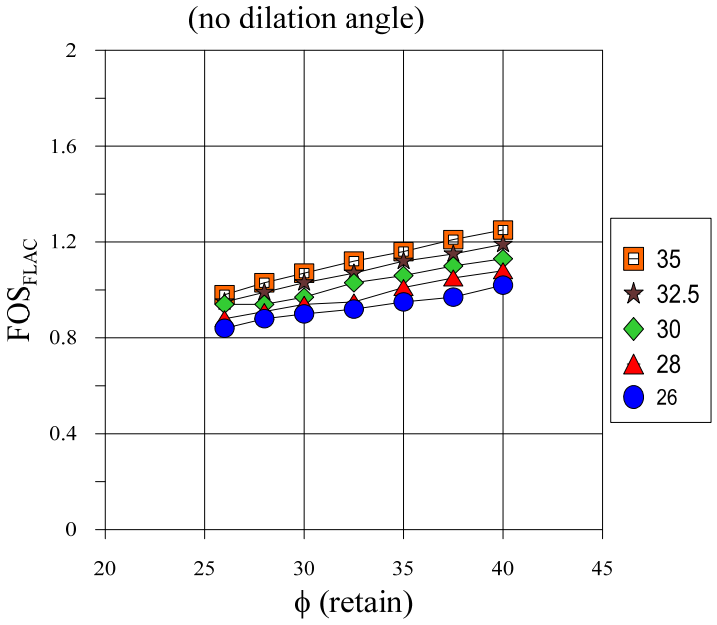

Figure 91. FLAC FOS with Respect to ϕ (Retain) for 20 ft Wall Height with 3H:1V Back Slope with No Dilation Angle.

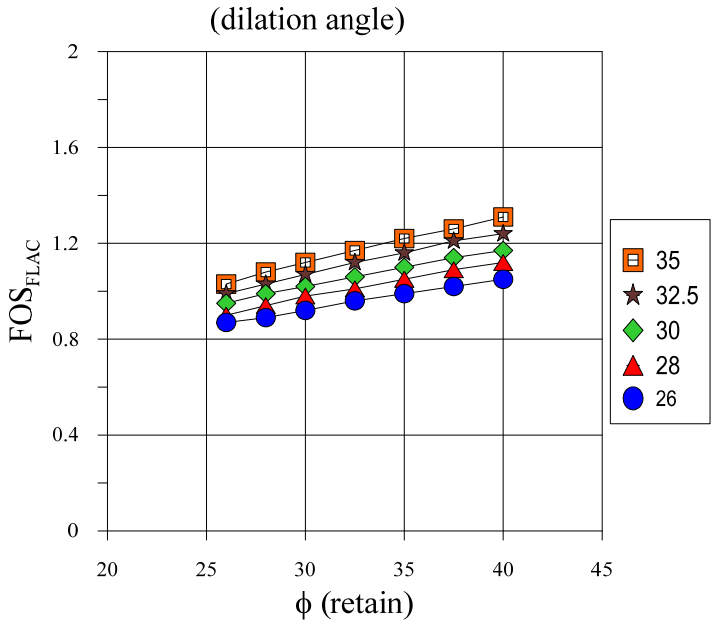

Figure 92. FLAC FOS with Respect to ϕ (Retain) for 20 ft Wall Height with 3H:1V Back Slope with Dilation Angle.

5.2.1.5 Calculation of Modified Design Parameters from FLAC Simulation

The stresses generated at failure conditions were used to find forces acting on the wall and used to find apparent design parameters such as apparent K_a (active earth coefficient), δ_w (wall friction of angle), δ_b (base friction of angle), and comparing them with design parameters recommended by AASHTO (2002).

The stresses used to find forces are integrated by Simpson's numerical integration rules. The following equations are used to find apparent design parameters. Total horizontal force, vertical force, and shear forces were calculated. The Figure 93 shows the direction at which forces are acting on the wall.

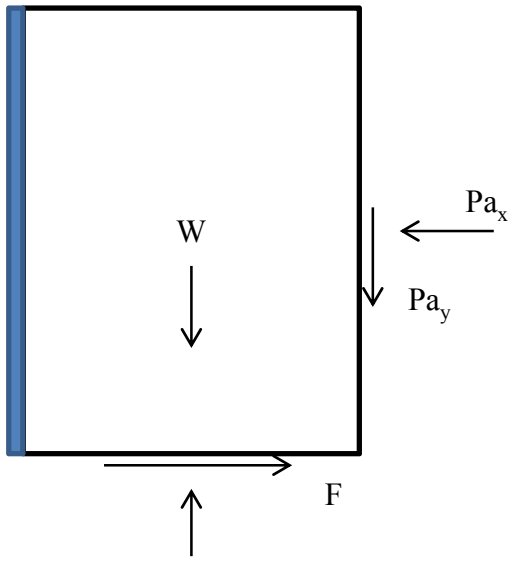

Figure 93. Free Body Diagram of Forces Acting on MSE Wall.

$$W = \gamma \times L \times H \quad \text{(Eq. 28)}$$

$$N = \int_0^L \sigma yy \, dx \quad \text{(Eq. 29)}$$

$$F = \int_0^L \sigma xy \, dx \quad \text{(Eq. 30)}$$

$$Pa_x = \int_0^H \sigma xx \, dx \quad \text{(Eq. 31)}$$

$$Pa_y = \int_0^H \sigma xy \, dx \quad \text{(Eq. 32)}$$

$$K_{a\ app} = \frac{Pax}{\frac{1}{2}\gamma \times L^2} \text{ (since } Pa = \frac{1}{2} Ka \times \gamma \times L^2) \quad \text{(Eq. 33)}$$

$$\delta_b = \tan^{-1}\left(\frac{F}{N}\right) \quad \text{(Eq. 34)}$$

$$\delta_w = \tan^{-1}\left(\frac{Pay}{Pax}\right) \quad \text{(Eq. 35)}$$

5.2.1.6 Results

Figure 94–Figure 99 show parameters starting with the apparent K_a deduced from the FLAC analyses to with the Rankine K_a for the case of zero back slope and the Coulomb K_a for the case of a back slope. The initial analysis series used no dilation angle. This was followed by a series of analyses using a dilation angle of 10°.

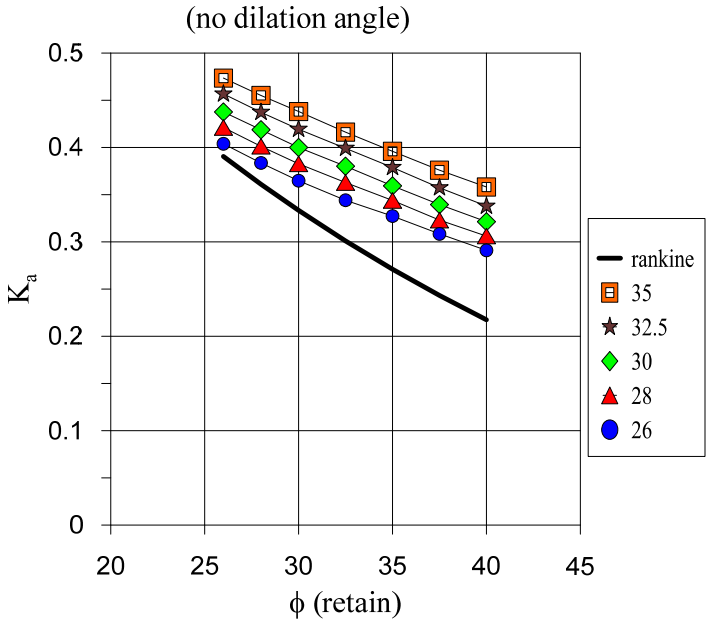

Figure 94. K_a FLAC Comparison with K_a_Rankine for Different ϕ (Retain) for 10 ft Wall Height with No Dilation Angle.

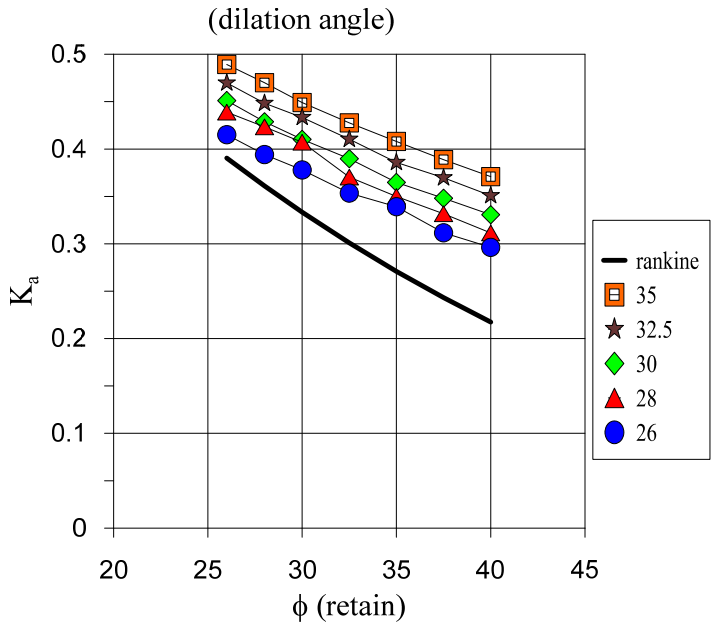

Figure 95. K_a_FLAC Comparison with K_a_Rankine for Different ϕ (Retain) for 10 ft Wall Height with Dilation Angle.

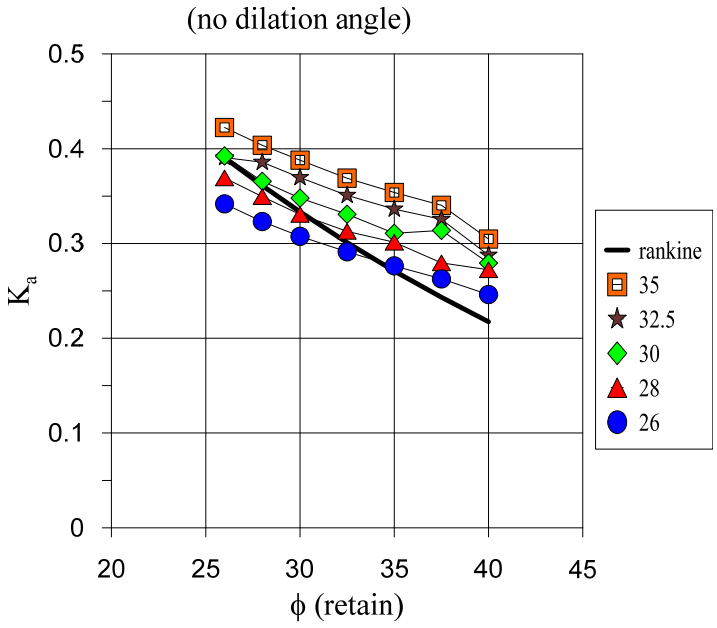

Figure 96. K_a_FLAC Comparison with K_a_Rankine for Different ϕ (Retain) for 20 ft Wall Height with No Dilation Angle.

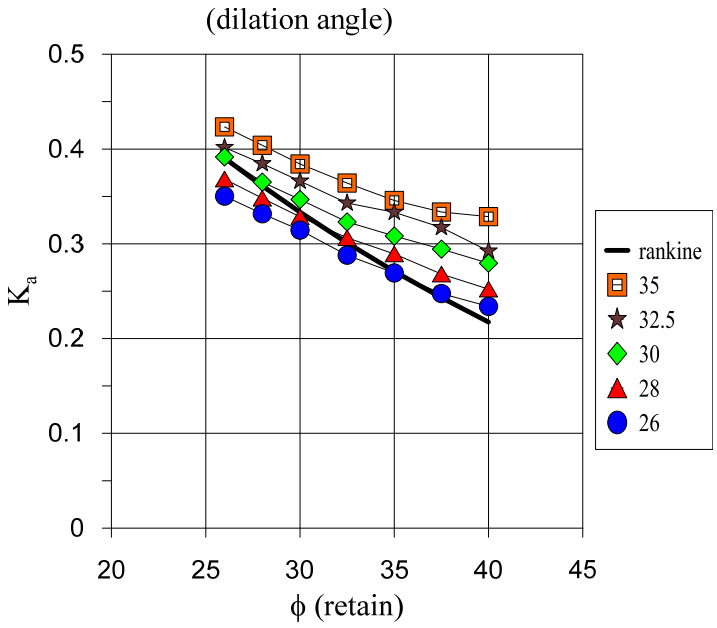

Figure 97. K_a_FLAC Comparison with K_a_Rankine for Different ϕ (Retain) for 20 ft Wall Height with Dilation Angle.

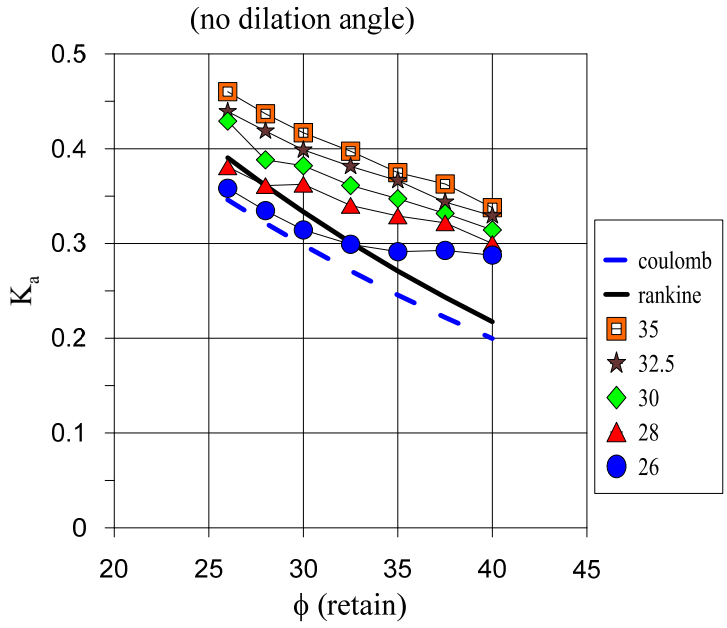

Figure 98. K_a_FLAC Comparison with K_a_Rankine for Different ϕ (Retain) for 20 ft Wall Height with 3H:1V Back Slope with No Dilation Angle.

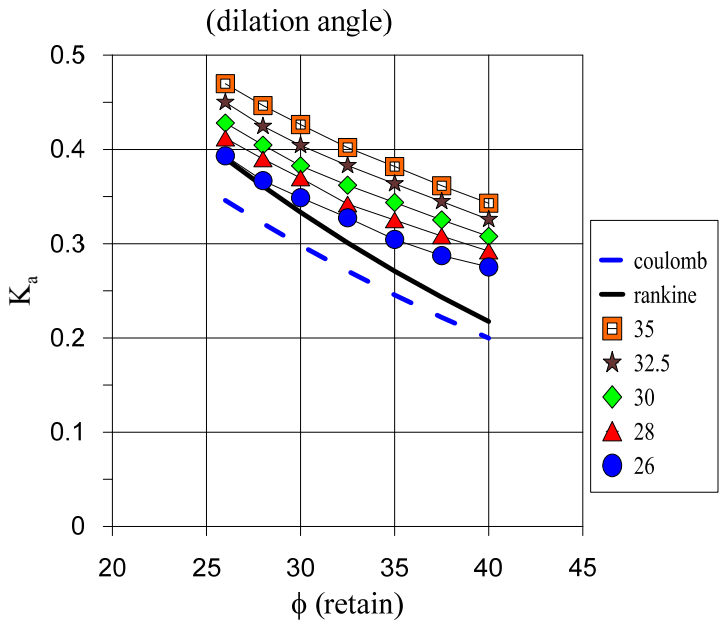

Figure 99. K_a_FLAC Comparison with K_a_Rankine for Different ϕ (Retain) for 20 ft Wall Height with 3H:1V Back Slope with Dilation Angle.

Once the K_a from FLAC simulation was calculated, the apparent interface friction was also calculated for same wall height and same parameters as mentioned earlier with using Eq. 35. The Figure 100–Figure 111 present the results for different cases.

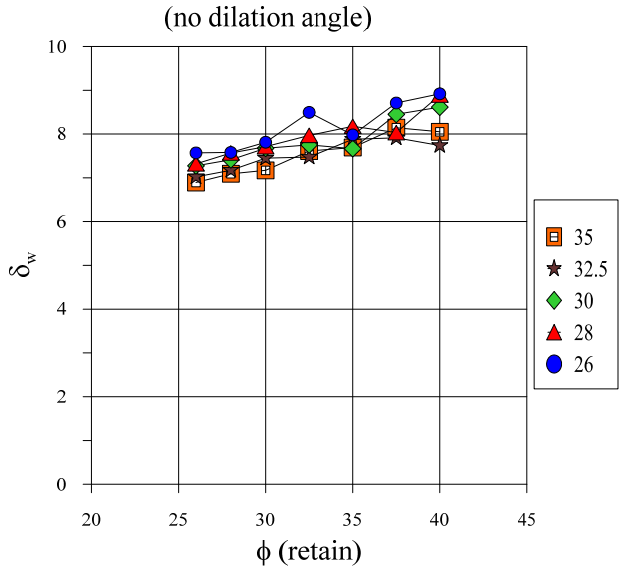

Figure 100. δ_w for Different ϕ (Retain) for 10 ft Wall Height with No Dilation Angle.

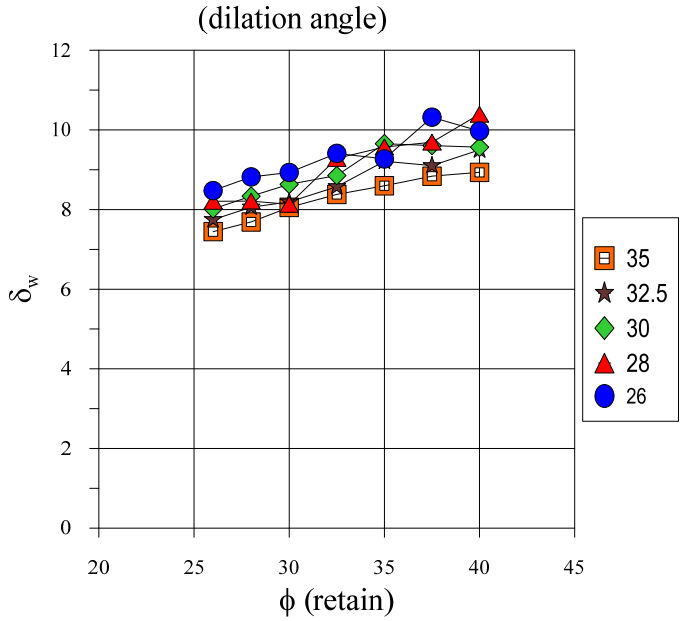

Figure 101. δ_w for Different ϕ (Retain) for 10 ft Wall Height with Dilation Angle.

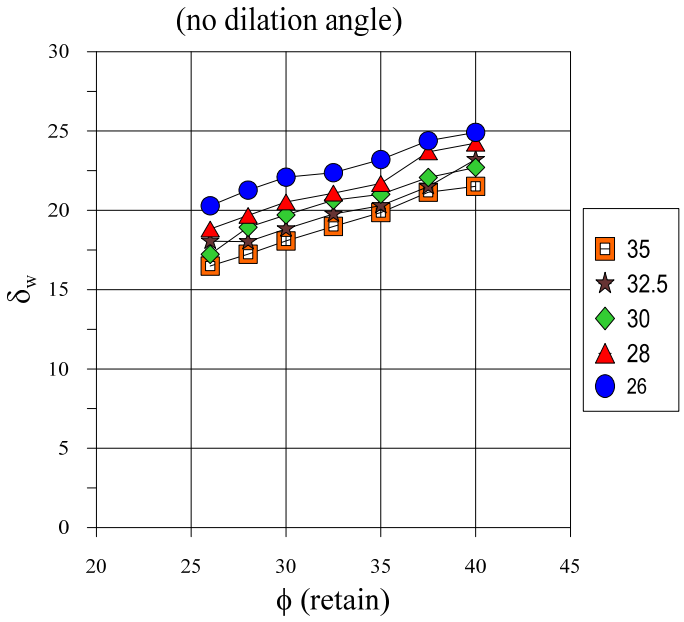

Figure 102. δ_w for Different ϕ (Retain) for 20 ft Wall Height with No Dilation Angle.

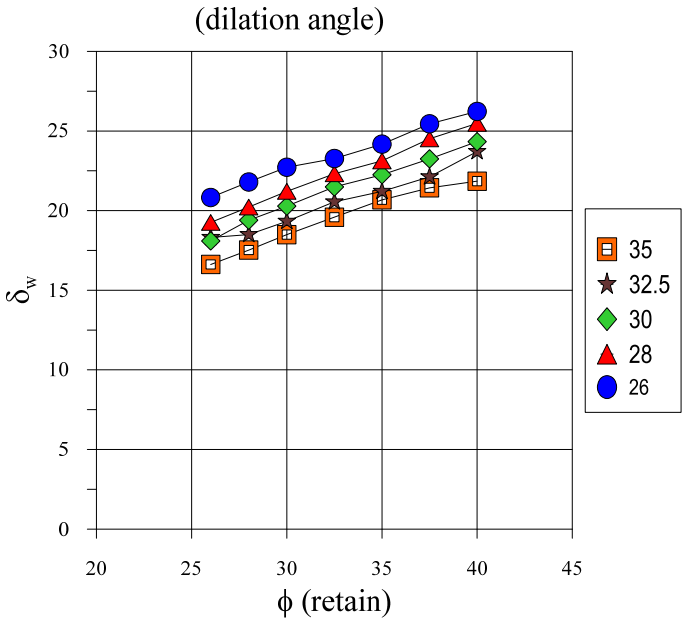

Figure 103. δ_w for Different ϕ (Retain) for 20 ft Wall Height with Dilation Angle.

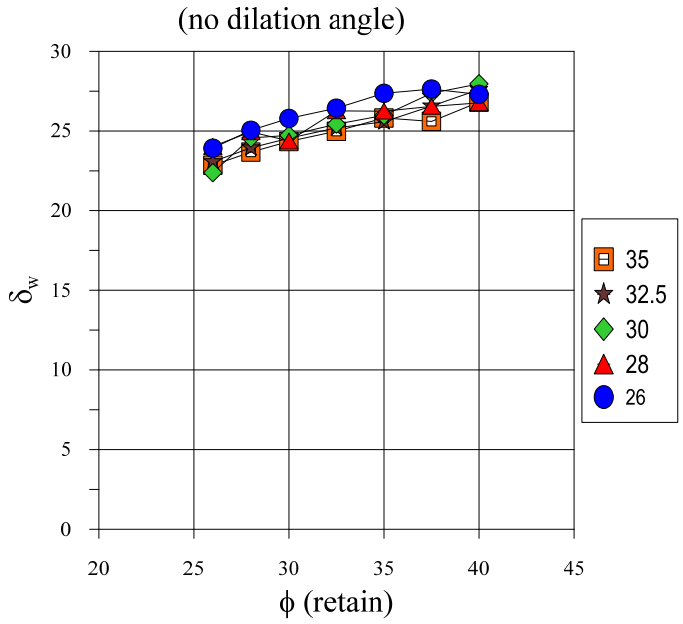

Figure 104. δ_w for Different ϕ (Retain) for 20 ft Wall Height with 3H:1V Back Slope with No Dilation Angle.

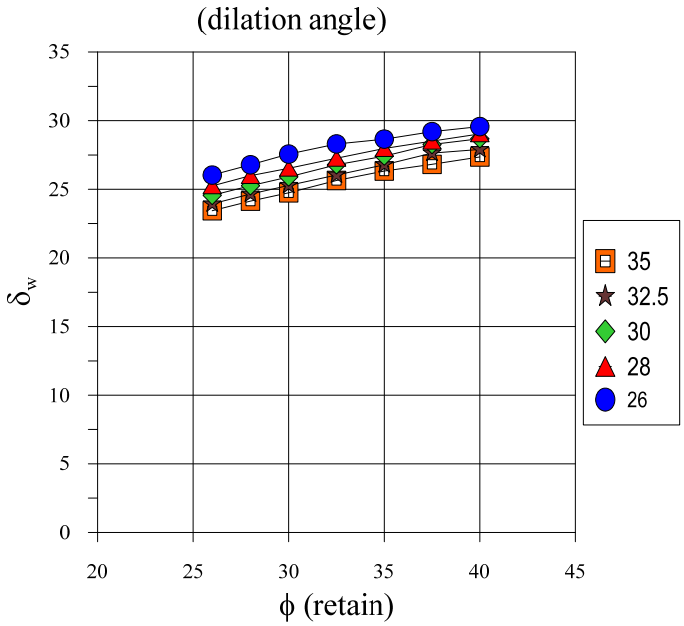

Figure 105. δ_w for Different ϕ (Retain) for 20 ft Wall Height with 3H:1V Back Slope with Dilation Angle.

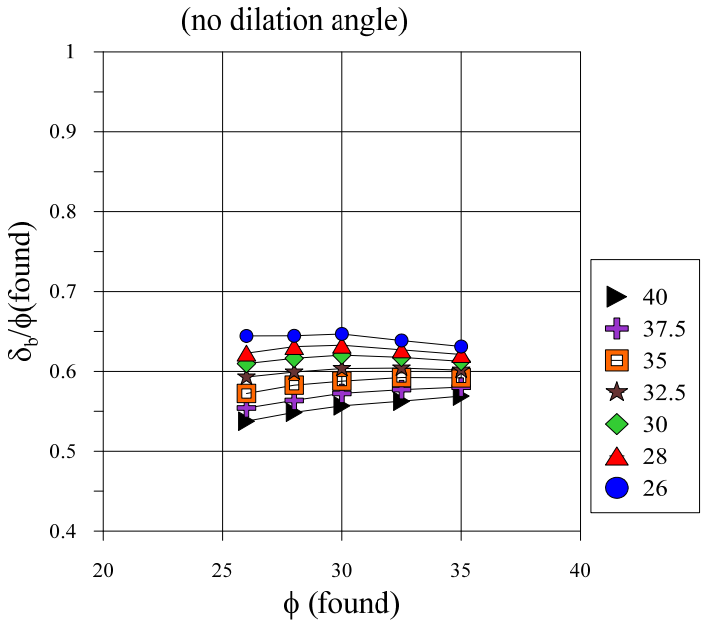

Figure 106. δ_b/ϕ (Found) for Different ϕ (Found) for 10 ft Wall Height with No Dilation Angle.

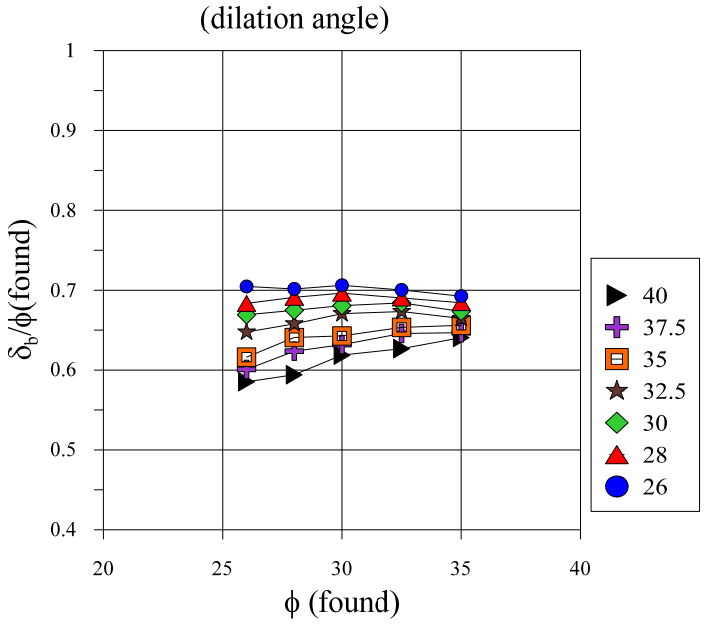

Figure 107. δ_b/ϕ (Found) for Different ϕ (Found) for 10 ft Wall Height with Dilation Angle.

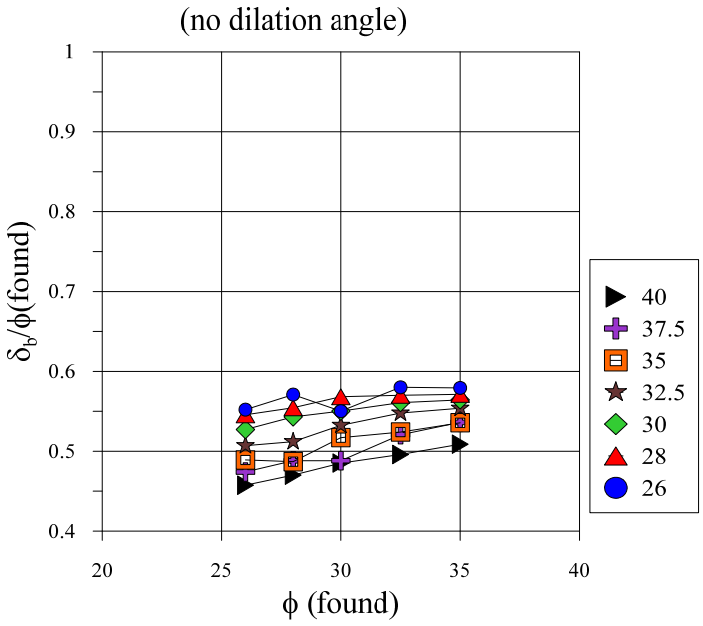

Figure 108. δ_b/ϕ (Found) for Different ϕ (Found) for 20 ft Wall Height with No Dilation Angle.

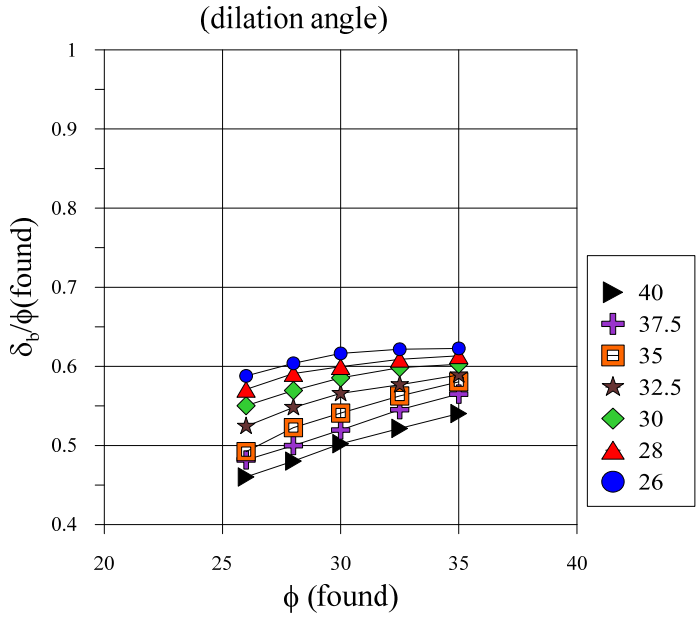

Figure 109. δ_b/ϕ (Found) for Different ϕ (Found) for 20 ft Wall Height with Dilation Angle.

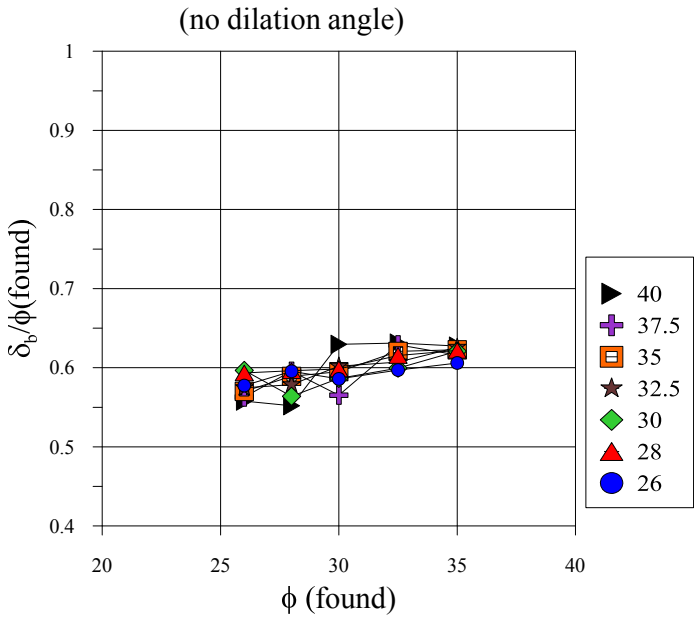

Figure 110. δ_b/ϕ (Found) for Different ϕ (Found) for 20 ft Wall Height with 3H:1V Back Slope with No Dilation Angle.

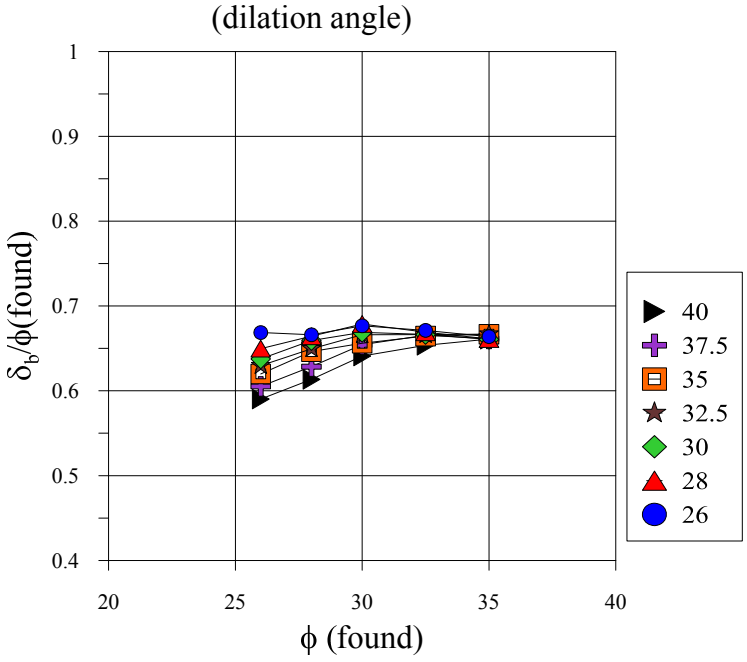

Figure 111. δ_b/ϕ (Found) for Different ϕ (Found) for 20 ft Wall Height with 3H:1V Back Slope with No Dilation Angle.

The design parameters calculated from FLAC analysis were used to find FOSs against sliding by the following steps. These steps are same as mentioned in AASHTO (2002) design manual for MSE walls, the only difference is that δ_b in the calculations are from a FLAC analysis. The results are shown in Figure 112-Figure 117 for different geometries and parameters.

- Calculate the driving force acting on the wall using K_a rankine for no back slope and K_a Coulomb for 3H:1V back slope.

$$F_{driving} = \frac{1}{2} K_a \times \gamma \times H^2 \quad \text{(Eq. 36)}$$

- Use δ_b from FLAC analysis to find resisting force from base of wall.

$$F_{resisting} = W \times tan\delta_b \quad \text{(Eq. 37)}$$

$$W = \gamma \times L \times H \quad \text{(Eq. 38)}$$

$$FOS_{Sliding} = \frac{F_{resisting}}{F_{driving}} \quad \text{(Eq. 39)}$$

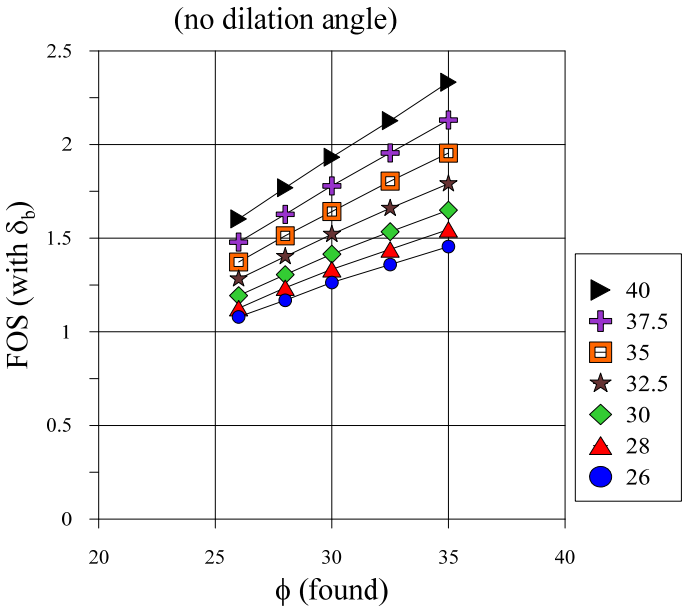

Figure 112. FOS Calculated with δ_b from FLAC for Different ϕ (Found) for 10 ft Wall Height with No Dilation Angle.

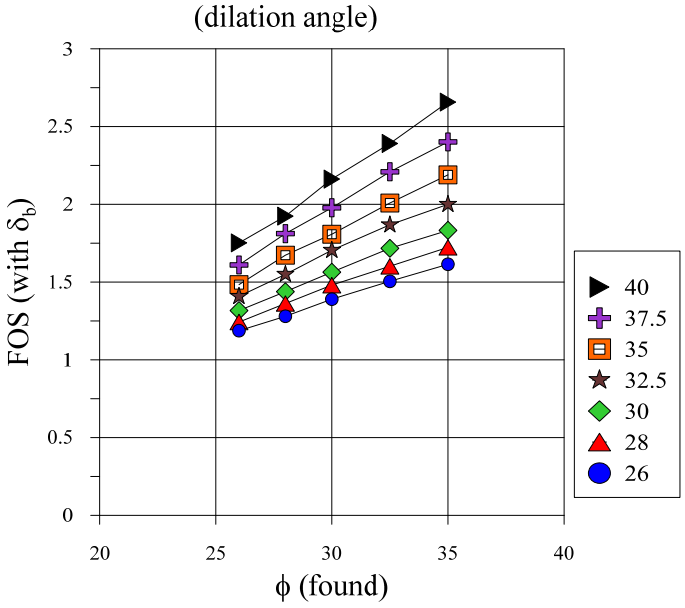

Figure 113. FOS Calculated with δ_b from FLAC for Different ϕ (Found) for 10 ft Wall Height with Dilation Angle.

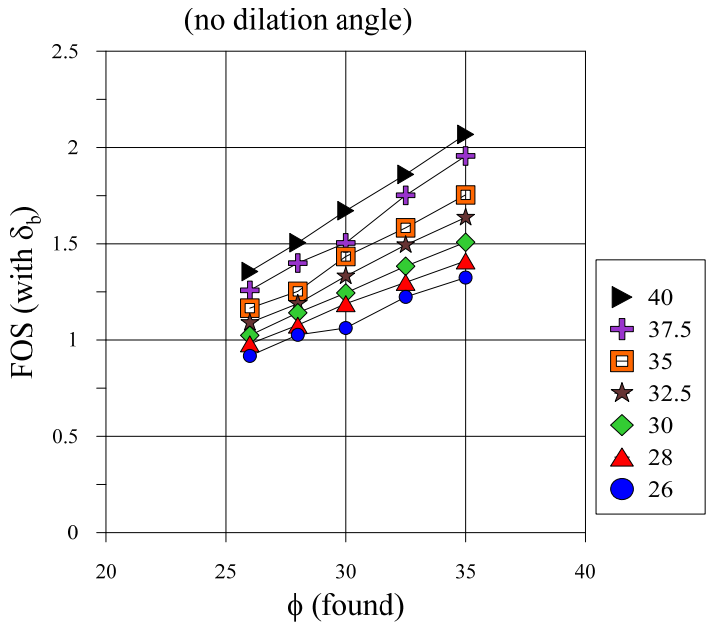

Figure 114. FOS Calculated with δ_b from FLAC for Different ϕ (Found) for 20 ft Wall Height with No Dilation Angle.

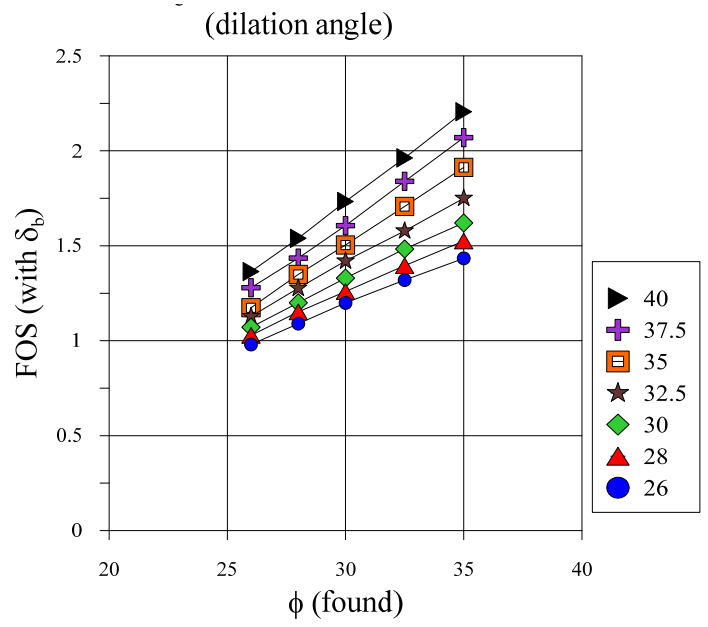

Figure 115. FOS Calculated with δ_b from FLAC for Different ϕ (Found) for 20 ft Wall Height with Dilation Angle.

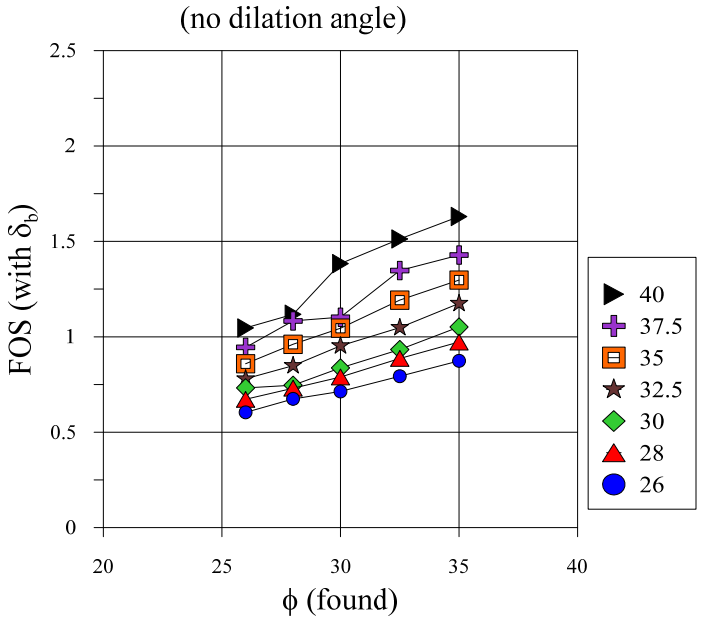

Figure 116. FOS Calculated with δ_b from FLAC for Different ϕ (Found) for 20 ft Wall Height with 3H:1V Back Slope with No Dilation Angle.

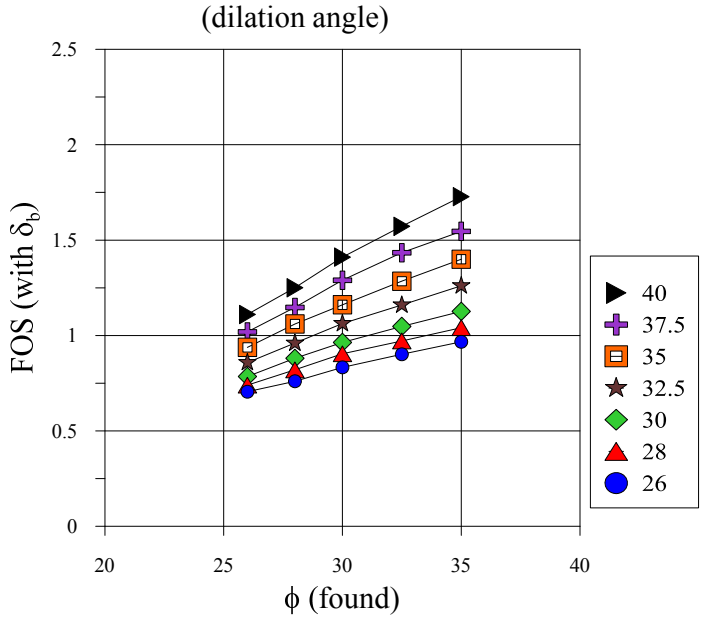

Figure 117. FOS Calculated with δ_b from FLAC for Different ϕ (Found) for 20 ft Wall Height with 3H:1V Back Slope with No Dilation Angle.

5.2.1.7 Conclusions

The FLAC simulations for different geometries and materials properties provided stress data which was used to do a calculations for modified design parameters. The outcomes of this study are concluded below.

- The K_a values back-calculated from FLAC stress distributions show higher values than those predicted from classical Rankine theory. This trend was verified for both cases i.e. retaining soil with dilation angle and without dilation angle for 20 ft wall height with no backslope.
- The modified K_a values from FLAC for 10 ft wall height with no backslope were close to K_a Rankine for no dilation angle and for dilation angle.
- For 3H:1V backslope and 20 ft wall height, the back-calculated K_a values are higher than K_a Rankine and K_a Coulomb.
- Using Eq.35 together with the forces calculated from FLAC simulations shows that for 10 ft wall height with no backslope, the apparent wall interface friction δ_w varies from 7^0-9^0 for the case of no dilation and between 8^0-$10^0$for the case of dilative retained soil.
- The apparent δ_w value for 20 ft wall height with no backslope is approximately 2/3 of ϕ(retain) values, with a tendency to increase with increasing ϕ(retain). The addition of dilation has negligible effect on δ_w values.
- The δ_w value for 20 ft wall height with 3H:1V backslope is 0.8 of ϕ(retain) values and it increases with ϕ(retain).

- The ratio of δ_b/ϕ (found) for 10 ft wall is between 0.6-0.65 with no dilation and with dilation it is between 0.7-0.8.
- The ratio of δ_b/ϕ (found) for a 20 ft wall with no backslope is between 0.5-0.6 with no dilation and with dilation it is between 0.6-0.65.
- The ratio of δ_b/ϕ (found) for a20 ft wall with 3H:1V backslope is 0.6 with no dilation and with dilation it is between 0.65.

5.3 Parametric Study for Bearing Capacity Analysis

In this section, an ultimate bearing capacity is calculated using different bearing capacity equations provided by AASTHO manual (AASHTO 2002), Vesic's equation, and a bearing capacity equation recommended by the German code for MSE walls (as recommended by Professor Dov Leshchinsky). The equation in AASHTO manual is the same as Meyerhof's equation. Using these equations and loads calculated from FLAC analysis for Figure 83 shown above, a parametric study was carried out for pure frictional soils and for pure cohesive soils as well as for c-ϕ foundation soils with frictional retaining soils.

5.3.1 Bearing Capacity Analysis for Pure Frictional Soils

For pure frictional soils the friction angle for foundation soils was considered between 26° and 35° and for retaining soils from 26° to 40° with dilation angle of 10° for both soils. Using these parameters for FLAC simulations a total of 35 simulations were performed. The loads considered for analysis are calculated from FLAC simulations and

from Rankine's K_a to see how it affects the FOS against a bearing failure. The effect of the additional vertical load associated with active thrust is also evaluated.

5.3.1.1 Loads Acting on the Base of Wall

According to AASHTO, loads acting on base of the wall without any external loads applied, are self-weight of the wall and a horizontal load from active thrust from the retained soil. By contrast, the German code considers the weight of wall, the horizontal component of active thrust, and the vertical component of active thrust. The horizontal and vertical components are correlated by interface friction angles between backfill and retaining soils. Adding an extra vertical load from active thrust reduces the eccentricity of loads on the base of the wall, which generally increases the effective width of base in bearing capacity calculations. The loads from active thrust are first calculated from FLAC simulations and from Rankine's K_a for a geometry shown in Figure 83. Three different retaining soil friction angles were considered for this parametric study. Figure 118 shows the loads acting on the base of wall for AASHTO and German code EBGEO (Johnson 2012).

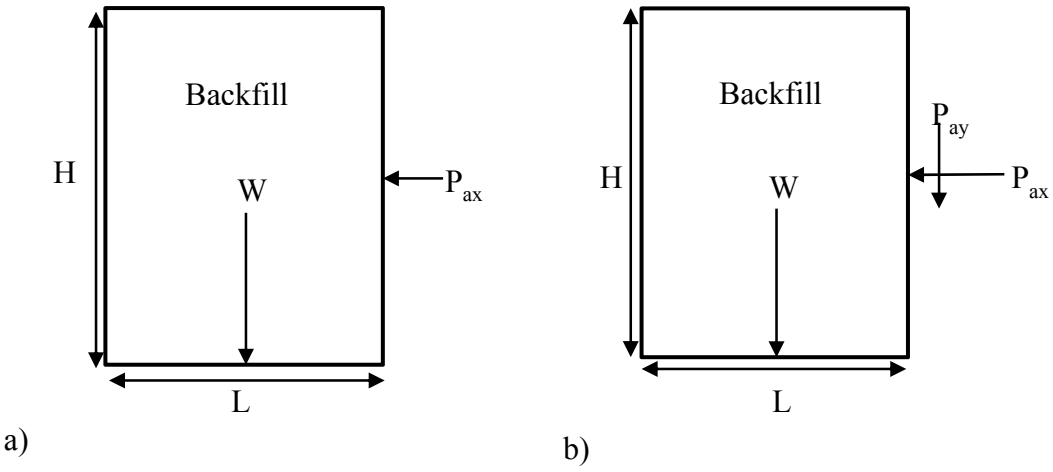

Figure 118. a) Loads Considered according to AASHTO (2002), b) Loads Considered According to German Code (EBGEO).

The total vertical load at the base of the wall predicted from the German code is higher than AASHTO, but the eccentricity of the loads is much lower when compared to AASHTO. Reduction of eccentricity has a significant contribution on FOS for bearing. The following equations are used for analysis.

- For eccentricity:

$$\text{AASHTO, 2002 } e = \frac{Pax \times H/3}{W} \quad \text{(Eq. 40)}$$

$$\text{EBGEO } e = \frac{Pax \times \frac{H}{3} - Pay \times L/2}{W + Pay} \quad \text{(Eq. 41)}$$

where $P_{ay}=P_{ax} \times \tan\delta_w$.

and $\delta_w=2/3\times \phi_{found}$.

- Total loads:

$$\text{AASHTO,2002 W= weight of the wall} \quad \text{(Eq. 42)}$$

$$\text{EBGEO } N_{total}=W+P_{ay} \quad \text{(Eq. 43)}$$

- Load Inclination:

AASHTO, 2002 $tan\delta = \frac{Pax}{W}$ (Eq. 44)

EBGEO $tan\delta = \frac{Pax}{Ntotal}$ (Eq. 45)

5.3.1.2 Bearing Capacity Equations Used for Comparison

For this study, equations of bearing capacity used are Meyerhof's, Vesic's, and an equation from German code DIN 4017 for geotechnical structures. The equation provided in AASHTO (2002) is identical to the Meyerhof equation. To compare an equation from German code (Johnson 2012) and Meyerhof's equation, an additional vertical load from the active thrust is added to the Meyerhof's equation to assess its effect on FOS for bearing. The factors for bearing capacity equation used for comparison study are tabulated in Table 32 and factors used in bearing capacity equations are for strip footing criteria.

Table 32. Factors for Bearing Capacity Equations Used from Different Codes and Authors.

Description	Meyerhof's	Vesic's	German code (DIN 4017)
Bearing capacity factors- N_q	$Nq = [e^{(\pi \tan\phi)}] \tan^2(45 + \frac{\phi}{2})$	Same as Meyerhof's	Same as Meyerhof's
N_γ	$N\gamma = (Nq - 1)\tan(1.4\phi)$	$N\gamma = 2(Nq + 1)\tan(\phi)$	$Nb = (Nq - 1)\tan\phi$ $N_\gamma = 2N_b$
N_c	$Nc = (Nq - 1)\cot\phi$ when $\phi > 0$ $Nc = 5.14$ when $\phi = 0$	Same as Meyerhof's	Same as Meyerhof's
Load inclination factors-i_q	$i_q = \left(1 - \frac{2\delta}{\pi}\right)^2$	$i_q = (1 - \tan\theta)^2$ θ is same as δ	$i_q = (1 - 0.7\tan\theta)^3$
i_c	$i_c = \left(1 - \frac{2\delta}{\pi}\right)^2$	$i_c = \frac{i_q N_q - 1}{N_q - 1}$ when $\phi > 0$ $i_c = 1 - \frac{2H}{L * c * N_c}$ when $\phi = 0$	$i_c = \frac{i_q N_q - 1}{N_q - 1}$ when $\phi > 0$ $i_c = 0.5 + 0.5\sqrt{\left(1 - \frac{H}{L * c}\right)}$ when $\phi = 0$
i_γ	$i_\gamma = \left(1 - \frac{\delta}{\phi}\right)^2$	$i_\gamma = (1 - \tan\theta)^3$	$i_\gamma = (1 - \tan\theta)^3$

According to AASHTO (2002) the embedment contribution to bearing capacity is neglected as most of MSE walls have a minimal embedment depth of one foot or less. The German code also recommends the same and the equations deduced to the overburden part and cohesion part. The bearing capacity equations are as follows.

- For Meyerhof's, Vesic's and for AASHTO (2002). Ultimate bearing capacity equation is:

$$Q= b' (cNc\ i_c +1/2\ b'\gamma\ N_\gamma\ i_\gamma) \quad \text{(Eq. 46)}$$

c = cohesion.

b'= L−2e.

γ = unit weight of foundation soil.

$$FOS = \frac{Q}{W} \quad \text{(Eq. 47)}$$

- From DIN 4017 the equation for ultimate bearing capacity is:

$$Q=b'(cNc\ i_c +b'\ \gamma\ N_b\ i_\gamma) \quad \text{(Eq. 48)}$$

c = cohesion.

b'= L−2e.

γ = unit weight of foundation soil.

$$FOS = \frac{Q}{W} \quad \text{(Eq. 49)}$$

The FOSs for bearing for pure frictional soils are plotted below for different foundation soils. In these plots Meyerhof's equation gives thelowest estimates of FOS while the Vesic equation (neglecting the vertical component of the active thrust) gives somewhat higher calculated FOSs. The DIN4017 analysis, which considers the vertical component of active thrust, gives a highest calculated FOS. A vertical component of active thrust was used in Meyerhof's equations to see the effect on FOS for bearing and was compared with German code (Johnson 2012). Figure 119–Figure 121 show FOS for bearing for pure frictional soils using loads from FLAC, and Figure 122–Figure 124 show loads calculated from Rankine's K_a.

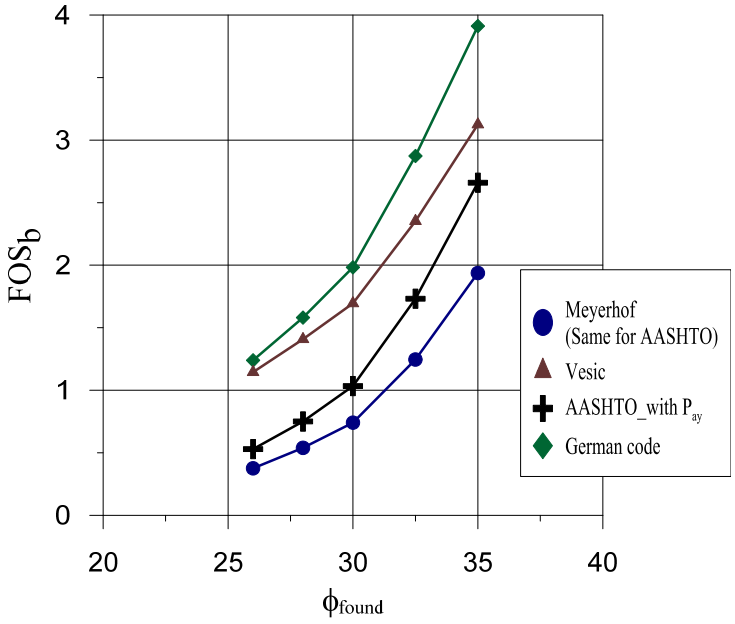

Figure 119. Factor of Safety for Bearing Using Different Equations for Different ϕ (Found) for a ϕ_{retain}=26° and Loads Calculated from FLAC Simulation.

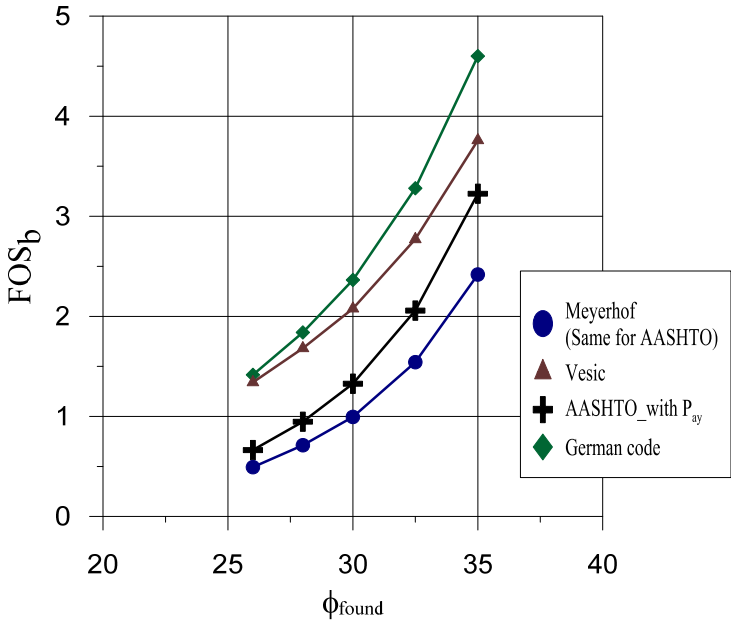

Figure 120. Factor of Safety for Bearing Using Different Equations for Different ϕ (Found) for a ϕ_{retain}=30° and Loads Calculated from FLAC Simulation.

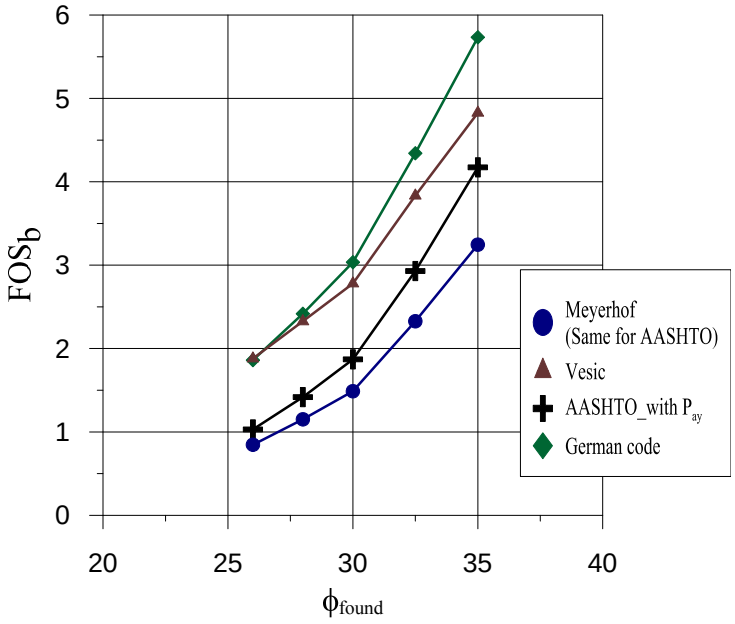

Figure 121. Factor of Safety for Bearing Using Different Equations for Different ϕ (Found) for a ϕ_{retain}=40° and Loads Calculated from FLAC Simulation.

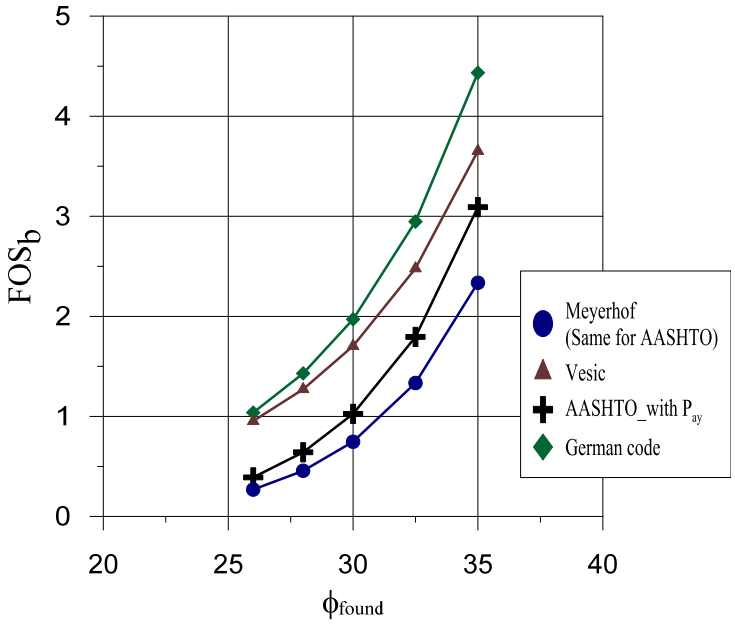

Figure 122. Factor of Safety for Bearing Using Different Equations for Different ϕ (Found) for a ϕ_{retain}=26° and Loads Calculated from Rankine's K_a.

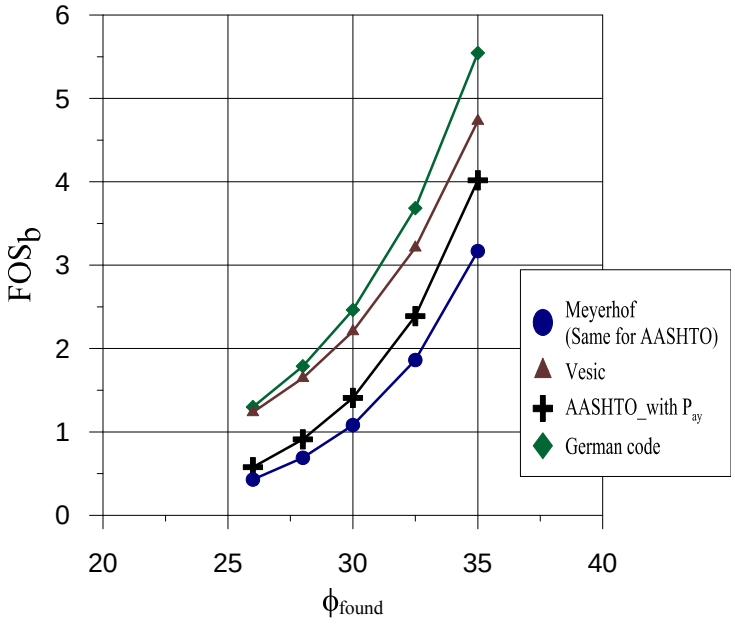

Figure 123. Factor of Safety for Bearing Using Different Equations for Different ϕ (Found) for a ϕ_{retain}=30° and Loads Calculated from Rankine's K_a.

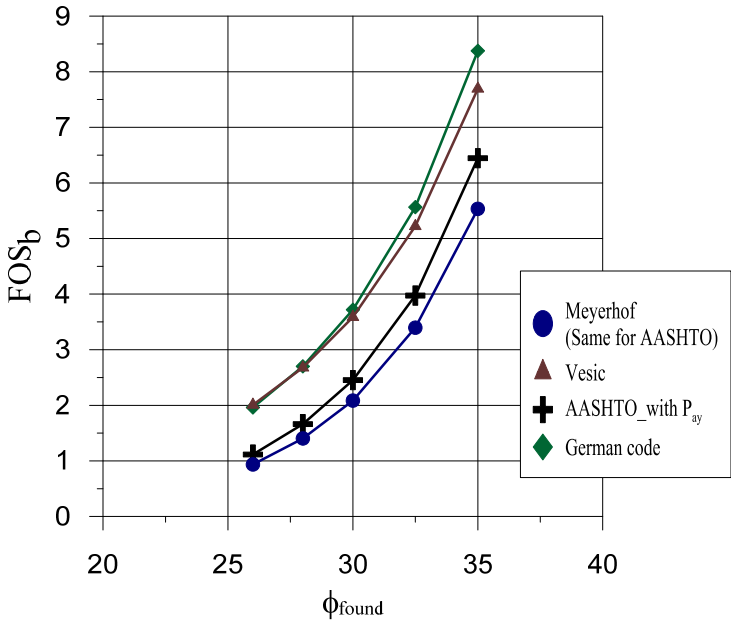

Figure 124. Factor of Safety for Bearing Using Different Equations for Different ϕ (Found) for a ϕ_{retain}=40° and Loads Calculated from Rankine's K_a.

5.3.1.3 Conclusions

The researchers found the following conclusions from this parametric study on bearing capacity equations:

- Active earth pressure forces from FLAC simulations are higher than forces calculated from Rankine's theory, especially for higher ϕ (retained) values. This is due the fact that numerical analysis trends to give a higher approximation. The FLAC analyses likely over-estimated active forces and under-estimated FOS.
- The Meyerhof's equation, which is used in the AASHTO analysis, gives a lower estimate of FOS for bearing than Vesic's equations.
- The German code (EBGEO) considers a vertical force associated with the active thrust. The FLAC simulations can also calculate the vertical component of the earth pressure force based on the stresses generated at the back of the wall. This vertical component increases the total vertical load at the base of the wall, but at the same time it decreases the eccentricity from the center of base of the wall. This decrease in eccentricity is generally beneficial as it increases the effective width of the base in the ultimate bearing capacity equation.
- FOSs for bearing from the German code (EBGEO) give higher values than Vesic's. This is due to the consideration of vertical component of the active thrust that decreases the eccentricity.
- Including the vertical component of active thrust in the Meyerhof analysis will increase the FOS against a bearing failure, but the predicted FOS will still be lower than that predicted from the Vesic analysis.
- Meyerhof's (AASHTO) gives a conservative FOS value for bearing capacity.

5.3.2 Bearing Capacity Analysis for Pure Cohesive Soils

FLAC simulations were carried out on a MSE wall with no back slope geometry for pure cohesive retaining soils and foundation soils. The unit weight of sandy backfill soil and retaining soils were both equal to 125 pcf. The geometry of the model is shown in Figure 83. The model properties are explained below for pure clays. After performing the simulations stresses were extracted from simulation for each case and forces acting on the wall from active thrust were calculated from stress data.

5.3.2.1 Model Properties Used for Pure Clay Used as Retaining and Foundation Soils

The backfill material used for this model was frictional soils with dilation angle of 10° and internal friction angle of 34°. The properties of retaining and foundation soils are tabulated in Table 33.

Table 33. Material Properties Used for Pure Cohesive Soils for FLAC Simulations.

Type	Strength	Unit weight (pcf)	Elastic modulus* (psf)	Bulk modulus (psf)	Shear modulus (psf)	C_u (psf)
Foundation and Retaining soils	Soft	125	0.08464 E6	0.1410 E6	0.0302 E6	500
	Medium-Firm	125	0.1269 E6	0.2116 E6	0.0453 E6	750
	Firm	125	0.1692 E6	0.2821 E6	0.0604 E6	1000
	Medium-Stiff	125	0.2962 E6	0.4937 E6	0.1058 E6	1500
	Stiff	125	0.4232 E6	0.7054 E6	0.1511 E6	2000

* Elastic modulus for sand is taken as $1000*P_{atm}$ where P_{atm}=2116.216 psf and Poisson ratio=0.4 (Kulhawy and Mayne 1990).

Using these material properties, a total of 25 simulations were performed to consider the effects of different foundation properties on different retaining soils. The model was first run for equilibrium condition under gravity and then it was run for failure condition under gravity loads.

5.3.2.2 Results

The loads acting on the wall due to an active thrust from retaining soils are calculated using FLAC simulations. The vertical component of active thrust was fairly small for all cohesive type retaining soils. Therefore this vertical force was not accounted in bearing capacity calculations. The equations used for bearing capacity are Meyerhof's, Vesic's, and German code (EBGEO). Since there is no vertical component from active thrust, bearing capacity values for German code and Vesic's are the same. The results presented below from Figure 125–Figure 127 are for soft, firm, and stiff clay retaining soils and for soft, med-firm, firm, med-stiff, and stiff clay foundation soils. The results are compared with FLAC FOS and the FOS for bearing calculated using Meyerhof's and Vesic's equations.

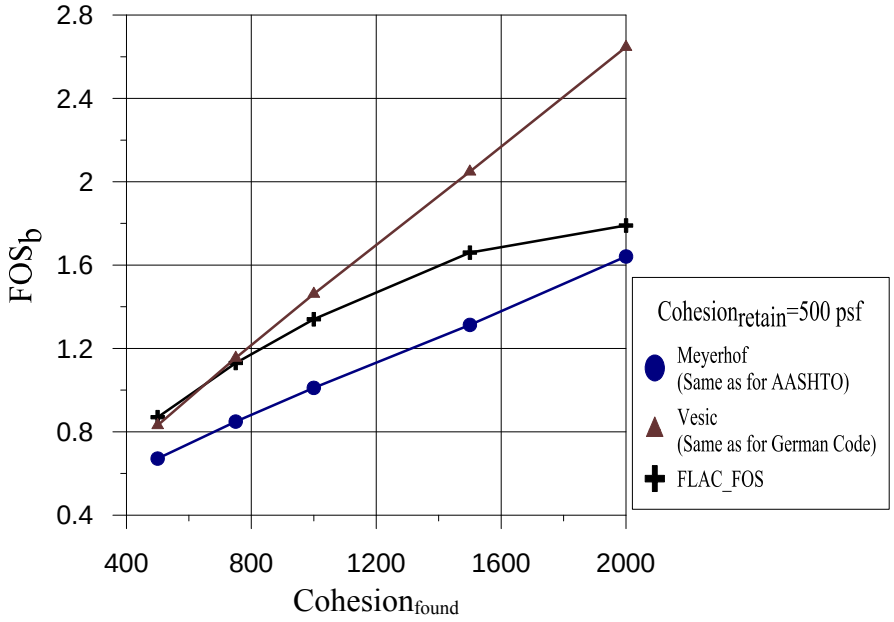

Figure 125. Factor of Safety for Bearing Using Different Equations for Different Cohesion (Found) for a cohesion$_{retatin}$=500 psf and Loads Calculated from FLAC.

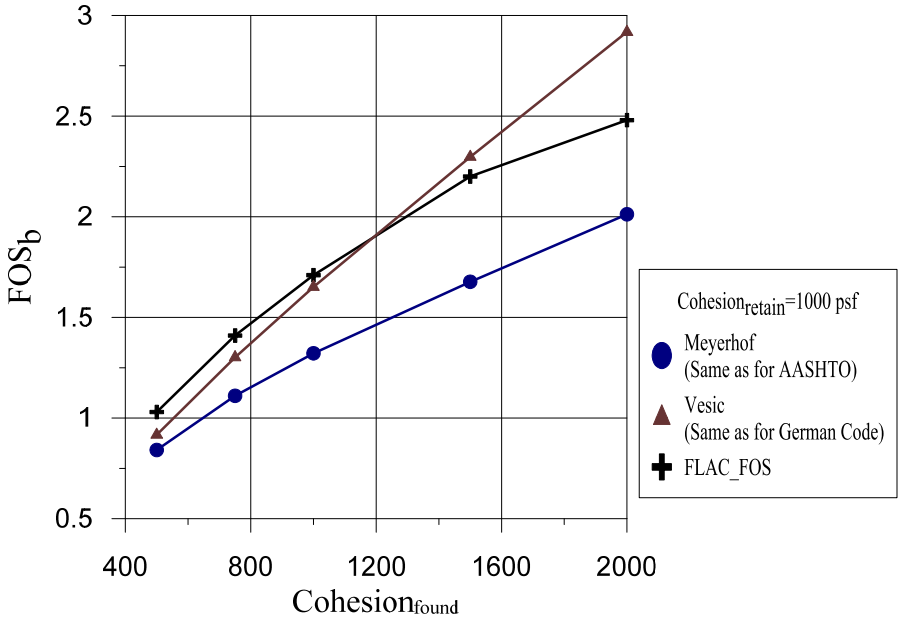

Figure 126. Factor of Safety for Bearing Using Different Equations for Different Cohesion (Found) for a cohesion$_{retatin}$=1000 psf and Loads Calculated from FLAC.

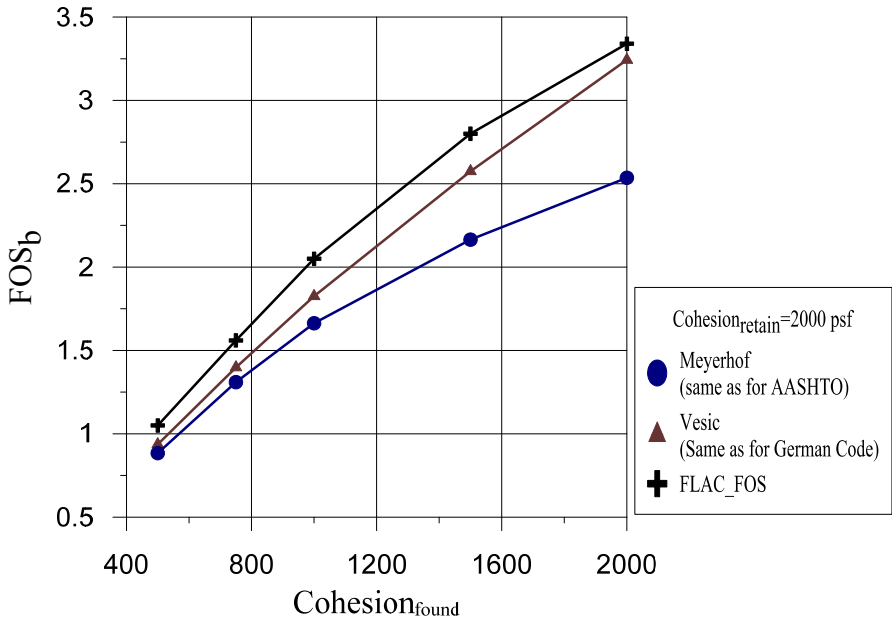

Figure 127. Factor of Safety for Bearing Using Different Equations for Different Cohesion (Found) for a cohesion$_{retatin}$=2000 psf and Loads Calculated from FLAC.

5.3.2.3 Conclusions

The following are the conclusions for using pure cohesive soils as foundation soils:

- The FOSs for soft retaining soils are lower because the softer retaining soils exert higher active thrust on the wall, especially horizontal load from active thrust.
- Safety factors predicted from the Meyerhof's (AASHTO) equations are lower than those predicted from Vesic's equation and FLAC.
- Vesic's equation agrees reasonably well with FLAC for medium and stiff soils, but appears unconservative for soft soil.
- The chief difference between the Meyerhof's and Vesic's equations for purely cohesive soils lies in the load inclination factor. Vesic's load inclination factor

accounts for the dimensions of the wall and cohesion at the base of wall; whereas, Meyerhof's load inclination factor accounts only for load inclination angle from vertical.

- For stiff clay retained soils, the FOS from FLAC is higher than FOS from the Meyerhof's and Vesic's equations, because of the smaller active thrust.
- Meyerhof's equations for bearing capacity can be used as a preliminary assessment tool for bearing capacity but if it gives a very low FOS, a FLAC simulation can be carried out to verify the calculations.

5.3.3 Bearing Capacity Analysis for c-ϕ Foundation Soils

To combine the effect of friction angle and cohesion on bearing capacity, a FLAC simulation was performed with foundation soils having both friction angle and cohesion. The properties of retaining soils are that of pure frictional soils with 26°, 30°, and 40° with a dilation angle of 10°.

5.3.3.1 Material Properties Used for FLAC Simulations

The material properties for retaining soils used here are of pure frictional soils to see the full effect of active thrust in both horizontal and vertical directions. Using frictional retaining soils also gives an option of comparing all possible bearing capacity equations and to see the effect of load inclination on both cohesion and overburden parts of the bearing capacity equation. The values used for material properties for FLAC simulations are tabulated below in Table 34.

Table 34. Material Properties for FLAC Simulations c-ϕ Foundations.

Type	Unit weight (pcf)	Elastic modulus* (psf)	Bulk modulus (psf)	Shear modulus (psf)	C_u (psf)	ϕ
Foundation soils	125	2.116 E6	3.6435 E6	0.3644 E6	500	26
					750	
					1000	
Retaining soils	125	2.116 E6	3.6435 E6	0.3644 E6	0	26
						30
						40

5.3.3.2 Results

Nine simulations were performed with different combinations of retaining and foundation soils. The results plotted below Figure 128-Figure 130 shows the FOS for sliding, for bearing using different equations and FOS from FLAC. The FLAC gives a FOS value by strength reduction method. This FOS is plotted as a reference for other calculated FOS from forces extracted from FLAC simulations.

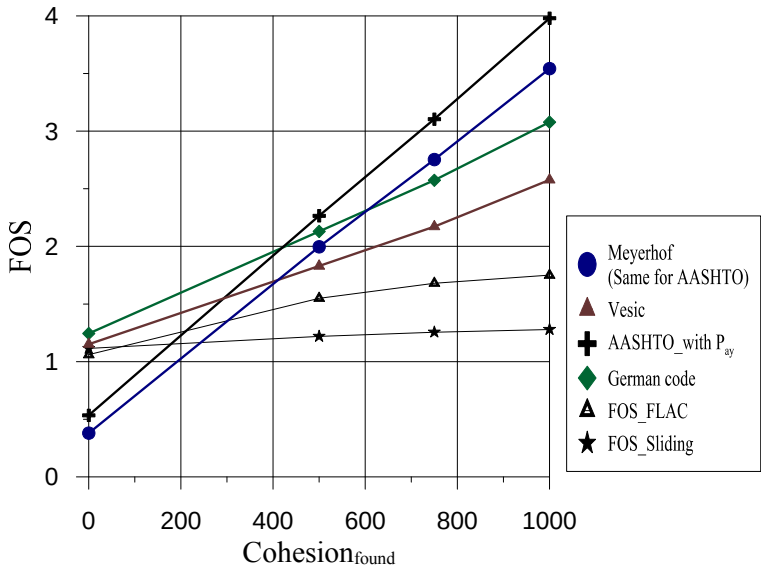

Figure 128. Factor of Safety Values for Bearing Analysis, Sliding Analysis and from FLAC Simulation for Different Cohesion (Found) for a Retaining ϕ=26°.

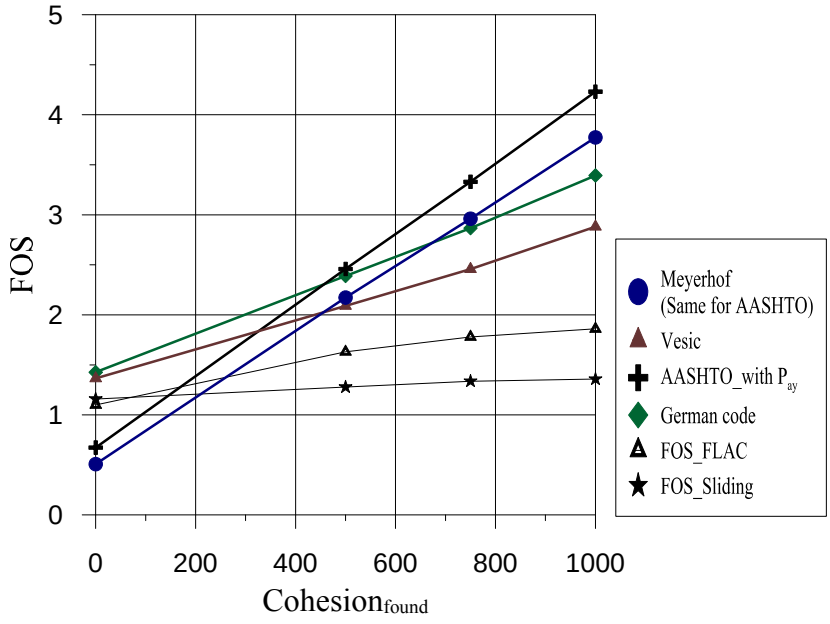

Figure 129. Factor of Safety Values for Bearing Analysis, Sliding Analysis and from FLAC Simulation for Different Cohesion (Found) for a Retaining ϕ=30°.

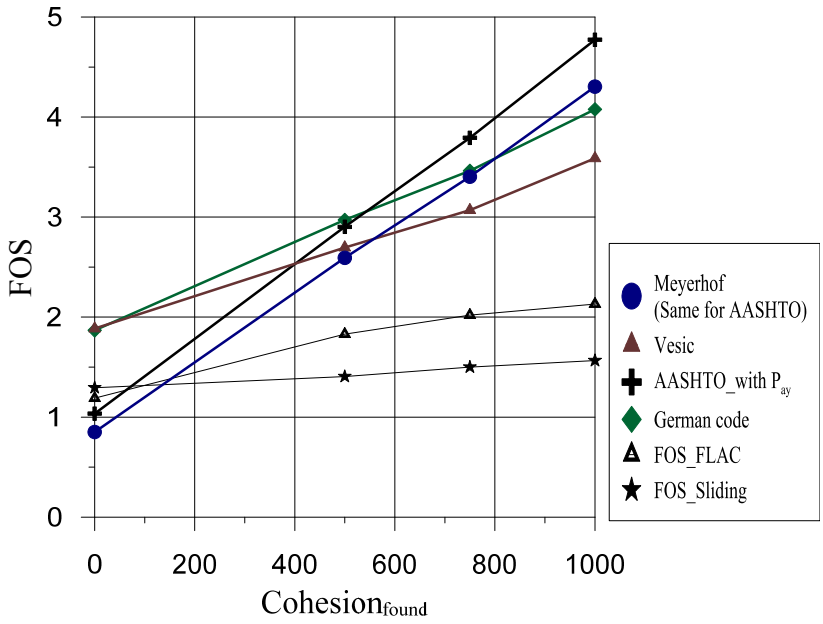

Figure 130. Factor of Safety Values for Bearing Analysis, Sliding Analysis and from FLAC Simulation for Different Cohesion (Found) for a Retaining ϕ=40°.

5.3.3.3 Conclusions

These are the conclusions for c-ϕ soils used as foundation soils.

- The FOS against sliding is calculated using forces from FLAC simulation. These FOS values are lower than FLAC values, because the sliding calculations assumed no cohesion.
- For lower retained soil friction values, the FOS from FLAC is higher value than the FOS for bearing from the Meyerhof analysis for foundation soils with low cohesion. However, for higher cohesion values the Meyerhof safety factors exceed the FLAC predictions.
- Accounting for the additional vertical load from active thrust in Meyerhof's equation generates a small increase in the predicted bearing capacity.

- The increase in bearing capacity with increasing cohesion predicted from the Meyerhof equation is nearly linear.
- The load inclination factor has a significant influence on both the embedment and cohesion contributions to bearing capacity predicted from the Meyerhof's and Vesic's equations.
- For lower cohesion and friction angle FOS for bearing from Meyerhof's should be verified by performing FLAC simulation for a particular cases.

6. SUMMARY AND CONCLUSIONS

This section summarizes the outcomes from this research discussed in the preceding sections. The conclusions from this research are provided at the end of this section.

6.1 Summary

The laboratory tests, numerical simulations and parametric studies conducted in this research for MSE retaining walls is summarized as follows

- The conclusions from laboratory test section on mentioned in section 3.7 shows that the angle of internal friction for backfill Type A, B & D can be higher than AASHTO, 2002 recommended value of 34^0. For Type C backfill material it is important to know the drainage condition of backfill. The angle of internal friction for this material depends on drainage conditions. If a backfill is having an undrained condition then the friction angle for this type of material can be as low as 23^0, whereas AASHTO,2002 recommends 30^0 for these type of materials.
- Amount of fines in the backfill has reasonable effect for Type A, B & D but has a significant effect for Type C backfill material.
- The global stability analysis performed in section 4. Numerical Simulations for different retaining geometries supported by MSE walls with different soil properties for retaining and foundation soils. The global stability analysis shows that the backfill soil friction angle does not contribute in global failure of MSE walls. For frictional retaining and foundation soils the global failure tends to be

sliding type with a formation of an active wedge of soil mass behind the MSE wall. The global stability analysis for cohesive retaining and foundation soils shows that the failure is more towards bearing type and the strength of foundation soils has an important role in FOS calculations. The detailed conclusions on this analysis are presented in section 4.1.2.

- The parametric study conducted for sliding and overturning analysis using AASHTO design guidelines shows that the ratio of unit of weight has a significant influence is calculating FOS for sliding and overturning especially for lower frictional values for retaining and foundation soils. The detailed conclusions are listed in section 5.1.3. Similarly, a parametric study performed for sliding and overturning analysis using FLAC computation results to find modified parameters has shown that there is an interaction effect and only 2/3 of friction angle of foundation soils is utilized in resisting sliding force. The complete results and conclusion on this part of parametric study is presented in section 5.2.1.7
- The parametric study for bearing capacity analysis was divided into three subsection depending the soil properties were for foundation and retaining soils. For each section, three bearing capacity equations were compared i.e. Meyerhof's, Vesic's and a bearing capacity equation from German code DIN 4017. Using these equations a FOS for bearing failure were calculated. The complete results and conclusion are presented in section 5.3.1 through section 5.3.3.

6.2 Conclusions

Following are the conclusions made by an author of this research.

- The laboratory test data for backfill materials such as Types A, B, and D show a friction angle values higher than what is recommended by AASHTO (2002). Therefore, the AASHTO strength recommendations may be considered as conservative estimates in the absence of site specific laboratory data. It is noted that the strength values reported in this thesis are based on material samples that strictly satisfy the AASTHTO particle size distribution requirements. Thus, this conclusion presumes that construction quality control procedures will ensure compliance with the AASHTO requirements.
- The material classification for backfill plays an important role in variability of soil parameters. For example, the amount of fines has a significant contribution on friction values for a given backfill material. Therefore it is necessary to perform a wet sieve analysis when possible to quantify an exact amount fines present in backfill material.
- The soil parameters for Type C backfill material should be quantified based on drainage condition at failure loading. Since the amount of fines for Type C recommended by TxDOT is between 0–30 percent and this amount fines changes the behavior of backfill material from cohesionless to cohesive. The friction values presented in this research are for drained and undrained conditions, and depending upon amount of fines present in this backfill a corresponding friction angle should be used as soil parameter for Type C backfill material. The

measured friction angles for Type C backfill, drained and undrained, were generally less than 30 degrees.

- The FLAC simulations conducted for global stability for purely frictional soils show that for lower friction values ($\phi < 30^0$) the failure surface is in form of a wedge behind the wall (Figure 33), which is consistent with Rankine or Coulomb theory. The dominant failure mechanism in these cases is a sliding failure type mechanism.
- For purely cohesive soils the dominant failure mechanism for soft type soils is typically bearing failure, whereas for firm and stiff soils sliding is typically the critical failure mechanism.
- The parametric study performed using AASHTO recommended soil parameters shows that the ratio of unit weight backfill to unit weight of retain soils plays important role on sliding FOS and over turning FOS. For lower retaining friction angle, the ratio of 0.85 gives a FOS of 1.5 for sliding with horizontal back slope geometry. For 3H:1V back slope ratio of 1.1 gives a FOS of 1.5 for sliding.
- A FLAC simulation performed using pure frictional soil parameters on retaining and foundation soils shows that there is an interaction effect on the base friction factor used in sliding analysis and it should be considered in the design process. Specifically, it is unconservative to assume that the full foundation frictional resistance can be mobilized at the base of the retained soil mass. The FLAC simulations indicate that interaction effects can reduce the available frictional resistance by as much as 33 percent.

- Field experience for low friction angle soils tends to indicate that the reduction in base friction angles in the sliding calculation to account for the interaction effect is overly conservative for foundation soils having friction angles less than 30 degrees. This is likely a consequence of the fact that soils with friction angles less than 30 degrees probably contain silt or clay that will generate a cohesive component to the soil strength. For the case of foundations having low friction angles, excessive conservatism in the analysis can be avoided by including the effects of cohesion in the sliding analysis.
- The bearing capacity analysis for pure frictional soil parameters using FLAC simulations has shown that a load eccentricity has an important role on ultimate bearing capacity. The vertical component of the active thrust reduces load eccentricity and therefore has a generally beneficial effect on wall stability. The FLAC simulations consistently indicate that the active thrust exerted by the retained soil exists, even for walls with horizontal backfills. Therefore, there is no reason not to take advantage of this effect when performing the bearing capacity calculations. The current German EBGEO code considers the vertical component of active thrust, which has a major influence in avoiding the apparently over-conservatism in the current AASTHTO guidelines.
- The comparison of bearing capacity equations recommended by AASHTO and EBGEO shows that additional vertical load from active thrust reduces the eccentricity of loads.

- The comparison between Meyerhof's equation and Vesic's equation shows that a different load inclination factor gives different ultimate bearing capacity values. The Meyerhof's equation gives a lower estimate and Vesic's gives a higher estimate; if compared with FLAC simulations, the FLAC FOS falls between FOS for bearing from Meyerhof's and Vesic's.

REFERENCES

AASHTO (2002). "Standarad Specifications for Highway Bridges (17th Edition) Retaining Walls." American Association of State Highway and Transportation Officials, Inc, Washington (DC).

AASHTO (2007). "T104-Standard Method of Test for Soundness of Aggregate by Use of Sodium Sulfate or Magnesium Sulfate." American Association of State Highway and Transportation Officials, Inc, Washington, DC, 10.

AASHTO (2008). "T267-Standard Method of Test for Determination of Organic Content in Soils by Loss of Ignition." American Association of State Highway and Transportation Officials, Inc, Washington, DC, 2.

Adams, M., Nicks, J., Stabile, T., Wu, J., Schlatter, W., and Hartmann, J. (2011). "Geosynthetic Reinforced Soil Integrated Bridge System, FHWA Synthesis Report." 68.

Allen, T., Christopher, B., Elias, V., and DeMaggio, J. (2001). "Development of the simplified method for internal stability design of mechanically stabilized earth walls." *FHWA Publication No. WA-RD*, 79.

Allen, W. M. (2013). "Selecting Backfill Materials for MSE Retaining Walls." <http://apps.trb.org/cmsfeed/TRBNetProjectDisplay.asp?ProjectID=721>. (2013).

Alzamora, D., and Barrows, R. J. (2007). "Research Pays Off: Mechanically Stabilized Earth Walls on the Interstate Highway System: Thirty Years of Experience." *TR News*(249).

ASTM (2007). "D422-63-Standard Test Method for Particle-Size Analysis of Soils." American Society for Testing and Materials, International, West Conshohocken, PA.

ASTM (2009). "C29-Standard Test Method for Bulk Density ("Unit Weight") and Voids in Aggregate." American Society for Testing and Materials, International, West Conshohocken, PA.

ASTM (2010). "D854-Standard Test Methods for Specific Gravity of Soil Solids by Water Pyconometer." American Society for Testing and Materials, International, West Conshohocken, PA.

ASTM (2011a). "D7181-Consolidated Drained Triaxial Compression Test for Soils." American Society for Testing and Materials, International, West Conshohocken, PA.

ASTM (2011b). "D4767-Standard Test Method for Consolidated Undrained Triaxial Compression Test for Cohesive Soils." American Society for Testing and Materials, International, West Conshohocken, PA.

ASTM (2012). "D698-12-Standard Test Method for Laboratory Compaction Characteristics of Soil Using Standard Effort." American Society for Testing and Materials, International, West Conshohocken, PA, 13.

Berg, R. R., Christopher, B. R., and Samtani, N. C. (2009). "Design of Mechanically Stabilized Earth Walls and Reinforced Soil Slopes–Volume II."

Bobet, A. (2002). "Design of MSE Walls for Fully Saturated Conditions." Joint Transportation Research Program, Purdue University, West Lafayette, IN., 163.

CalTrans (2004). "Bridge Design Specifications " *Retaining Walls*, California Department of Transportation, Sacramento, CA.

Chalermyanont, T., and Benson, C. H. (2005). "Reliability-Based Design for External Stability of Mechanically Stabilized Earth Walls." *International Journal of Geomechanics*, 5(3), 196-205.

Chew, S., Schmertmann, G., and Mitchell, J. (1991). "Reinforced soil wall deformations by finite element method." *Performance of Reinforced Soil Structures, A. McGown, K. Yeo and KZ Andrawes (Eds.), London: Thomas Telford Ltd*, 35-40.

Christopher, B. R., Leshchinsky, D., and Stulgis, R. (2005). "Geosynthetic-Reinforced Soil Walls and Slopes: US Perspective." *Proc., Geo-Frontiers Congress 2005*, Austin, TX, ASCE, 12.

Dodson, M. D. (2010). "Lessons Learned from Settlement of Three Highway Embankment MSE Walls." *Earth Retention Conference 3*, 588-595.

Duncan, J. M. (2000). "Factors of Safety and Reliability in Geotechnical Engineering." *Journal of Geotechnical and Geoenvironmental Engineering*, 126(4), 307-316.

Elias, V., Fishman, K. L., Christopher, B. R., and Berg, R. R. (2009). "Corrosion/Degradation of Soil Reinforcements for Mechanically Stabilized Earth Walls and Reinforced Soil Slopes." Federal Highway Adminstration, Washington, DC, 142.

FHWA (2001). "Mechanically Stabilized Earth Walls and Reinforced Soil Slopes Design and Construction Guidelines." V. Elias, Christopher, B. R., Berg, R. R., ed., Federal Highway Adminstration, Washington, DC.

FHWA (2009). "Design and Construction of Mechanically Stabilized Earth Walls and Reinforced Soil Slopes-Vol.1." Federal Highway Adminstration, Washington, D.C.

Galvan, M. (2007). "Presentation titled "Retaining wall design and construction issues"." <https://ftp.dot.state.tx.us/pub/txdot-info/des/presentations/desbrgconf07/galvan%20retaining_wall_issues.pdf>. (2011).

Garton , M. K. (2013). "Large Scale Triaxial Testing of Mechanically Stabilized Earth Retaining Wall Backfill." Master of Science, Texas A&M University, College Station, Texas.

Germaine, J. T., and Ladd, C. C. (1988). "State-of-the-Art Paper: Triaxial Testing of Saturated Cohesive Soils." *Advanced Triaxial Testing of Soil and Rock, ASTM*, Vol. STP 977, 39.

Harr, M. E. (1984). *Reliability-based design in civil engineering*, Dept. of Civil Engineering, School of Engineering, North Carolina State University, Raleigh, N.C.

Holtz, R. D., and Kovacs, W. D. (2011). *An Introduction to Geotechnical Engineering*, Pearson, Upper Saddle River, NJ.

Holtz, R. D., and Lee, W. F. (2002). "Internal stability analyses of geosynthetic reinforced retaining walls." Washington State Dept. of Transportation, 379.

Johnson, A. (2012). *Recommendations for Design and Analysis of Earth Structures Using Geosynthetic Reinforcements-EBGEO*, John Wiley & Sons.

Keller, G. R. (1995). " Experiences with Mechanically Stabilized Structures and Native Soil Backfill." *Journal of the Transportation Research Record*, 1474, 30-38.

Kuerbis, R. H., and Vaid, Y. P. (1990). "Corrections for Membrane Strength in the Triaxial Test." *Geotechnical Testing Journal, ASTM*, 13(4), 9.

Kulhawy, F. H. (1992). "On the evaluation of soil properties." *ASCE Geotech. Spec. Publ.*, 31, 95-115.

Kulhawy, F. H., and Mayne, P. W. (1990). "Manual on estimating soil properties for foundation design." Electric Power Research Inst., Palo Alto, CA (USA); Cornell Univ., Ithaca, NY (USA). Geotechnical Engineering Group.

Leshchinsky, D. (2006). "ASD and LRFD of Reinforced SRW with the use of software Program MSEW (3.0)." *Geosynthetics*, 14-20.

Leshchinsky, D., and Han, J. (2004). "Geosynthetic reinforced multitiered walls." *Journal of Geotechnical and Geoenvironmental Engineering*, 130, 1225.

Liang, R. Y. (2004). "MSE Wall and Reinforcement Testing at MUS-16-7.16 Bridge Site." University of Akron, Dept. of Civil Engineering. FHWA, 616.

Ling, H., and Leshchinsky, D. (2003). "Finite element parametric study of the behavior of segmental block reinforced-soil retaining walls." *Geosynthetics International*, 10(3), 77-94.

Ling, H. I., Liu, H., and Mohri, Y. (2005). "Parametric studies on the behavior of reinforced soil retaining walls under earthquake loading." *Journal of Engineering Mechanics*, 131, 1056.

Mooney, M. A., Nocks, C. S., Selden, K. L., Bee, G. T., and Senseney, C. T. (2008). "Improving Quality Assurance of MSE Wall and Bridge Approach Earthwork Compaction." Colorado Dept. of Transportation, DTD Applied Research and Innovation Branch.

Morrison, K. F., Harrison, F. E., Collin, J. G., Dodds, A. M., and Arndt, B. (2006). "Shored Mechanically Stabilized Earth (SMSE) Wall systems Design Guidelines." Golder Associates Inc, Lakewood, CO, 230.

NCMA (2002). "Segmental Retaining Wall Design Manual: 2nd edition." National Concrete Masonry Association Herndon, VA, 289.

Rathje, E. M., Rauch, A. F., Trejo, D., Folliard, K. J., Viyanant, C., Esfellar, M., Jain, A., and Ogalla, M. (2006). "Evaluation of crushed concrete and recycled asphalt pavement as backfill for mechanically stabilized earth walls." Center for Transportation Research, Austin, TX., 182.

Reddy, D., Navarrete, F., Rosay, C., Cira, A., Ashmawy, A., and Gunaratne, M. (2003). "Long-Term Behavior Of Geosynthetic Reinforced Mechanically Stabilized Earth (MSE) Wall System-Numerical/Analytical Studies, Full Scale Field Testing, and Design Software Development." 281.

Terzaghi, K. (1943). *Theoretical Soil Mechanics*, Wiley, New York.

TxDOT (1999a). "Tex-128-E Determining Soil pH." Texas Department of Transportation, Austin,TX, 3.

TxDOT (1999b). "Tex-129-E Measuring the Resistivity of Soil Materials." Texas Department of Transportation, Austin,TX.

TxDOT (2004). "Standard Specifications for Construction and Maintenance of Higways, Streets, and Bridges." Texas Department of Transportation, Austin, Texas, 1028.

TxDOT (2005). "Tex-620-J Determining Chloride and Sulfate Contents in Soil." Texas Department of Transportation, Austin,TX.

TxDOT (2012). "Geotechnical Manual." Texas Department of Transportation, Austin, Texas, 60.

WisDOT (2006). "Bridge Manual." *Retaining Walls*, Wisconsin Department of Transportation, Madison,WI.

Yoon, S. (2011). "Backfill Material Parameters used by TxDOT (Personal Communication)."Austin,TX.

APPENDIX A

LABORATORY TEST RESULTS

The results presented here are for Type-A, B and D which were tested under consolidated drained condition. A consolidated undrained test was performed on a Type-C backfill material and the results are presented here below. The table- below shows an overview of test results and following are the detailed test results for each Type of backfill materials.

Table A. 1. Friction angles for Type-A,B& D backfill tested

Gradation	Maximum Friction Angles (°)	Minimum Friction Angles (°)	p-q Friction Angles (°)
A1	49.9	43.0	45.5
A2	46.8	41.8	43.7
A3	47.5	41.8	42.9
A4	45.9	39.8	42.8
B1	53.4	48.5	51.9
B2	53.2	48.3	52.5
B3	48.4	43.5	45.7
B4	41.7	31.8	39.2
D1	47.2	41.6	44.2
D2	47.0	36.5	40.7
D3	51.6	38.4	43.8
D4	41.7	35.8	38.0

Table A. 2. Laboratory test results for type-C material.

Gradation	Maximum undrained Friction Angles (°)	Minimum undrained Friction Angles (°)	Maximum drained Friction Angles (°)	Minimum drained Friction Angles (°)	Dry Unit Weight (pcf)
C1	29.4	26.2	40.3	27.8	120.6
C2	28.3	26.2	47.4	30.1	129.4
C3	32.0	22.6	50.9	33.7	128.4
C4	32.3	23.6	26.4	14.5	126.3

Table A. 3. Type A test results

Test Name	Date	Gradation	Cell Pressure (psi)	γ Sample Tested	Void Ratio	% RC	Friction Angle	Comments
A1_10_1_52012	20-May	A1	4.3	87.90	0.85	93%	49.9	
A1_10_2_60412	4-Jun	A1	4.3	87.80	0.85	93%	49.7	Possible leak: dilation up to 5%
A1_15_1_60512	5-Jun	A1	6.5	86.00	0.89	91%	47.0	
A1_15_2_61412	14-Jun	A1	6.5	86.40	0.88	91%	45.2	
A1_20_1_60512	5-Jun	A1	8.7	83.60	0.94	88%	43.3	
A1_20_2_61412	14-Jun	A1	8.7	84.90	0.91	90%	43.0	Contraction at 3%
A2_10_1_70312	3-Jul	A2	4.3	87.80	0.85	88%	46.8	
A2_10_2_71312	13-Jul	A2	4.3	95.82	0.69	96%	42.7	Compliant load curve
A2_15_1_71612	16-Jul	A2	6.5	87.24	0.86	88%	43.6	
A2_15_2_71712	17-Jul	A2	6.5	87.43	0.86	88%	43.1	
A2_20_1_71812	18-Jul	A2	8.7	91.80	0.77	92%	44.7	
A2_20_2_71812	18-Jul	A2	8.7	93.17	0.74	93%	41.8	Leak: volume change=24%
A3_10_1_71912	19-Jul	A3	4.3	96.49	0.68	97%	47.5	Inconsistent load curve
A3_10_2_72012	20-Jul	A3	4.3	84.90	0.91	86%	44.8	
A3_15_1_73012	30-Jul	A3	6.5	100.89	0.61	102%	42.1	
A3_15_2_73012	30-Jul	A3	6.5	94.44	0.72	95%	41.7	Jump in load curve at 7.5%
A3_20_1_73112	31-Jul	A3	8.7	101.45	0.60	102%	42.4	Leak: volume change=18%
A3_20_2_73112	31-Jul	A3	8.7	100.49	0.61	101%	42.1	Leak: volume change 14%
A4_10_2_62212	22-Jun	A4	4.3	115.00	0.41	98%	52.5	Inconsistent load curve
A4_10_3_62412	24-Jun	A4	4.3	108.40	0.50	92%	45.9	
A4_15_1_62612	26-Jun	A4	6.5	102.50	0.58	87%	41.4	Leak: volume change=8%
A4_15_2_62712	27-Jun	A4	6.5	98.90	0.64	84%	40.2	Compliant load curve
A4_20_1_70212	2-Jul	A4	8.7	101.40	0.60	86%	39.8	
A4_20_2_70212	2-Jul	A4	8.7	101.00	0.61	86%	40.7	

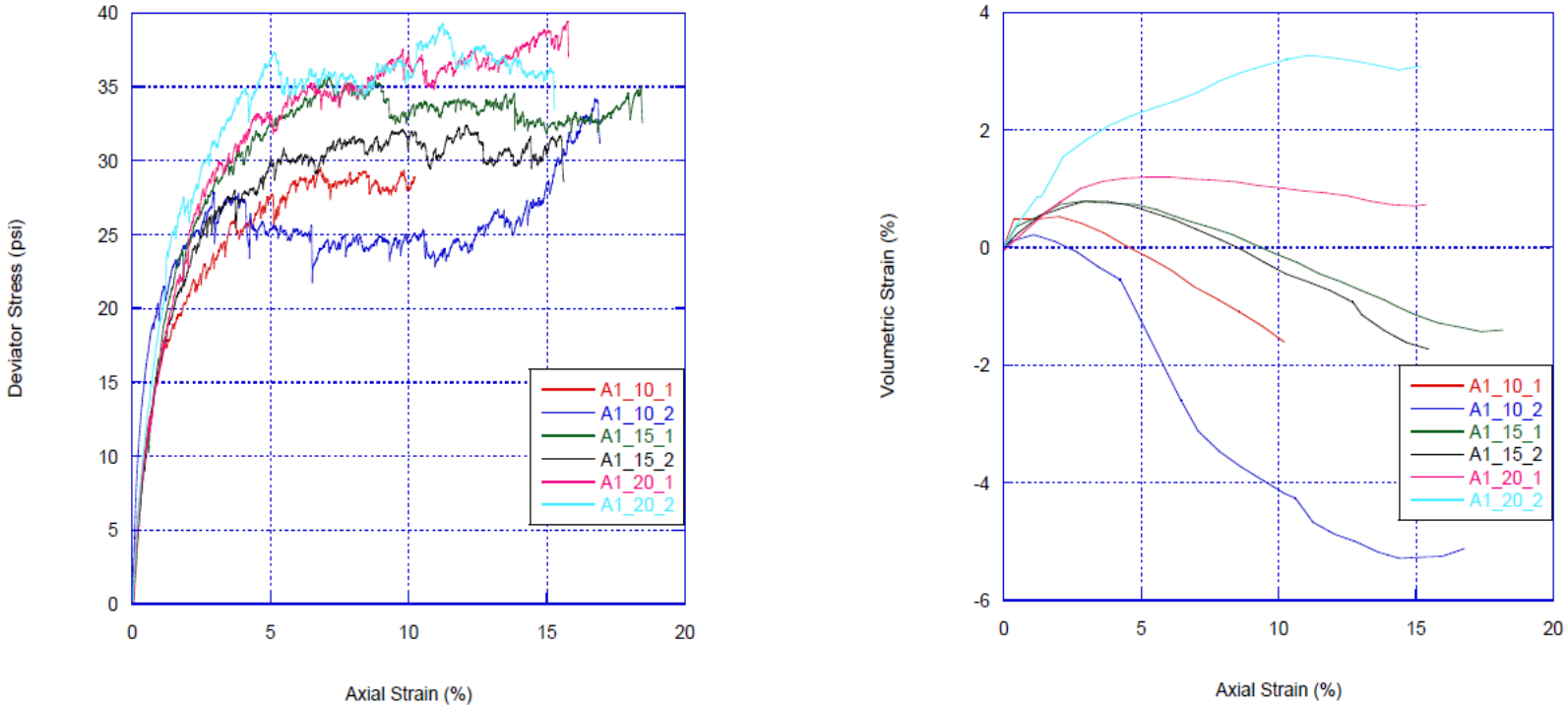

Figure A. 1. Gradation A1 stress-strain and volumetric strain curves

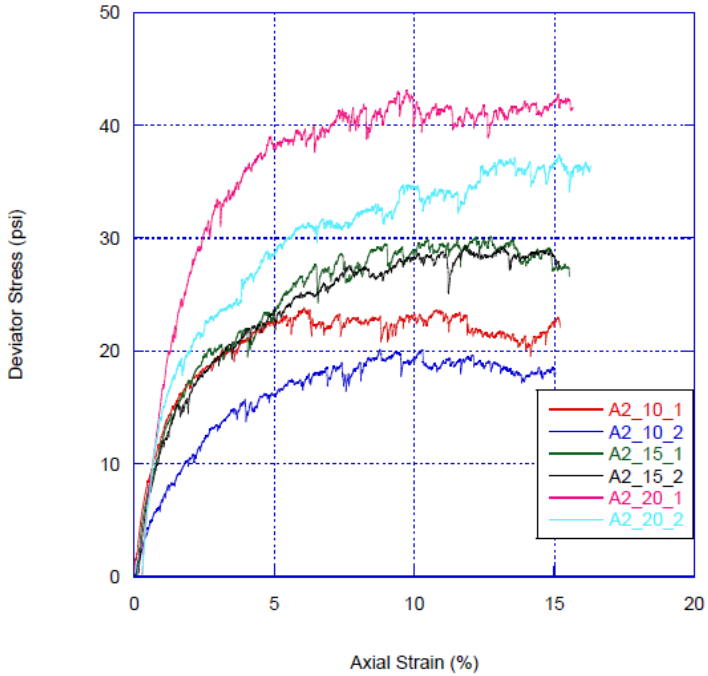

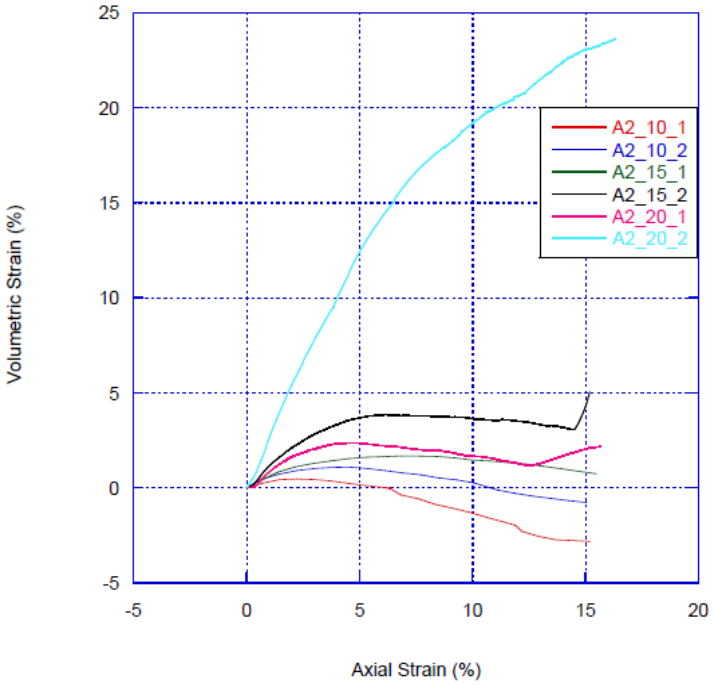

Figure A. 2. Gradation A2 stress-strain and volumetric strain curves

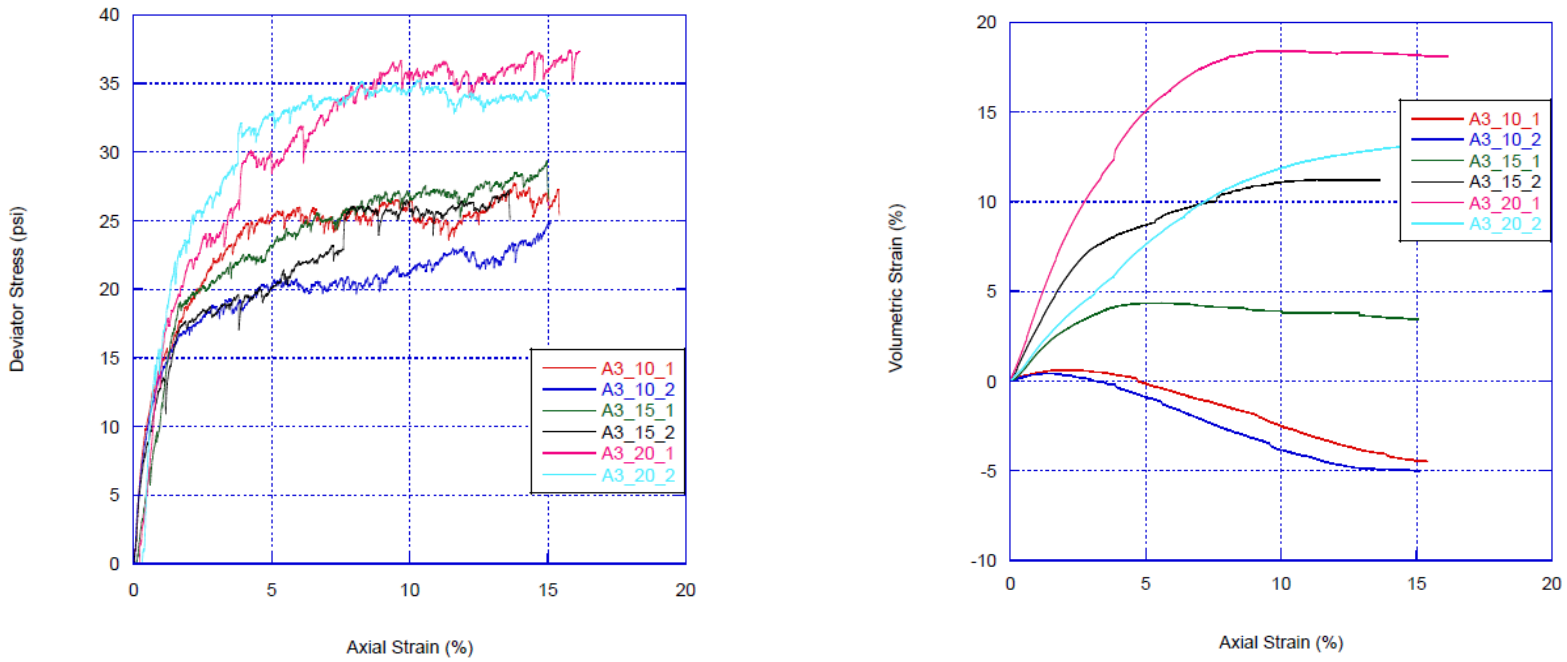

Figure A. 3. Gradation A3 stress-strain and volumetric strain curves

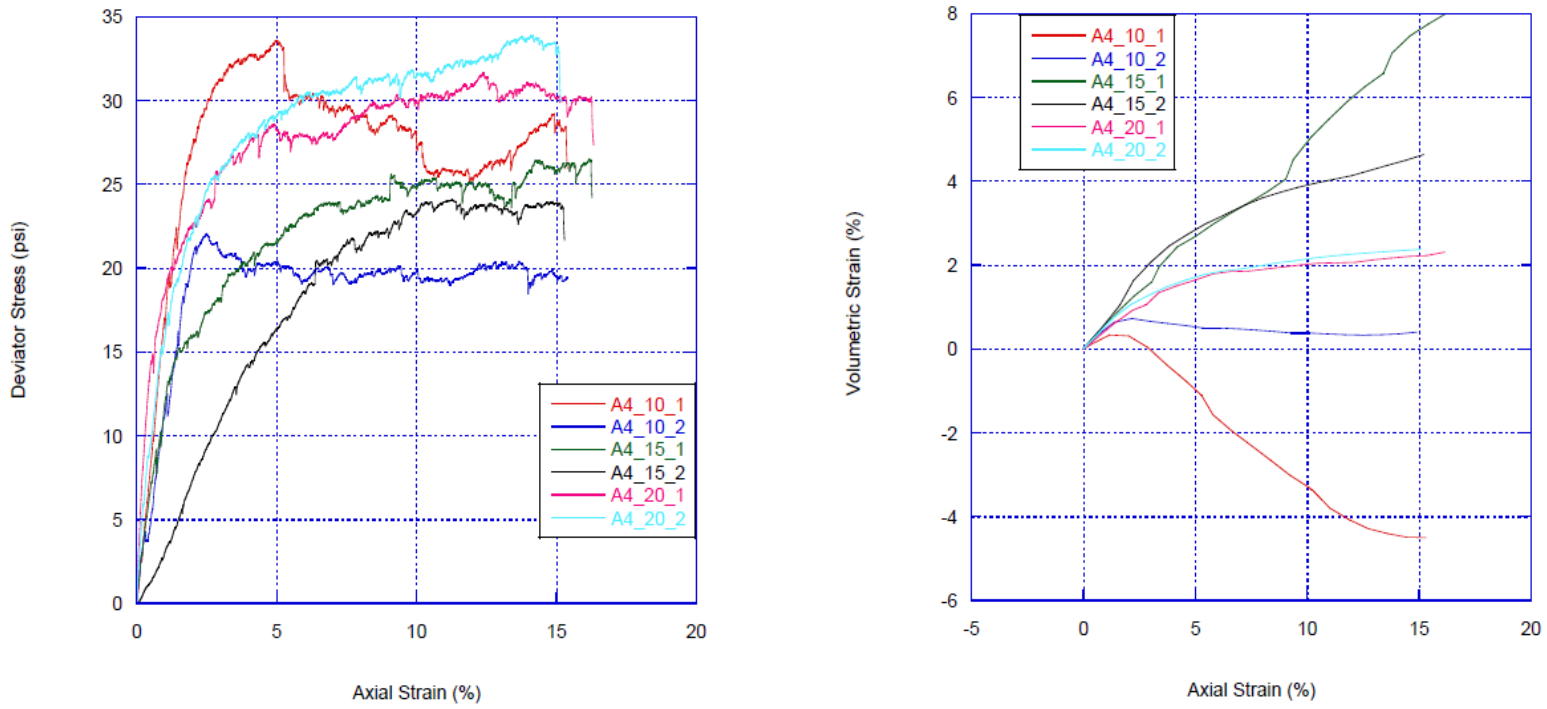

Figure A. 4. Gradation A4 stress-strain and volumetric strain curves

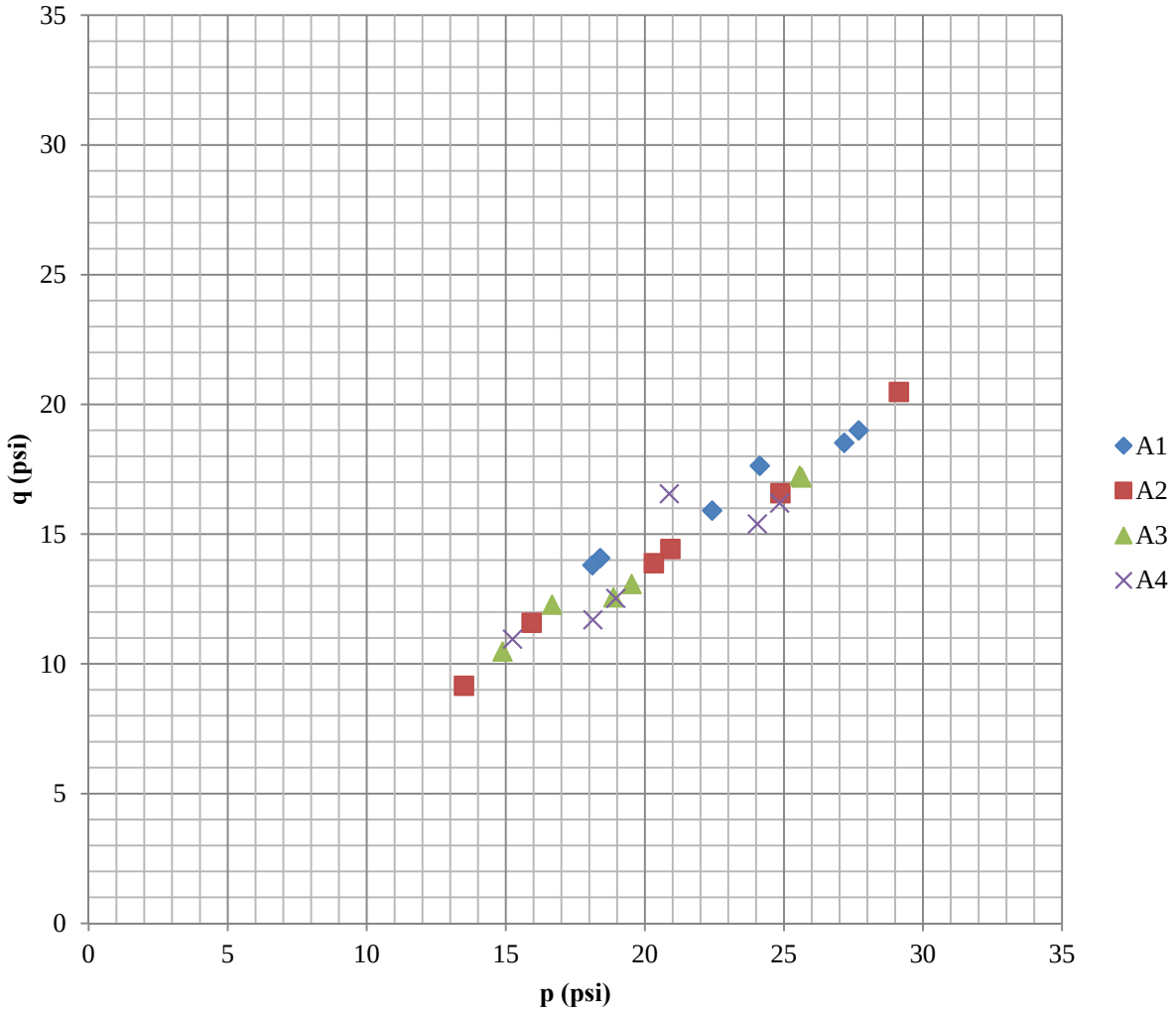

Figure A. 5. Type A material p-q diagram

Table A. 4. Type B test results

Test Name	Date	Gradation	Cell Pressure (psi)	γ Sample Tested	Void Ratio	% RC	Friction Angle	Comments
B1_10_1_60612	6-Jun	B1	4.3	-	-	-	53.3	
B1_10_2_61312	13-Jun	B1	4.3	94.20	0.75	87%	53.4	
B1_15_1_60712	7-Jun	B1	6.5	95.00	0.73	88%	51.5	
B1_15_2_61212	12-Jun	B1	6.5	97.20	0.69	90%	51.4	Sample touching chamber at strain <10%
B1_20_1_61112	11-Jun	B1	8.7	91.20	0.81	84%	53.8	
B1_20_2_61212	12-Jun	B1	8.7	91.40	0.80	85%	48.5	
B2_10_1_80112	1-Aug	B2	4.3	114.40	0.44	101%	49.6	
B2_10_2_80112	1-Aug	B2	4.3	114.70	0.44	101%	49.4	
B2_15_1_80212	2-Aug	B2	6.5	113.10	0.46	100%	53.2	Leak: volume change=100%
B2_15_2_80212	2-Aug	B2	6.5	111.60	0.48	98%	48.3	
B2_20_1_80312	3-Aug	B2	8.7	115.20	0.43	102%	50.7	
B2_20_2_80312	3-Aug	B2	8.7	116.90	0.41	103%	48.4	
B3_10_1_80412	4-Aug	B3	4.3	119.33	0.38	106%	45.9	Membrane rupture volume change large after 8%
B3_10_2_80612	6-Aug	B3	4.3	117.44	0.40	105%	48.4	
B3_15_1_80612	6-Aug	B3	6.5	118.27	0.39	106%	47.1	
B3_15_2_80712	7-Aug	B3	6.5	117.79	0.40	105%	46.0	
B3_20_1_80712	7-Aug	B3	8.7	118.48	0.39	106%	43.5	Inconsistent load curve trend
B3_20_2_80812	8-Aug	B3	8.7	115.89	0.42	103%	45.4	
B4_10_1_71812	18-Jul	B4	4.3	120.53	0.37	111%	31.8	
B4_15_1_82012	20-Aug	B4	6.5	119.40	0.38	110%	34.5	
B4_20_2_82312	23-Aug	B4	8.7	136.00	0.21	125%	41.7	

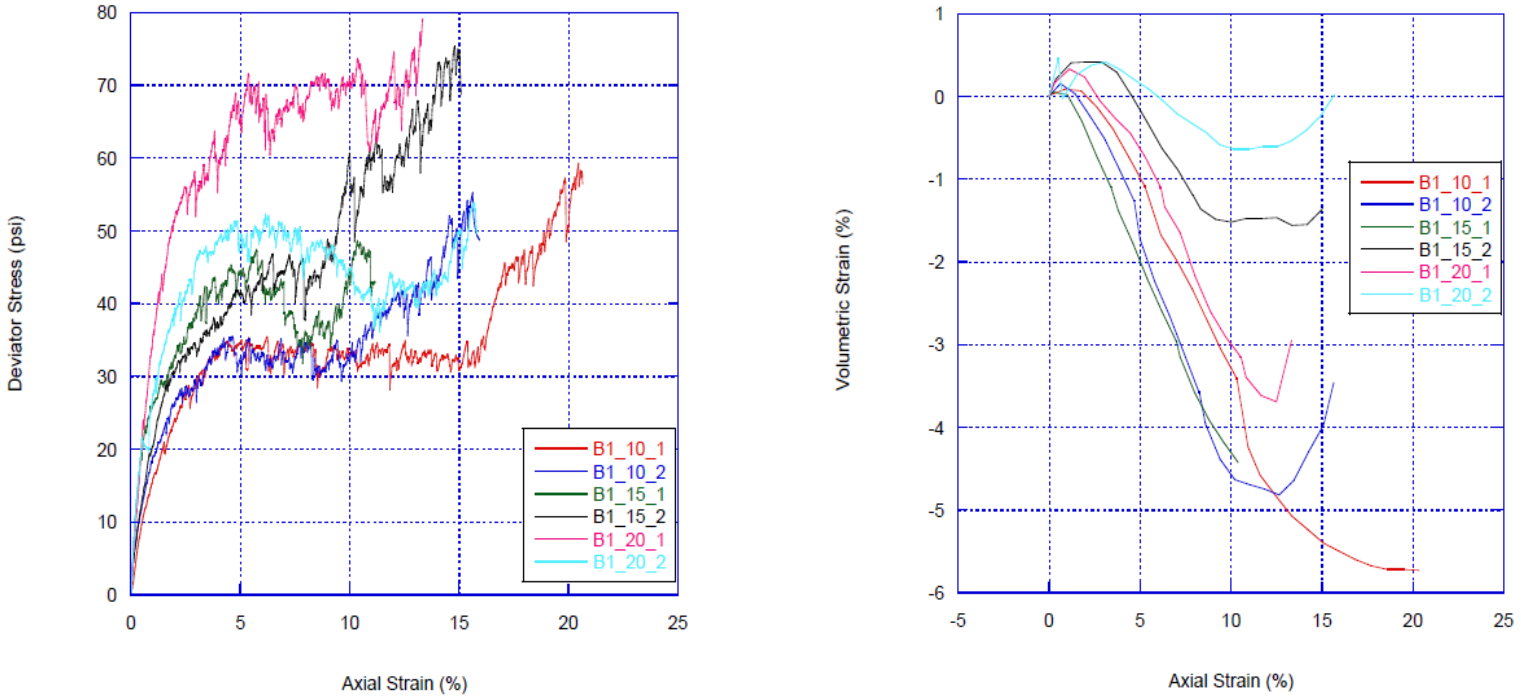

Figure A. 6. Gradation B1 stress-strain and volumetric strain curves

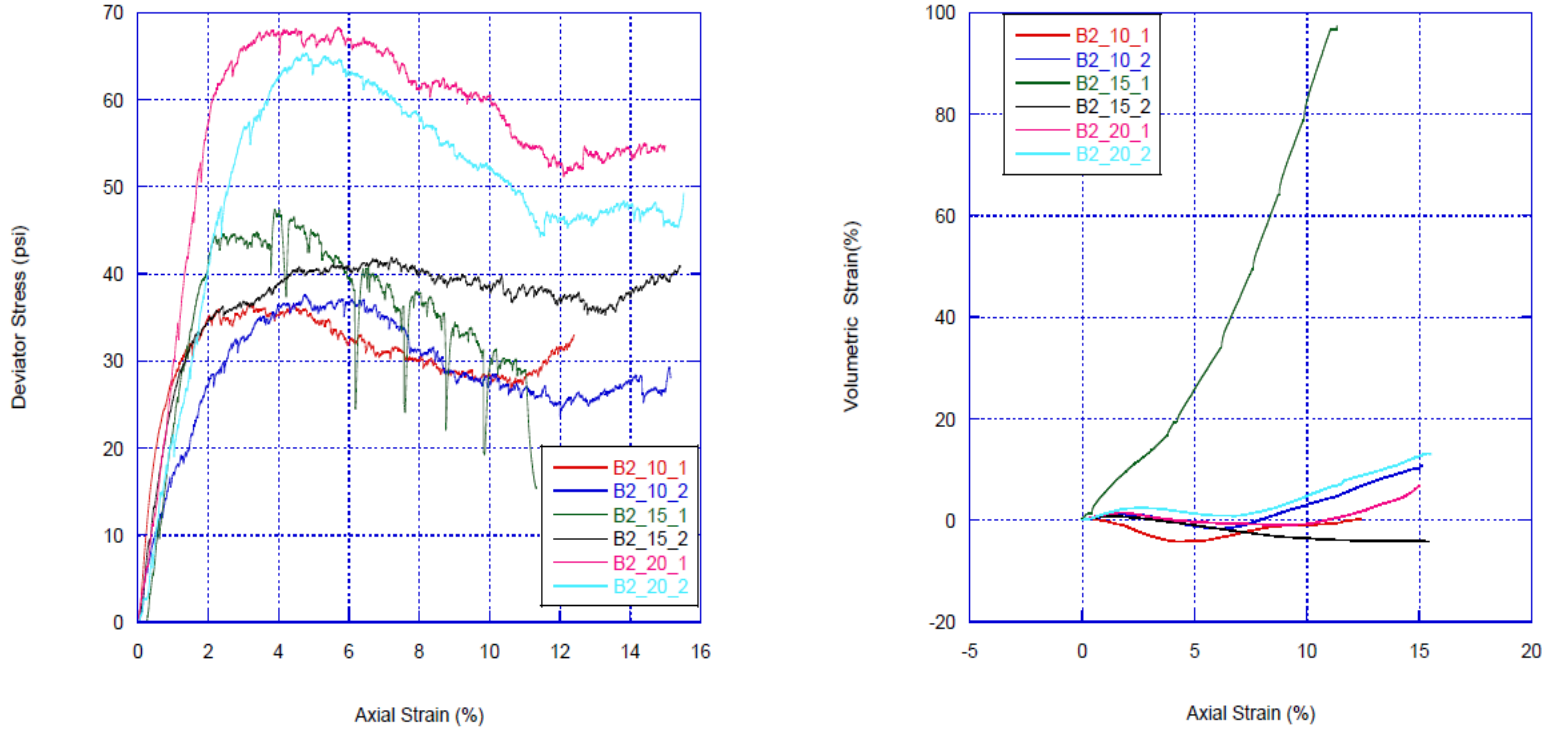

Figure A. 7. Gradation B2 stress-strain and volumetric strain curves

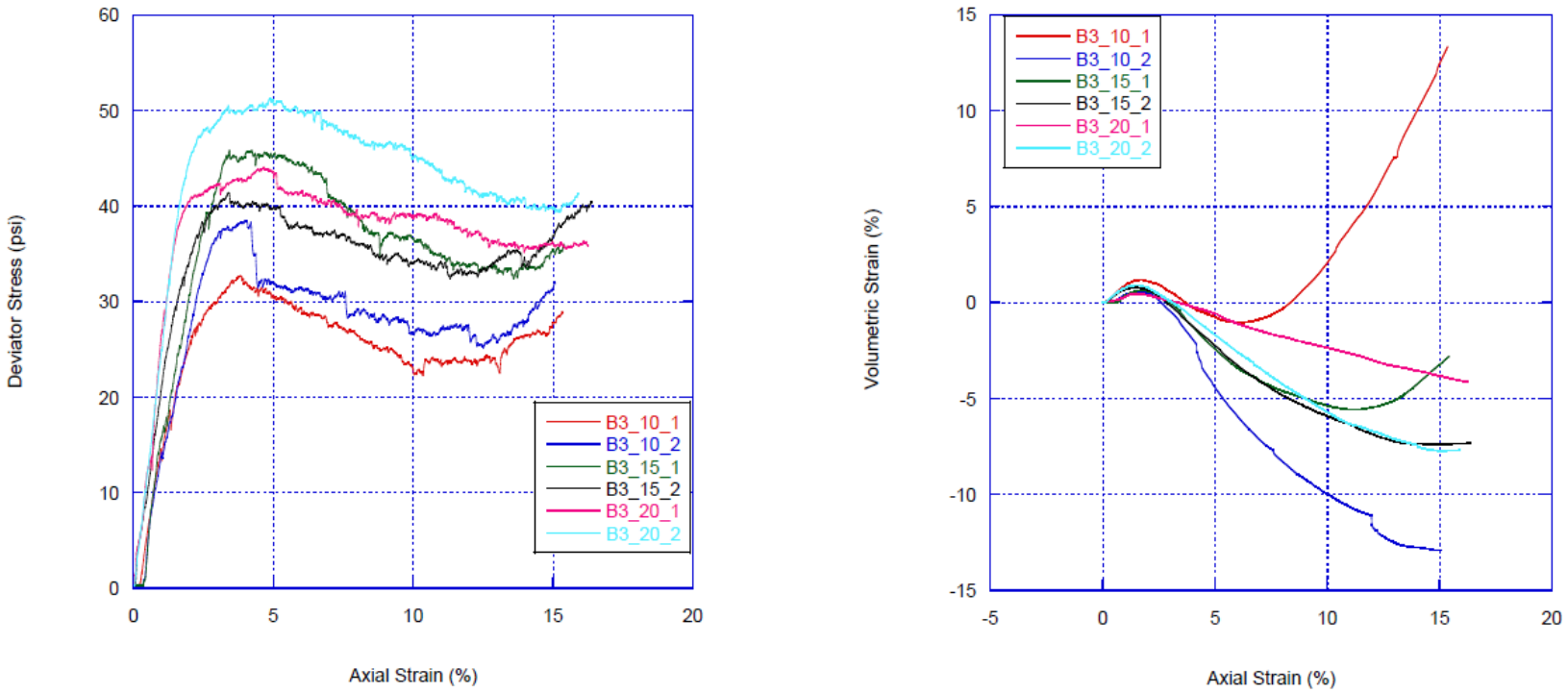

Figure A. 8. Gradation B3 stress-strain and volumetric strain curves

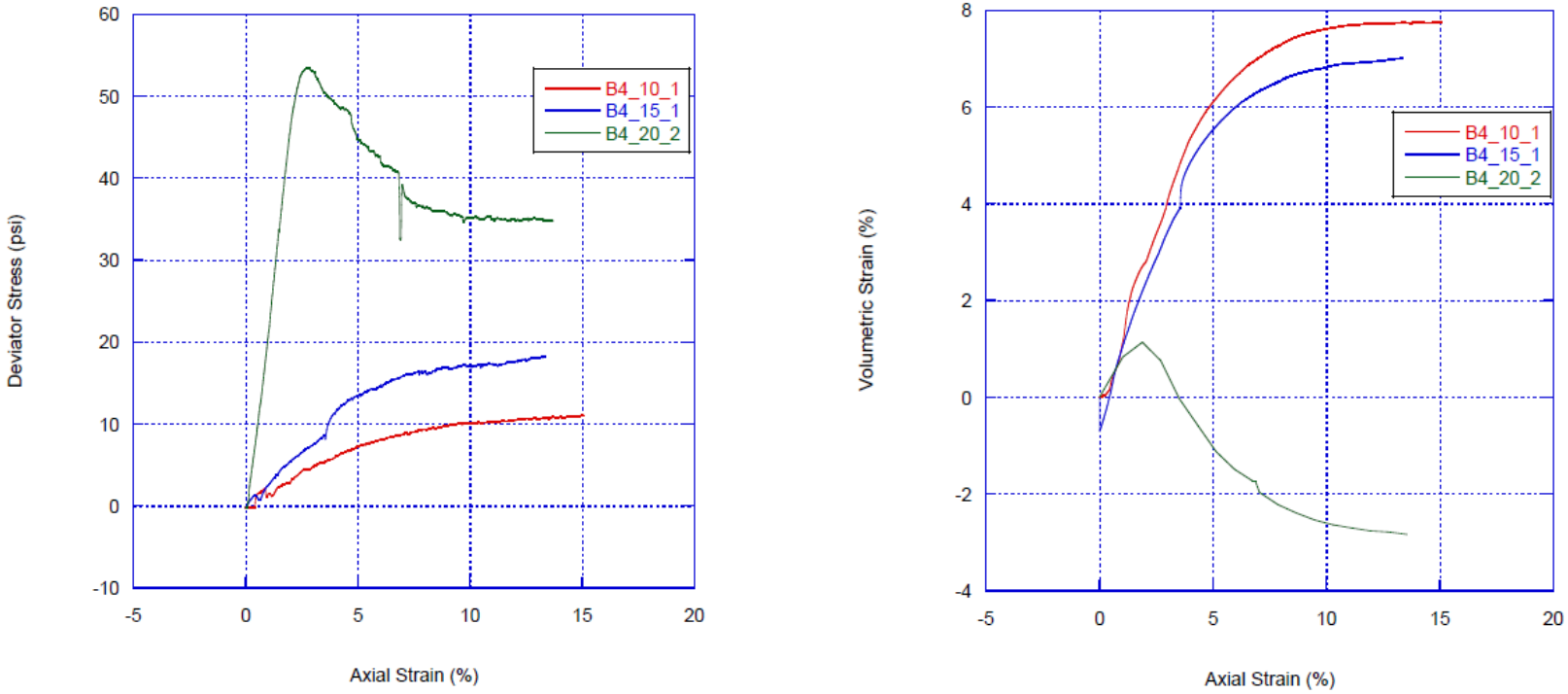

Figure A. 9. Gradation B4 stress-strain and volumetric strain curves

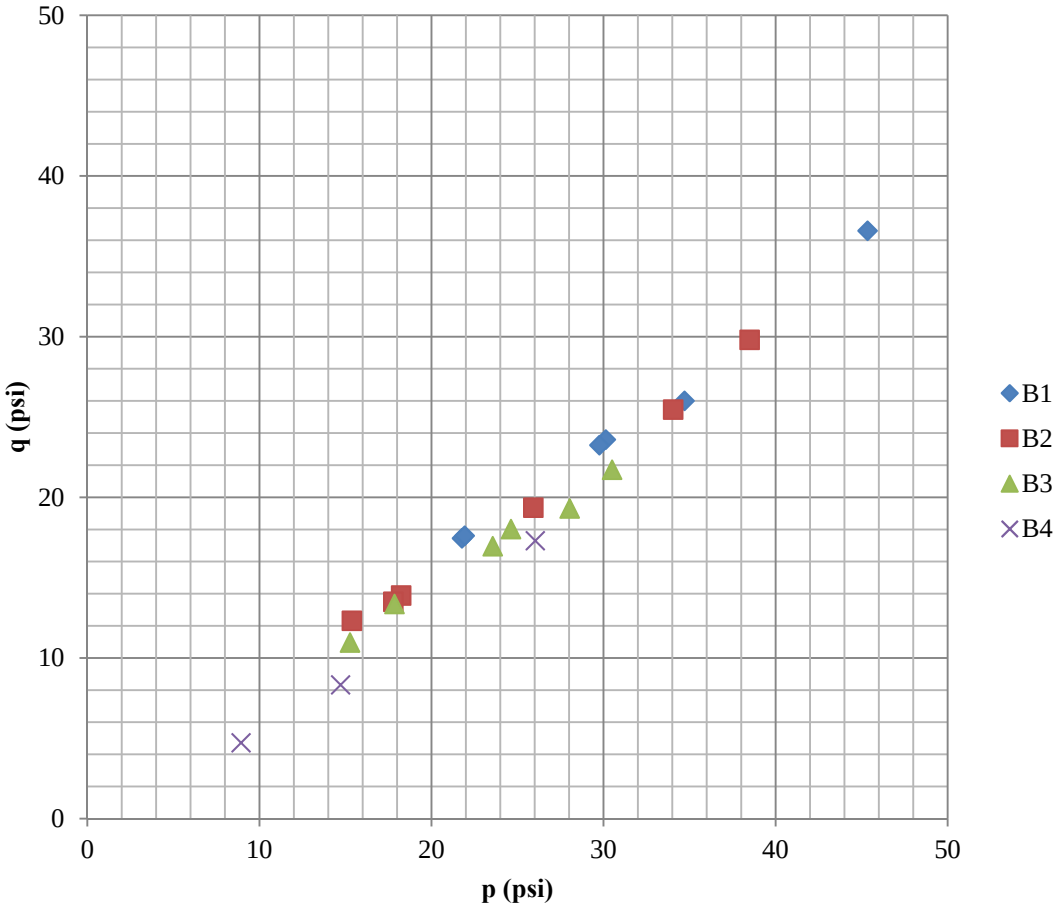

Figure A. 10. Type B material p-q diagram

Table A. 5. Type C test results

Test Name	Date	Soil Type	Gradation	Confining Stress (psf)	Confining Stress (psi)	Wall Height (ft)	Unit Weight of Sample Tested	Void Ratio	% RC	Friction Angle (undrained)	Friction Angle (drained)
C1_10_1_S_10412	4-Oct	C	C1	625	4.34	10	120.12	-	99.60	27.50	40.27
C1_10_2_S_10412	4-Oct	C	C1	625	4.34	10	123.44	-	102.35	29.19	39.08
C1_15_1_S_10612	6-Oct	C	C1	937.5	6.51	15	119.96	-	99.48	27.23	34.49
C1_15_2_S_10612	6-Oct	C	C1	937.5	6.51	15	125.31	-	103.93	29.45	34.48
C1_20_1_S_10812	8-Oct	C	C1	1250	8.68	20	117.73	-	97.62	26.23	27.97
C1_20_2_S_10812	8-Oct	C	C1	1250	8.68	20	124.11	-	102.91	28.10	30.94
C2_10_1_S_92812	28-Sep	C	C2	625	4.34	10	125.86	-	97.57	26.91	47.45
C2_10_2_S_10112	1-Oct	C	C2	625	4.34	10	131.97	-	101.52	28.33	44.24
C2_15_1_S_92812	28-Sep	C	C2	937.5	6.51	15	130.05	-	100.04	28.20	45.39
C2_15_2_S_10312	3-Oct	C	C2	937.5	6.51	15	128.70	-	99.00	29.22	35.96
C2_20_1_S_93012	30-Sep	C	C2	1250	8.68	20	124.96	-	96.12	26.24	30.06
C2_20_2_S_10112	1-Oct	C	C2	1250	8.68	20	131.79	-	101.38	28.82	41.12
C3_10_1_S_101012	10-Oct	C	C3	625	4.34	10	129.33	-	100.72	22.66	41.10
C3_10_2_S_101012	10-Oct	C	C3	625	4.34	10	133.23	-	103.76	32.02	50.90
C3_15_1_S_101112	11-Oct	C	C3	937.5	6.51	15	129.26	-	100.67	26.18	35.37
C3_15_2_S_101112	11-Oct	C	C3	937.5	6.51	15	132.89	-	103.49	28.48	44.03
C3_20_1_S_101212	12-Oct	C	C3	1250	8.68	20	133.02	-	103.60	26.99	33.67
C3_20_2_S_101212	12-Oct	C	C3	1250	8.68	20	129.99	-	101.24	27.80	35.41
C4_10_1_S_101612	16-Oct	C	C4	625	4.34	10	125.10	-	98.97	25.82	26.41
C4_10_1_S_101612	16-Oct	C	C4	625	4.34	10	121.01	-	95.81	32.31	20.44
C4_15_1_S_101912	19-Oct	C	C4	937.5	6.51	15	119.57	-	94.59	23.66	14.49
C4_15_2_S_101712	17-Oct	C	C4	937.5	6.51	15	126.87	-	100.29	30.68	22.00
C4_20_1_S_101812	18-Oct	C	C4	1250	8.68	20	128.64	-	101.69	27.68	22.79
C4_20_1_S_101812	18-Oct	C	C4	1250	8.68	20	124.28	-	98.32	32.29	13.37

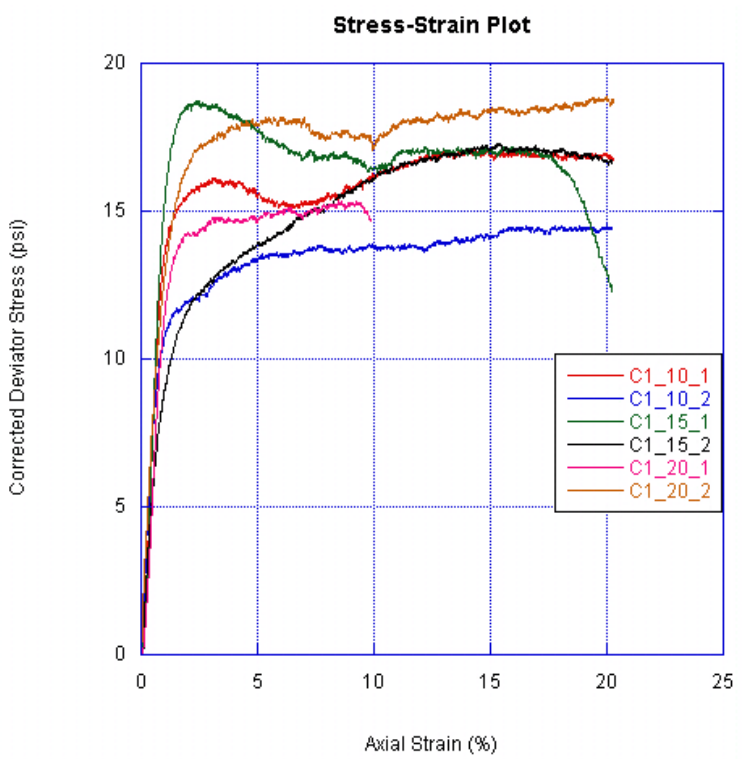

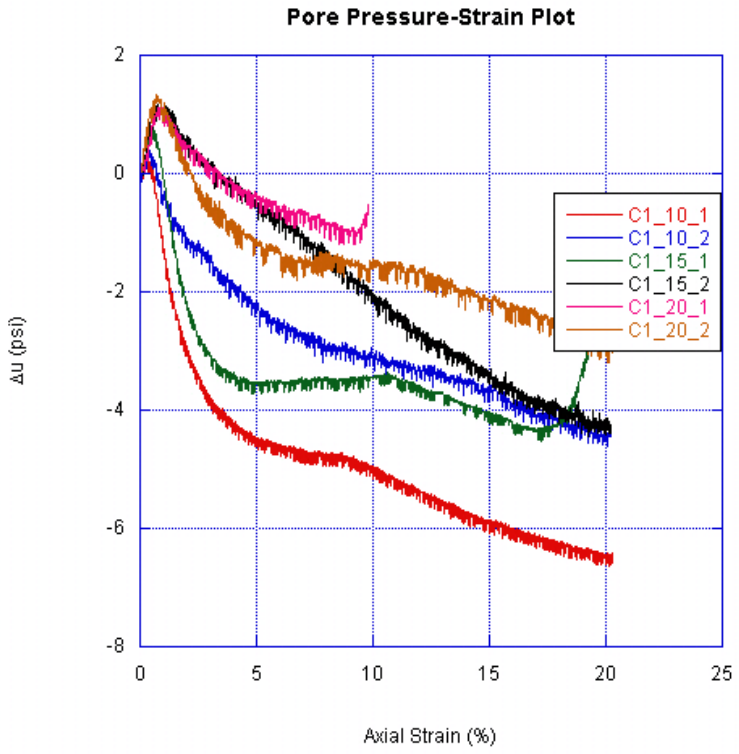

Figure A. 11. Gradation C1 stress-strain and pore pressure-strain curves

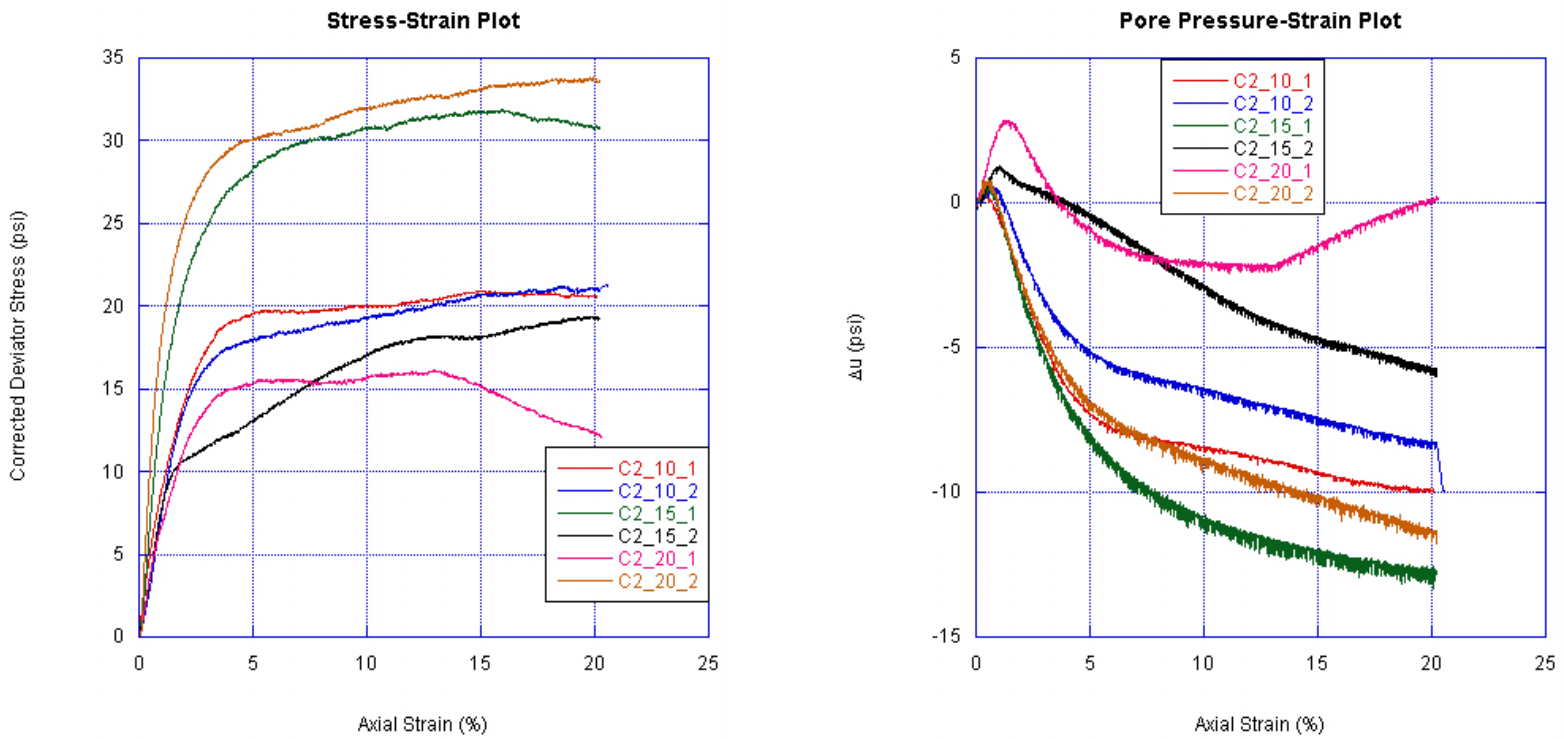

Figure A. 12. Gradation C2 stress-strain and pore pressure-strain curves

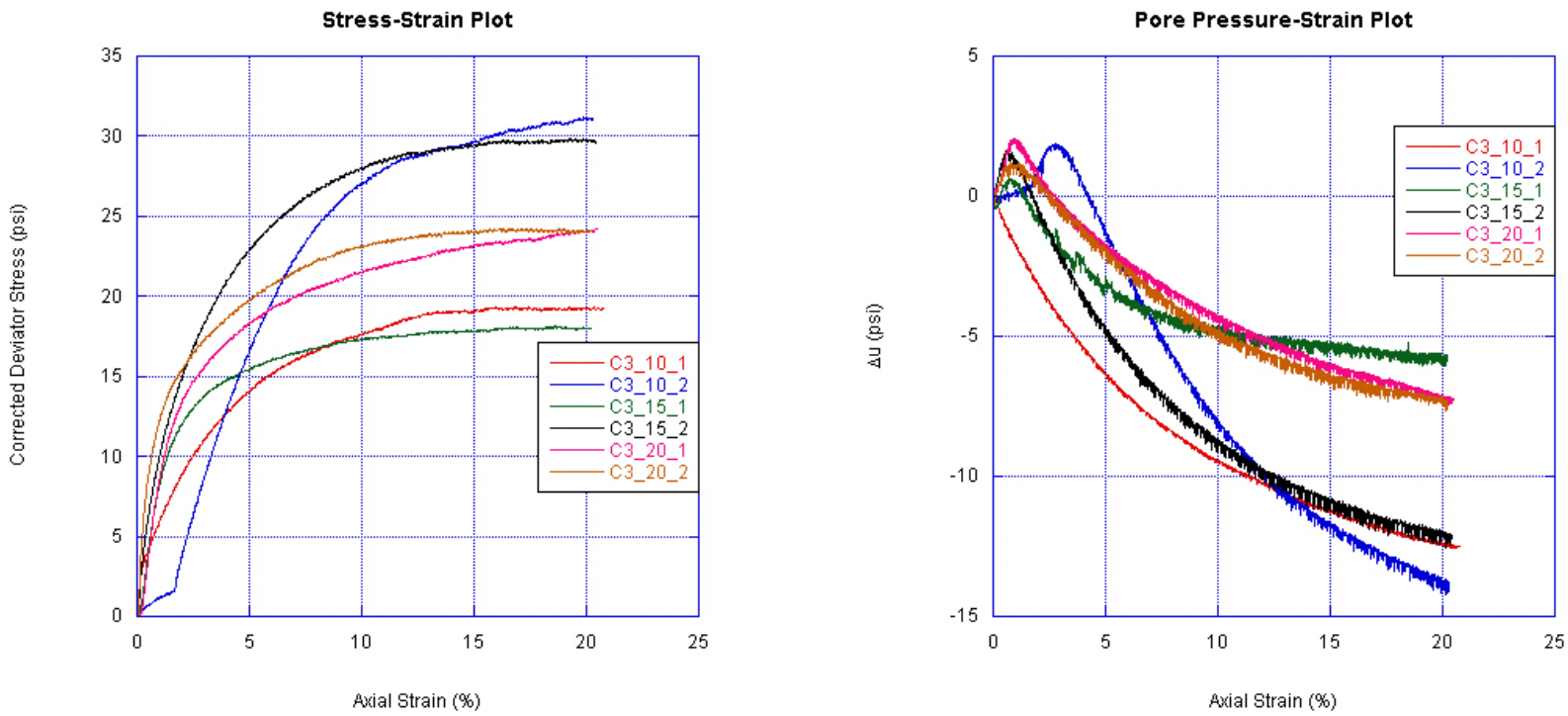

Figure A. 13. Gradation C3 stress-strain and pore pressure-strain curves

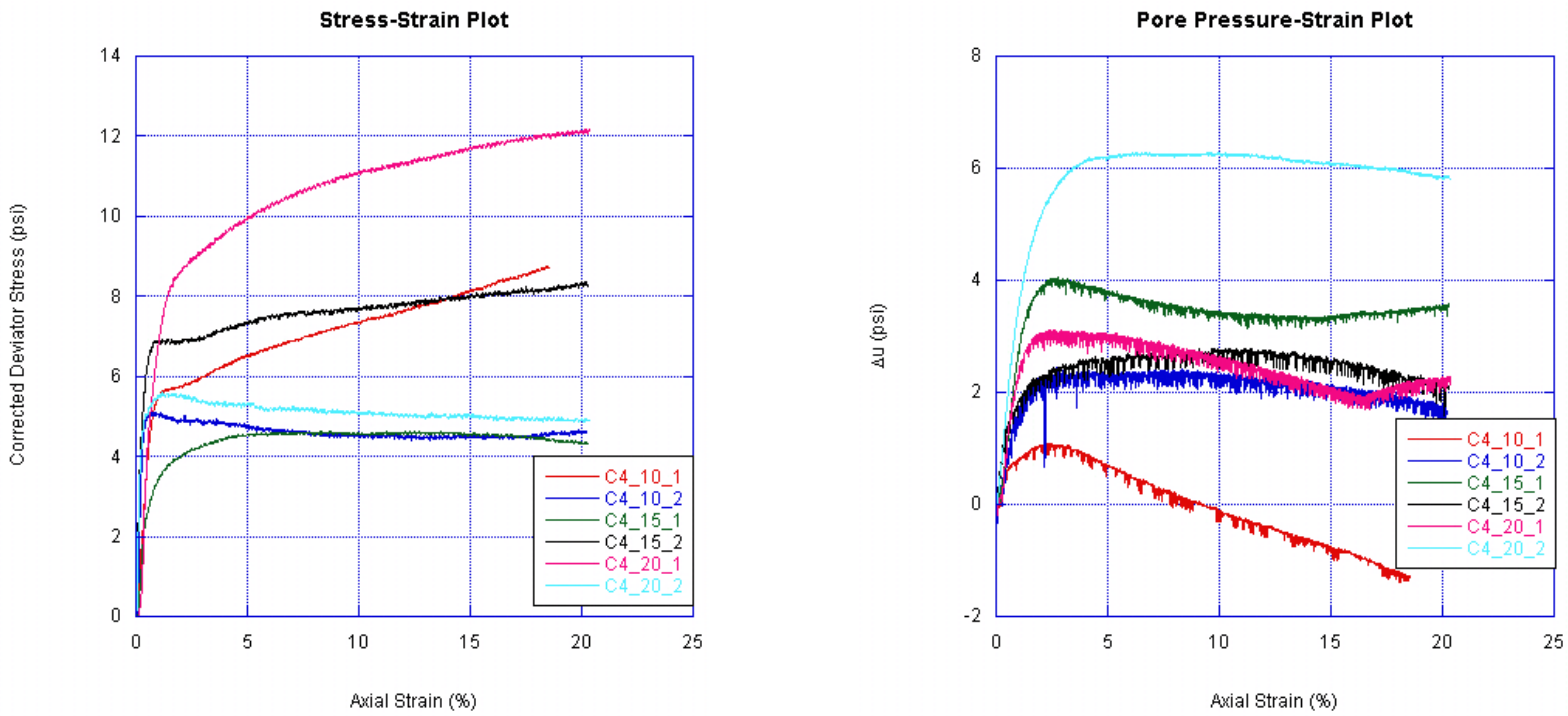

Figure A. 14. Gradation C4 stress-strain and pore pressure-strain curves

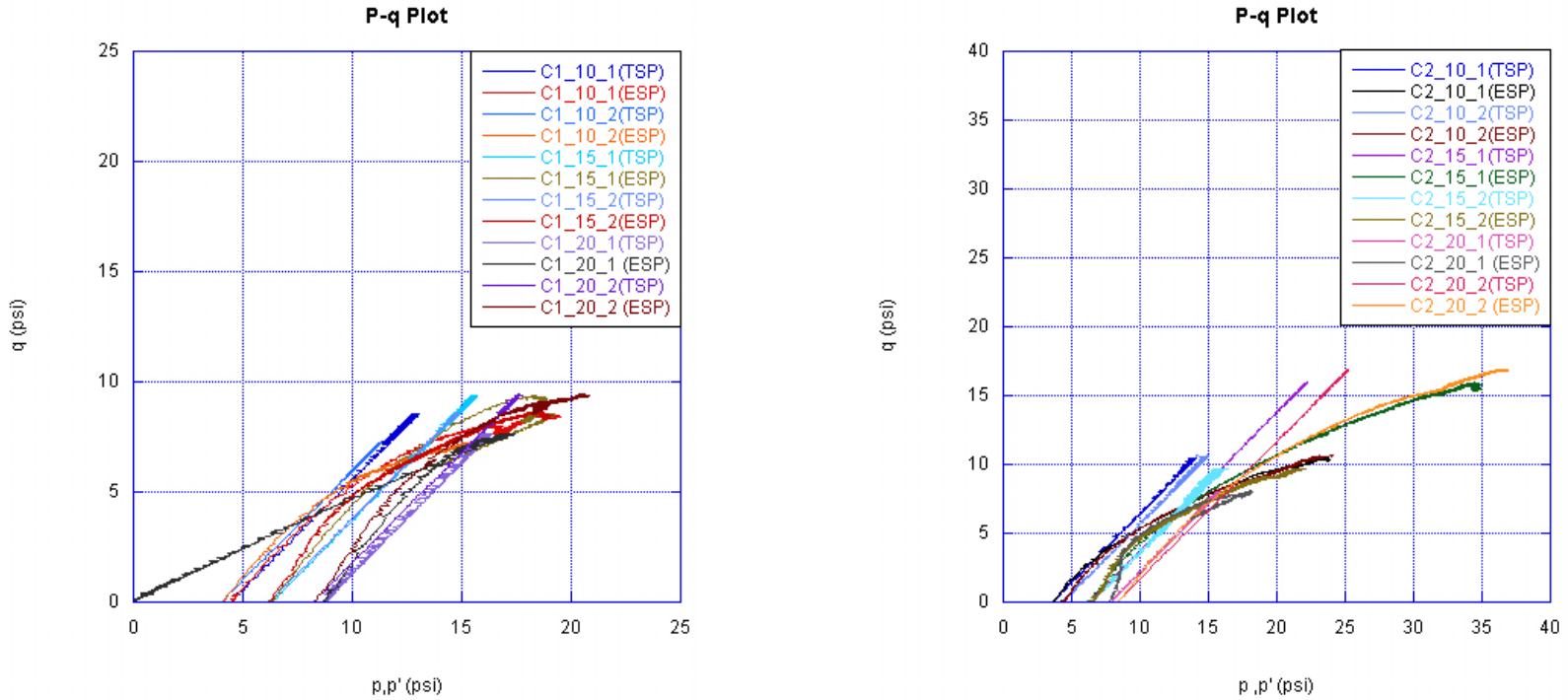

Figure A. 15. Type C-1 and C-2 p-q plots

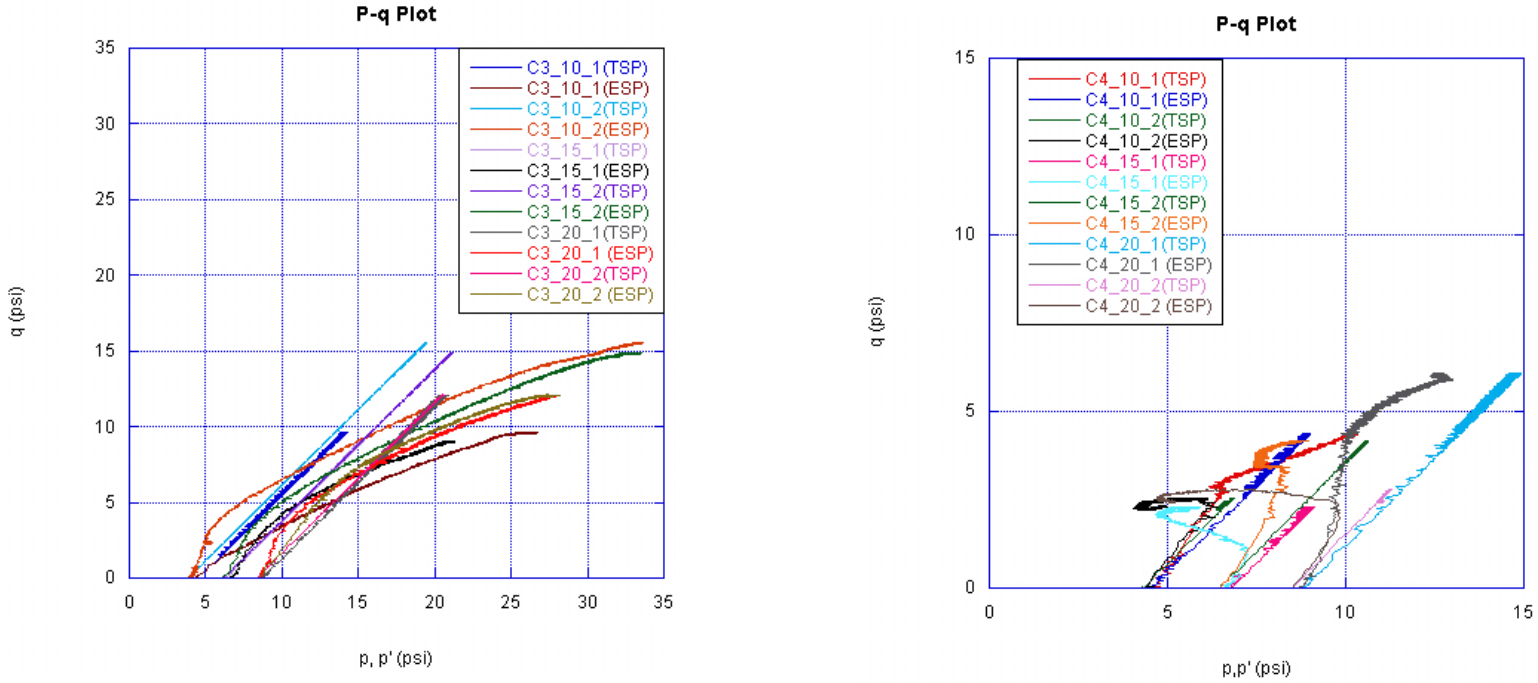

Figure A. 16. Type C-3 and C-4 p-q plots

Table A. 6. Type D test results

Test Name	Date	Gradation	Cell Pressure (psi)	γ of Sample Tested	Void Ratio	% RC	ϕ	Comments
D1_10_1_52012	20-May	D1	4.3	-		-	46.9	
D1_10_2_53012	30-May	D1	4.3	87.50	0.93	94%	47.2	
D1_15_1_52112	21-May	D1	6.5	-		-	42.3	
D1_15_2_61812	18-Jun	D1	6.5	86.20	0.95	92%	45.2	
D1_20_1_52212	22-May	D1	8.7	-		-	41.6	
D1_20_2_61912	19-Jun	D1	8.7	90.00	0.87	96%	45.0	Leak. volume change=10%
D2_10_1_71112	11-Jul	D2	4.3	89.10	0.89	86%	47.0	
D2_10_2_71112	11-Jul	D2	4.3	82.00	1.05	79%	39.6	Inconsistent load curve trend, leak. volume change 9%
D2_15_1_71212	12-Jul	D2	6.5	88.50	0.90	85%	44.6	Inconsistent load curve trend
D2_15_2_71212	12-Jul	D2	6.5	84.80	0.99	82%	41.2	
D2_20_1_71312	13-Jul	D2	8.7	82.90	1.03	80%	36.5	
D2_20_2_71312	13-Jul	D2	8.7	85.68	0.97	83%	38.0	
D3_10_1_72312	23-Jul	D3	4.3	101.80	0.66	107%	51.59	Inconsistent load curve
D3_10_2_72312	23-Jul	D3	4.3	103.60	0.63	109%	50.95	Same as above
D3_15_1_72412	24-Jul	D3	6.5	95.00	0.77	100%	39.93	Leak: volume change=16%
D3_15_2_72412	24-Jul	D3	6.5	88.00	0.91	93%	42.06	
D3_20_1_72512	25-Jul	D3	8.7	90.11	0.87	95%	38.40	
D3_20_2_73112	31-Jul	D3	8.7	88.33	0.91	93%	42.41	
D4_10_1_62512	25-Jun	D4	4.3	90.00	0.87	90%	41.00	Inconsistent volume behavior
D4_10_2_62612	26-Jun	D4	4.3	89.60	0.88	90%	41.70	
D4_15_1_62712	27-Jun	D4	6.5	93.00	0.81	93%	39.40	Inconsistent load curve trend
D4_15_2_62912	29-Jun	D4	6.5	79.40	1.12	80%	35.80	Compliant load curve
D4_20_1_62812	28-Jun	D4	8.7	81.50	1.07	82%	36.10	
D4_20_2_62912	29-Jun	D4	8.7	88.00	0.91	88%	37.90	

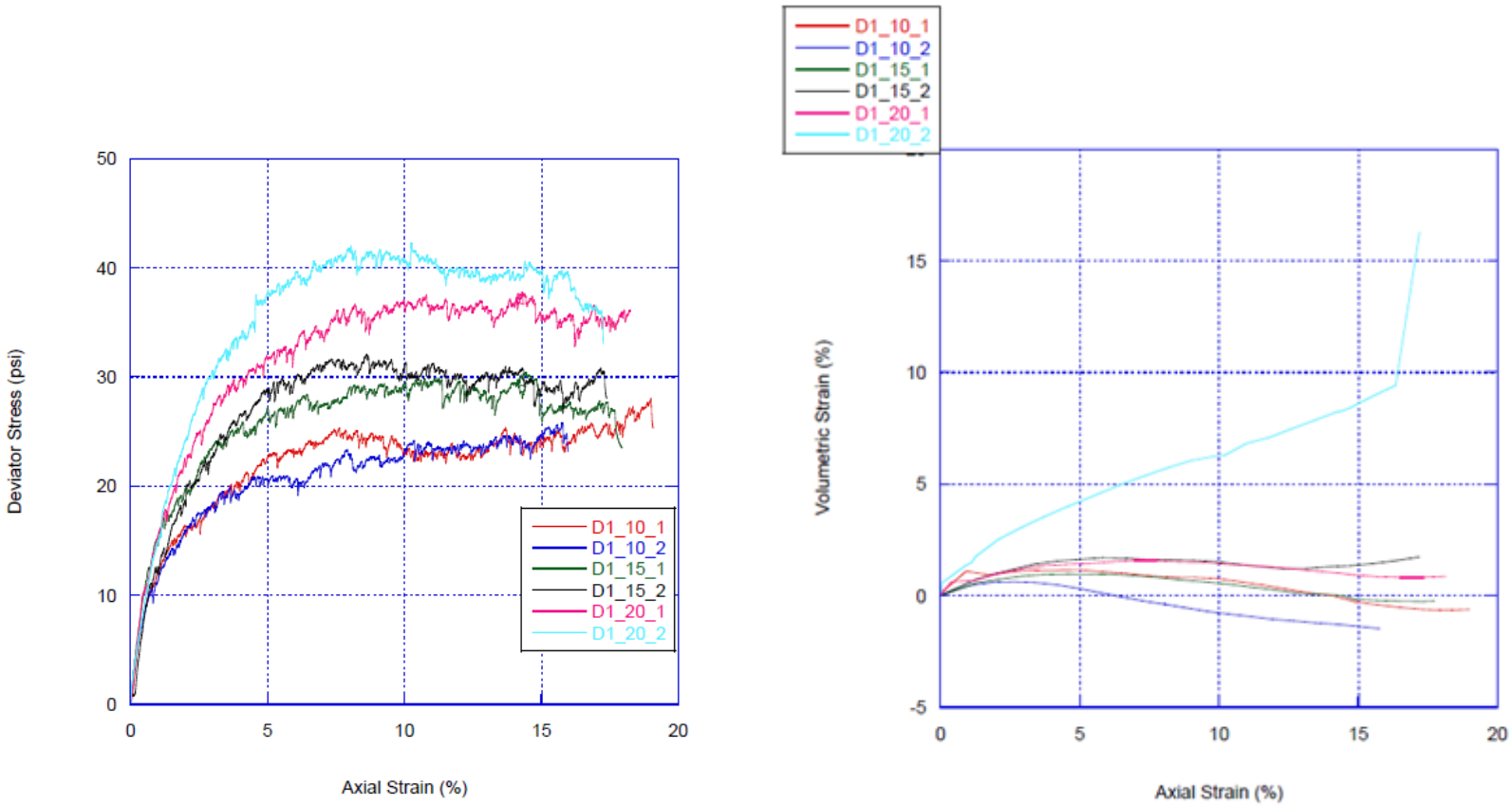

Figure A. 17. Gradation D1 stress-strain and volumetric strain curves

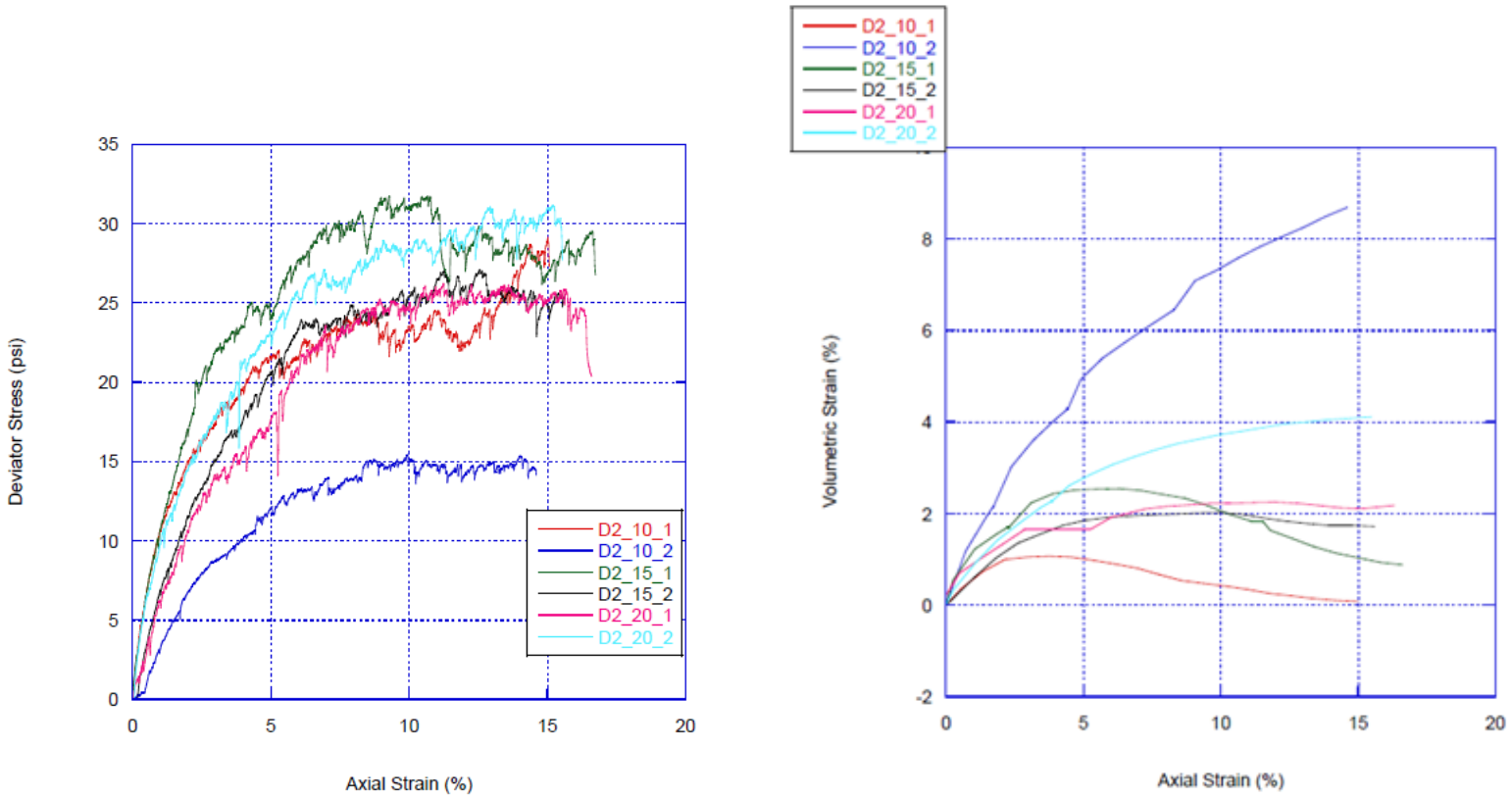

Figure A. 18. Gradation D2 stress-strain and volumetric strain curves

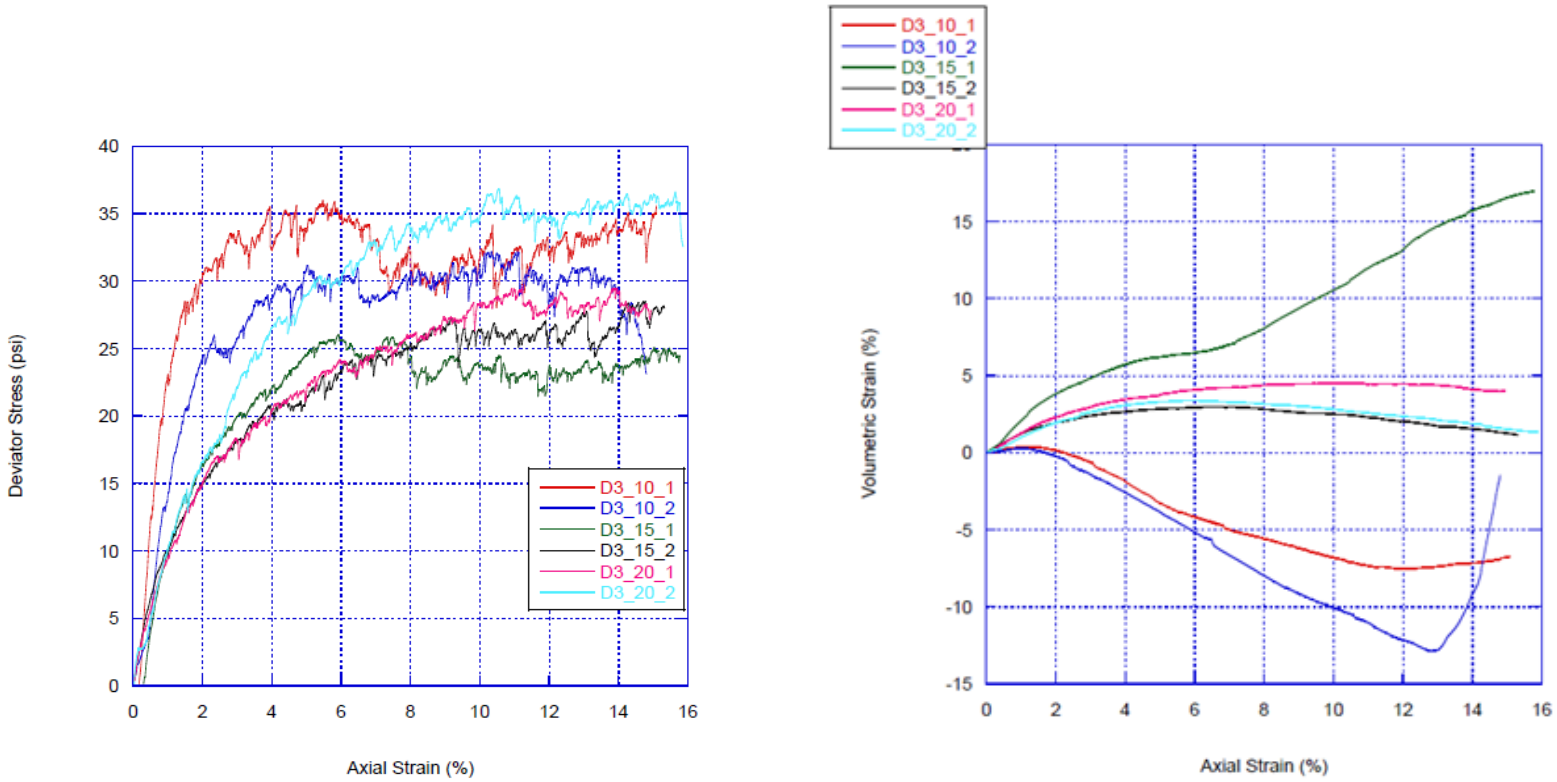

Figure A. 19. Gradation D3 stress-strain and volumetric strain curves

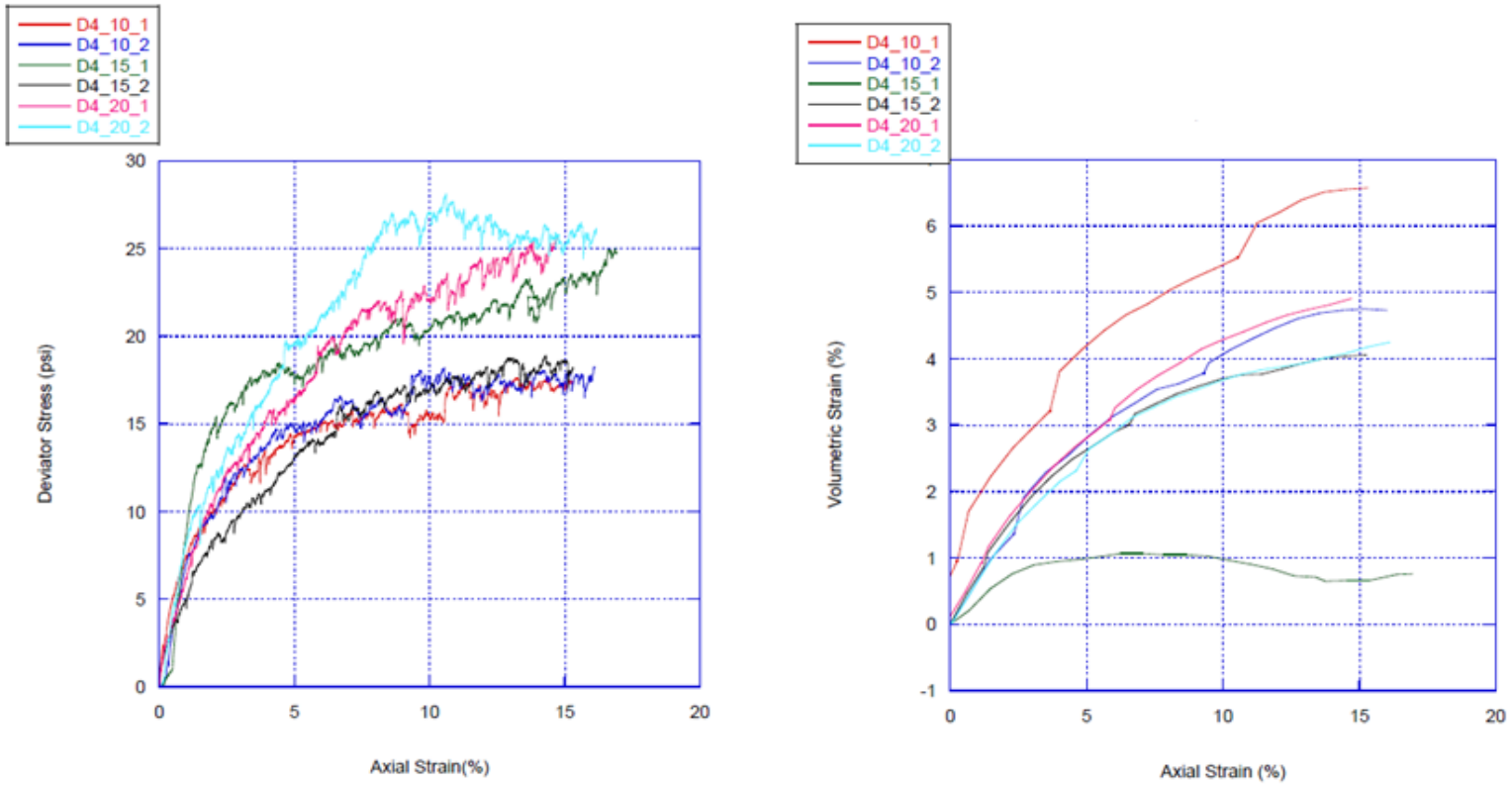

Figure A. 20. Gradation D4 stress-strain and volumetric strain curves

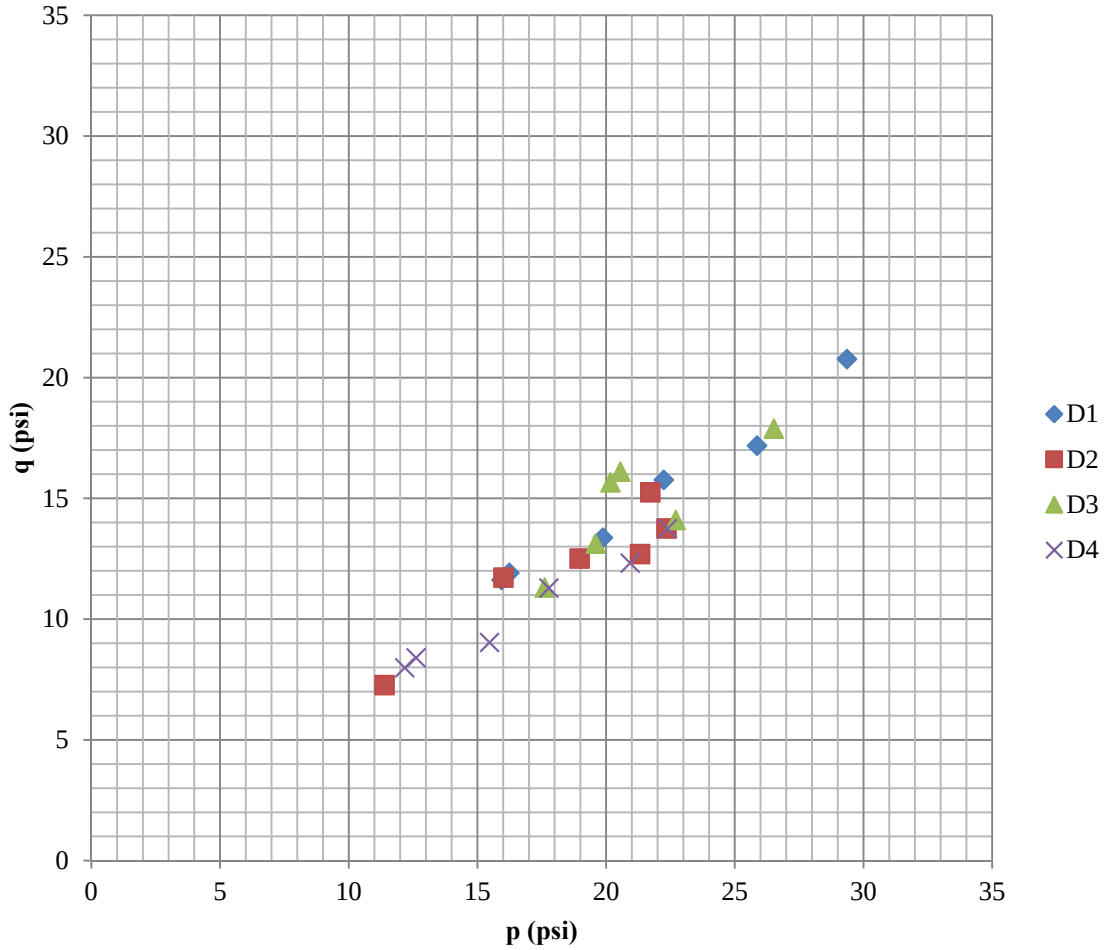

Figure A. 21. Type D material p-q diagram

APPENDIX B

RESULTS FROM FLAC SIMULATIONS

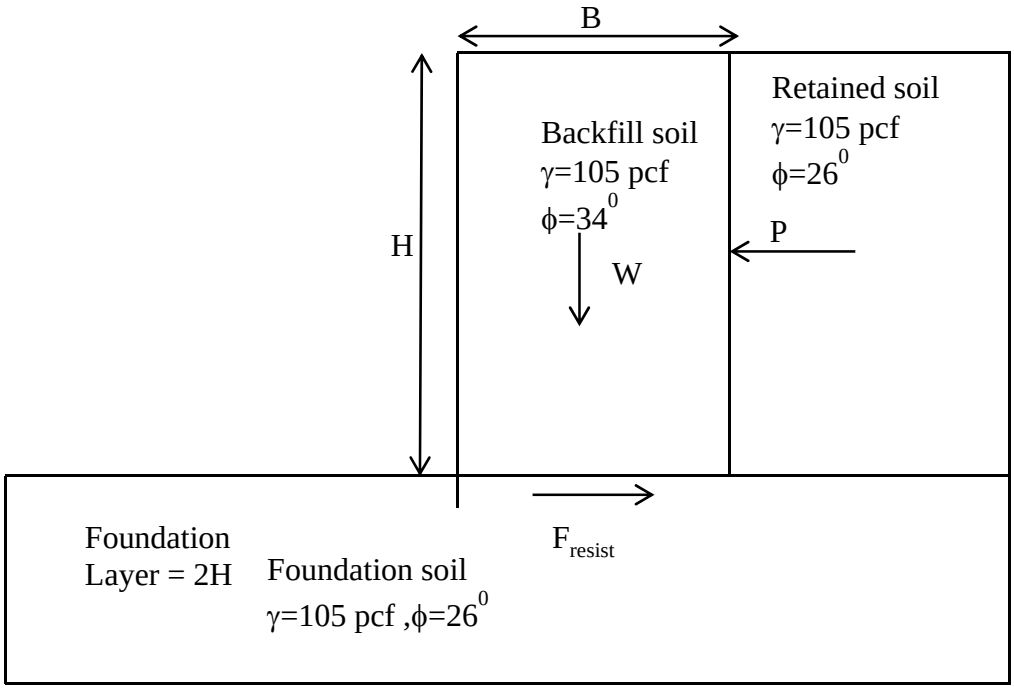

Figure B. 1. Dimensions and properties used for Series 1 Case 1.

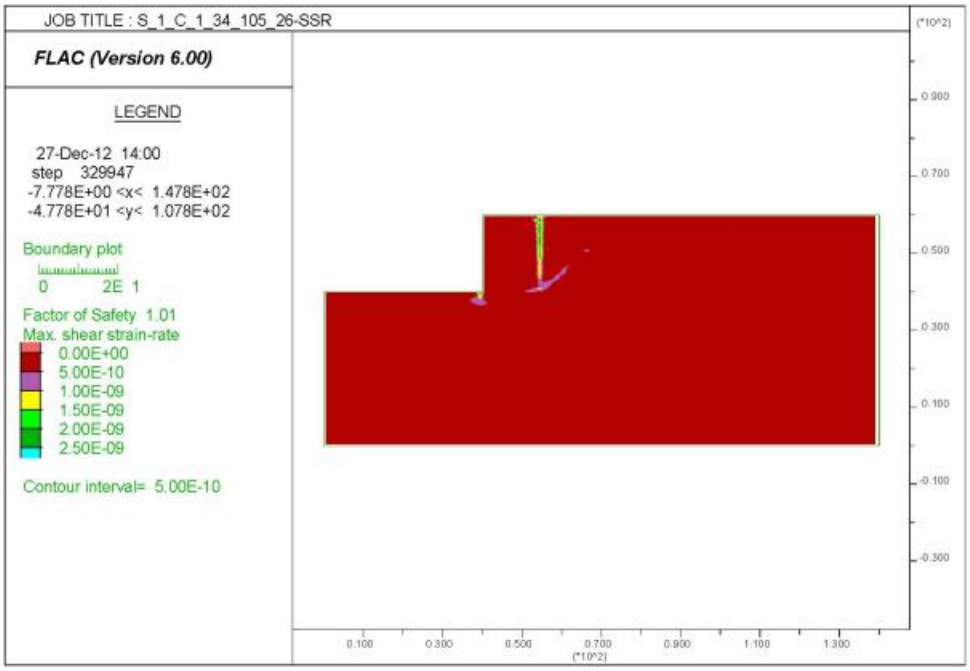

Figure B. 2. Series 1 Case 1 Foundation angle ϕ=26^0, Backfill angle ϕ=34^0 and γ=105pcf Maximum Shear Strain Rate.

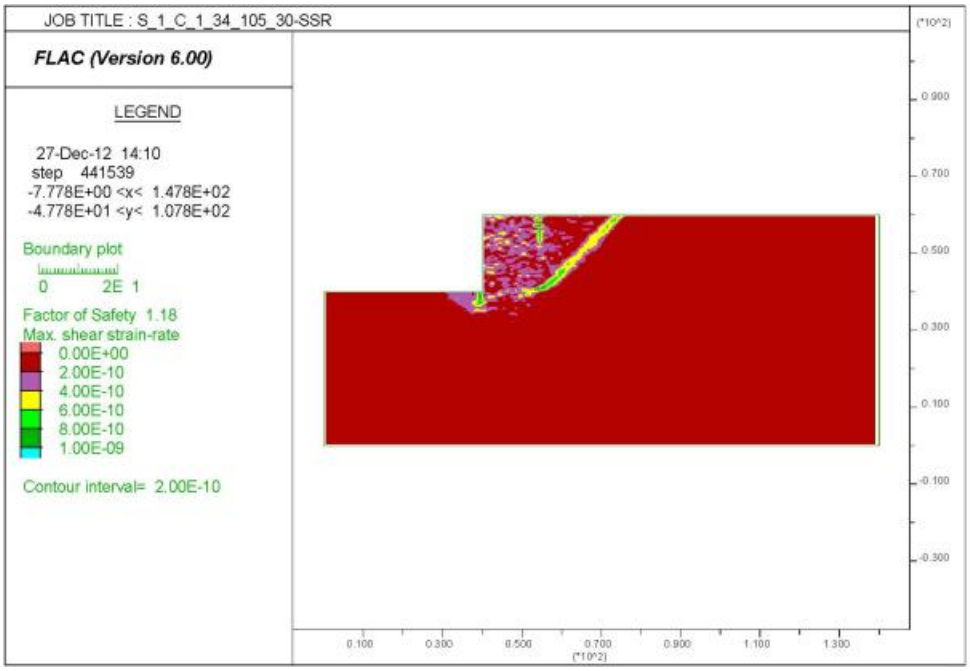

Figure B. 3. Series 1 Case 1 Foundation angle ϕ=30^0, Backfill angle ϕ=34^0 and γ=105pcf Maximum Shear Strain Rate.

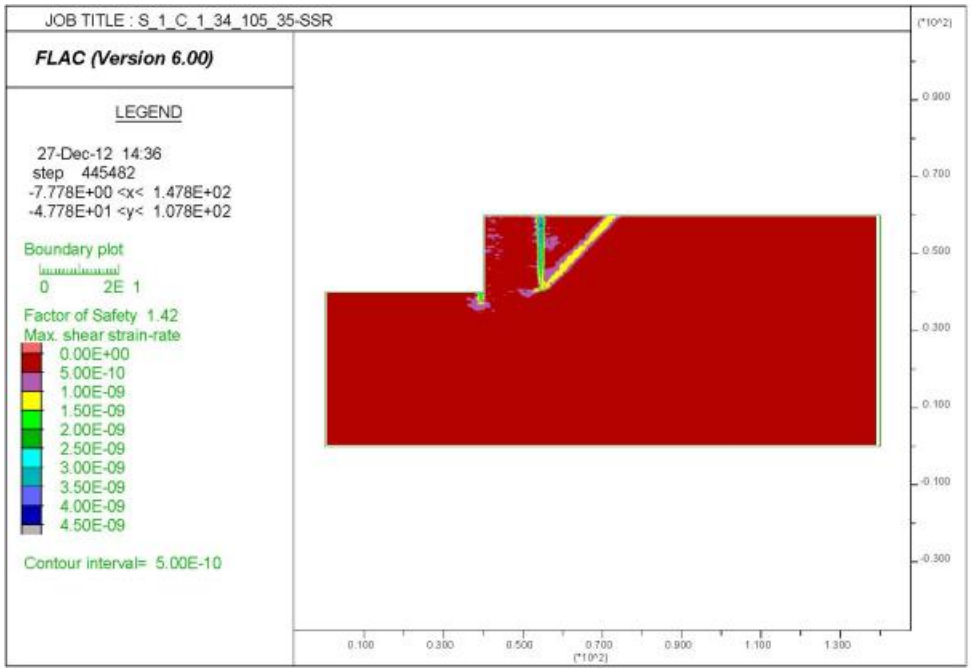

Figure B. 4. Series 1 Case 1 Foundation angle ϕ=35^0, Backfill angle ϕ=34^0 and γ=105pcf Maximum Shear Strain Rate.

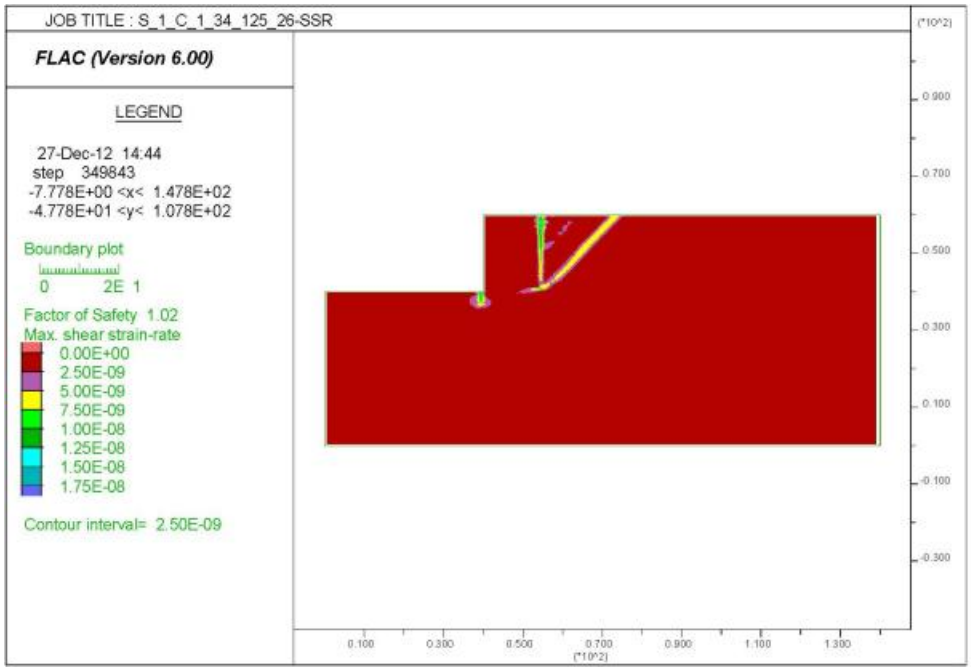

Figure B. 5. Series 1 Case 1 Foundation angle ϕ=26^0, Backfill angle ϕ=34^0 and γ=125pcf Maximum Shear Strain Rate.

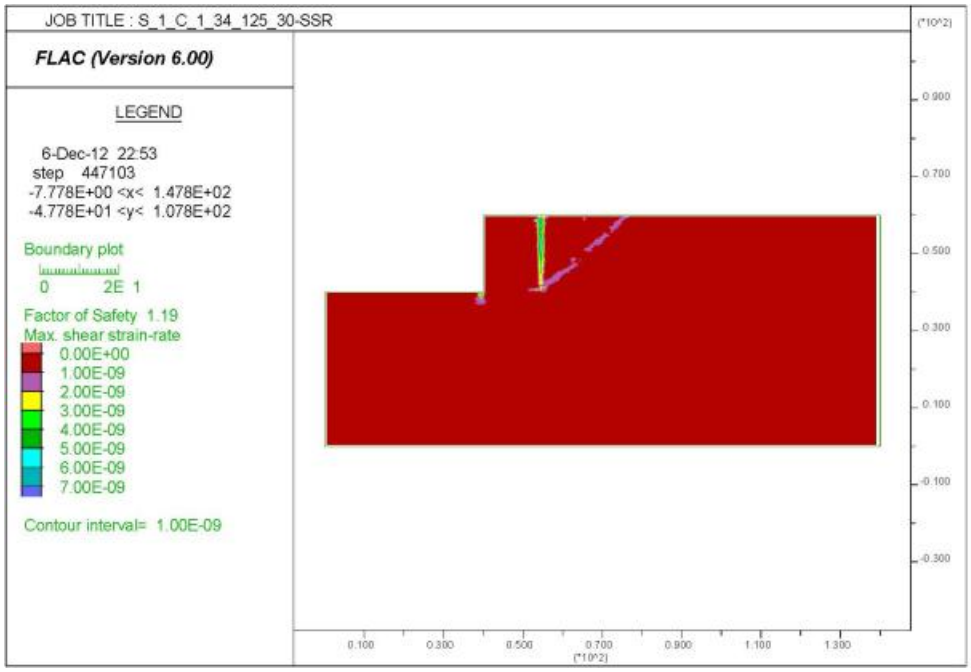

Figure B. 6. Series 1 Case 1 Foundation angle $\phi=30^{0}$, Backfill angle $\phi=34^{0}$ and γ=125pcf Maximum Shear Strain Rate.

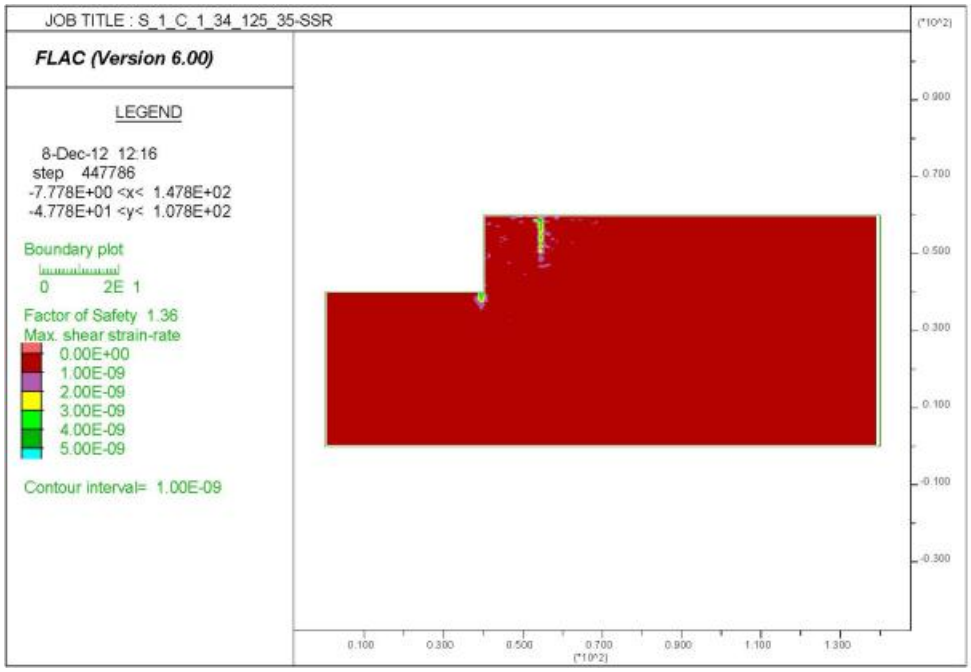

Figure B. 7. Series 1 Case 1 Foundation angle $\phi=35^{0}$, Backfill angle $\phi=34^{0}$ and γ=125pcf Maximum Shear Strain Rate.

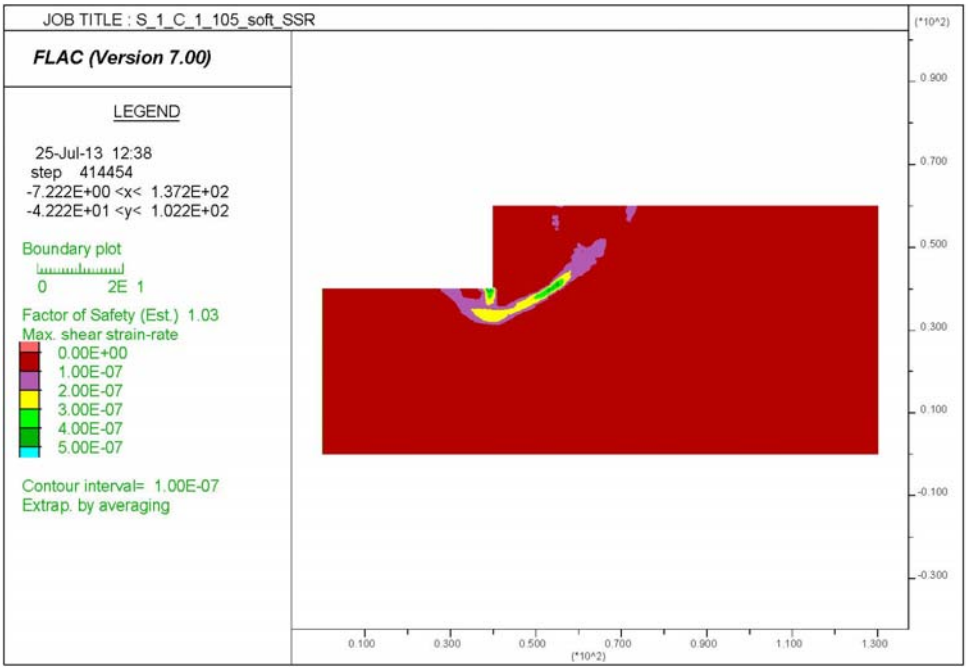

Figure B. 8. Series 1 Case 1 Foundation C_u=500 psf, Backfill angle ϕ=34^{o}and γ=105pcf Maximum Shear Strain Rate.

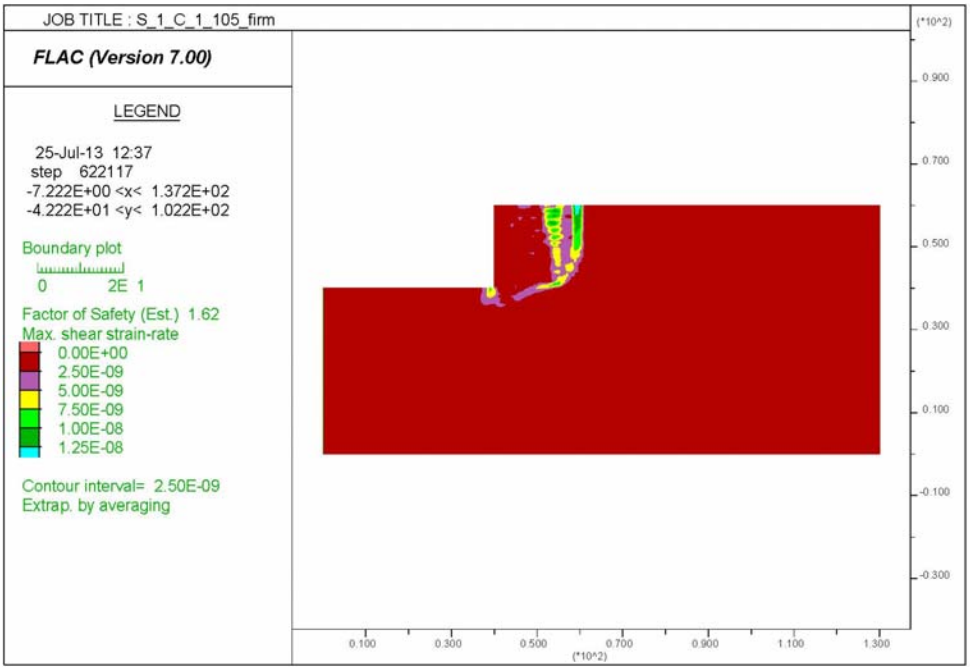

Figure B. 9. Series 1 Case 1 Foundation C_u=1000 psf, Backfill angle ϕ=34^{o}and γ=105pcf Maximum Shear Strain Rate.

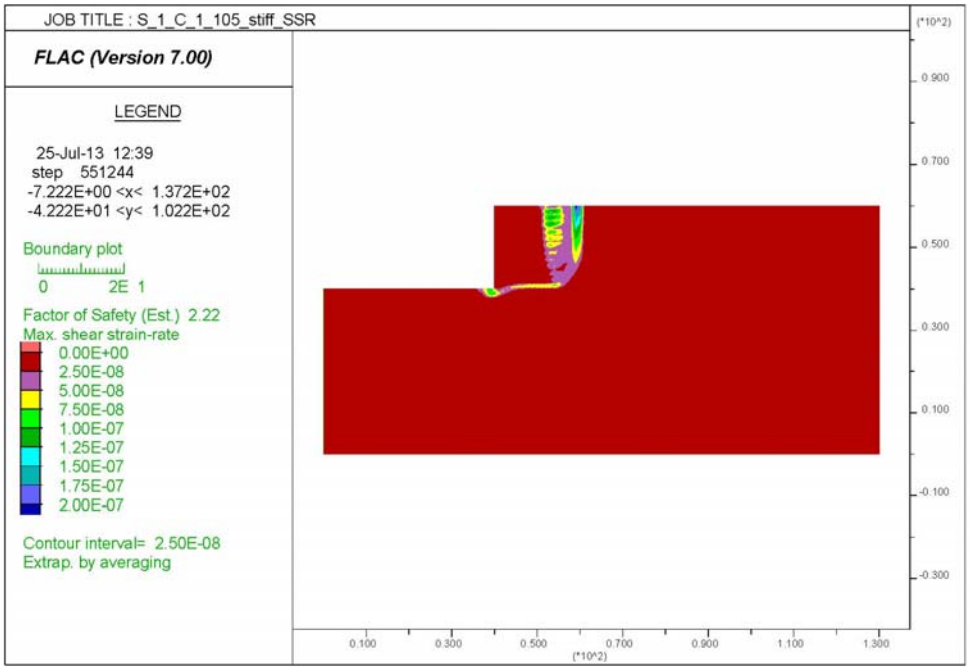

Figure B. 10. Series 1 Case 1 Foundation C_u=2000 psf, Backfill angle ϕ=34^{0}and γ=105pcf Maximum Shear Strain Rate.

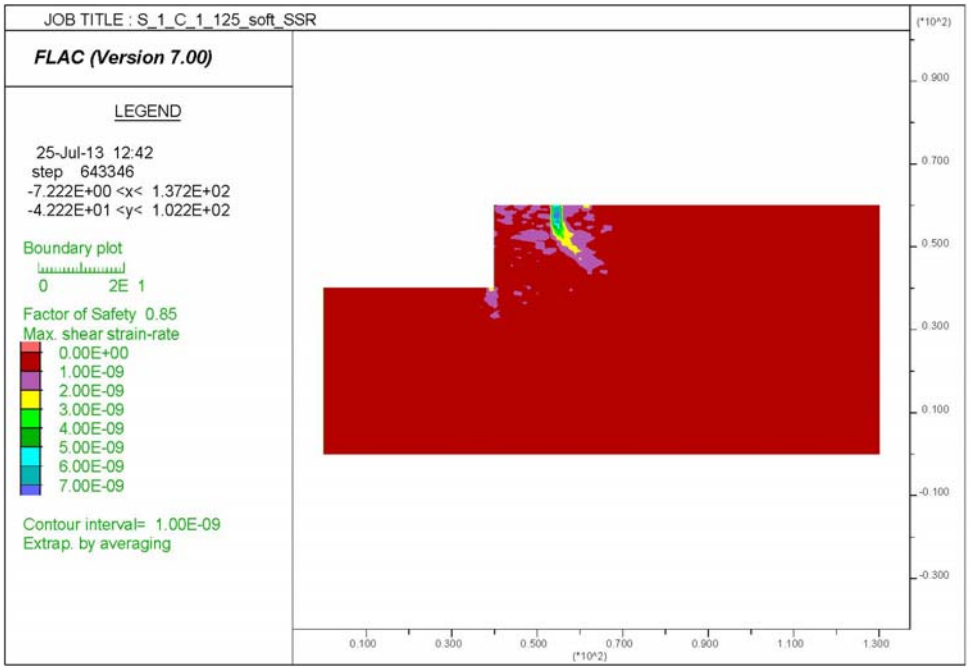

Figure B. 11. Series 1 Case 1 Foundation C_u=500 psf, Backfill angle ϕ=34^{0}and γ=125pcf Maximum Shear Strain Rate.

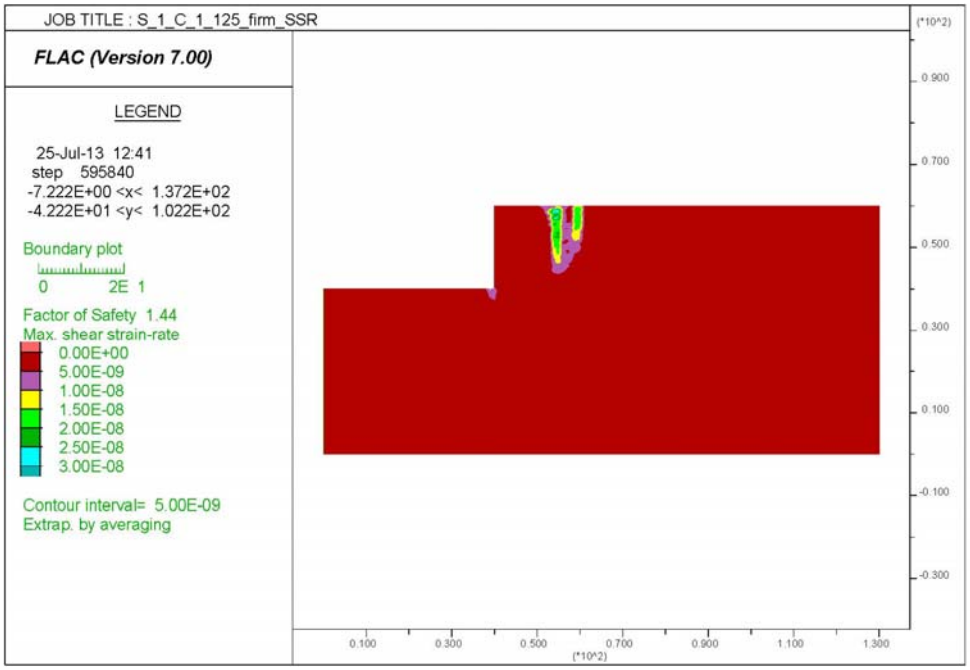

Figure B. 12. Series 1 Case 1 Foundation C_u=1000 psf, Backfill angle ϕ=34^{0}and γ=125pcf Maximum Shear Strain Rate.

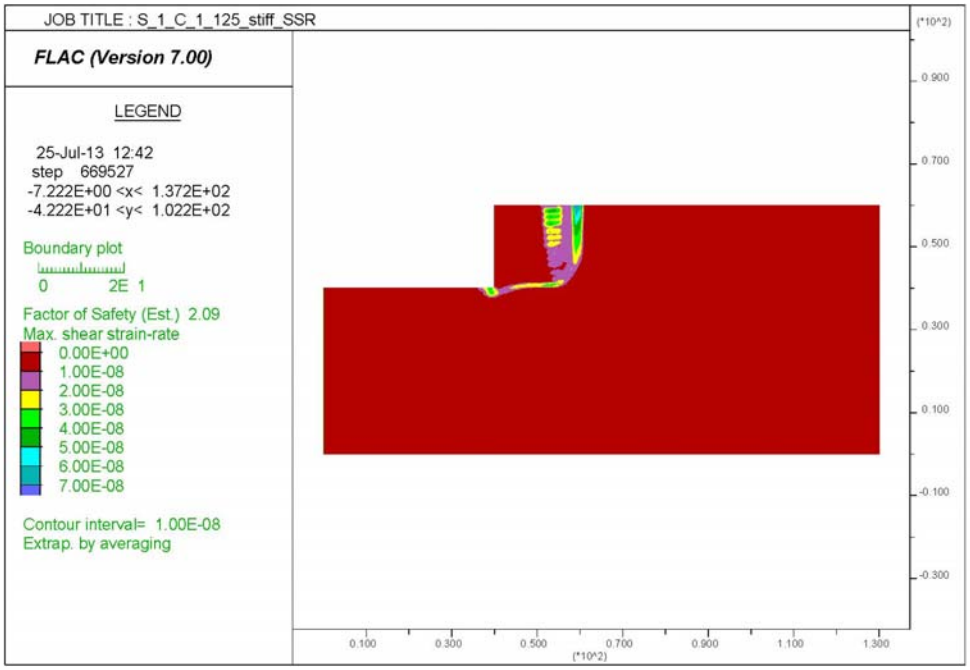

Figure B. 13. Series 1 Case 1 Foundation C_u=2000 psf, Backfill angle ϕ=34^{0}and γ=125pcf Maximum Shear Strain Rate.

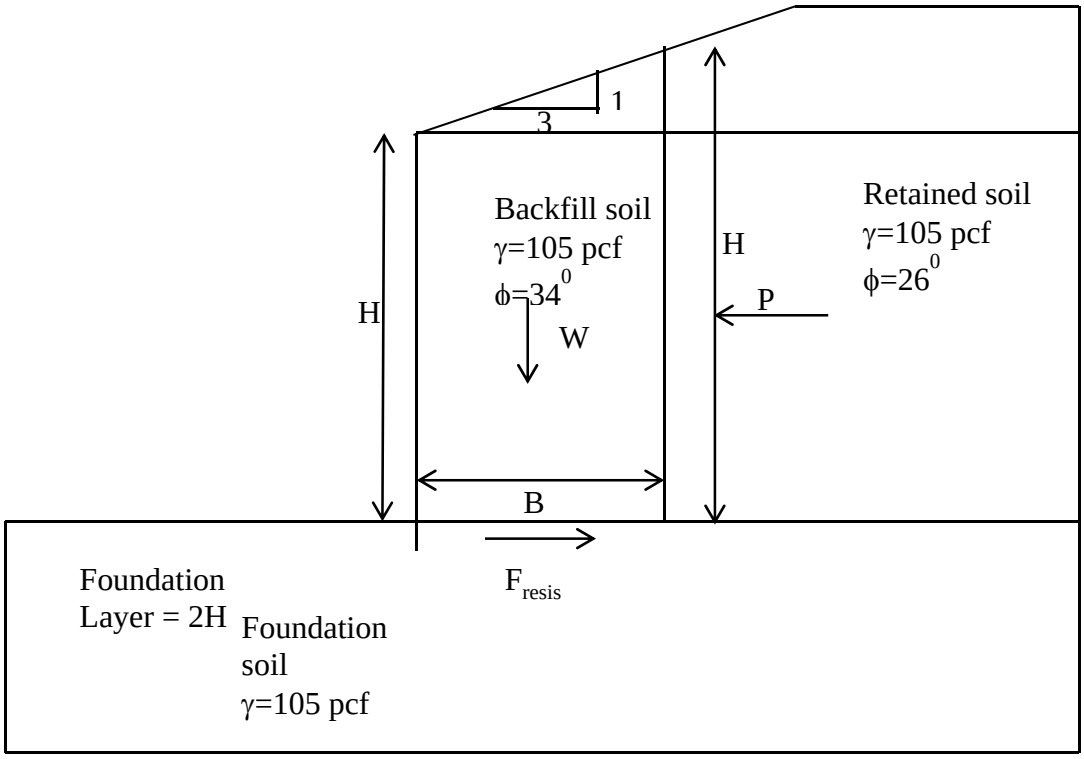

Figure B. 14. Dimensions and properties used for Series1 Case 2.

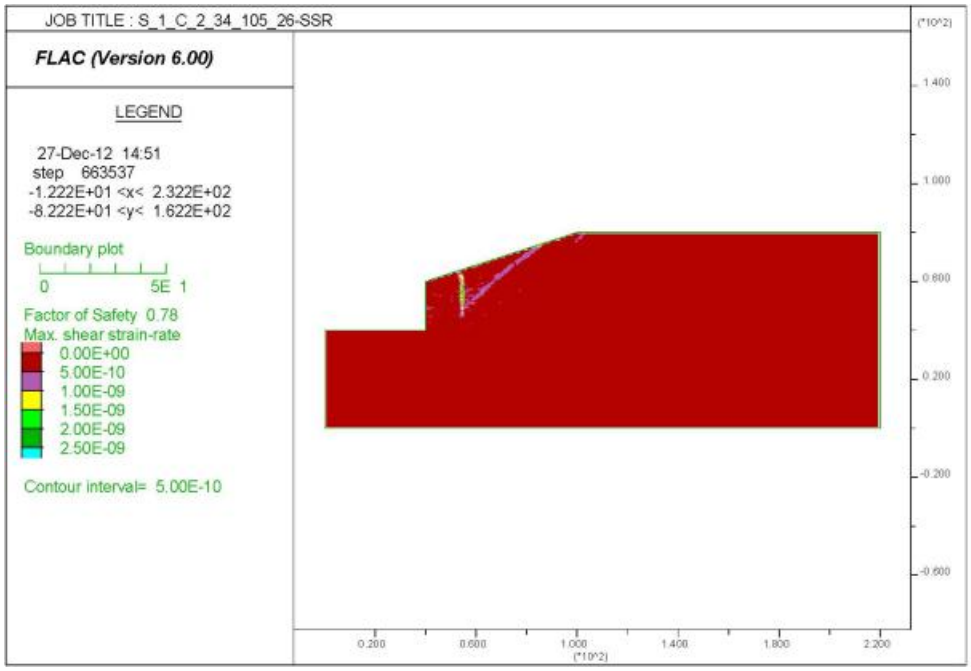

Figure B. 15. Series 1 Case 2 Foundation angle ϕ=26^0, Backfill angle ϕ=34^{0}and γ=105pcf Maximum Shear Strain Rate.

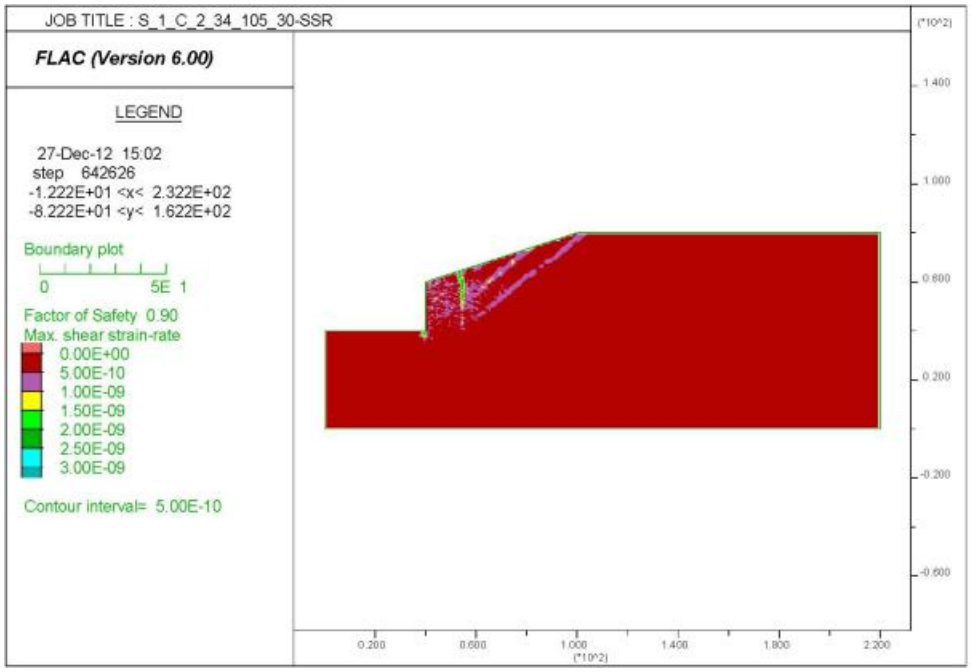

Figure B. 16. Series 1 Case 2 Foundation angle ϕ=30^0, Backfill angle ϕ=34^{0}and γ=105pcf Maximum Shear Strain Rate.

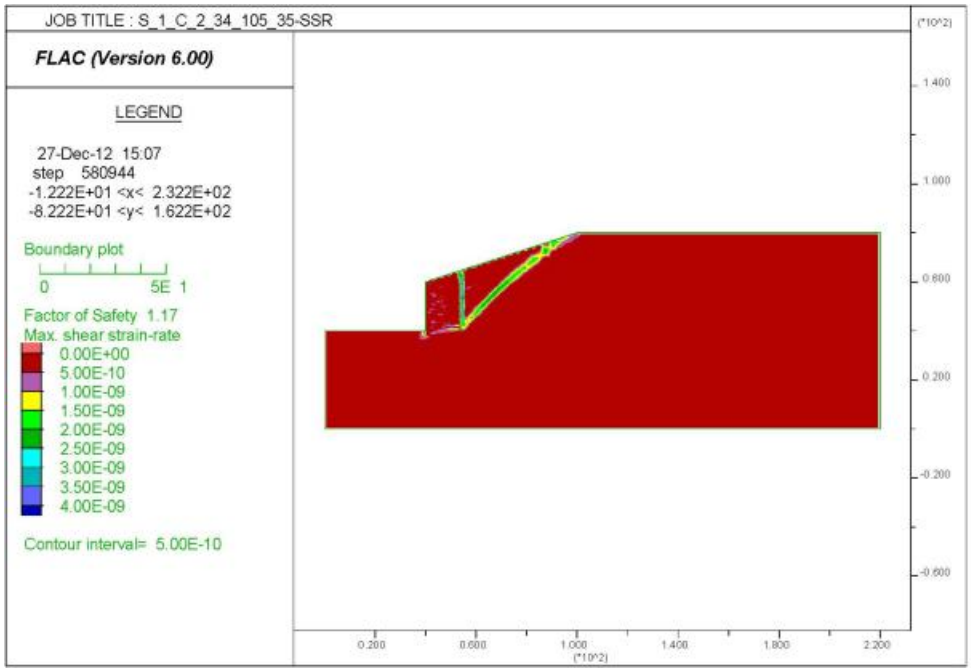

Figure B. 17. Series 1 Case 2 Foundation angle ϕ=35^0, Backfill angle ϕ=34^{0}and γ=105pcf Maximum Shear Strain Rate.

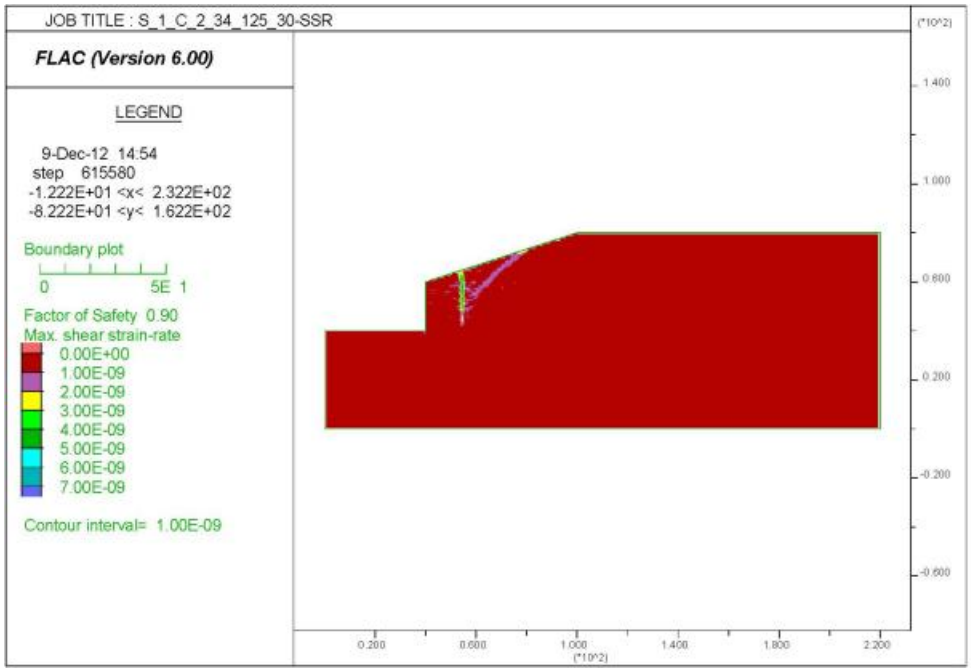

Figure B. 18. Series 1 Case 2 Foundation angle ϕ=26^0, Backfill angle ϕ=34^{0}and γ=125pcf Maximum Shear Strain Rate.

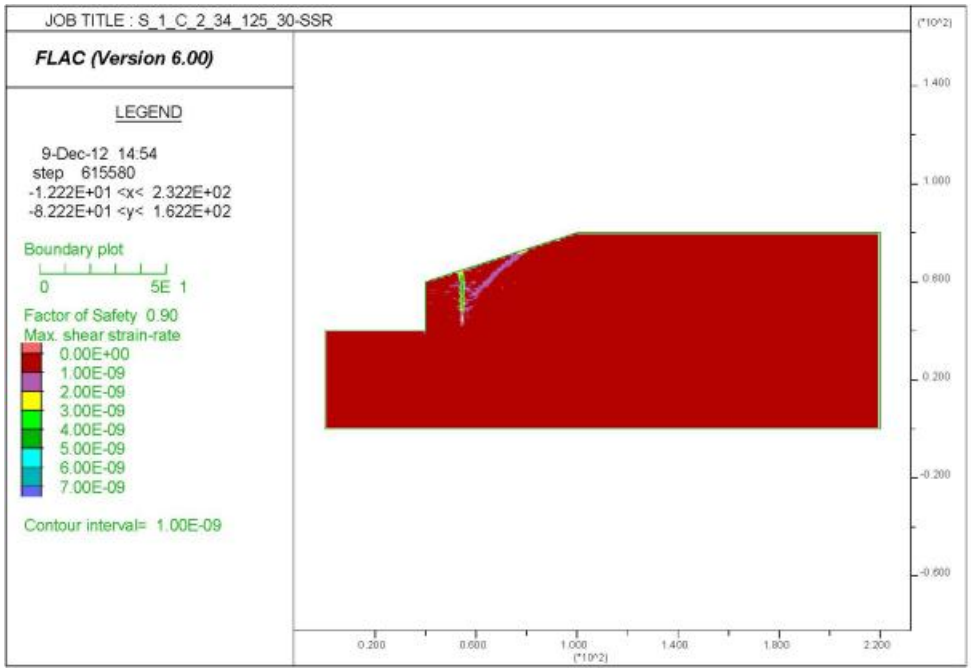

Figure B. 19. Series 1 Case 2 Foundation angle ϕ=30^0, Backfill angle ϕ=34^{0}and γ=125pcf Maximum Shear Strain Rate.

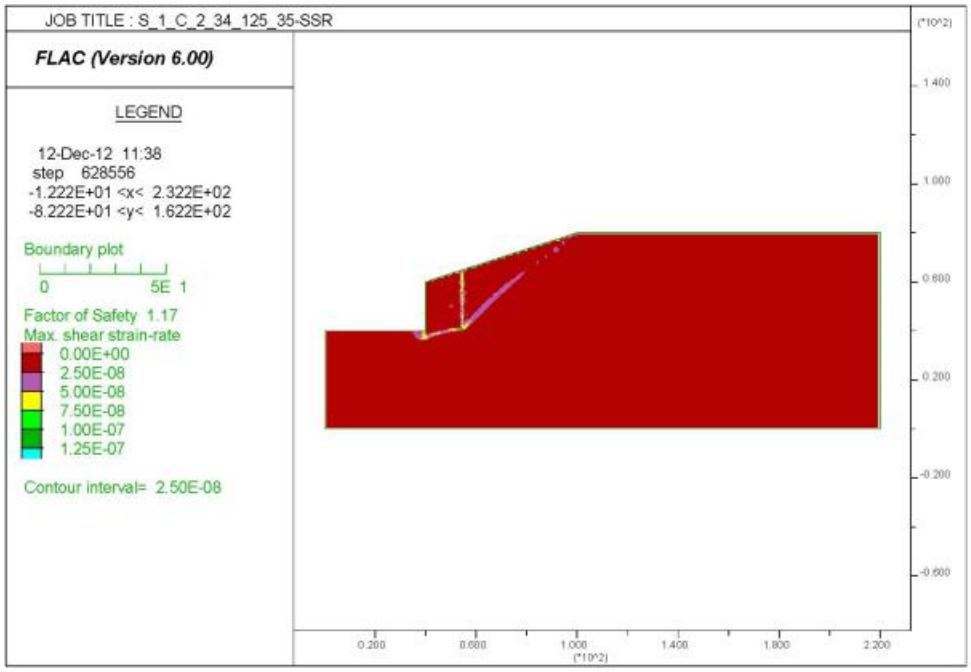

Figure B. 20. Series 1 Case 2 Foundation angle ϕ=35^{0}, Backfill angle ϕ=34^{0}and γ=125pcf Maximum Shear Strain Rate.

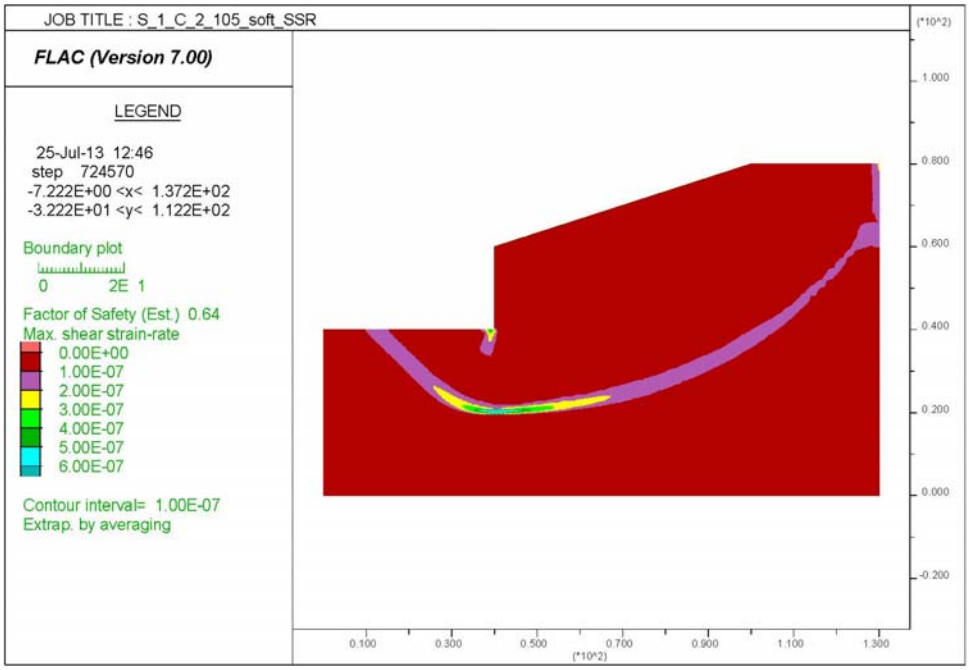

Figure B. 21. Series 1 Case 2 Foundation C_u=500 psf, Backfill angle ϕ=34^{0}and γ=105pcf Maximum Shear Strain Rate.

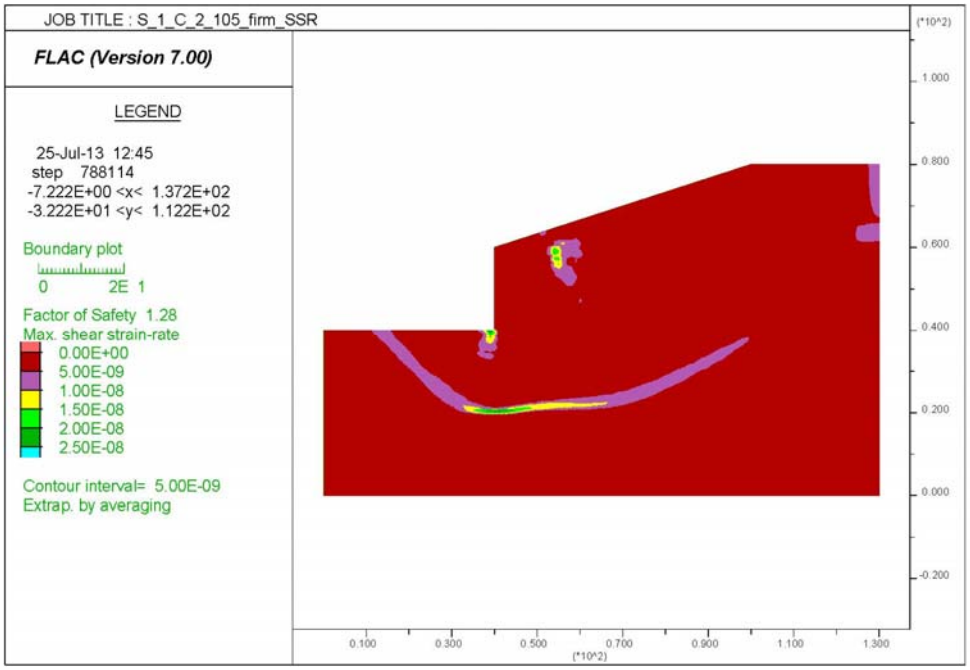

Figure B. 22. Series 1 Case 2 Foundation C_u=1000 psf, Backfill angle ϕ=34^{o}and γ=105pcf Maximum Shear Strain Rate.

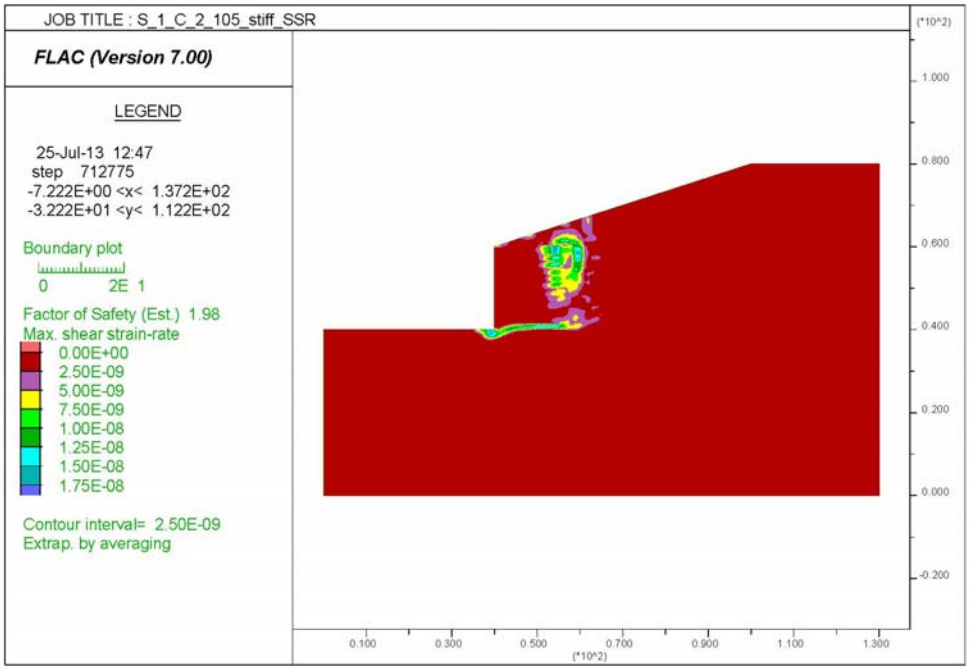

Figure B. 23. Series 1 Case 2 Foundation C_u=2000 psf, Backfill angle ϕ=34^{o}and γ=105pcf Maximum Shear Strain Rate.

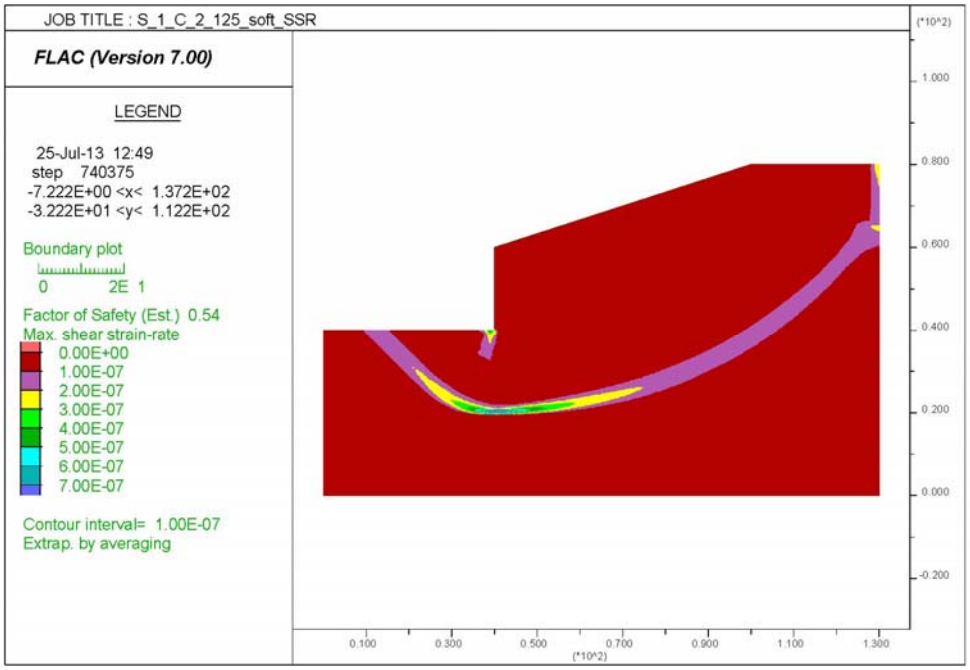

Figure B. 24. Series 1 Case 2 Foundation C_u=500 psf, Backfill angle ϕ=34^{o}and γ=125pcf Maximum Shear Strain Rate.

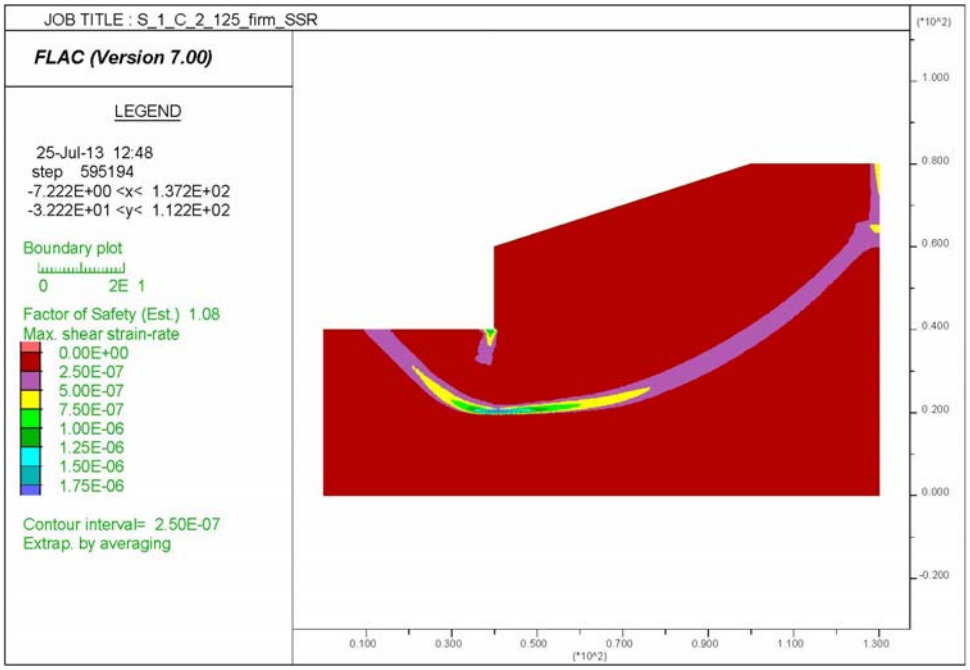

Figure B. 25. Series 1 Case 2 Foundation C_u=1000 psf, Backfill angle ϕ=34^{o}and γ=125pcf Maximum Shear Strain Rate.

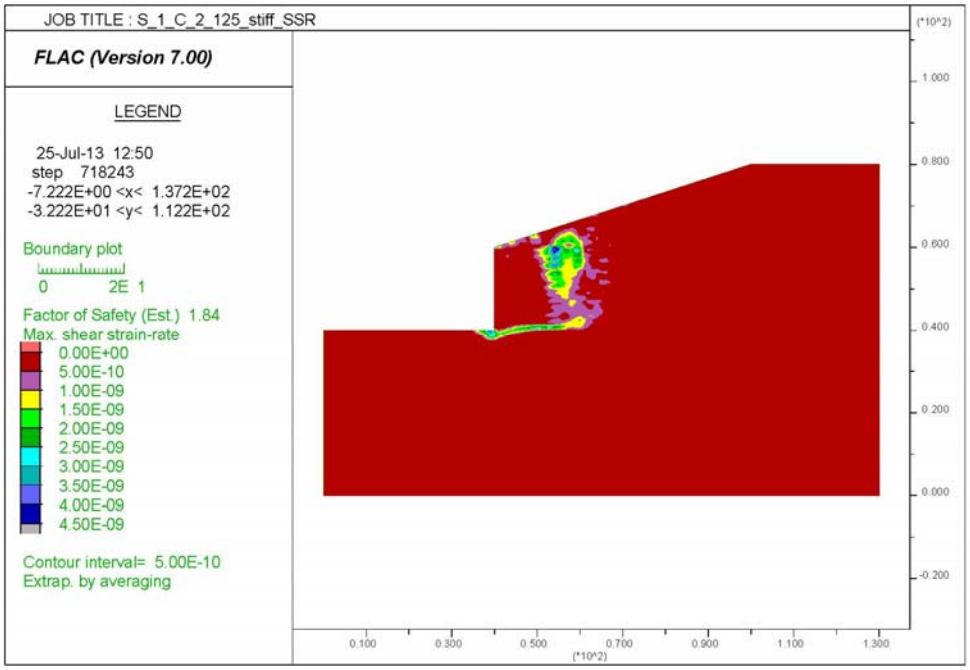

Figure B. 26. Series 1 Case 2 Foundation C_u=2000 psf, Backfill angle ϕ=34^{0}and γ=125pcf Maximum Shear Strain Rate.

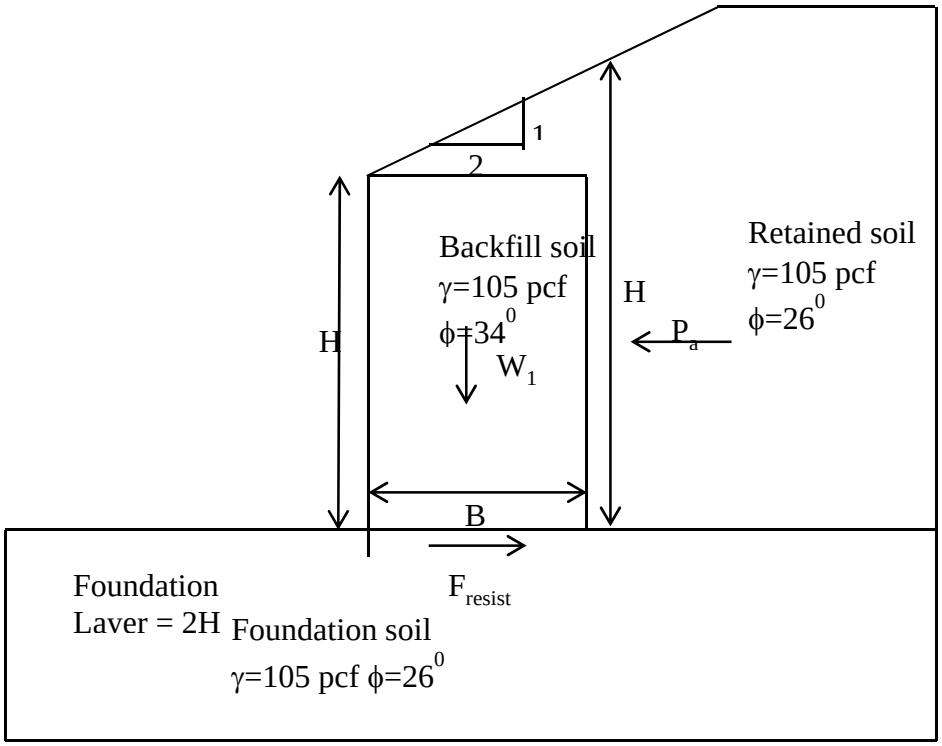

Figure B. 27. Dimensions and Properties used for Series 1 Case 3.

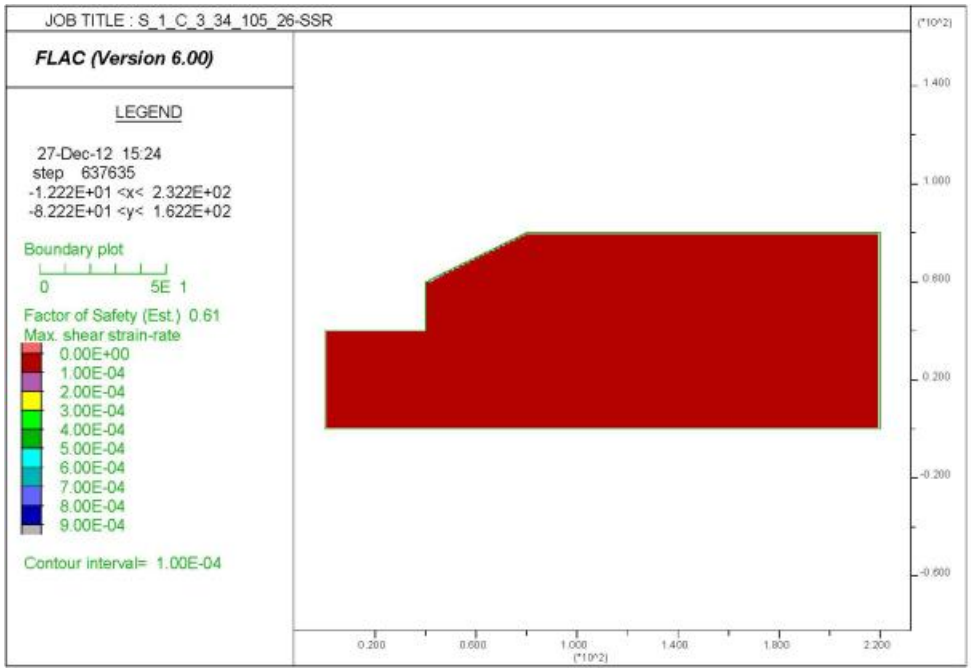

Figure B. 28. Series 1 Case 3 Foundation angle ϕ=26^0, Backfill angle ϕ=34^{0}and γ=105pcf Maximum Shear Strain Rate.

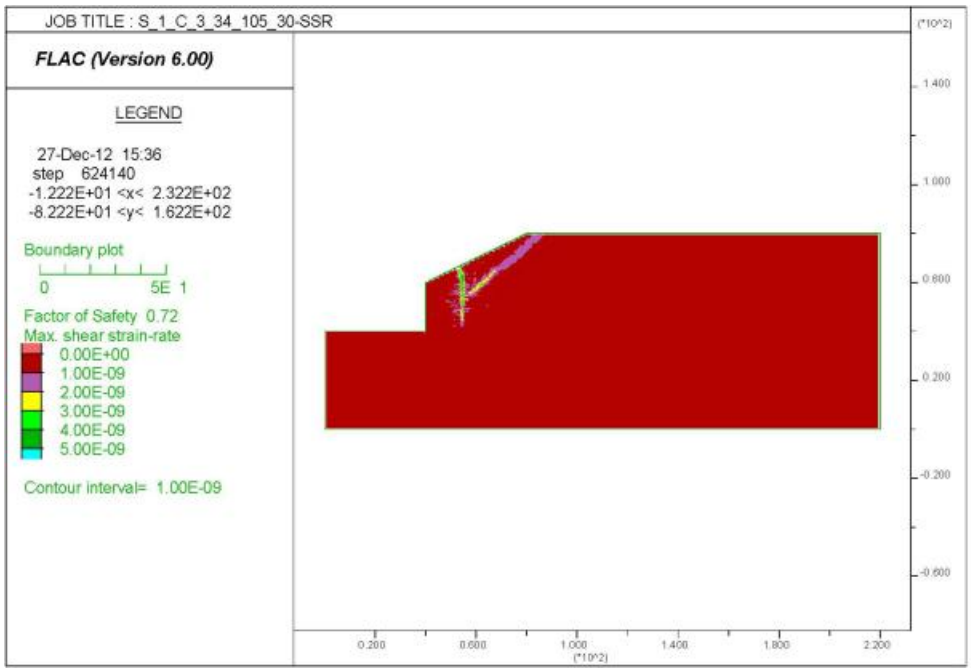

Figure B. 29. Series 1 Case 3 Foundation angle ϕ=30^0, Backfill angle ϕ=34^{0}and γ=105pcf Maximum Shear Strain Rate.

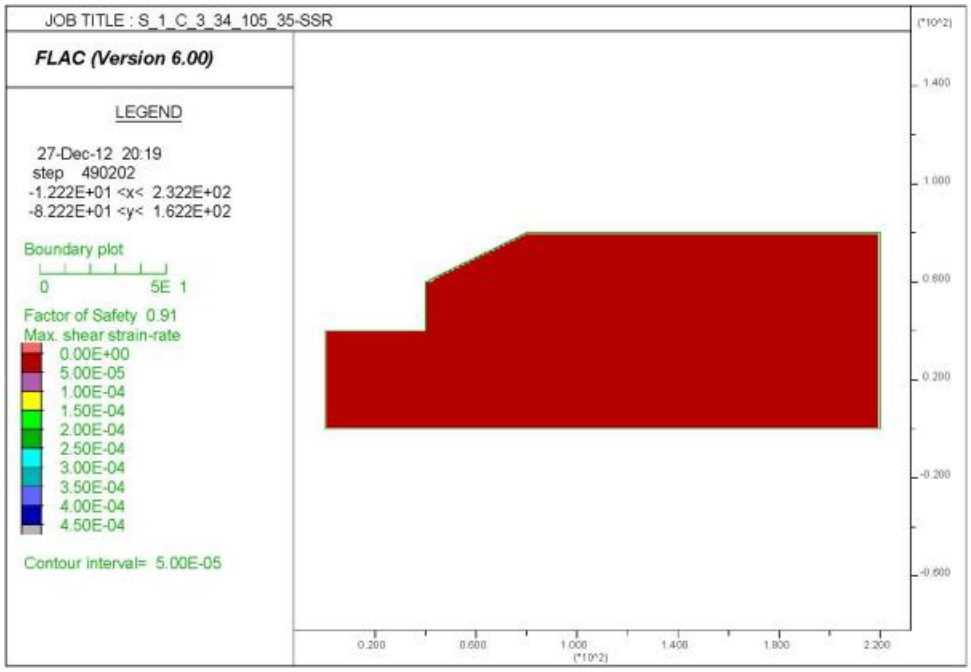

Figure B. 30. Series 1 Case 3 Foundation angle ϕ=35^0, Backfill angle ϕ=34^{0}and γ=105pcf Maximum Shear Strain Rate.

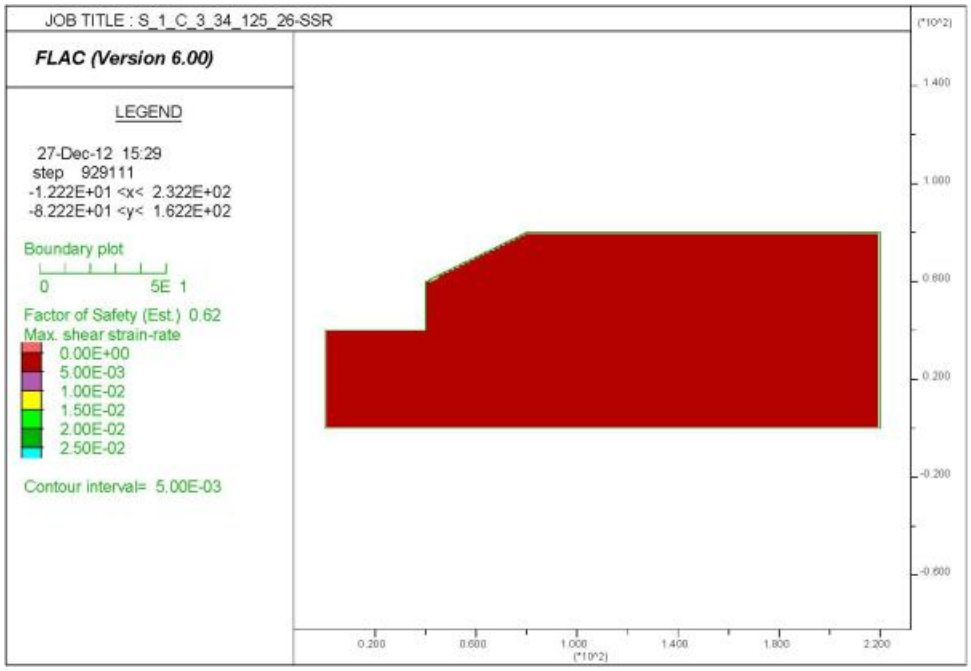

Figure B. 31. Series 1 Case 3 Foundation angle ϕ=26^0, Backfill angle ϕ=34^{0}and γ=125pcf Maximum Shear Strain Rate.

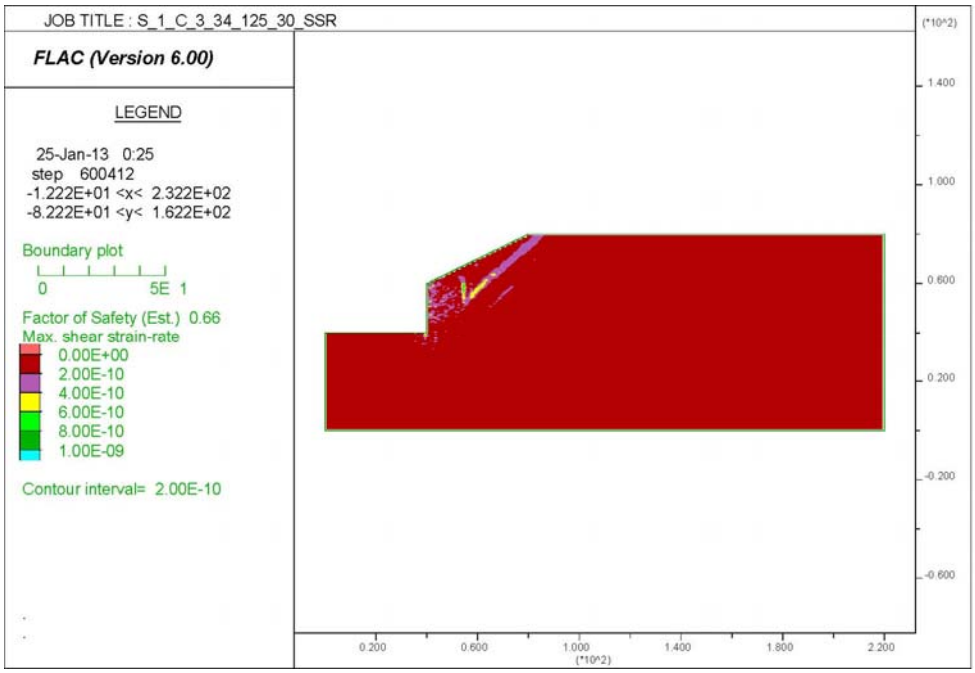

Figure B. 32. Series 1 Case 3 Foundation angle ϕ=30^{o}, Backfill angle ϕ=34^{o}and γ=125pcf Maximum Shear Strain Rate.

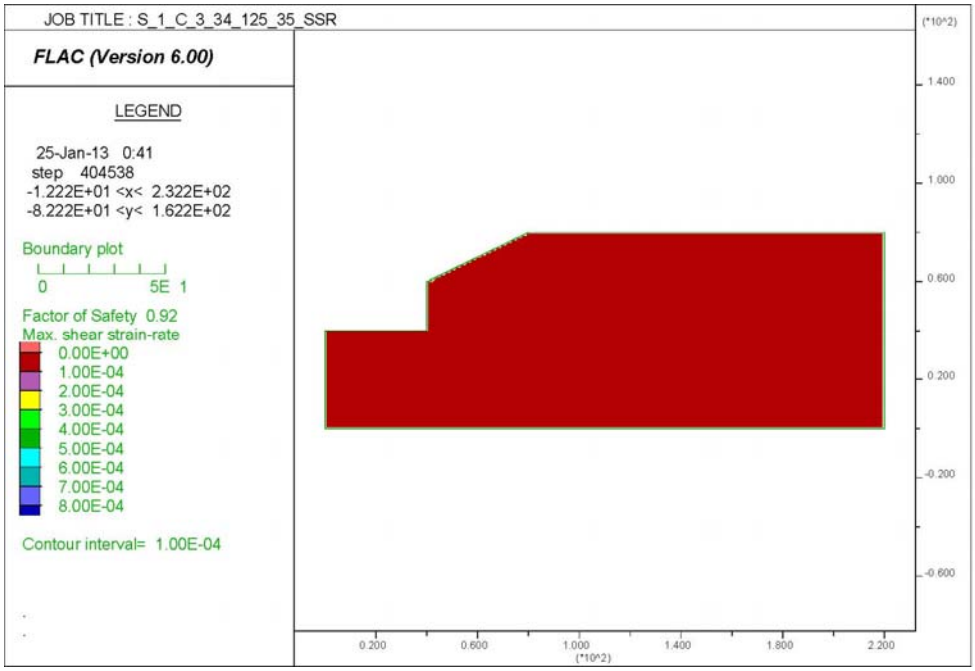

Figure B. 33. Series 1 Case 3 Foundation angle ϕ=35^{o}, Backfill angle ϕ=34^{o}and γ=125pcf Maximum Shear Strain Rate.

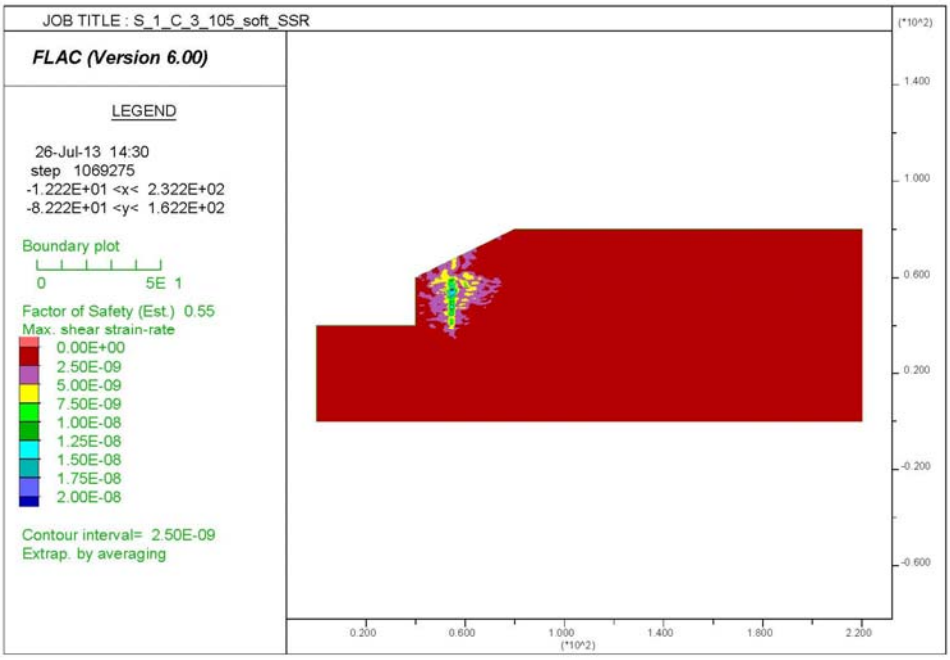

Figure B. 34. Series 1 Case 3 Foundation C_u=500 psf, Backfill angle ϕ=34^{0}and γ=105pcf Maximum Shear Strain Rate.

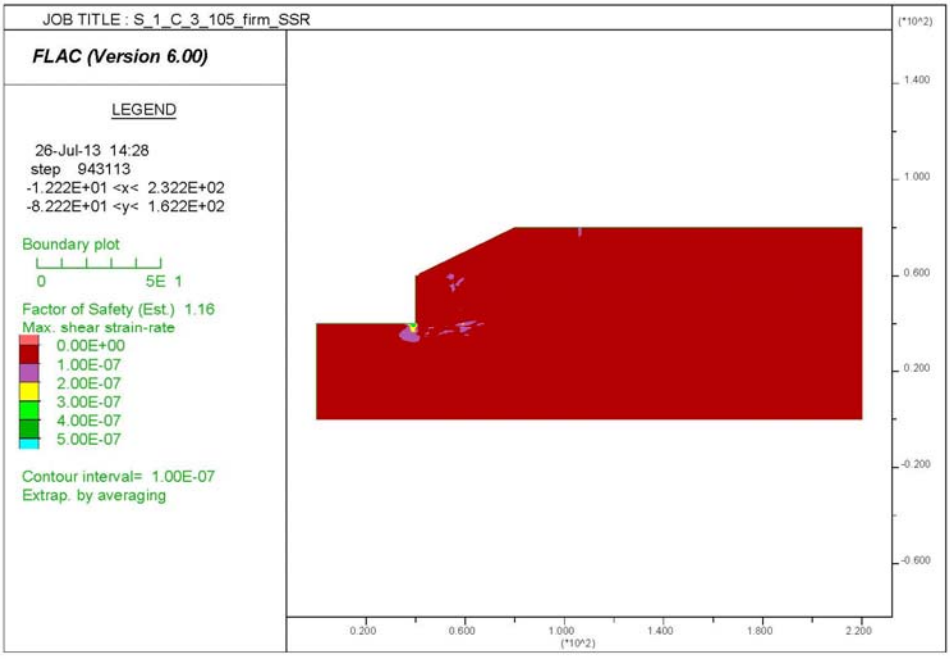

Figure B. 35. Series 1 Case 3 Foundation C_u=1000 psf, Backfill angle ϕ=34^{0}and γ=105pcf Maximum Shear Strain Rate.

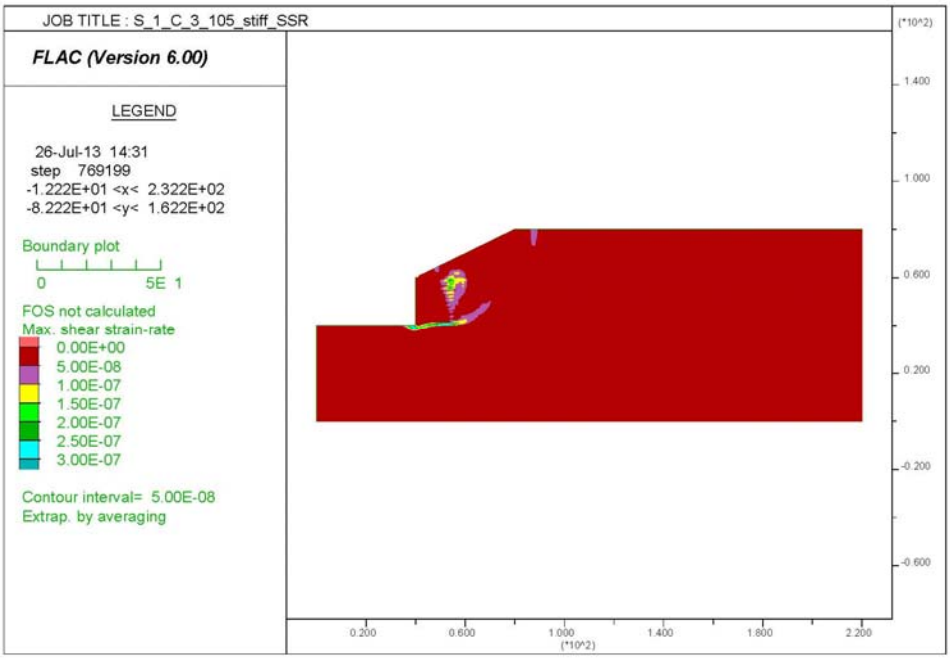

Figure B. 36. Series 1 Case 3 Foundation C_u=2000 psf, Backfill angle ϕ=34^{0}and γ=105pcf Maximum Shear Strain Rate.

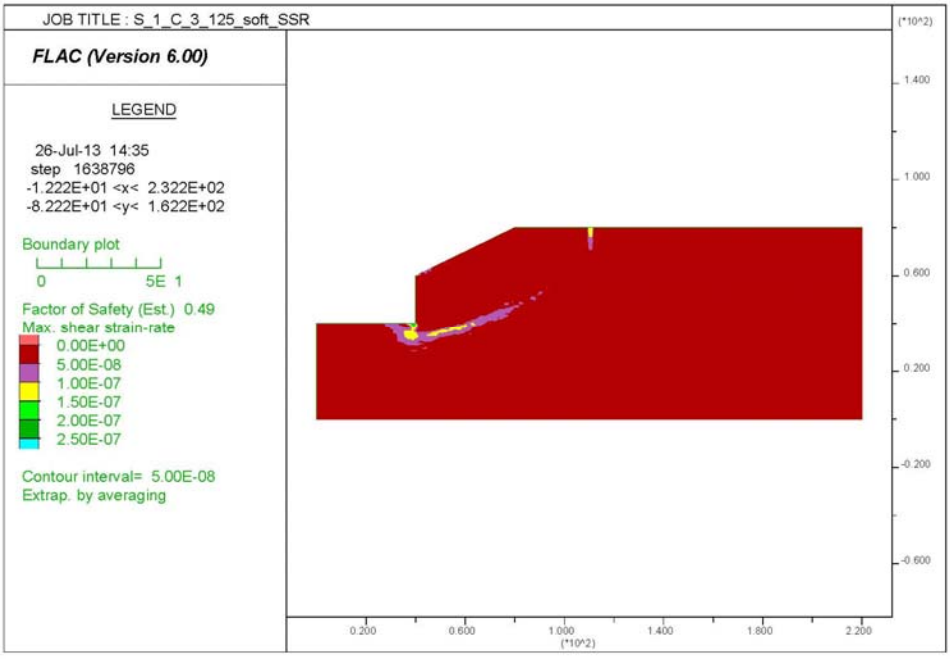

Figure B. 37. Series 1 Case 3 Foundation C_u=500 psf, Backfill angle ϕ=34^{0}and γ=125pcf Maximum Shear Strain Rate.

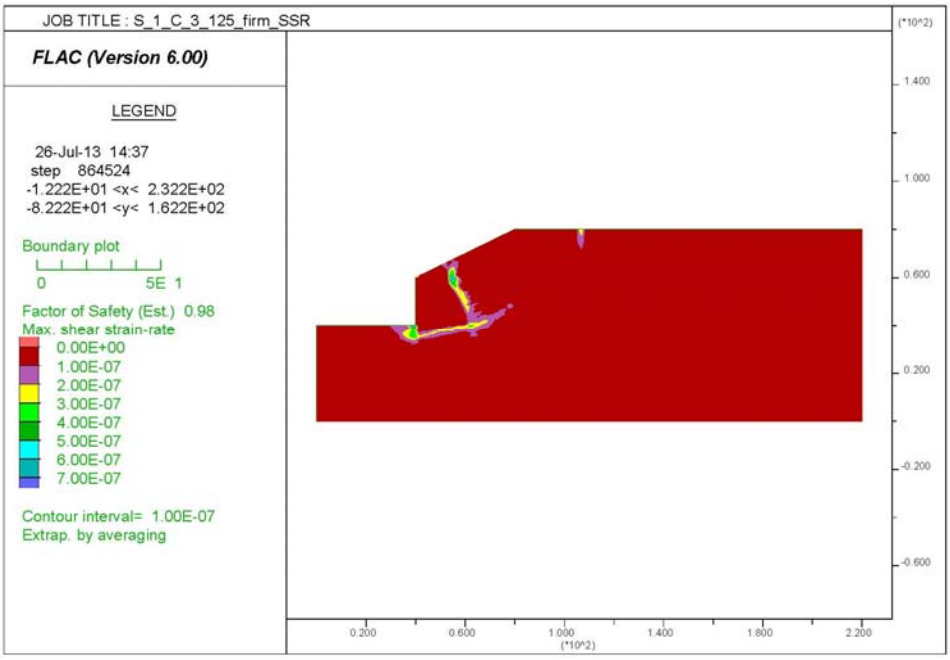

Figure B. 38. Series 1 Case 3 Foundation C_u=1000 psf, Backfill angle ϕ=34^{0}and γ=125pcf Maximum Shear Strain Rate.

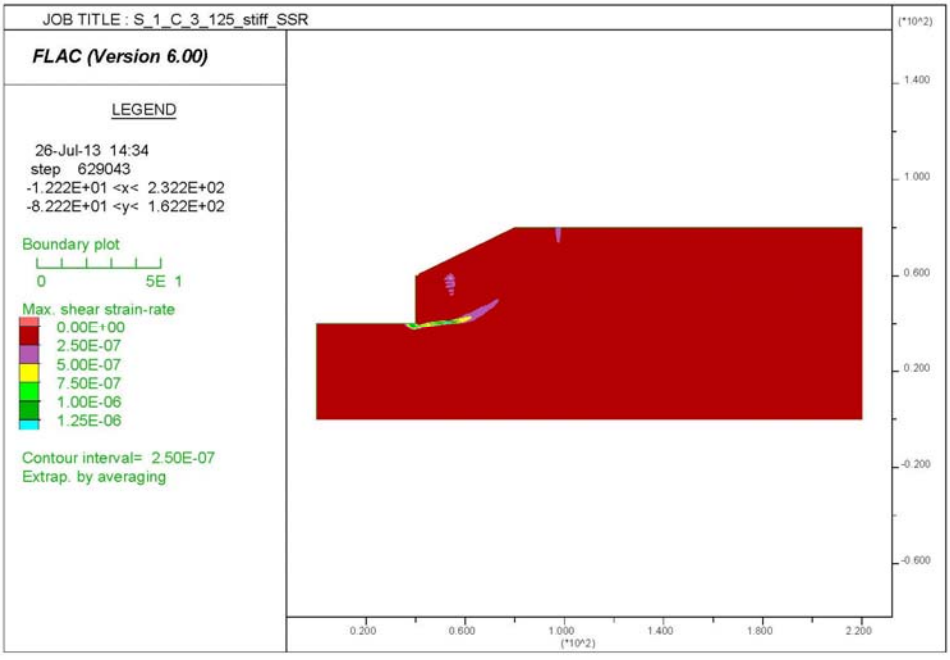

Figure B. 39. Series 1 Case 3 Foundation C_u=2000 psf, Backfill angle ϕ=34^{0}and γ=125pcf Maximum Shear Strain Rate.

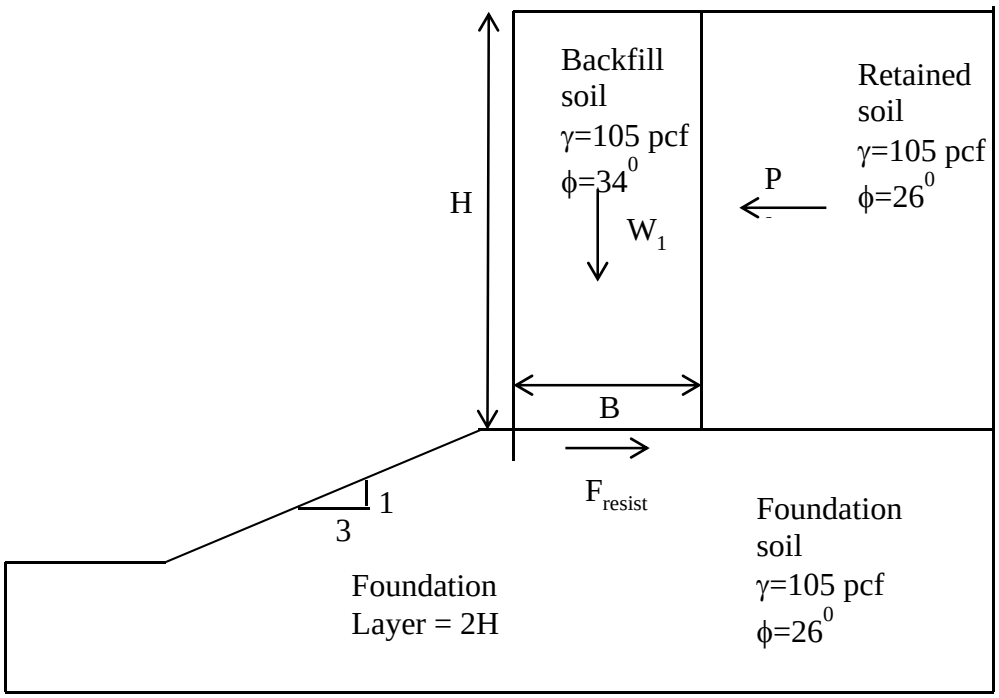

Figure B. 40. Dimensions and properties used for Series 2 Case 2.

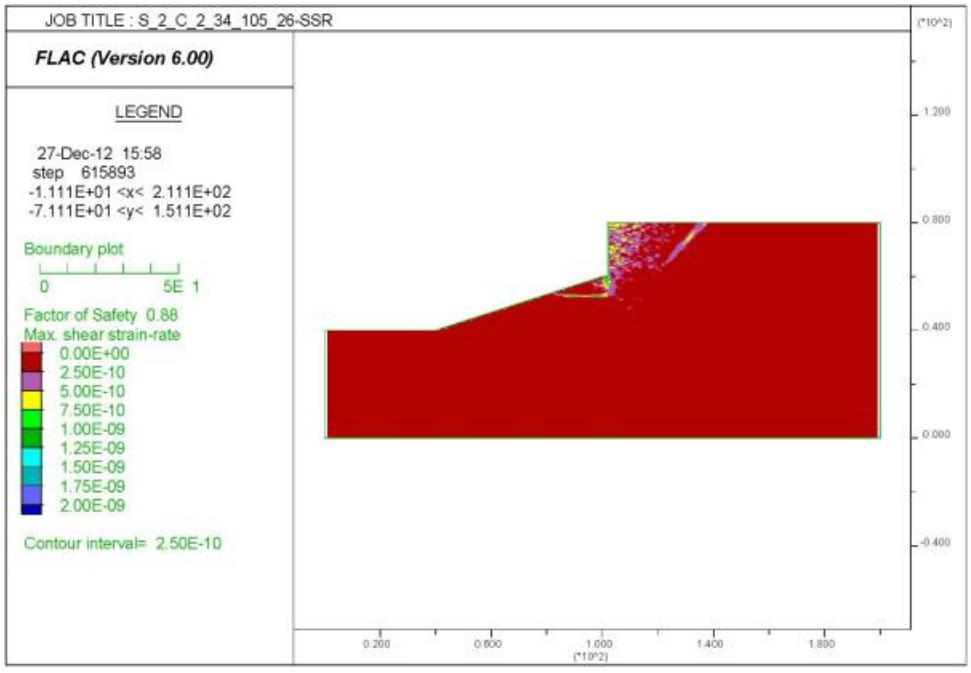

Figure B. 41. Series 2 Case 2 Foundation angle ϕ=26^0, Backfill angle ϕ=34^{0}and γ=105pcf Maximum Shear Strain Rate.

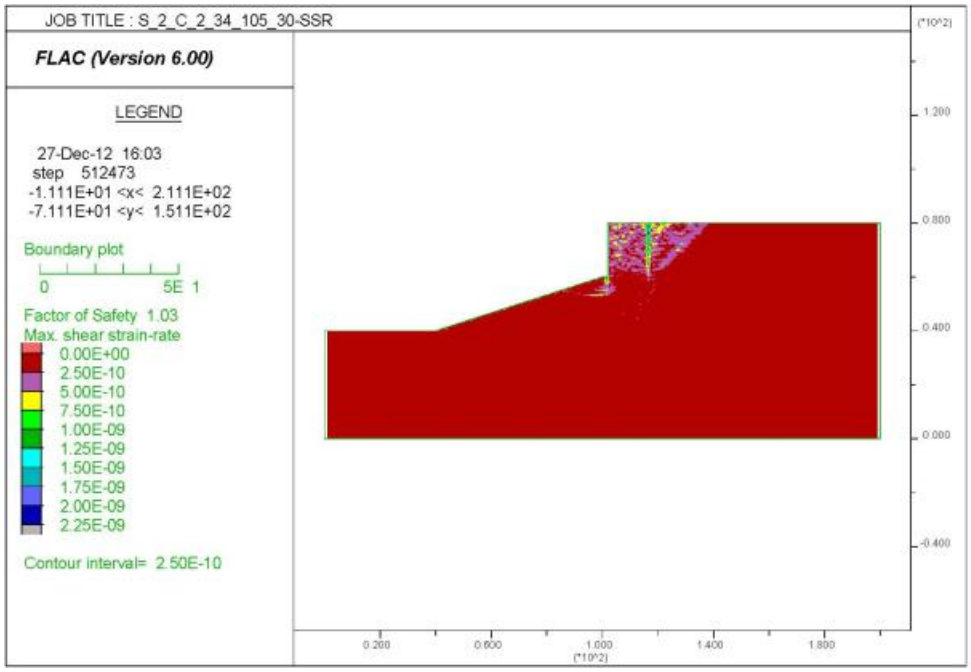

Figure B. 42. Series 2 Case 2 Foundation angle ϕ=30^0, Backfill angle ϕ=34^{0}and γ=105pcf Maximum Shear Strain Rate.

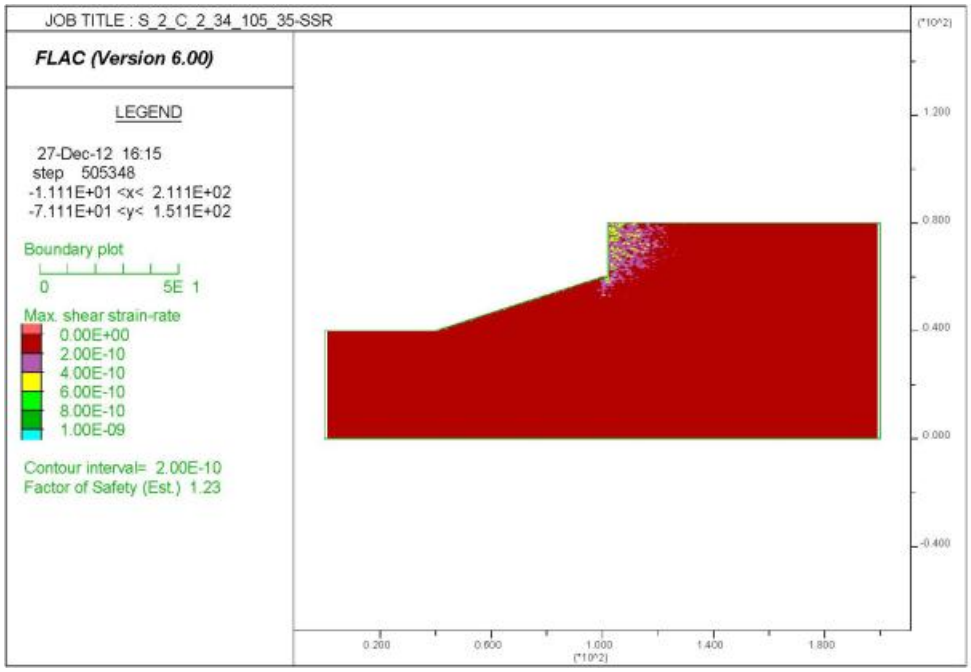

Figure B. 43. Series 2 Case 2 Foundation angle ϕ=35^0, Backfill angle ϕ=34^{0}and γ=105pcf Maximum Shear Strain Rate

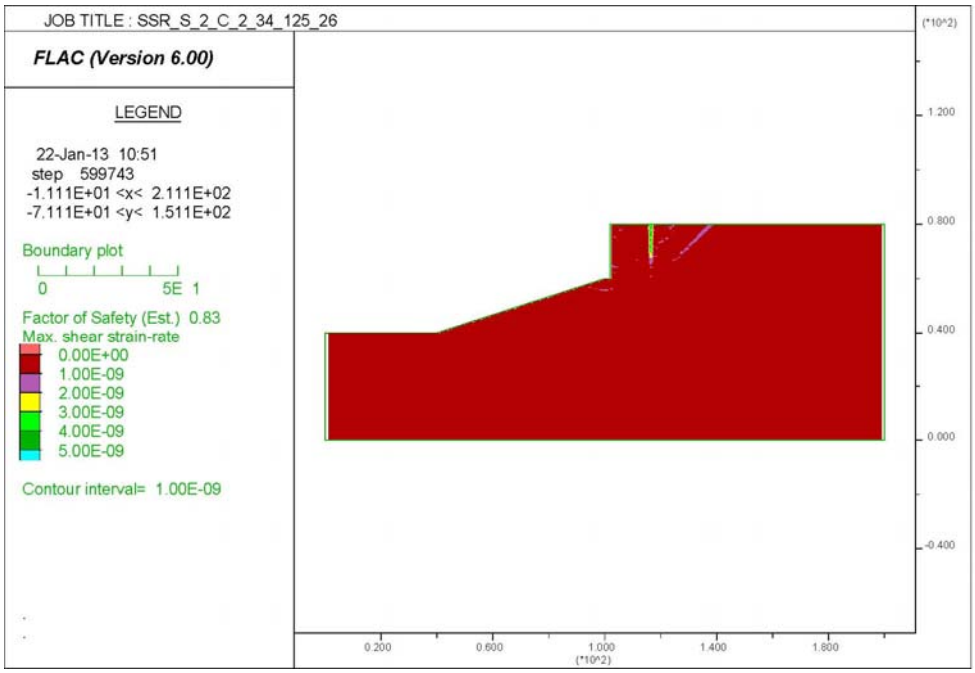

Figure B. 44. Series 2 Case 2 Foundation angle ϕ=26^0, Backfill angle ϕ=34^{0}and γ=125pcf Maximum Shear Strain Rate.

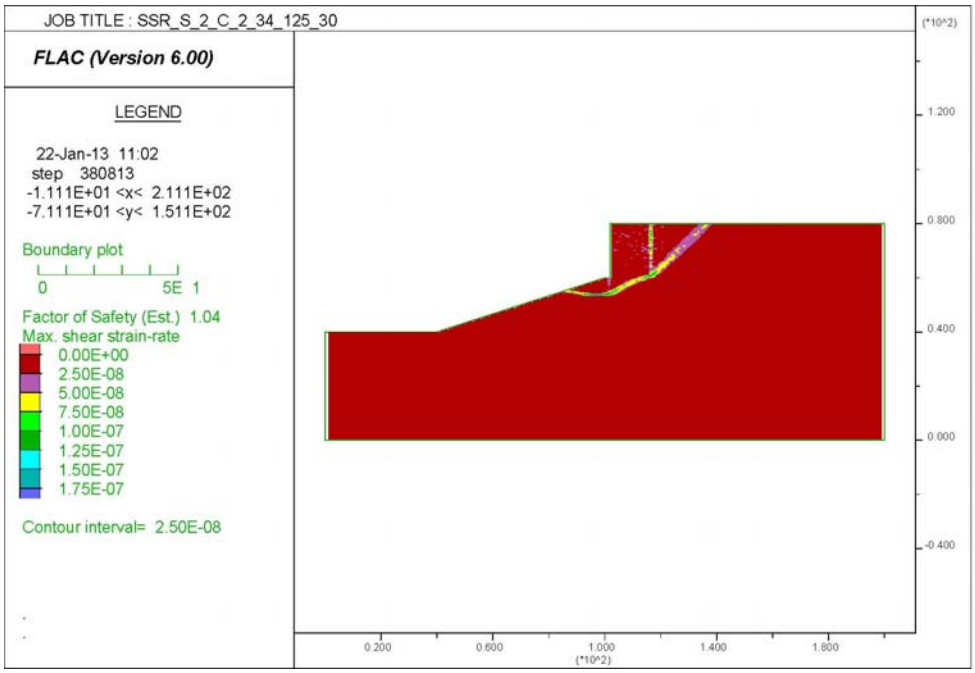

Figure B. 45. Series 2 Case 2 Foundation angle ϕ=30^0, Backfill angle ϕ=34^{0}and γ=125pcf Maximum Shear Strain Rate.

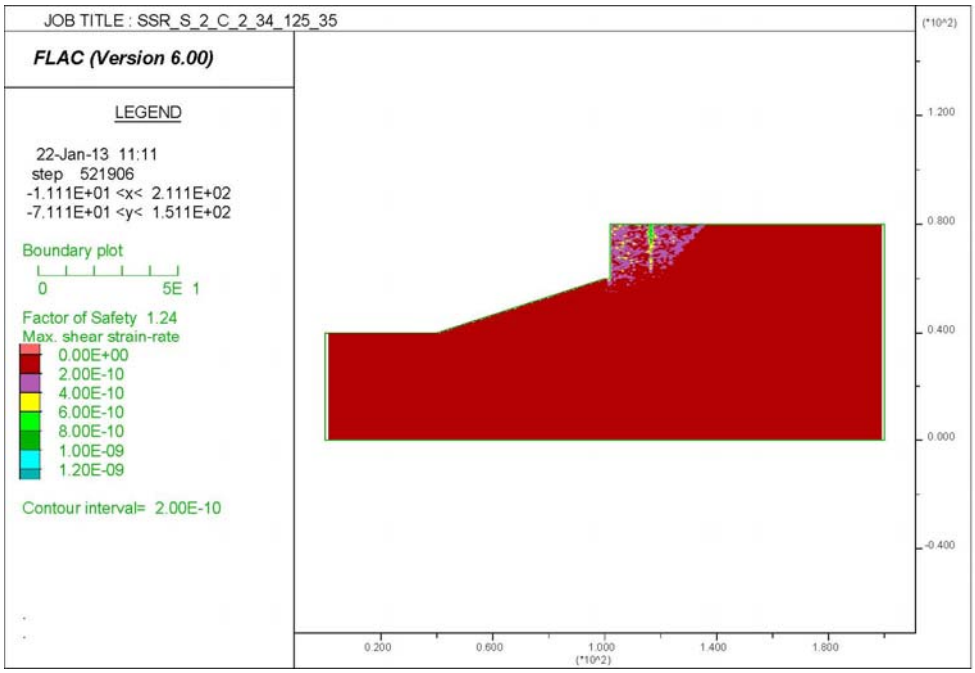

Figure B. 46. Series 2 Case 2 Foundation angle ϕ=35^0, Backfill angle ϕ=34^{0}and γ=125pcf Maximum Shear Strain Rate.

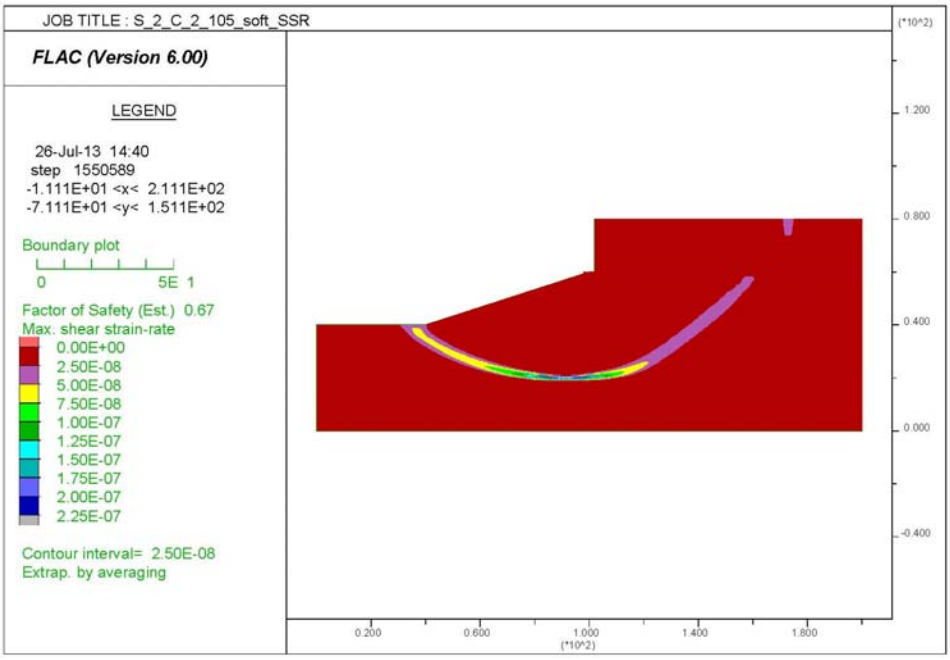

Figure B. 47. Series 2 Case 2 Foundation C_u=500 psf, Backfill angle ϕ=34^{0}and γ=105pcf Maximum Shear Strain Rate.

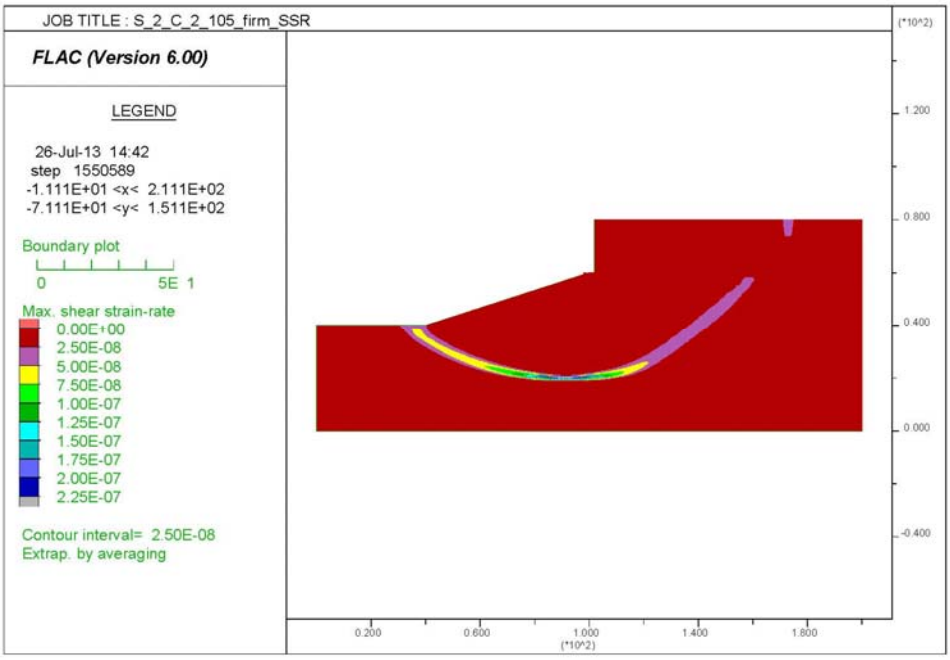

Figure B. 48. Series 2 Case 2 Foundation C_u=1000 psf, Backfill angle ϕ=34^{0}and γ=105pcf Maximum Shear Strain Rate.

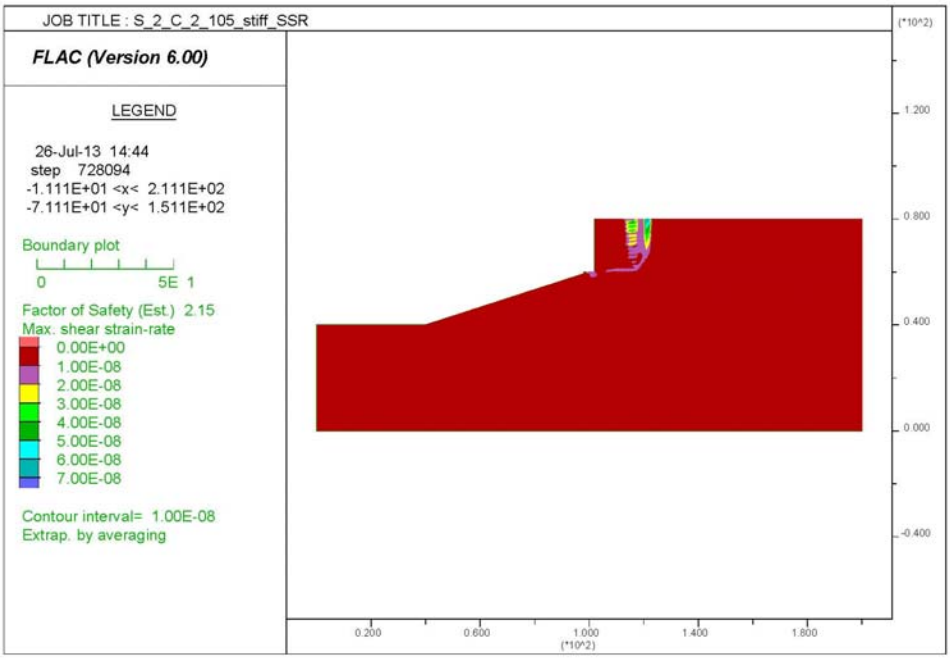

Figure B. 49. Series 2 Case 2 Foundation C_u=2000 psf, Backfill angle ϕ=34^{0}and γ=105pcf Maximum Shear Strain Rate.

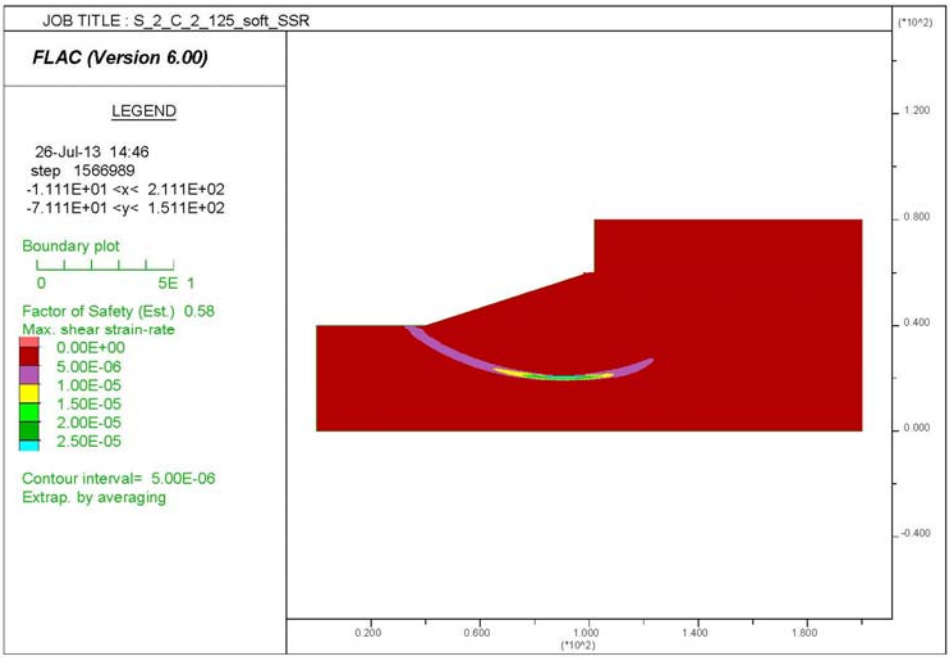

Figure B. 50. Series 2 Case 2 Foundation C_u=500 psf, Backfill angle ϕ=34^{o}and γ=125pcf Maximum Shear Strain Rate.

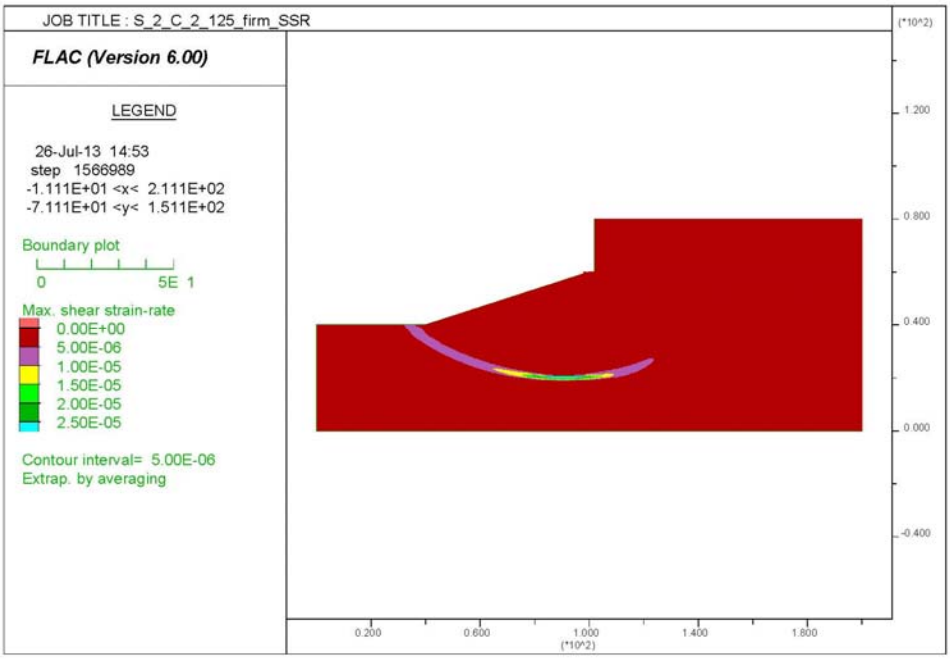

Figure B. 51. Series 2 Case 2 Foundation C_u=1000 psf, Backfill angle ϕ=34^{o}and γ=125pcf Maximum Shear Strain Rate.

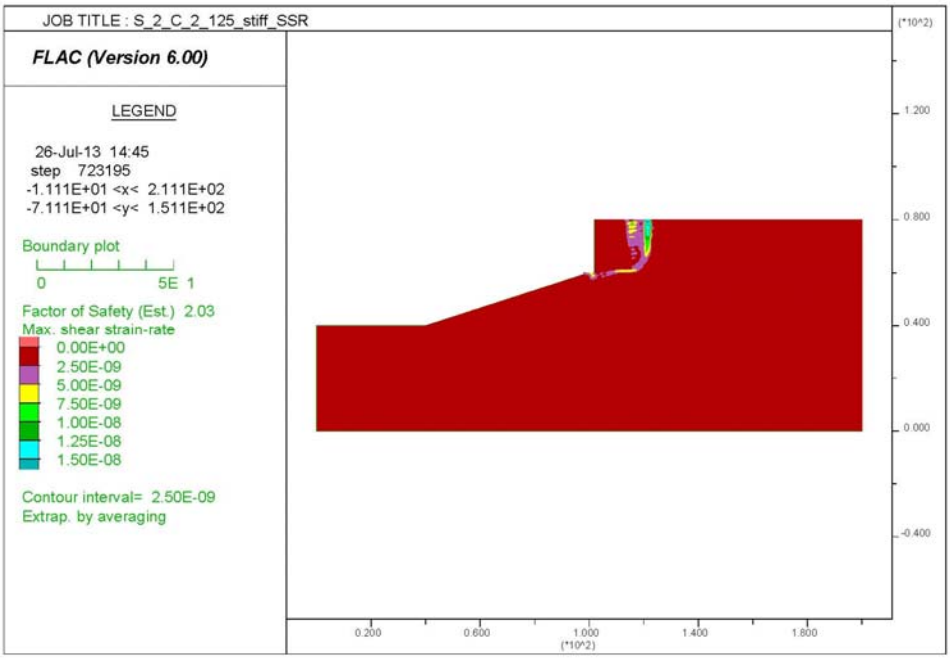

Figure B. 52. Series 2 Case 2 Foundation C_u=2000 psf, Backfill angle ϕ=34^{0}and γ=125pcf Maximum Shear Strain Rate.

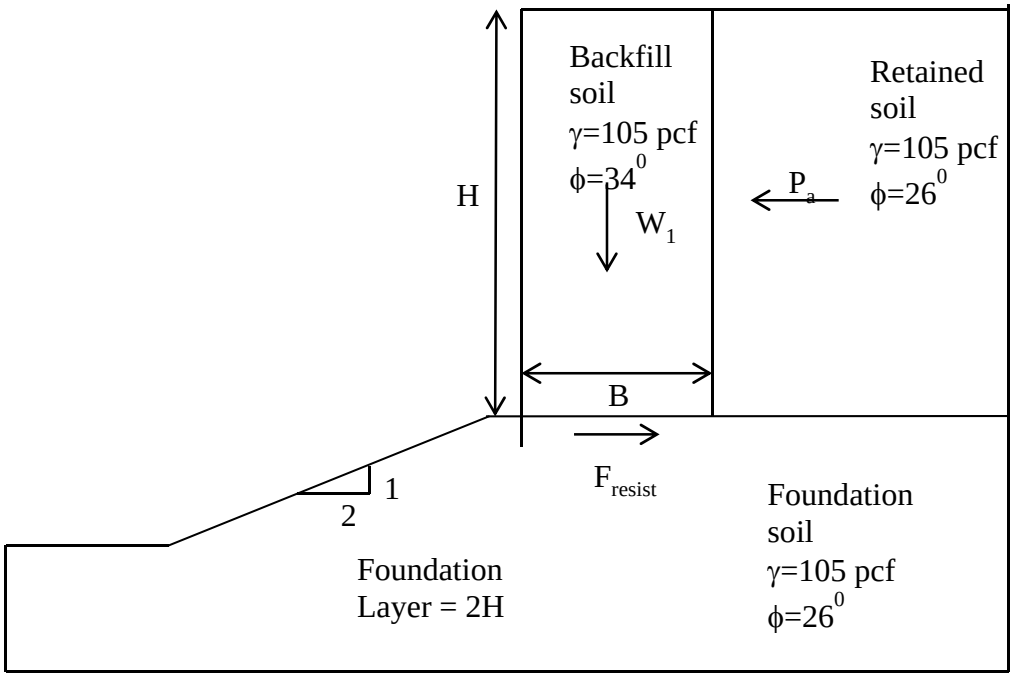

Figure B. 53. Dimensions and properties used for Series 2 case 3.

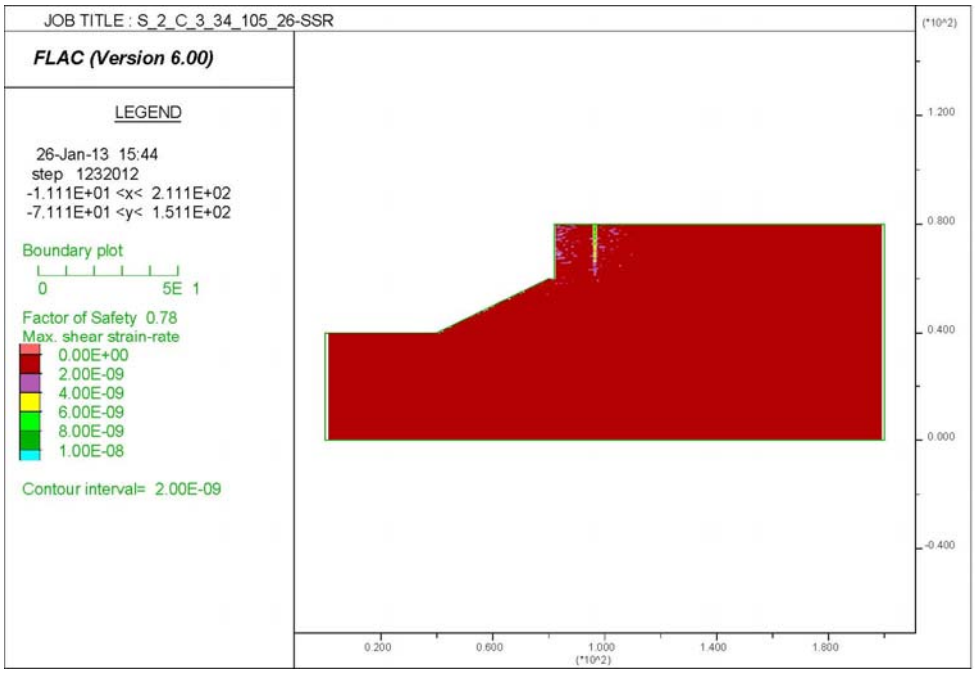

Figure B. 54. Series 2 Case 3 Foundation angle ϕ=26^0, Backfill angle ϕ=34^{0}and γ=105pcf Maximum Shear Strain Rate.

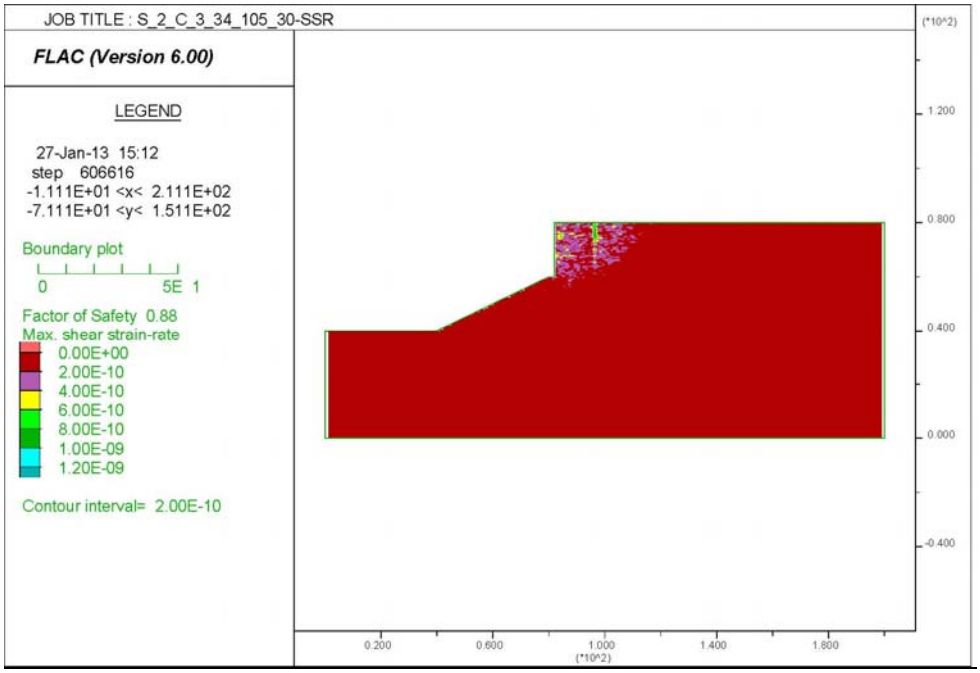

Figure B. 55. Series 2 Case 3 Foundation angle ϕ=30^0, Backfill angle ϕ=34^{0}and γ=105pcf Maximum Shear Strain Rate.

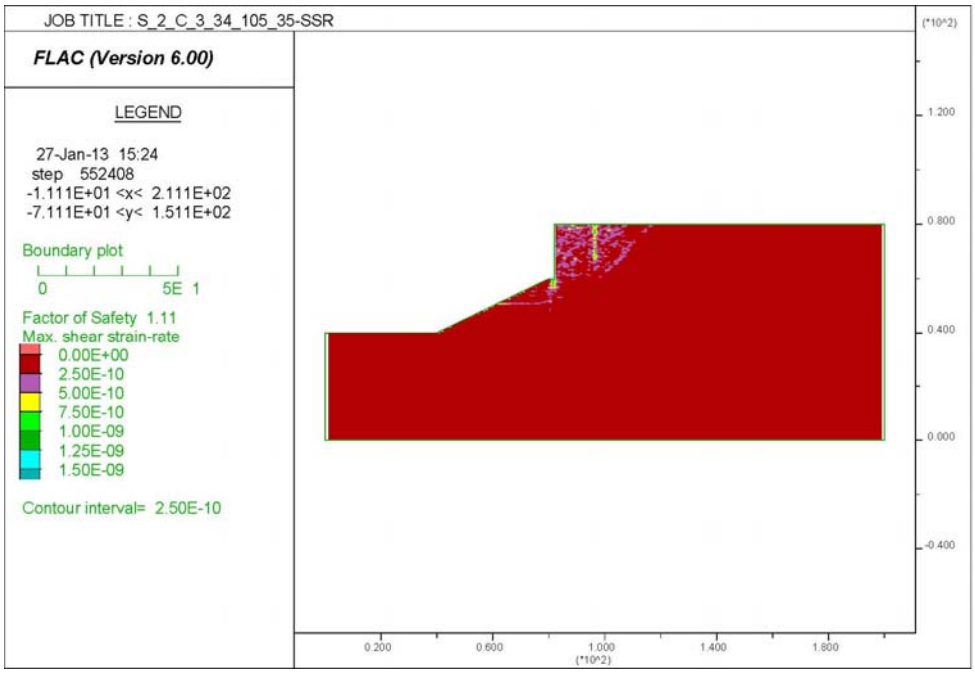

Figure B. 56. Series 2 Case 3 Foundation angle ϕ=35^0, Backfill angle ϕ=34^{0}and γ=105pcf Maximum Shear Strain Rate.

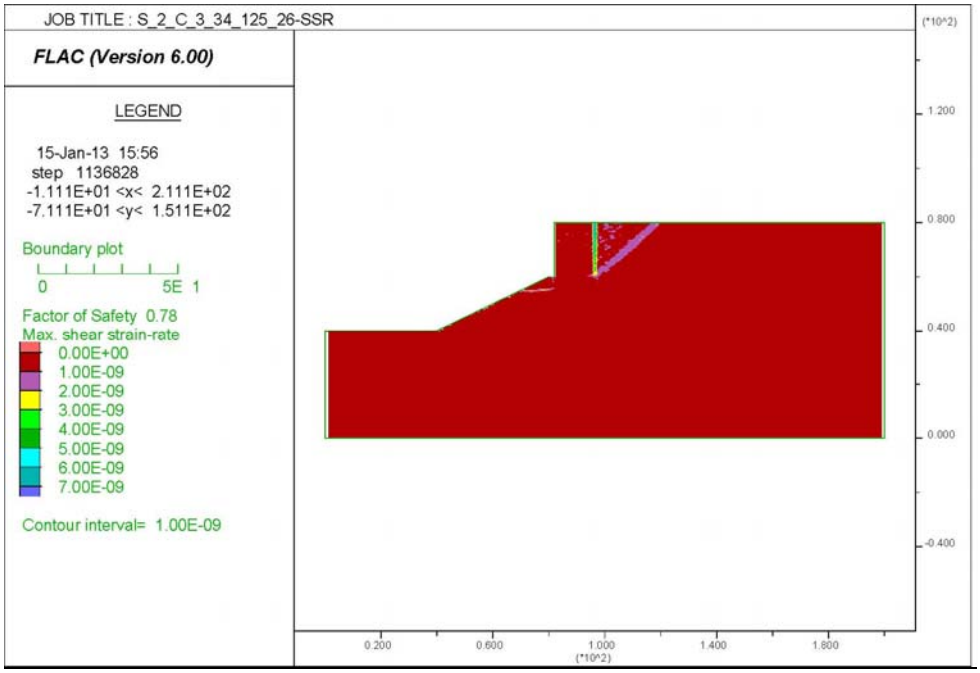

Figure B. 57. Series 2 Case 3 Foundation angle ϕ=26^0, Backfill angle ϕ=34^{0}and γ=125pcf Maximum Shear Strain Rate.

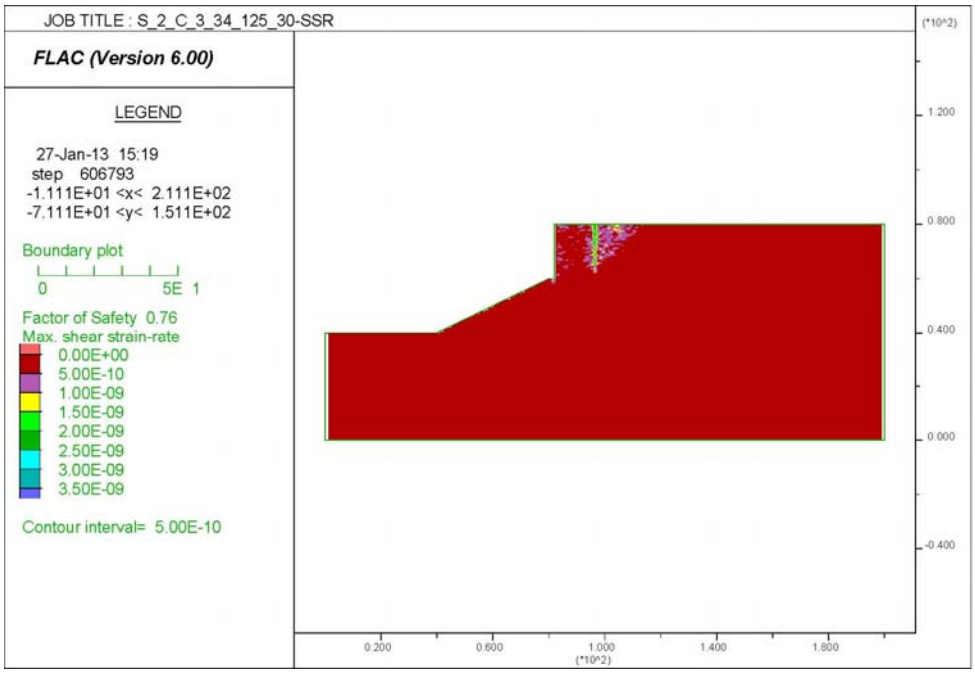

Figure B. 58. Series 2 Case 3 Foundation angle ϕ=30^{o}, Backfill angle ϕ=34^{o}and γ=125pcf Maximum Shear Strain Rate.

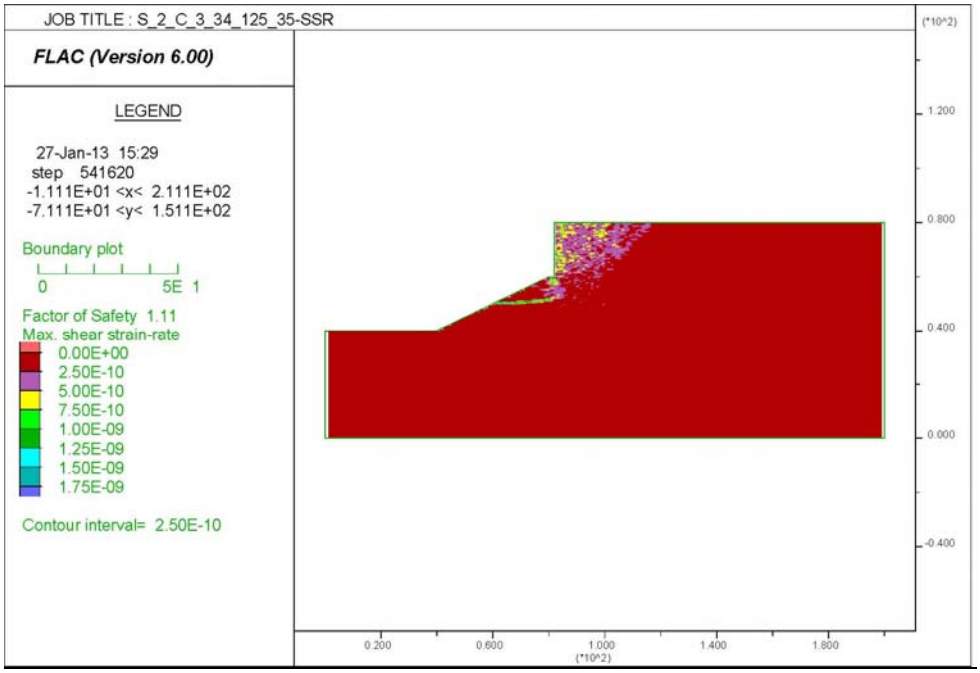

Figure B. 59. Series 2 Case 3 Foundation angle ϕ=35^{o}, Backfill angle ϕ=34^{o}and γ=125pcf Maximum Shear Strain Rate.

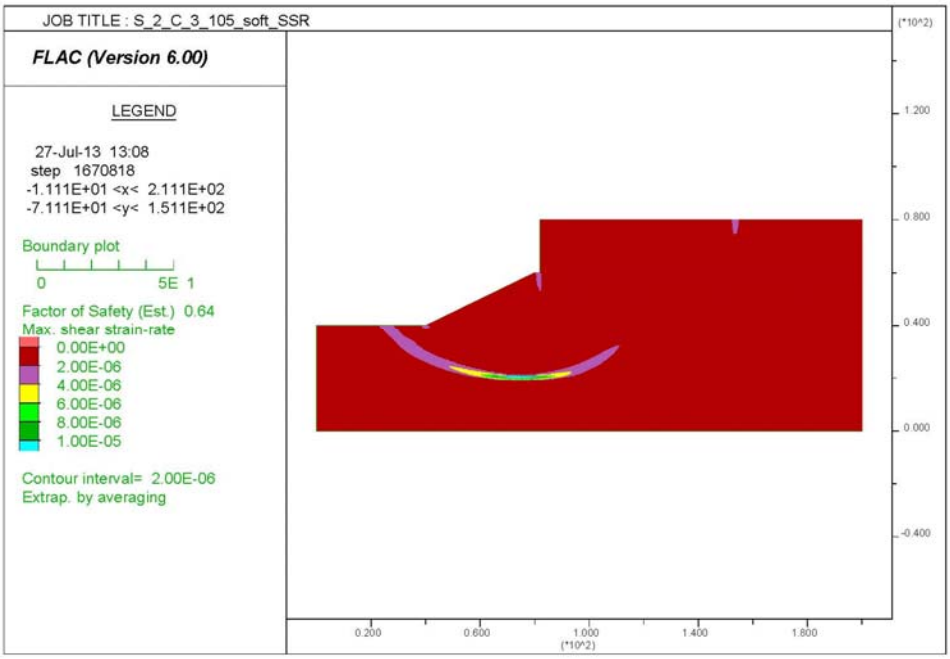

Figure B. 60. Series 2 Case 3 Foundation C_u=500 psf, Backfill angle ϕ=34^{o}and γ=105pcf Maximum Shear Strain Rate.

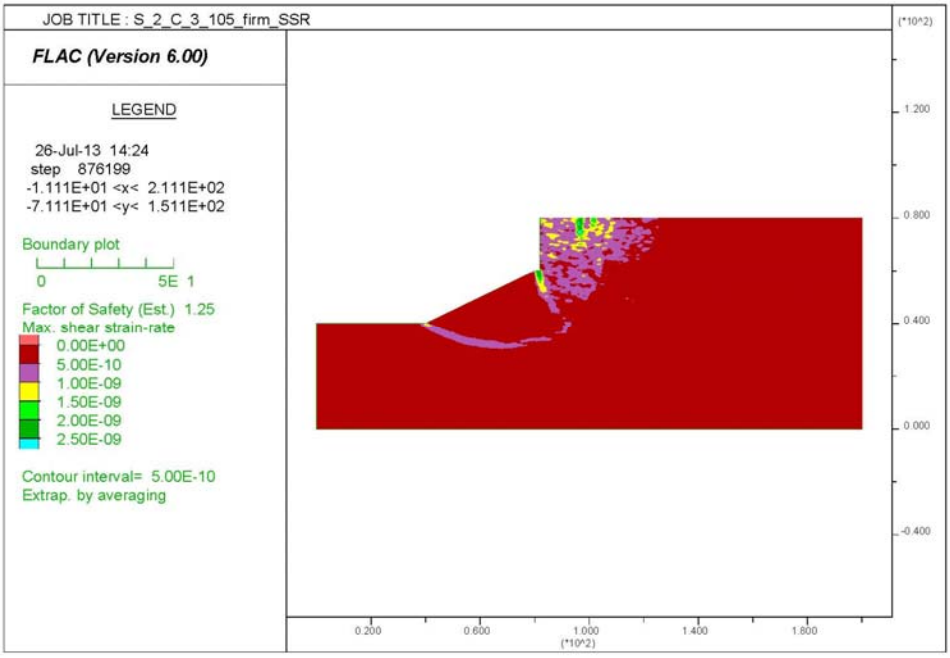

Figure B. 61. Series 2 Case 3 Foundation C_u=1000 psf, Backfill angle ϕ=34^{o}and γ=105pcf Maximum Shear Strain Rate.

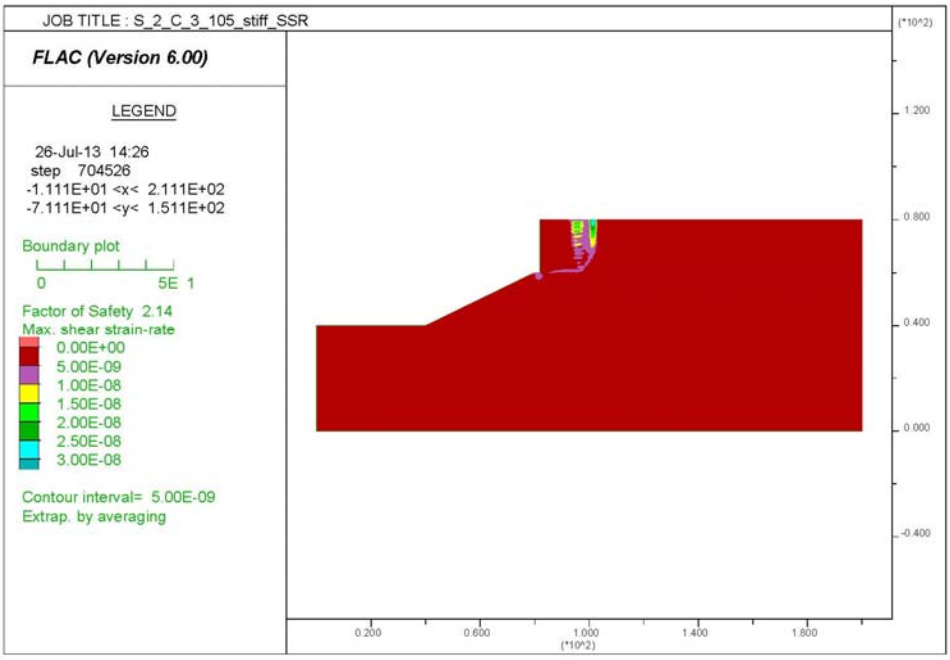

Figure B. 62. Series 2 Case 3 Foundation C_u=2000 psf, Backfill angle ϕ=34^{0}and γ=105pcf Maximum Shear Strain Rate.

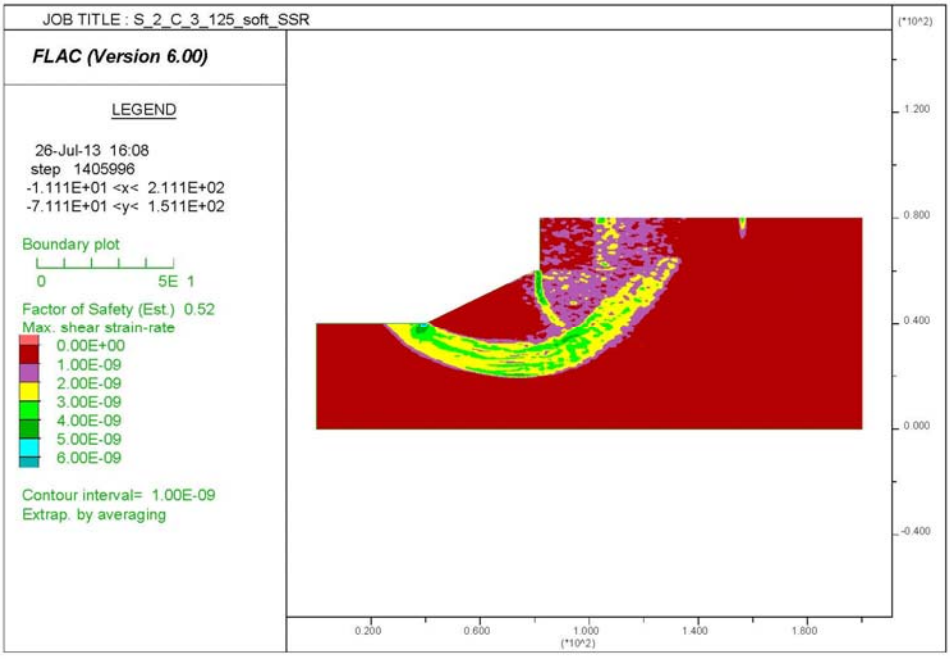

Figure B. 63. Series 2 Case 3 Foundation C_u=500 psf, Backfill angle ϕ=34^{0}and γ=125pcf Maximum Shear Strain Rate.

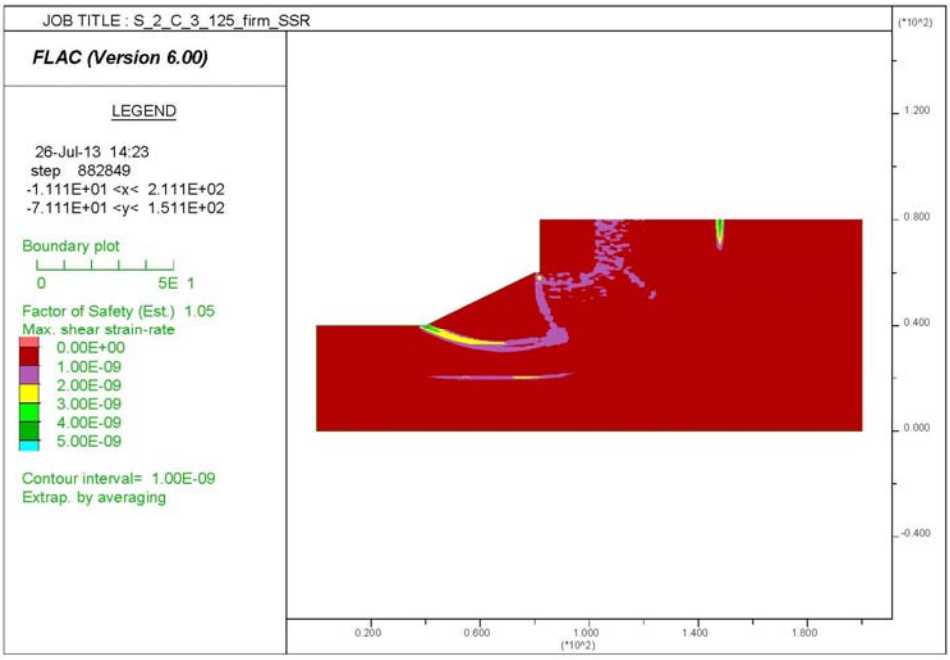

Figure B. 64. Series 2 Case 3 Foundation C_u=1000 psf, Backfill angle ϕ=34^{0}and γ=125pcf Maximum Shear Strain Rate.

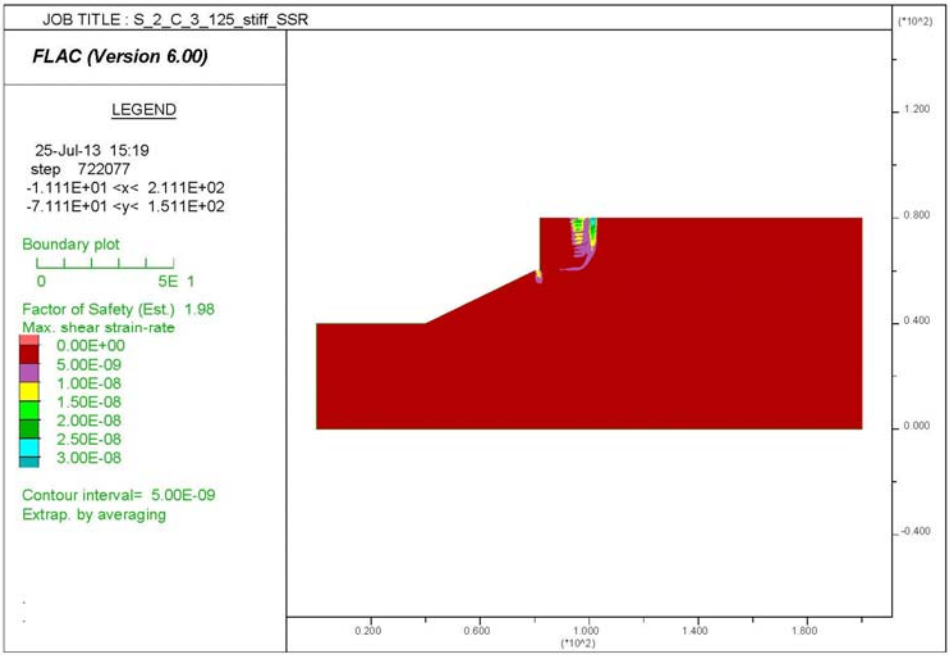

Figure B. 65. Series 2 Case 3 Foundation C_u=2000 psf, Backfill angle ϕ=34^{0}and γ=125pcf Maximum Shear Strain Rate.